

**UNIVERSIDAD COMPLUTENSE DE MADRID**  
**FACULTAD DE CIENCIAS QUÍMICAS**



**TESIS DOCTORAL**

**New selective molecular recognition elements and  
amplification methods for the development of optical  
(bio)sensors**

**Nuevos elementos de reconocimiento molecular selectivo y  
métodos de amplificación para el desarrollo de (bio)sensores  
ópticos**

MEMORIA PARA OPTAR AL GRADO DE DOCTOR

PRESENTADA POR

**Álvaro Luque Uría**

Directores

**María Cruz Moreno Bondi**  
**Elena Benito Peña**

Madrid

**UNIVERSIDAD COMPLUTENSE DE MADRID**

**FACULTAD DE CIENCIAS QUÍMICAS**



**TESIS DOCTORAL**

NEW SELECTIVE MOLECULAR RECOGNITION ELEMENTS AND  
AMPLIFICATION METHODS FOR THE DEVELOPMENT OF OPTICAL  
(BIO)SENSORS

NUEVOS ELEMENTOS DE RECONOCIMIENTO MOLECULAR SELECTIVO Y  
MÉTODOS DE AMPLIFICACIÓN PARA EL DESARROLLO DE (BIO)SENSORES  
ÓPTICOS

MEMORIA PARA OPTAR AL GRADO DE DOCTOR

PRESENTADA POR

**Álvaro Luque Uría**

Directoras

**Dra. María Cruz Moreno Bondi**

**Dra. Elena Benito Peña**

Madrid, 2022





## ACNOWLEDGEMENTS

This research was conducted between 2017 and 2021 in the Optical Chemosensors and Applied Photochemistry group (GSOLFA), at the Department of Analytical Chemistry of Complutense University of Madrid. I would like to thank the Spanish Ministry of Science and Innovation for the financial support (BES-2016-078137, CTQ2015-69278-C2-1-R and RTI2018-096410-B-C21).

My supervisor Prof. María Cruz Moreno Bondi is greatly acknowledged for trusting me and giving me the opportunity to work in her group. I want to express that I have learnt a lot from her both on a professional and a personal level. Furthermore, I want to point out that this thesis could not have been possible without her enormous passion for science and dedication, because it has given me the strength that I needed when I was feeling weaker. I also want to thank her for her guidance and thorough supervision during all these years, and for investing in my professional development, offering me the chance to carry out two highly enriching research stages.

Also, I want to warmly acknowledge Prof. Elena Benito Peña for being there for me when I needed it the most, not only at work, but also on a personal level. She has been the biggest help for me during this thesis, and I will never thank her enough for all the things she has done for me. She has been incredibly helpful with everything related to the laboratory experiments, and she has even contributed firsthand to some of the results presented on this thesis.

I also want to thank Prof. Guillermo Orellana for his highly interesting scientific talks and the rest of the team members of GSOLFA, especially Jose and Bettina, since they supported me from the beginning until the end of my journey, and they have been great confidants and a big support for me. Lopuksi, haluan kiittää sinua, J, aivan erityisellä tavalla. Olet ollut suurin apuni ja tukeni laboratoriossa, myös lähtösi jälkeen. Sinusta on tullut minulle todellinen ystävä. Olet uskomaton ihminen, ja ihailen sinua niin paljon. Kiitos paljon.

I do not want to forget Prof. Karsten Haupt and his group from the University of Technology of Compiègne, where I learnt a lot of things regarding molecularly imprinted polymers. Also, I want to thank Dr. Tarja Nevanen from VTT Technical Research Centre of Finland, because I was able to obtain there one of the most valuable results from this thesis.

I also want to thank my friends from Badajoz and those scattered all over the world for their love and support and for sharing both the good and bad times. Por último, y no menos importante, agradecer a mi madre y al resto de mi familia todo el apoyo incondicional que me habéis dado en todas las cosas que he hecho.

Gracias, thank you, merci, kiitos, salamats, ขอขอบคุณครับ, ありがとう.



## TABLE OF CONTENTS

Figures and tables .....	5
Abbreviations.....	17
Abstract .....	21
Resumen.....	23
<b>1. INTRODUCTION.....</b>	<b>25</b>
<b>1.1. Mycotoxins .....</b>	<b>26</b>
1.1.1. Origins.....	26
1.1.2. Mycotoxins as immunosuppressant drugs.....	35
<b>1.2. Analytical methods for the analysis of mycotoxins.....</b>	<b>38</b>
1.2.1. Chromatographic methods .....	38
1.2.2. Non-chromatographic methods.....	45
<b>1.3. Biosensors for analytical applications.....</b>	<b>48</b>
1.3.1. Principles of biosensors: definitions and concepts .....	48
1.3.2. Optical biosensors.....	49
<b>1.4. Recognition elements in biosensors and bioassays.....</b>	<b>54</b>
1.4.1. Biorecognition elements .....	54
1.4.2. Biomimetic recognition elements.....	57
<b>1.5. Phage display as an analytical tool for the selection of mimopeptides and recombinant antibodies .....</b>	<b>59</b>
1.5.1. Introduction to phage display.....	59
1.5.2. Bacteriophages .....	59
1.5.3. Principles and applications of phage display.....	62
1.5.4. Applications of phage display to the analysis of small molecules.....	63
<b>1.6. Bibliography.....</b>	<b>65</b>
<b>2. AIMS OF THE STUDY.....</b>	<b>83</b>
<b>3. SELECTION OF MIMOPEPTIDES BY PHAGE DISPLAY .....</b>	<b>85</b>
<b>3.1. Introduction.....</b>	<b>87</b>
3.1.1. Phage-display libraries.....	87
3.1.2. Selection of mimopeptides by phage display.....	89
<b>3.2. Objectives .....</b>	<b>92</b>
<b>3.3. Experimental part.....</b>	<b>93</b>
3.3.1. Reagents and solutions .....	93
3.3.2. Analytical instrumentation and materials.....	97
3.3.3. Experimental procedures .....	97

3.4.	Results and discussion .....	103
3.4.1.	Selection of mimopeptides for mycophenolic acid .....	103
3.4.2.	Selection of mimopeptides for ochratoxin A .....	114
3.4.3.	Selection of mimopeptides for alternariol (AOH) .....	116
3.5.	Conclusions .....	129
3.6.	Bibliography .....	130
4.	<b>IMMUNODETECTION OF MYCOPHENOLIC ACID IN BLOOD OF TRANSPLANTED PATIENTS USING A RECOMBINANT PEPTIDE MIMETIC BIOLUMINESCENT TRACER.....</b>	<b>135</b>
4.1.	Introduction.....	137
4.2.	Objectives .....	139
4.3.	Experimental part.....	140
4.3.1.	Reagents and solutions .....	140
4.3.2.	Analytical instrumentation and materials.....	144
4.3.3.	Experimental procedures .....	144
4.4.	Results and discussion .....	151
4.4.1.	Synthetic peptide-based ELISA.....	151
4.4.2.	Analysis of the mimopeptide binding kinetics by SPR .....	154
4.4.3.	Construction of the mimopeptide-NanoLuc fusions.....	156
4.4.4.	Structural characterization of the mimopeptide and the fusion protein.. .....	158
4.4.5.	Optimization of the measuring conditions .....	161
4.4.6.	Analytical characteristics of the bioluminescent assay.....	168
4.4.7.	Sample analysis .....	174
4.5.	Conclusions .....	177
4.6.	Bibliography.....	179
5.	<b>PERFORMANCE OF TWO LUCIFERASE PROTEIN FUSIONS WITH A FUMONISIN MIMOPEPTIDE FOR THE ANALYSIS OF THE TOXIN IN WHEAT SAMPLES .....</b>	<b>183</b>
5.1.	Introduction.....	185
5.2.	Objectives .....	187
5.3.	Experimental part.....	188
5.3.1.	Reagents and solutions .....	188
5.3.2.	Analytical instrumentation and materials.....	191
5.3.3.	Experimental procedures .....	191
5.4.	Results and discussion .....	195



5.4.1.	Construction of the protein fusions.....	195
5.4.2.	Bioluminescent characterization of the fusion proteins.....	196
5.4.3.	Immunoassay optimization.....	197
5.4.4.	Analytical characteristics of the bioluminescent immunoassays .....	202
5.4.5.	Sample analysis .....	207
5.5.	Conclusions .....	209
5.6.	Bibliography.....	210
6.	FINAL REMARKS .....	215
	ANNEX: Publications .....	217



## Figures and tables

- Figure 1.** Chemical structure of the most abundant legislated mycotoxins. .... 33
- Figure 2.** Chemical structure of AOH and AME. .... 34
- Figure 3.** Chemical structures of the fungal metabolite cyclosporin A and the bacterial metabolites tacrolimus and rapamycin. .... 36
- Figure 4.** Chemical structure of MPA and its two main metabolites, the active form Acyl-MPAG and the inactive form MPAG. .... 37
- Figure 5.** Schematic representation of different types of ELISAs. A. Direct ELISA, based on the interaction between an immobilized antigen and a labelled antibody. B. Indirect ELISA, based on the same interaction as the direct ELISA, but using an unlabeled antibody for the interaction with the antigen. A labelled secondary antibody is required to detect the first antibody. C. Sandwich ELISA, based on the immobilization of an antibody on the surface. The antigen interacts with the immobilized antibody and then a secondary antibody interacts either with the antigen-antibody complex or with the antigen alone. If needed, a labelled antibody selective for the secondary antibody is added to obtain the analytical signal. D. Competitive ELISA, based on the initial interaction of the antibody with a solution containing the antigen and then adding the mixture to antigen-coated wells. Already-bound antibodies would be washed away, whereas the rest of antibodies would interact with the bound antigens on the plate. A labelled secondary antibody selective for the first antibody is added to provide the analytical signal. .... 46
- Figure 6.** Schematic representation of the SPR principle. Molecular interactions are monitored on a gold surface. In this representation, IgG antibodies are coupled to the gold surface, and the analyte is delivered there through a microfluidic system. The sensor consists of a glass surface with a thin gold layer on top in which the antibody is attached. Polarized p-light is propagated generally over a prism until it reaches the gold surface, where it generates a plasmon and it is reflected. At a specific angle, the incident light resonates with the plasmon, producing a decay in the light intensity (beam 1). When the analyte interacts with the antibody, the refractive index slightly changes, causing a shift in the light angle that resonates with the plasmon generated on the gold surface (beam 2). The representation of the shift between the first angle that produces the decay in the light intensity and the second angle *versus* the time is called sensogram. .... 50
- Figure 7.** Top: Schematic representation of the five antibody isotypes found in humans. Bottom: Scheme of the different parts of an IgG antibody. IgGs are “Y” shaped proteins composed of two heavy chains (marked in red) and two light chains (marked in green). Each heavy chain consists of a variable domain ( $V_H$ ) and three constant domains ( $C_H$ ), whereas the light chains are made of one variable ( $V_L$ ) and one constant ( $C_L$ ) domain. The recognition normally takes place in the variable regions of the light and/or heavy chains. .... 56
- Figure 8.** Transmission electron micrograph of filamentous phages M13 acquired with negative staining using a JEOL JEM-1400PLUS instrument operating at 120 kV, with a LaB6 electron source and a GATAN US1000 CCD camera. .... 61
- Figure 9.** Structure of a filamentous Ff phage. M13 phage is illustrated as a representative of the Ff class of filamentous phages. The phage virion consists of five structural proteins, the major coat protein, pVIII (blue), and four minor coat proteins, pIII (grey),

pVI (orange), pVII (purple) and pIX (yellow). Phages can be engineered to display different protein sequences in any of the structural proteins. In this figure, at the end of protein pIII, five copies of a protein (green) are displayed. The phage vector is represented as a grey line in between the major coat protein..... 61

**Figure 10.** Two different examples of phage-displayed peptide libraries. On both cases, the sequences are displayed on pIII of an M13 phage. On the left hand, a pentavalent display of a 12-amino acid linear sequence is portrayed, whereas on the right hand, a sequence of 7 amino acids forming a loop-shaped peptide is depicted. .... 88

**Figure 11.** Selection of biorecognition elements by phage display. A. Schematic representation of panning rounds. First, a binding step from the whole pool of phages to the target antibody or peptide is required. Second, a washing step removes all the unbound phages. Next, an elution of the phages that interact with the target is carried out. The fourth and last step of the panning is an amplification of the selectively eluted phages. This process is generally repeated between three to five times. B. Selection and characterization of individual clones. Phage clones are picked from fresh agar plates after the panning rounds. These selected clones are screened, typically by phage-based ELISAs and the best clones are sequenced for further characterization. .... 90

**Figure 12.** Phage output obtained from the eluates of the three selection rounds. .... 105

**Figure 13.** ELISA with polyclonal phages for the first panning strategy for MPA. The three rounds showed binding to the target wells (blue bars) but also high nonspecific binding to the background wells (grey). The phage concentration tested was  $10^{10}$  pfu mL<sup>-1</sup>. The results are shown as the mean values of the absorbance  $\pm$  the standard deviation of the mean ( $n = 3$ ). .... 106

**Figure 14.** Phage output obtained from the eluates of the three selection rounds. A. Output for the Ph.D.-12 library and B. Output for the Ph.D.-C7C library. .... 108

**Figure 15.** ELISA with polyclonal phages for the second panning strategy for MPA. A. Results obtained for the Ph.D.-12 amplified fractions, in which phages have high specificity for target wells (blue) and negligible signal in background wells (grey) and B. Results for the Ph.D.-C7C amplified fractions, showing high nonspecific binding for background wells. In both cases, the phage concentration tested was  $5 \cdot 10^9$  pfu mL<sup>-1</sup>. The results are shown as the mean values of the absorbance  $\pm$  the standard deviation of the mean ( $n = 3$ ). .... 108

**Figure 16.** ELISA with monoclonal phages of the 32 clones selected from the second plate-based panning strategy with the Ph.D.-12 library for MPA. Only one clone showed significant affinity towards background wells (grey), whereas more than half selectively bound to the target wells containing the monoclonal antibody (blue). The results show the absorbance value for each clone ( $n=1$ ). .... 110

**Figure 17.** Competitive ELISA with monoclonal phages for the 16 clones with the highest affinity for the antibody. Not a single clone presented affinity for the background wells (grey), and most of them bound to the target wells containing the monoclonal antibody (blue). However, none of the clones showed competition when  $1 \mu\text{g mL}^{-1}$  free MPA was added to the wells (orange). The results are shown as the average absorbance value  $\pm$  the standard deviation of the mean ( $n = 2$ ). .... 111

**Figure 18.** ELISA with monoclonal phages for the eight clones selected from the second and third round of the magnetic bead-based panning strategy for MPA. Phage clones did not show any background signal (grey) and only one of the clones, clone A2, presented affinity for the target antibody (blue). Additionally, background and target

wells in the absence of phage (Blank) were tested, providing the similar signal as those phages that showed no interaction with the anti-MPA Fab antibody. The results are shown as the average absorbance value  $\pm$  the standard deviation of the mean ( $n = 3$ ).

..... 112

**Figure 19.** Competitive phage-based ELISA for clone A2 with increasing free MPA concentrations ranging from 0 ng mL<sup>-1</sup> to 3200 ng mL<sup>-1</sup>. The results represent the average absorbance values  $\pm$  the standard error of the mean ( $n = 3$ ). ..... 113

**Figure 20.** Confirmatory bead-based phage ELISA for clone A2. The phage clone A2 was incubated together with different MPA concentrations, ranging from 0 ng mL<sup>-1</sup> to 3200 ng mL<sup>-1</sup>. The results show the mean fluorescence intensity values  $\pm$  the standard error of the mean ( $n = 3$ ). ..... 113

**Figure 21.** ELISA with monoclonal phages for the 24 individual clones selected from the second round of the magnetic bead-based panning for OTA. A positive control (MPA clone A2 for anti-MPA Fab antibody) was also tested. The clones showed a similar behavior for the background (grey) and the target wells with anti-OTA Fab (blue). The results show the average absorbance values  $\pm$  the standard deviation of the mean ( $n = 2$ ). ..... 115

**Figure 22.** ELISA with monoclonal phages for the 23 individual clones selected from the third round of the magnetic bead-based panning for OTA. In the same way as the ELISA for the clones of the second round, the same positive control (MPA clone A2 for anti-MPA Fab) was tested. None of the clones tested showed any remarkable difference between the background (grey) and target wells with anti-OTA Fab (blue). The results show the average absorbance values  $\pm$  the standard deviation of the mean ( $n = 2$ ). ... 115

**Figure 23.** Phage output obtained from the eluates of the four selection rounds from the first panning strategy for AOH mimopeptides. A. Output for the Ph.D.-12 library and B. Output for the Ph.D.-C7C library..... 117

**Figure 24.** ELISA with polyclonal phages for the first two pannings for AOH mimopeptides. A. Results obtained for the Ph.D.-12 amplified fractions, in which phages have similar specificity for target wells (blue) and background wells (grey) and B. Results for the Ph.D.-C7C amplified fractions, showing high specificity for target wells and little binding for background wells. In both cases, the phage concentration tested was 5 · 10<sup>9</sup> pfu mL<sup>-1</sup>. The results are shown as the mean values of the absorbance  $\pm$  the standard deviation of the mean ( $n = 3$ ). ..... 118

**Figure 25.** Phage output obtained from the eluates of the three selection rounds from the second panning strategy for AOH mimopeptides. A. Output for the Ph.D.-12 library and B. Output for the Ph.D.-C7C library. .... 119

**Figure 26.** ELISA with polyclonal phages for the second panning strategy for AOH mimopeptides. A. Results obtained for the Ph.D.-12 amplified fractions, in which phages gain specificity for target wells (blue), maintaining a negligible signal in background wells (grey) until the third round, in which the nonspecificity was amplified and, B. Results for the Ph.D.-C7C amplified fractions, showing high specific binding for target wells since the second round in comparison to background wells. In both cases, the phage concentration tested was 5 · 10<sup>9</sup> pfu mL<sup>-1</sup>. The results are shown as the mean values of the absorbance  $\pm$  the standard deviation of the mean ( $n = 3$ ). ..... 120

**Figure 27.** Phage output obtained from the eluates of the three selection rounds from the last panning strategy for AOH mimopeptides. .... 121

**Figure 28.** ELISA with polyclonal phages for the last panning strategy for AOH mimopeptides. High specificity for target wells (blue) is achieved only in the third round. The other two rounds present very low affinity for both target and background (grey) wells. The phage concentration tested was  $5 \cdot 10^9$  pfu mL<sup>-1</sup>. The results are shown as the mean values of the absorbance  $\pm$  the standard deviation of the mean ( $n = 3$ ). .. 122

**Figure 29.** ELISA with monoclonal phages for the 47 individual clones selected from the third (top) and fourth (bottom) rounds of the first panning strategy with the Ph.D.-C7C library for AOH. Nearly half of the clones presented specificity for the target wells (blue) and negligible signal for background wells (grey). The results show the absorbance value for each clone ( $n=1$ )...... 123

**Figure 30.** Competitive ELISA with monoclonal phages for the 20 clones with the highest affinity for the antibody. Only one clone presented affinity for the background wells (grey), and all of them bound to the target wells containing the monoclonal antibody (blue). However, none of the clones showed exceptional competition when 100 ng mL<sup>-1</sup> free AOH was added to the wells (orange). The results are shown as the average absorbance value  $\pm$  the standard deviation of the mean ( $n = 3$ )...... 124

**Figure 31.** ELISA with monoclonal phages for the 48 individual clones selected from the second (top) and third (bottom) rounds of the second panning strategy with the Ph.D.-C7C library for AOH. Nearly a third of the clones presented specificity for the background wells (grey) and only a few clones showed specificity for target wells (blue). The results show the absorbance value for each clone ( $n=1$ )...... 125

**Figure 32.** Competitive ELISA with monoclonal phages for the 10 clones with the highest affinity for the antibody. Two of the clones presented affinity for the background wells (grey), and seven of them bound selectively to the target wells containing the monoclonal antibody (blue). However, none of the clones showed exceptional competition when 100 ng mL<sup>-1</sup> free AOH was added to the wells (orange). The results are shown as the average absorbance value  $\pm$  the standard deviation of the mean ( $n = 3$ ). ..... 126

**Figure 33.** ELISA with monoclonal phages for the 24 individual clones selected from the third round of the last panning strategy with the Ph.D.-C7C library for AOH. None of the clones presented specificity for the background wells (grey) and roughly half of the clones showed specificity for target wells (blue). The results are shown as the average absorbance value  $\pm$  the standard deviation of the mean ( $n = 2$ )...... 127

**Figure 34.** Competitive ELISA with monoclonal phages for the 10 clones with the highest affinity for the antibody. None of the clones presented affinity for the background wells (grey), and eight of them bound selectively to the target wells containing the monoclonal antibody (blue). Some of the clones showed a slight competition when 100 ng mL<sup>-1</sup> free AOH was added to the wells (orange). The results are shown as the average absorbance value  $\pm$  the standard deviation of the mean ( $n = 3$ )...... 127

**Figure 35.** Scheme of the synthetic peptide-based ELISA using magnetic beads. The biotinylated MPA mimopeptide is first attached to neutravidin-coupled magnetic beads. Then, the anti-MPA Fab and free MPA are added to the solution and a competition is established between the mimopeptide bound on the beads and free MPA for the anti-MPA Fab binding sites. At low MPA concentrations, more anti-MPA Fab will remain bound to the mimopeptide. A secondary HRP-coupled anti-IgG monoclonal antibody is added to detect the remaining anti-MPA Fab bound to the beads. After addition of the substrate of the enzyme the fluorescence is measured in a microplate reader. .... 145

**Figure 36.** Scheme of the assembly process of the MPA mimopeptide (orange) and the NanoLuc (blue) inserts on pMAL vector. PCR-amplified-pMAL vector containing the MPA mimopeptide insert on different sites of the vector is incubated with the PCR-amplified NanoLuc insert to obtain two different products. In case A, the MPA mimopeptide is located on the N-terminus of the NanoLuc sequence, whereas in case B the mimopeptide is on the C-terminus of the NanoLuc. .... 147

**Figure 37.** Scheme of the bioluminescent bead-based immunoassay for MPA detection. Streptavidin-coated magnetic beads were incubated with the biotinylated anti-MPA Fab. Then, the NanoLuc-MPA mimopeptide fusion protein and varying concentrations of free MPA were simultaneously added and incubated. Finally, the substrate for NanoLuc was added to the wells and the bioluminescence was monitored with a CLARIOstar microplate reader. .... 149

**Figure 38.** Checkerboard titration for the optimization of the mimopeptide and antibody concentrations of the synthetic peptide-based ELISA in the absence (top) and presence (bottom) of 16 ng mL<sup>-1</sup> free MPA (RSD < 16.5%). .... 152

**Figure 39.** Comparison of the bead-based ELISAs with the MPA synthetic mimopeptide (black) and the phage clone A2 (red). The fluorescence emission ( $\lambda_{\text{ex}} = 530 \text{ nm}$ ,  $\lambda_{\text{em}} = 590 \text{ nm}$ ) was measured immediately after the addition of the Amplex UltraRed as substrate. The results represent the normalized mean values  $\pm$  the standard error of the mean (n = 3) with a logistic fit (OriginPro 2019). .... 154

**Figure 40.** SPR sensograms of the interaction between free MPA and the anti-MPA Fab antibody using Biacore T200. The colors observed refer to the different nanomolar concentrations of MPA added. .... 155

**Figure 41.** SPR sensograms of the interaction between the mimopeptide and the anti-MPA Fab antibody using Biacore T200. The colors observed refer to the different nanomolar concentrations of the mimopeptide added. .... 155

**Figure 42.** Expression test with the four clones that showed successful alignment after the transformation of NEB 5-alpha cells and a blank. The results show the bioluminescence of each product (n = 1). .... 157

**Figure 43.** SDS-PAGE analysis for the C-terminal fusion protein with Coomassie brilliant blue protein staining: lane A, molecular marker (Thermo Scientific™ PageRuler™ Prestained Protein Ladder, 10 to 180 kDa), B, C-terminal fusion, C, C-terminal fusion with a 5 min boiling step at 95 °C. .... 157

**Figure 44.** <sup>1</sup>H-<sup>1</sup>H TOCSY bidimensional spectrum of the MPA mimopeptide A(CEGLYAHWC)GGGSK(Bio)-NH<sub>2</sub>. The amino acids were assigned in the spectrum according to NMR charts. .... 158

**Figure 45.** <sup>1</sup>H-NMR spectra of the MPA mimopeptide in the presence (red) and the absence (blue) of a few drops of DTT. The structural change is observed in the anomeric region between 9 and 5 ppm of the amplified spectra. The H $\alpha$  assignment of the amino acids can be observed in the amplified spectrum of the mimopeptide in the absence of DTT. .... 159

**Figure 46.** Structural simulation of the MPA mimopeptide with MAESTRO software. .... 160

**Figure 47.** <sup>1</sup>H-<sup>15</sup>N HSQC spectrum of the NanoLuc-mimopeptide fusion protein. .... 160

**Figure 48.** Binding test of the NanoLuc-mimopeptide fusion proteins on neutravidin-coated wells. Both products present very high nonspecific interaction for background wells (grey) in comparison to the signal obtained in the target wells with the anti-MPA

Fab (blue). The results are shown as the mean values of the bioluminescence signal  $\pm$  the standard deviation of the mean ( $n = 3$ )..... 161

**Figure 49.** Binding test of the NanoLuc-mimopeptide fusion proteins on neutravidin-coated wells previously blocked. Both fusion proteins, N-terminal (A) and C-terminal (B) present very high nonspecific interactions with both of the blocking agents for background wells (grey) in comparison to the signal obtained in the target wells with the anti-MPA Fab (blue). The results are shown as the mean values of the bioluminescence signal  $\pm$  the standard deviation of the mean ( $n = 3$ )..... 162

**Figure 50.** Neutravidin bead-based assay with SuperBlock blocking buffer supplemented with 0.05% T20. A. Bioluminescence observed with different dilutions of the fusion protein in the assay. B. Comparison of the signal obtained with a 1:10 dilution of the fusion protein with three negative controls, in which the assay was reproduced in the same conditions but in the absence of anti-MPA Fab (no Fab), neutravidin-coated magnetic beads (no beads) and the NanoLuc-MPA mimopeptide fusion protein (no protein). The results are shown as the average bioluminescence values  $\pm$  the standard deviation of the mean ( $n=3$ )..... 163

**Figure 51.** Neutravidin bead-based assay with Protein Free blocking buffer supplemented with 0.05% T20. A. Bioluminescence observed with different dilutions of the fusion protein in the assay. B. Comparison of the signal obtained with a 1:10 dilution of the fusion protein with three negative controls, in which the assay was reproduced in the same conditions but in the absence of anti-MPA Fab (no Fab), neutravidin-coated magnetic beads (no beads) and the NanoLuc-MPA mimopeptide fusion protein (no protein). The results are shown as the average bioluminescence values  $\pm$  the standard deviation of the mean ( $n=3$ )..... 163

**Figure 52.** Streptavidin cellulose bead-based assay for (A) the N-terminal and (B) the C-terminal fusions at two different dilution factors, in the presence (blue) and absence (grey) of 32 ng mL<sup>-1</sup> MPA. Under the same conditions, the C-terminal fusion shows ten times higher bioluminescence than the N-terminal product. The results are shown as the average bioluminescence values  $\pm$  the standard deviation of the mean ( $n=3$ )..... 164

**Figure 53.** Streptavidin cellulose bead-based assay for (A) the N-terminal and (B) the C-terminal fusions in the presence (blue) and absence (grey) of 32 ng mL<sup>-1</sup> MPA with two different negative controls: the absence of anti-MPA Fab and the absence of streptavidin beads. Under the same assay conditions, the C-terminal fusion shows slightly better signal to background ratio than the N-terminal product. The results are shown as the average bioluminescence values  $\pm$  the standard deviation of the mean ( $n=3$ )..... 165

**Figure 54.** Scheme of the developed assays for NanoLuc fusion proteins. A. Plate-based method. B. Neutravidin beads-based method. C. Streptavidin beads-based method. 165

**Figure 55.** Checkerboard titration for the optimization of the antibody and magnetic bead concentrations for the immunoassay with the NanoLuc-mimopeptide fusion protein in the absence (top) and presence (bottom) of 32 ng mL<sup>-1</sup> free MPA (RSD < 17.5%)..... 167

**Figure 56.** Calibrate comparison between the N-terminal (grey) and the C-terminal (blue) fusions. The previously optimized conditions were applied in both calibrates. The results are presented as the normalized bioluminescence mean values  $\pm$  the standard error of the mean ( $n = 3$ ) with a logistic fit (OriginPro 2019)..... 168

**Figure 57.** Calibration curve of the bioluminescent immunoassay for the determination of MPA in buffer using the C-terminal fusion. Several MPA concentrations were



incubated together with the fusion protein and streptavidin magnetic beads coupled to the biotinylated anti-MPA. The bioluminescence signals ( $\lambda_{em} = 470 \pm 80$  nm) were measured after the addition of the NanoLuc substrate, and the values were normalized to the maximum and minimum signals. The results represent as the mean values  $\pm$  the standard error ( $n = 3$ ) adjusted to a logistic fit using OriginPro 2019. .... 169

**Figure 58.** Chemical structures of mycophenolic acid (MPA), its two main metabolites, (Acyl-MPAG and MPAG) and two immunosuppressant drugs commonly co-administered to transplanted patients (Tacrolimus and Cyclosporin A)..... 171

**Figure 59.** Cross-reactivity test of the bioluminescent immunoassay. Acyl-MPAG, an active form of MPA, shows a significant cross-reactivity to MPA, contrary to the inactive form MPAG. The two other immunosuppressant drugs evaluated, tacrolimus and cyclosporin A, showed no significant cross-reactivity at the concentration levels assessed. The bioluminescence values were normalized to the maximum and minimum signals, and the results are shown as the mean values  $\pm$  the standard error of the mean ( $n = 3$ ) adjusted to a logistic fit using OriginPro 2019. .... 171

**Figure 60.** Evaluation of the long-term stability for the C-terminal fusion protein stored at  $-20$  °C in PBS. The bioluminescent immunoassay was performed under the same conditions and the IC50 values were consequently compared. The results are shown as the values  $\pm$  the standard error given by OriginPro 2019..... 172

**Figure 61.** SDS-PAGE analysis for the fusion proteins after more than one year of storage with Coomassie brilliant blue protein staining: lane A: C-terminal fusion, B, C-terminal fusion with a 5 min boiling step at  $95$  °C, C, molecular marker (Thermo Scientific™ PageRuler™ Prestained Protein Ladder, 10 to 180 kDa), D, N-terminal product, E, N-terminal product with a 5 min boiling step at  $95$  °C..... 173

**Figure 62.** Calibration curves obtained for the bead-based immunoassay using various dilutions of ultrafiltered serum samples in PBS  $1\times$  supplemented with 0.05% T20. The bioluminescence values were normalized to the maximum and minimum signals and the results are shown as the mean values  $\pm$  the standard error of the mean ( $n = 3$ ) adjusted to a logistic fit using OriginPro 2019. .... 173

**Figure 63.** Comparison of the results obtained for the analysis of MPA in blood samples from transplanted patients by the immunoassay and the chromatographic method. H patients received no previous treatment with MPA, whereas T patients were previously treated with MPA. The results are presented as the mean values  $\pm$  the standard error of the mean ( $n = 3$ ). .... 174

**Figure 64.** RRLC elution profile of MPAG, Acyl-MPAG and MPA. The MPA solution was prepared at  $80$  ng mL<sup>-1</sup>, whereas the MPAG and the Acyl-MPAG solutions were prepared at  $250$  ng mL<sup>-1</sup>..... 175

**Figure 65.** SDS-PAGE results obtained for the two fusion proteins. A. A2-GLuc fusion protein; Lane 1: protein ladder (Bio-Rad Precision Plus Protein Dual Color Standard); Lane 2: unpurified protein; Lane 3: flow through of the column; Lanes 4 to 9: elution fractions of the purified protein. B. A2-NLuc fusion protein; Lane 1: protein ladder (Thermo Scientific™ PageRuler™ Prestained Protein Ladder, 10 to 180 kDa); Lane 2: unpurified protein; Lane 3: flow through of the HisTrap™ column; Lane 4: washing solution collected; Lane 5: purified protein eluted from the column. .... 195

**Figure 66.** Kinetic curves obtained for A2-GLuc (blue dashed line), A2-NLuc with furimazine (red dotted line) and A2-NLuc with NanoGLO reagent (black straight line). In all cases,  $50$   $\mu$ L of each substrate (coelenterazine for A2-GLuc and furimazine or

NanoGLO for A2-NLuc) were added to a solution of 50  $\mu\text{L}$  containing the same molar concentration of each of the fusion proteins. Different concentrations of the fusion proteins were assessed in the experiment, obtaining equivalent results in the signal drop for all of them. The graphs represent the normalized bioluminescence of three replicates.

..... 196

**Figure 67.** Evaluation of the ability of the A2-GLuc fusion protein to act as a mimopeptide on a plate-based (left) or bead-based (right) format. The mimopeptide signal in the presence of antibody (blue) was considerably higher than that in the absence (red) of the antibody for all the different concentrations tested. The results are displayed as average bioluminescence signals  $\pm$  the standard error of the mean ( $n = 3$ ). .....

**Figure 68.** Competition evaluation in the bead-based format for A2-GLuc. Left. Preliminary experiments in the absence (blue) and presence (red) of  $10 \text{ ng mL}^{-1}$  free  $\text{FB}_1$  for different fusion protein concentrations. Right. Evaluation of the response of the two A2-GLuc concentrations with the best signal-to-background ratios,  $1.5 \mu\text{g mL}^{-1}$  (green) and  $3 \mu\text{g mL}^{-1}$  (magenta), for different  $\text{FB}_1$  concentrations, between 0 and  $1000 \text{ ng mL}^{-1}$ . The results are presented as the average luminescence signals  $\pm$  the standard error of the mean ( $n = 3$ ).....

**Figure 69.** Assay response of factor Xa-cleaved A2-GLuc in the absence (blue) or presence (red) of  $5 \text{ ng mL}^{-1}$  free  $\text{FB}_1$  with different concentrations of the fusion protein ( $0.375\text{--}3 \mu\text{g mL}^{-1}$ ). Signal-to-background ratios are represented in black squares, with the corresponding scale on the right y axis.....

**Figure 70.** Checkerboard titration for the bead-based immunoassay using A2-GLuc. Different concentrations of the antibody (x-axis) and the fusion protein (z-axis) were tested in the absence (up) and the presence (down) of  $10 \mu\text{g mL}^{-1}$  free  $\text{FB}_1$ . The ratio between these two signals (C) was utilized to determine the optimal concentrations for the immunoassay (RSD $<16.2\%$ ). .....

**Figure 71.** Assay comparison for the A2-NLuc fusion protein where the competition was established with the antibody in solution (left) or previously bound onto magnetic beads (right). Signal-to-background ratios are presented in black squares, with the corresponding scale on the right y axis.....

**Figure 72.** Checkerboard titration for the bead-based immunoassay using A2-NLuc. Different concentrations of magnetic beads (x-axis) and antibody (z-axis) were tested in the absence (up) and the presence (down) of  $10 \mu\text{g mL}^{-1}$  free  $\text{FB}_1$ . The ratio between both signals (C) was utilized to determine the optimal concentrations for the immunoassay (RSD  $<14.4\%$ ). .....

**Figure 73.** Calibration curves for the two bead-based bioluminescent immunoassays developed with either A2-GLuc (red diamonds) and A2-NLuc (blue circles) for the detection of  $\text{FB}_1$  in assay buffer. The competition between the fusion protein and free  $\text{FB}_1$  for the binding sites of the antibody was set in solution. After the corresponding incubation step, the antibody was collected with protein G-coated magnetic beads. The bioluminescence (total luminescence for A2-GLuc,  $\lambda_{\text{em}} = 470 \pm 40 \text{ nm}$  for A2-NLuc) was measured once the substrate was added to the wells. The values presented were normalized to the maximum and minimum values. The results are displayed as the mean values  $\pm$  the standard error of the mean ( $n = 3$ ) and were adjusted to a logistic fit with OriginPro 2019 software.....

**Figure 74.** Cross reactivity evaluation for the developed immunoassays using (A) A2-GLuc and (B) A2-NLuc. Under identical experimental conditions as the calibration

curves, the most abundant mycotoxins that can potentially be found in combination with FB<sub>1</sub> were assessed. The bioluminescent signal values were normalized to the maximum and minimum values. The results are displayed as the average values ( $n = 3$ )  $\pm$  the standard error of the mean. The calibration curves were adjusted to a logistic fit using OriginPro 2019 software..... 204

**Figure 75.** Calibration curves obtained for the evaluation of the matrix effect in the bioluminescent immunoassays with (A) A2-GLuc and (B) A2-NLuc. Under identical experimental conditions as the calibration curves, the wheat extracts were diluted at different concentrations (extract concentration: 5%, 7%, 10%) in the assay buffer and the calibration curves are compared with that in buffer solution. The bioluminescence was normalized to the maximum and minimum signals. The results are presented as the mean bioluminescence  $\pm$  the standard error of the mean ( $n = 3$ ). The calibration curves were adjusted to a sigmoidal fit with OriginPro 2019 software..... 206

<b>Table 1.</b> Legislated mycotoxins by the European Commission. ....	28
<b>Table 2.</b> Fungal species producing some of the most widespread non-legislated mycotoxins. ....	34
<b>Table 3.</b> Analytical characteristics of the most relevant chromatographic methods for the determination of AOH, AME, fumonisins and MPA .....	40
<b>Table 4.</b> Analytical characteristics of non-chromatographic methods for the determination of MPA, FB1 and AOH. ....	57
<b>Table 5.</b> Classification of bacteriophages according to their shape and basic properties. <sup>a</sup> .....	60
<b>Table 6.</b> Experimental conditions of the first panning strategy for the selection of MPA mimopeptides. ....	104
<b>Table 7.</b> Experimental conditions of the second panning strategy for the selection of MPA mimopeptides. ....	107
<b>Table 8.</b> Experimental conditions of the first panning strategy for the selection of AOH mimopeptides. ....	116
<b>Table 9.</b> Experimental conditions of the second panning strategy for the selection of AOH mimopeptides. ....	119
<b>Table 10.</b> Experimental conditions of the third panning strategy for the selection of AOH mimopeptides. ....	121
<b>Table 11.</b> Identified amino acid sequences from the AOH pannings. The conserved amino acid sequences between the different clones are reflected in bold. ....	128
<b>Table 12.</b> Ratios between the signals obtained in the checkerboard titration in the presence and the absence of free MPA in solution for every peptide and antibody amount tested. The optimal combination selected is shown in bold (RSD < 13.1%)....	153
<b>Table 13.</b> Kinetic constants determined for the interaction of the anti-MPA Fab with free MPA and the mimopeptide using Biacore T200. The values are shown as the average ± the standard error of seven different analyte concentrations. ....	156
<b>Table 14.</b> Ratios between the signals obtained in the checkerboard titration in the presence and the absence of free MPA in solution for every antibody and magnetic bead concentration tested. The optimal combination selected is shown in bold (RSD < 14.8%). .....	166
<b>Table 15.</b> Comparison of different immunoassays and chromatographic methods for the determination of total and free MPA. ....	170
<b>Table 16.</b> MPA doses administered to the analyzed transplanted patients. ....	174
<b>Table 17.</b> Concentration levels of MPAG determined in the analyzed samples. ....	176
<b>Table 1.</b> Sequence of the PCR primers used for the construction of the two fusion proteins. The overlapping region with the template plasmid for each case is underlined. The FB <sub>1</sub> mimopeptide sequence appears in bold. ....	192
<b>Table 19.</b> Signal-to-noise ratios obtained in the checkerboard titration in the presence and the absence of free FB <sub>1</sub> for every fusion protein concentration and antibody amount assessed. The optimal combination selected is shown in bold red color (RSD<16.2%). .....	200
<b>Table 20.</b> Signal-to-noise ratios obtained in the checkerboard titration in the presence and the absence of free FB <sub>1</sub> for every antibody and bead amount assessed. The optimal combination selected is shown in bold red color. (RSD <14.4%) .....	202
<b>Table 21.</b> Analytical characteristics of the two immunoassays described for FB <sub>1</sub> . ....	203

**Table 22.** Cross reactivity results for the bioluminescent immunoassays with the two fusion proteins, A2-GLuc and A2-NLuc..... 205

**Table 23.** Analysis of spiked wheat samples with FB<sub>1</sub>. ..... 207

**Table 24.** Analysis of real samples and validation with HPLC-MS/MS reference method.  
..... 208



**Abbreviations**

Ab	Antibody
Acyl-MPAG	Mycophenolic acid acyl- $\beta$ -D-glucuronide
Afs	Aflatoxins
Ag	Antigen
ALT	Altenuene
AME	Alternariol monomethyl ether
AMP	Ampicillin
AOH	Alternariol
AP	Alkaline phosphatase
BB	Binding buffer
BEA	Beauvericin
BSA	Bovine serum albumin
BUT	Butenolide
CI	Confidence interval
C <sub>H</sub>	Constant heavy domain of antibody
C <sub>L</sub>	Constant light domain of antibody
CPA	Cyclopiazonic acid
CUL	Culmorin
CV	Coefficient of variation
DAD	Diode array detector
DON	Deoxynivalenol
dsDNA	Double-stranded DNA
EAs	Ergot Alkaloids
EB	Elution buffer
ELISA	Enzyme-linked immunosorbent assay
EMO	Emodin
EN	Enniantins
FA	Fusaric acid

Fab	Fragment antigen binding
FAO	Food and Agriculture Organization of the US
FBs	Fumonisin
FB <sub>1</sub>	Fumonisin B <sub>1</sub>
FB <sub>2</sub>	Fumonisin B <sub>2</sub>
FD	Fluorescent detection
FDA	US Food and Drug Administration
FP	Fusaproliferin
GC	Gas chromatography
GLuc	<i>Gaussia</i> luciferase
HPLC	High performance liquid chromatography
HRP	Horse-radish peroxidase
IC <sub>50</sub>	Half maximal inhibitory concentration
IPTG	Isopropyl-β-d-thiogalactopyranoside
K <sub>D</sub>	Dissociation constant
LB	Luria broth
LOD	Limit of detection
LOQ	Limit of quantification
MBP	Maltose binding protein
MIP	Molecularly imprinted polymer
MON	Moniliformin
MPA	Mycophenolic acid
MPAG	Mycophenolic acid β-D-glucuronide
MS	Mass spectrometry
NLuc	NanoLuc luciferase
OD	Optical density
OTA	Ochratoxin A
PAGE	Polyacrylamide gel electrophoresis
PBS	Phosphate buffer saline



PCR	Polymerase chain reaction
RSD	Relative standard deviation
SDS	Sodium dodecyl sulphate
SPE	Solid phase extraction
ssDNA	Single-stranded DNA
STE	Sterigmatocystin
UV	Ultraviolet
V <sub>H</sub>	Variable heavy domain of antibody
V <sub>L</sub>	Variable light domain of antibody
WHO	World Health Organization
ZEA	Zearalenone



## Abstract

### **New selective molecular recognition elements and amplification methods for the development of optical (bio)sensors**

Mycotoxins are low molecular weight substances produced as secondary metabolites by a wide variety of filamentous fungi that can be found as natural contaminants in many foods and feeds. The number of toxic fungal metabolites currently known exceeds the thousand units, but only a few of them are considered a threat to humans and animal health. Exposure to mycotoxins can be due to the consumption of contaminated foodstuff, but also by inhalation of dust containing mycotoxigenic fungal spores. It has been estimated that nearly 40% of the global crops can be contaminated with mycotoxins. Hence, the development of analytical methods that can detect these mycotoxins in foodstuff are essential. On the other hand, despite their elevated risk in food quality, several mycotoxins present medical applications, for example as immunosuppressant drugs for organ transplantation. However, a limitation for this application is the narrow therapeutic window presented by these drugs, *e.g.*, mycophenolic acid. High doses of these compounds can cause serious adverse health effects in humans, but little doses could not be sufficient to prevent organ rejection in transplanted patients. Thus, it is also of utmost importance to monitor the levels of these compounds in blood to improve the clinical efficacy of the immunosuppressant.

The traditional way of analyzing these mycotoxins has been through chromatographic methods. Nevertheless, novel immunoassays and biosensors have proven to be suitable alternatives to overcome the limitations of chromatographic techniques, since they can provide fast, sensitive, cheap, and even on-site analyses. A biosensor is a device that includes a recognition element of biological nature, such as antibodies or enzymes, in contact with a transducer, which is in charge of transforming the biomolecular recognition event into an analytical signal. This thesis was focused on the development of new optical biosensors for the analysis of mycotoxins in foodstuff and immunosuppressant drugs in human blood. To accomplish this aim, novel recognition elements were selected or designed in order to provide fast, selective and sensitive determinations of two mycotoxins, mycophenolic acid (MPA), applied as immunosuppressant in heart-transplanted patients, and fumonisin B<sub>1</sub> (FB<sub>1</sub>).

The first part of the thesis was focused on the selection of mycotoxin mimopeptides applying the phage display technology. Mimopeptides are described as epitope-mimicking peptides since they can bind to the same antibody paratope as the corresponding antigen. The synthesis of toxin-conjugates for their application in competitive immunoassays is usually time-consuming and challenging and may result in randomly crosslinked and unstable molecules which might reduce assay sensitivity. The main advantage of the use of these peptides is that cumbersome conjugation steps of the toxin either to a carrier protein or to a label are avoided overcoming the above-mentioned limitations.

Phage display technology consists of the selection of novel biorecognition elements, from recombinant antibodies to mimopeptides, for specific targets. To achieve this, it is

important to carry out an efficient selection and screening of the phage library which are typically comprised of  $10^7$ – $10^{10}$  different phage clones displaying a randomized peptide sequence, or antibody fragments. By conducting the aforementioned selection rounds, also known as pannings, those phage clones that exhibit high affinity for the target are selected and amplified from the initial pool. After several panning rounds, the enriched phages are scrutinized in ELISAs in order to choose the best binder with the desired properties. In this thesis, different selection rounds were carried out for three different mycotoxins: mycophenolic acid, ochratoxin A and alternariol, obtaining satisfactory results for the first one.

In the second part of this thesis, different immunoassays were developed based on the use of mimopeptides. First, the mimopeptide for mycophenolic acid obtained by phage display was used to design a competitive immunoassay for the detection of the immunosuppressant in human serum. To this aim, the binding kinetics of the mimopeptide were first evaluated and compared to those presented by the mycotoxin for an anti-MPA recombinant antibody (Fab fragment). Then, a fusion protein of the mimopeptide with a bioluminescent protein, NanoLuc luciferase, which acted as the reporter of the immunoassay, was synthesized and characterized. The use of the recombinant fusion enabled its direct use in competitive immunoassays without the need for secondary antibodies or further labeling. For the development of the bioluminescent sensor a biotinylated anti-MPA Fab antibody was immobilized on streptavidin-coupled magnetic beads and MPA was analyzed with a detection limit of  $0.26 \text{ ng mL}^{-1}$  and an  $\text{IC}_{50}$  of  $2.9 \pm 0.5 \text{ ng mL}^{-1}$ . The biosensor showed good selectivity toward MPA and was applied to the analysis of the immunosuppressive drug in clinical samples, of both healthy and MPA-treated patients, followed by validation by liquid chromatography coupled to diode array detection.

The last part of the thesis was focused on the comparison of the analytical performance of a previously reported mimopeptide for fumonisin B<sub>1</sub> fused to two different enzymes, *Gaussia* luciferase (A2-GLuc) and NanoLuc (A2-NLuc) luciferase, for the determination of the mycotoxin in wheat samples. The assay showing the best performance used the A2-NLuc recombinant protein, providing a limit of detection of  $0.61 \text{ ng mL}^{-1}$  and a dynamic range from 1.9 to  $95 \text{ ng mL}^{-1}$ , and was employed for the analysis of the toxin in a certified reference matrix material, as well as in spiked and naturally contaminated wheat samples. The recoveries obtained in the spiked samples were between 81.5 and 109%, with relative standard deviations lower than 14%. The analysis of naturally contaminated wheat samples was validated by liquid chromatography coupled to tandem mass spectrometry.

## Resumen

### Nuevos elementos de reconocimiento molecular selectivo y métodos de amplificación para el desarrollo de (bio)sensores ópticos

Las micotoxinas son sustancias de bajo peso molecular producidas como metabolitos secundarios por una gran variedad de hongos filamentosos que pueden encontrarse como contaminantes naturales en muchos alimentos y piensos. El número de metabolitos fúngicos tóxicos que se conocen en la actualidad supera las mil unidades, pero sólo unas pocas docenas se consideran una amenaza para la salud humana y animal. La exposición a las micotoxinas puede deberse al consumo de alimentos contaminados, pero también a la inhalación de polvo que contiene esporas de hongos micotoxigénicos. Se calcula que aproximadamente el 40% de los cultivos del mundo pueden estar contaminados con micotoxinas, de ahí que sea esencial el desarrollo de métodos analíticos que permitan detectar estas micotoxinas en los alimentos. Por otro lado, a pesar de su elevado riesgo en la calidad de los alimentos, varias micotoxinas presentan aplicaciones médicas, por ejemplo, como fármacos inmunosupresores para el trasplante de órganos. Sin embargo, una limitación para esta aplicación es la estrecha ventana terapéutica que presentan estos fármacos, por ejemplo, el ácido micofenólico. Altas dosis de estos compuestos pueden causar graves efectos adversos para la salud de los seres humanos, pero pequeñas dosis pueden provocar el rechazo de órganos en pacientes trasplantados. Por ello, también es de suma importancia controlar los niveles de estos compuestos en sangre para mejorar la eficacia clínica del inmunosupresor.

La forma tradicional de analizar estas micotoxinas ha sido mediante métodos cromatográficos. Sin embargo, novedosos inmunoensayos y biosensores han demostrado ser alternativas adecuadas para superar las limitaciones de las técnicas cromatográficas, ya que pueden proporcionar análisis rápidos, sensibles, baratos e incluso *in situ*. Un biosensor es un dispositivo que incluye un elemento de reconocimiento de naturaleza biológica, como anticuerpos o enzimas, en contacto con un transductor, que se encarga de transformar el evento de reconocimiento biomolecular en una señal analítica. Esta tesis se ha centrado en el desarrollo de nuevos biosensores ópticos para el análisis de micotoxinas en alimentos y de fármacos inmunosupresores en sangre humana. Para lograr este objetivo, se seleccionaron o diseñaron nuevos elementos de reconocimiento para proporcionar determinaciones rápidas, selectivas y sensibles de dos micotoxinas, el ácido micofenólico (MPA), aplicado como inmunosupresor en pacientes trasplantados del corazón, y la fumonisina B<sub>1</sub> (FB<sub>1</sub>).

La primera parte de la tesis se centró en la selección de mimopéptidos de micotoxinas aplicando la tecnología de *phage display*. Los mimopéptidos se describen como péptidos imitadores de epítomos, ya que pueden unirse al mismo parátipo de anticuerpos que el antígeno correspondiente. La síntesis de conjugados de toxinas para su aplicación en inmunoensayos competitivos suele llevar mucho tiempo y suponer un reto, y puede dar lugar a moléculas inestables y reticuladas al azar que podrían reducir la sensibilidad del ensayo.

La tecnología de *phage display* consiste en la selección de nuevos elementos de biorreconocimiento, desde anticuerpos recombinantes hasta mimopéptidos, para objetivos específicos. Para conseguirlo, es importante llevar a cabo una selección y un

cribado eficientes de la biblioteca de fagos, que suele estar compuesta por  $10^7$ - $10^{10}$  clones de fagos diferentes que muestran una secuencia peptídica aleatoria, o fragmentos de anticuerpos. Al llevar a cabo las rondas de selección antes mencionadas, también conocidas como paneo, se seleccionan y amplifican de la muestra inicial aquellos clones de fagos que presentan una alta afinidad por la molécula analito. Tras varias rondas de paneo, los fagos enriquecidos se analizan en ensayos ELISA para elegir aquél que presente las propiedades deseadas. En esta tesis se han realizado diferentes rondas de selección para tres micotoxinas diferentes: ácido micofenólico, ocratoxina A y alternariol, obteniendo resultados satisfactorios para la primera.

En la segunda parte de esta tesis, se desarrollaron diferentes inmunoensayos basados en el uso de mimopéptidos. En primer lugar, el mimopéptido para el ácido micofenólico obtenido mediante *phage display* se utilizó para diseñar un inmunoensayo competitivo para la detección del inmunosupresor en suero humano. Para ello, primero se evaluó la cinética de unión del mimopéptido y se comparó con la que presenta la micotoxina para un anticuerpo recombinante anti-MPA (fragmento Fab). A continuación, se sintetizó y caracterizó una proteína de fusión del mimopéptido con una proteína bioluminiscente, la luciferasa NanoLuc, que actuó como marcador del inmunoensayo. El uso de la fusión recombinante permitió su uso directo en inmunoensayos competitivos sin necesidad de anticuerpos secundarios ni de marcaje adicional. Para el desarrollo del sensor bioluminiscente se inmovilizó un anticuerpo Fab anti-MPA biotinilado en partículas magnéticas funcionalizadas con estreptavidina, obteniendo un límite de detección de  $0,26 \text{ ng mL}^{-1}$  y un  $\text{IC}_{50}$  de  $2,9 \pm 0,5 \text{ ng mL}^{-1}$ . El biosensor mostró una buena selectividad hacia el MPA y se aplicó al análisis del fármaco inmunosupresor en muestras clínicas, tanto de pacientes sanos como tratados con MPA, seguido de una validación por cromatografía líquida acoplada a detección por matriz de diodos.

La última parte de la tesis se centró en la comparación del rendimiento analítico de un mimopéptido para la fumonisina B<sub>1</sub> previamente descrito en bibliografía, y fusionado con dos enzimas diferentes, la *Gaussia* luciferasa (A2-GLuc) y la *NanoLuc* luciferasa (A2-NLuc), para la determinación de la micotoxina en muestras de trigo. El ensayo que mostró el mejor rendimiento utilizó la proteína recombinante A2-NLuc, proporcionando un límite de detección de  $0,61 \text{ ng mL}^{-1}$  y un rango dinámico de 1,9 a  $95 \text{ ng mL}^{-1}$ . Este ensayo se empleó para el análisis de la toxina en un material de matriz de referencia certificado, así como en muestras de trigo contaminadas de forma natural. Las recuperaciones obtenidas en las muestras contaminadas se situaron entre el 81,5 y el 109%, con desviaciones estándar relativas inferiores al 14%. El análisis de las muestras de trigo contaminadas naturalmente se validó mediante cromatografía líquida acoplada a espectrometría de masas en tándem.

## **1. INTRODUCTION**

### **1.1. Mycotoxins**

#### 1.1.1. Origins

##### 1.1.1.1. Legislated mycotoxins

##### 1.1.1.2. Non-legislated mycotoxins

#### 1.1.2. Mycotoxins as immunosuppressive drugs

### **1.2. Analytical methods for the analysis of mycotoxins**

#### 1.2.1. Chromatographic

#### 1.2.2. Non-chromatographic

### **1.3. Biosensors for analytical applications**

#### 1.3.1. Principles of biosensors: definitions and concepts

#### 1.3.2. Optical biosensors

##### 1.3.2.1. Label based and label free biosensors

##### 1.3.2.2. Chemical and biological-derived optical labels

### **1.4. Recognition elements in biosensors and bioassays**

#### 1.4.1. Biorecognition elements

#### 1.4.2. Biomimetic recognition elements

### **1.5. Phage display as an analytical tool for the selection of mimopeptides and recombinant antibodies**

#### 1.5.1. Introduction to phage display

#### 1.5.2. Bacteriophages

#### 1.5.3. Principles and applications of phage display

#### 1.5.4. Applications of phage display for biosensing of small molecules

### **1.6. Bibliography**

## 1.1. Mycotoxins

The decades of the 1940s and 1950s were very active in the quest of new antibiotics, as infectious diseases were the main cause of death worldwide.<sup>1,2</sup> Naturally-produced substances, including those generated by fungi, were constantly isolated and tested as potential antibiotics. Nonetheless, all the substances that proved to have slight (or acute) toxic effects were immediately discarded and eventually unrecalled.<sup>2</sup> It was not until the 1960s when scientists raised awareness of those substances that resulted toxic for humans and animals and were produced naturally by some organisms. These toxins ended up becoming the needed answer to several important, yet unexplained, health crises that occurred throughout human history. Besides the “golden era” of antibiotics,<sup>3</sup> the second half of the XX century was also the “mycotoxin gold rush”,<sup>4</sup> as most of the currently known mycotoxins were then discovered.

### 1.1.1. Origins

There is a wide diversity of organisms in nature, both prokaryotic and eukaryotic. Among eukaryotic organisms, fungi have caught the eyes of humans for centuries, and even milleniums.<sup>5</sup> However, it has been subject of debate for many years which organisms should be included in the Fungi kingdom, as they were initially mistaken for plants.<sup>5,6</sup> Fungi are a very heterogeneous group, involving organisms of very diverse evolutionary backgrounds which share a similar mode of nutrition, as well as morphological and ecological characteristics.<sup>5</sup> Fungi are ubiquitous in almost all kinds of habitats and commonly produce spores that help them reproduce under favorable environmental conditions.<sup>5,7</sup> As a way to survive and thrive, they have developed several defense mechanisms and communication techniques, one of them being the production of secondary metabolites.<sup>8</sup>

The metabolism is the combination of biochemical reactions fulfilled by an organism. Consequently, a metabolite can be defined as an intermediate or a final product of the metabolism and it predominantly comprises small molecules.<sup>9</sup> Metabolites can either be primary, if they are found in every living cell and are of utmost importance for the organism's survival, or secondary, if their occurrence is not as widespread and they are not essential for the organism.<sup>9</sup> Most of the secondary metabolites known come from plants, although fungi are also very prominent in its production. There is a myriad of different fungal secondary metabolites found in nature and they show very diverse properties and applications. Some beneficial applications are, for example, their use as food colorants and pigments, but also as pharmaceuticals.<sup>10,11</sup> Back in 1928, Alexander Fleming observed that a compound produced by *Penicillium notatum*, penicillin, was able to kill bacteria. This fungal secondary metabolite ended up becoming a very famous antibiotic for humans. Moreover, other fungal metabolites such as cyclosporin A are currently used in immunosuppressant treatments after organ transplantation.<sup>12</sup> Nonetheless, some fungal products can be very detrimental for food, plants, and human health.<sup>8</sup> In this sense, the term mycotoxin can be defined as a fungal secondary metabolite that can cause adverse effects to exposed humans, animals and even other species such as plants and microorganisms.<sup>13,14</sup>

Mycotoxins are low molecular weight compounds that are produced in the mycelium (the vegetative part) of filamentous fungi, but can also be found in some spores.<sup>15</sup> There are a wide variety of mycotoxins produced by a great extent of different



fungi; around 1000 toxic fungal metabolites have been described in the literature.<sup>13</sup> One particularity of mycotoxins is that despite their diversity, each one is only produced by a very few number of fungal species.<sup>15</sup> For example, roquefortine C is considered one of the most widespread mycotoxin, but only 25 species are able to produce it.<sup>13</sup> *Aspergillus*, *Penicillium*, *Fusarium*, *Alternaria* and *Cladosporium* species are the most predominant in mycotoxin production, although mycotoxigenic fungi can also be found, among others, in species of the genres *Claviceps*, *Diplodia*, *Phoma*, *Phomopsis* and *Strachybotrys*.<sup>16</sup> The diseases contracted due to the dietary, respiratory, dermal or other exposure to mycotoxins are referred to as mycotoxicoses. However, the pathologies provoked by the presence of infectious fungi are collectively known as mycoses.<sup>14</sup>

Mycotoxin contamination is a global concern that affects many regions in the world, from the warmest ones to more temperate regions. Mycotoxin production in stored crops is inevitable; depending on the environmental conditions, only a few days are enough for these crops to be subject to mold growth.<sup>8</sup> Dietary intake of mycotoxins can lead to severe health problems since they have been reported to cause carcinogenic, cytotoxic, hepatotoxic, neurotoxic, nephrotoxic, immunotoxic and estrogenic effects, and even death in human beings and animals.<sup>17</sup>

#### **1.1.1.1. Legislated mycotoxins**

Among the hundreds of different mycotoxins that are currently discovered, a few of them are regarded as a threat to humans and animals.<sup>14</sup> National and international organizations, such as the US Food and Drug Administration (FDA), the Food and Agriculture Organization of the US (FAO), the European Commission or the World Health Organization (WHO) have acknowledged the potential risks of mycotoxin uptake and have regulated maximum limits for some of them in food and feed.<sup>18</sup> Currently, the mycotoxins that are of greatest relevance worldwide for food safety and therefore need to be regulated are aflatoxins (AFs), ochratoxin A (OTA), patulin, deoxynivalenol (DON), zearalenone (ZEA), fumonisins (FBs), T-2 and HT-2 toxins, citrinin and ergot alkaloids (EAs).<sup>19</sup> **Table 1** presents a list of mycotoxins legislated by the European Commission in different food commodities and their corresponding maximum residue levels.<sup>20</sup>

**Table 1.** Legislated mycotoxins by the European Commission.

Mycotoxin	Foodstuff		Maximum levels ( $\mu\text{g}/\text{kg}$ )		
	Product	Particularities	AFB <sub>1</sub>	Sum of AFB <sub>1</sub> , AFB <sub>2</sub> , AFG <sub>1</sub> and AFG <sub>2</sub>	AFM <sub>1</sub>
Aflatoxins (AF) AFB <sub>1</sub> , AFB <sub>2</sub> , AFG <sub>1</sub> , AFG <sub>2</sub> , AFM <sub>1</sub>	Groundnuts (peanuts) and other oilseeds	T	8.0	15.0	—
		D	2.0	4.0	—
	Almonds, pistachios and apricot kernels	T	12.0	15.0	—
		D	8.0	10.0	—
	Hazelnuts and Brazil nuts to be treated before human consumption	T	8.0	15.0	—
		D	5.0	10.0	—
	Other tree nuts	T	5.0	10.0	—
		D	2.0	4.0	—
	Dried fruit (other than dried figs)	T	5.0	10.0	—
		D	2.0	4.0	—
	Dried figs		6.0	10.0	—
	Cereals	Including all products derived from cereals and processed cereal products	2.0	4.0	—
	Maize and rice	T, or as an ingredient in foodstuffs	5.0	10.0	—
	Milk	Raw, heat-treated and for the manufacture of milk-based products	—	—	0.0500
	Following species of spices: <i>Capsicum</i> spp., <i>Piper</i> spp., <i>Myristica fragrans</i> , <i>Zingiber officinale</i> , <i>Curcuma longa</i>	Including mixtures of spices containing at least one of the aforementioned	5.0	10.0	—
	Processed cereal-based and baby foods	For infants and young children	0.10	—	
Infant formulae and follow-on formulae	Including infant milk and follow-on milk		—	0.025	
Dietary foods for special medical purposes	Specifically for infants	0.10	—	0.025	

Table 1 cont.

Mycotoxin	Foodstuff		Maximum levels ( $\mu\text{g}/\text{kg}$ )
<b>Ochratoxin A (OTA)</b>	Cereals	Unprocessed	5.0
		D, derived products and processed cereals	3.0
	Dried vine fruits (currants, raisins and sultanas)		10.0
	Coffee	Roasted coffee beans and ground roasted coffee	5.0
		Soluble coffee	10.0
	Wine	Sparkling, fruit wine	2.0
		Aromatized wine, and related drinks and cocktails	2.0
	Grape products	D, juice, concentrated juice, nectar, must and concentrated must	2.0
	Processed cereal-based and baby foods	For infants and young children	0.50
	Dietary foods for special medical purposes	Specifically for infants	
	Following species of spices	<i>Piper spp., Myristica fragrans, Zingiber officinale and Curcuma longa</i>	15.0
		<i>Capsicum spp.</i>	20.0
		Mixture of spices containing at least one of the aforementioned	15.0
	Licorice	Root, ingredient for herbal infusion	20.0
		Extract for beverages and confectionary	80.0
Wheat gluten	Not sold directly to the consumer	8.0	
<b>Patulin</b>	Fruit juices	Including concentrated juices and nectars	50.0
	Spirit drinks, cider and fermented drinks derived from apples	Also containing apple juice	50.0
	Solid apple products	D, apple compote and puree	25.0
	Baby foods	Apple juice and solid apple products, including apple compote and puree, for infants and young children	10.0
		Other than processed cereal-based foods for infants and young children	10.0

Table 1 cont.

Mycotoxin	Foodstuff		Maximum levels ( $\mu\text{g}/\text{kg}$ )
<b>Deoxynivalenol (DON)</b>	Unprocessed cereals	Others than durum wheat, oats, and maize	1250.0
		Durum wheat, oats, and maize	1750.0
	Maize	Unprocessed, except unprocessed maize intended to be processed by wet milling	1750.0
		Milling fractions of maize with more than 500-micron particle size	750.0
		Milling fractions of maize with less than or equal to 500-micron particle size	1250.0
	Cereals	D, flour, bran, and end marketed for direct human consumption (except maize)	750.0
		Processed foods and baby foods for infants and young children	200.0
	Pasta	Dry	750.0
	Bread, pastries, biscuits, cereal snacks, and breakfast cereals	Including small bakery wares	500.0
	<b>Zearalenone (ZEA)</b>	Unprocessed cereals	Other than maize
Maize		Unprocessed, except unprocessed maize intended to be processed by wet milling	350.0
		Milling fractions of maize with more than 500-micron particle size	200.0
		Milling fractions of maize with less than or equal to 500-micron particle size	300.0
		Refined maize oil	400.0
		D, maize-based snacks, and breakfast cereals	100.0
		Processed foods and baby foods for infants and young children	20.0
Bread, pastries, biscuits, cereal snacks, and breakfast cereals		Including small bakery wares, excluding maize products	50.0
Cereals		D, flour, bran, and end marketed for direct human consumption (except maize)	75.0
		Processed foods and baby foods for infants and young children	20.0

Table 1 cont.

Mycotoxin	Foodstuff		Maximum levels ( $\mu\text{g}/\text{kg}$ )
<b>Fumonisin (FBs)</b> (considered as the sum of $\text{FB}_1$ and $\text{FB}_2$ )	Maize	Unprocessed, except unprocessed maize intended to be processed by wet milling	4000.0
		Milling fractions of maize with more than 500-micron particle size	1400.0
		Milling fractions of maize with less than or equal to 500-micron particle size	2000.0
		Maize-based breakfast cereals and snacks	800.0
		D, maize-based foods	1000.0
		Processed foods and baby foods for infants and young children	200.0
<b>T-2 and HT-2 toxin</b> (considered as a sum)	Unprocessed cereals and cereal products		–
<b>Citrinin</b>	Food supplements	Based on rice, fermented with red yeast <i>Monascus purpureus</i>	100.0
			<b>Maximum levels (g/kg)</b>
<b>Ergot sclerotia</b>	Unprocessed cereals	Except corn and rice	0.50
<b>Ergot alkaloids</b>	Unprocessed cereals	Except corn and rice	–
	Cereals	Milling products, except corn and rice	–
		For infants and young children	–
	Bread, pastries, biscuits, cereal snacks, breakfast cereals and pasta	Including small bakery wares	–

D: Direct human consumption; T: Treated before human consumption.

As can be observed in **Table 1**, aflatoxins and ochratoxin A present by far the most restrictive levels in a wide variety of foodstuffs, followed by patulin. Some toxins, such as T-2, HT-2 and ergot alkaloids have been assigned maximum recommended levels, but there are still no legal regulations for them.

Aflatoxins (AFs) are mainly produced by the *Aspergillus* species *A. flavus* and *A. parasiticus*, although they are also produced by *A. bombycis*, *A. nomius*, *A. ochraceoroseus* and *A. pseudotamari*.<sup>8,14</sup> These toxins were first isolated in the 1960s, after a health crisis in which more than 100,000 turkeys died from consuming contaminated peanut meals.<sup>21</sup>  $\text{B}_1$ ,  $\text{B}_2$ ,  $\text{G}_1$  and  $\text{G}_2$  are the most abundant, naturally-produced aflatoxins, whereas other conventional aflatoxins, such as  $\text{M}_1$  and  $\text{M}_2$ , are produced after the hydroxylation of  $\text{AFB}_1$  and  $\text{AFB}_2$ , respectively.<sup>14</sup> Aflatoxins can cause carcinogenicity, hepatotoxicity, or

immunotoxicity, among other serious illnesses, both in humans and animals. Moreover, it has been proven that they can instigate growth suppression in animals.<sup>22,23</sup> Among the different aflatoxins, AFB<sub>1</sub> presents the highest toxicity, and it is regarded as the most powerful natural carcinogen known.<sup>14,24</sup>

Ochratoxin A (OTA) was first isolated in 1965 from *Aspergillus ochraceus*,<sup>25</sup> although it can be produced from different species of *Aspergillus* and *Penicillium* fungi.<sup>26</sup> OTA is mainly found in barley, oats, wheat and other plant products.<sup>14</sup> It has carcinogenic and toxic effects in humans and animals, being the kidney one of the main targets of the mycotoxin.<sup>27</sup>

Patulin is a metabolite from some species of *Penicillium*, *Aspergillus* and *Byssoschlamys*. Although it presents genotoxic and immunotoxic effects, it was first isolated in the 1940s as an antimicrobial active principle.<sup>8,14</sup> It was not until the 1960s when patulin was reclassified as a mycotoxin. Patulin is the most widespread mycotoxin in apple and apple products, even though it has been also found in grapes and other fruit juices.<sup>8,28</sup>

Trichothecenes comprise a big family of more than 100 fungal metabolites from *Fusarium*, *Cephalosporium*, *Cylindrocarpon*, *Myrothecium*, *Phomopsis*, *Stachybotrys*, *Trichoderma*, *Trichothecium* and *Verticimonosporium* species.<sup>29</sup> The common denominator of all trichothecenes is that they contain a 12,13-epoxytrichothene skeleton, as well as an olefinic bond with side-chain substitutions.<sup>14</sup> Deoxynivalenol (DON), also known as vomitoxin, belongs to this big family and it is produced by *Fusarium graminearum* and *F. culmorum*. DON is not a very toxic mycotoxin, albeit it causes nausea, diarrhea and vomiting.<sup>14</sup> It is the most ubiquitous trichothecene, found in grains like wheat, oats or maize.<sup>8</sup> Two other mycotoxins belonging to this family are T-2 and HT-2 toxins. These closely-related toxins are produced by some *Fusarium* species like *F. armeniacum*, *F. langsethiae*, *F. sporotrichioides* and *F. poae*.<sup>30,31</sup> T-2 is quickly converted into HT-2, the major metabolite, after ingestion.<sup>32</sup> They have an equivalent toxicity, and it has been reported that they inhibit protein synthesis and cause apoptosis of proliferating cells.<sup>30,31</sup> They are detected mainly in oats and cereal products.<sup>31</sup>

Zearalenone (ZEA) is a secondary metabolite primarily produced by *Fusarium graminearum*, but also by other species like *F. culmorum* or *F. equiseti*.<sup>32</sup> ZEA is mainly found in cereal crops worldwide before and after harvest.<sup>14,32</sup> Several controversies have arisen regarding the categorization of this compound. Even though it is considered a mycotoxin, the actual toxicity is not very high. However, ZEA has a remarkably high biological potency, binding to estrogenic receptors. Therefore, it is believed that ZEA could be reclassified as a mycoestrogen.<sup>14</sup>

Fumonisin were reported and characterized in 1988, relatively recently when compared to other mycotoxins.<sup>33,34</sup> They are mainly produced by the *Fusarium* species *F. verticillioides* and *F. proliferatum*, which are common pathogens of maize and sorghum.<sup>8</sup> Among the different mycotoxins belonging to this group, fumonisin B<sub>1</sub> is the rifest. They are related to the equine leukoencephalomalacia disease, and possess carcinogenic, genotoxic and teratogenic effects.<sup>8</sup>

Contrary to fumonisins, citrinin was one of the first mycotoxins discovered back in the early 1930s.<sup>35</sup> It was first isolated from *Penicillium citrinum*, but it has also been detected in different *Penicillium*, *Aspergillus* and *Monascus* species.<sup>14,36</sup> The consumption of this mycotoxin, that can be found in rice, corn, oats, rye, barley and wheat produces nephrotoxic and hepatotoxic effects.<sup>14,36</sup>

Ergot alkaloids are a big family of secondary metabolites produced by *Claviceps* fungi. Up to date, there are more than 50 different ergot alkaloids characterized, with ergotamine being one of the most abundant.<sup>14,37</sup> All ergot alkaloids have the common structure of a tetracyclic ergoline ring.<sup>38</sup> They are normally found in the sclerotia (a compacted mycelium containing food reserves) of the fungi.<sup>32</sup> Human ergotism can be contracted after consuming cereals, and derived products, infected with ergot sclerotia, since these alkaloids can survive baking and boiling temperatures.<sup>37</sup> Nevertheless, novel methods for grain cleaning have almost entirely discarded ergotism as a human disease.<sup>14</sup>

**Figure 1** shows the chemical structure of the legislated mycotoxins. For the mycotoxin families that include more than one different metabolite, the most relevant one has been included in the Figure.

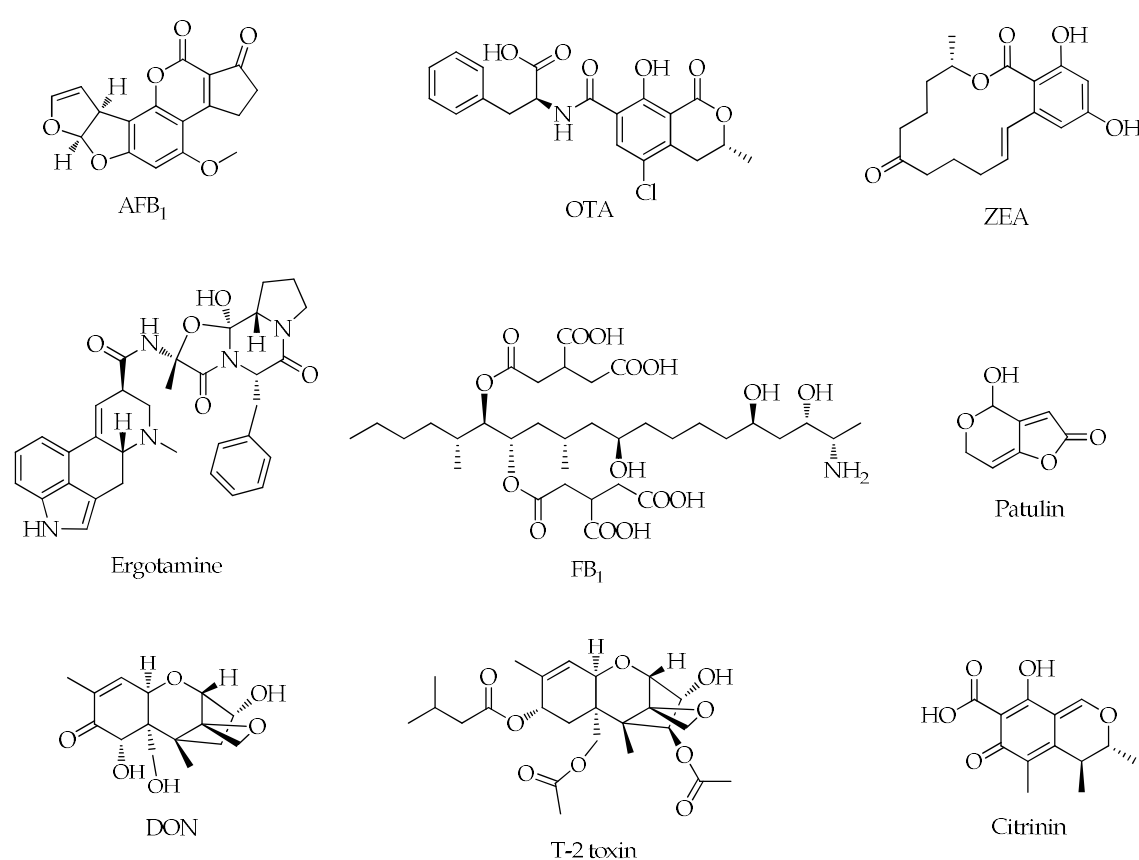


**Figure 1.** Chemical structure of the most abundant legislated mycotoxins.

#### 1.1.1.2. Non-legislated mycotoxins

Besides the aforementioned group of mycotoxins, there are many others that are not regulated yet. This can be due to the fact that there is still not enough information about their occurrence or toxicity.<sup>39</sup> The term “emerging mycotoxins” refers to all the mycotoxins that are not routinely analyzed nor legislatively regulated.<sup>40</sup> This term can often be misinterpreted as “new mycotoxins from different fungal species”. However, it has been observed that the so-called emerging mycotoxins are typically co-produced

with many of the legislated mycotoxins by the same fungus, but have never been studied in depth.<sup>41</sup>

**Table 2** shows some of the most widespread non-legislated mycotoxins and the fungal species that produce them.<sup>40,42</sup> One of the motivations of this doctoral thesis is the study of several non-legislated mycotoxins and the development of analytical methods for their analysis. Concretely, in this Ph.D. work we have focused on the study of mycophenolic acid (MPA), alternariol (AOH) and alternariol monomethyl ether (AME), three non-legislated mycotoxins which are discussed below.

**Table 2.** Fungal species producing some of the most widespread non-legislated mycotoxins.

Fungal species	Mycotoxins produced
<i>Fusarium</i> spp.	Beauvericin (BEA), moniliformin (MON), fusaproliferin (FP), enniatins (EN), fusaric acid (FA), culmorin (CUL), butenolide (BUT)
<i>Aspergillus</i> spp.	Sterigmatocystin (STE), emodin (EMO), cyclopiazonic acid (CPA)
<i>Penicillium</i> spp.	Mycophenolic acid (MPA), cyclopiazonic acid (CPA)
<i>Alternaria</i> spp.	Alternariol (AOH), alternariol monomethyl ether (AME), altenuene (ALT), tenuazonic acid (TEA)

AOH and its derivative, AME (**Figure 2**) are two of the most prevailing *Alternaria* mycotoxins, which were isolated for the first time in 1953.<sup>43</sup> They are produced by a large number of *Alternaria* species, including *A. alternata*, *A. brassicae*, *A. cucumerina*, *A. dauci*, *A. kikuchiana*, *A. solani*, *A. tenuissima* and *A. tomato*.<sup>44</sup> Since *Alternaria* species need high-moisture conditions to grow, they are normally found in relatively highly moisturized foodstuffs, such as grains before harvest, vegetables and fruits.<sup>42</sup> There are many works that describe the high occurrence of AOH and AME in food products. For example, in a detailed study published by the European Food Safety Authority (EFSA), AOH was found in 31% of the agricultural samples analyzed, in concentrations ranging from 6.3 to 1840 µg/kg, with the maximum levels found in sunflower seeds.<sup>45</sup> Moreover, another study revealed that AOH and AME were found at very high levels, up to 53 mg/kg in sum, in tomato samples after analyzing very heavily spoiled tomatoes.<sup>46</sup> Even if it seems that the acute toxicity of AOH and AME is not very high, they have shown genotoxic and mutagenic effects in cell cultures *in vitro*.<sup>45,47</sup> Additionally, a report proved the perfect stability of both toxins under simulated gastrointestinal conditions, although it has been observed that they are poorly adsorbed by the gastrointestinal track of rats.<sup>48,49</sup>

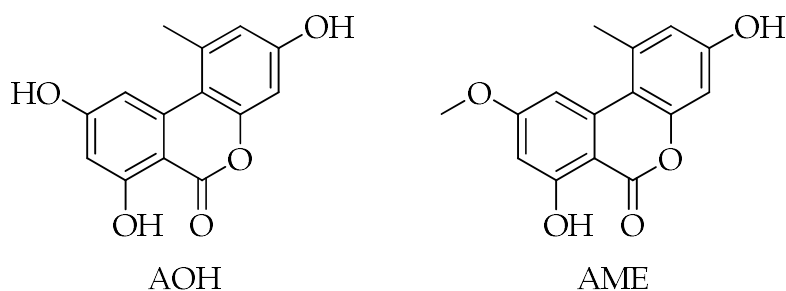


**Figure 2.** Chemical structure of AOH and AME.



MPA is produced by some *Penicillium* species, such as *P. brevicompactum*, *P. roqueforti* and *P. carneum*, as well as in *Byssoschlamys nivea*, a common producer of patulin.<sup>40,50</sup> This mycotoxin was identified at the end of the XIX century, in 1893, becoming one of the first fungal metabolites ever discovered.<sup>51</sup> MPA contamination occurs at higher concentrations than most fungal metabolites, and it has been found in blue cheese,<sup>52</sup> grapes, wine<sup>53</sup> and ginger,<sup>54</sup> among others. Some controversies have aroused with the categorization of MPA as a mycotoxin. The acute toxicity of MPA has been extensively studied, and it is proven to be relatively low, however, some authors consider MPA to be an indirect mycotoxin, due to its strong immunosuppressive properties.<sup>50,51</sup> The use of MPA as an immunosuppressive drug will be discussed more extensively in the following section.

### 1.1.2. Mycotoxins as immunosuppressant drugs

The history of transplantation began a few centuries ago, with several attempts of plastic surgery rebuilds as well as various trials of organ exchange in animals.<sup>55</sup> As time passed by, scientists and doctors found a common pattern in organ transplantations, autografts (transplants from different parts of the same individual) were almost always successful whereas, allografts (transplants between individuals with different genotypes) were initially promising, but always ended up being ineffective, since the organs or tissues transplanted were eventually rejected by the patient's organism.<sup>55</sup>

Immunosuppressant drugs can be defined as those substances able to dampen the immune system, in particular T and B lymphocytes. They can lower the number of functional lymphocytes, and therefore drastically decrease the chances of organ rejection in transplanted patients.<sup>56</sup> Immunosuppressants can also be employed in different medicinal areas such as nephrology, gastroenterology, rheumatology, dermatology or ophthalmology.<sup>56</sup> The first clinical implementation of an immunosuppressive drug was reported by Schwartz and Dameshek in the 1960s. They proved that the intake of 6-mercaptopurine led to a delayed rejection of skin allografts in rabbits.<sup>57</sup>

As stated at the beginning of this chapter, the XX century was characterized for the perseverant search of new antibiotics. Besides these antimicrobial substances, many mycotoxins showed different properties, such as antitumor agents, enzyme inhibitors or immunosuppressant agents.<sup>9</sup> Some of the most important and currently used immunosuppressant drugs are indeed fungal secondary metabolites, such as cyclosporin A or MPA; although other common immunosuppressants like tacrolimus and rapamycin are found in bacteria. The structures of cyclosporin A, tacrolimus and rapamycin are displayed in **Figure 3** whereas the structure of MPA, one of the analytes studied in the present doctoral thesis, is shown in **Figure 4**.<sup>58,59</sup>

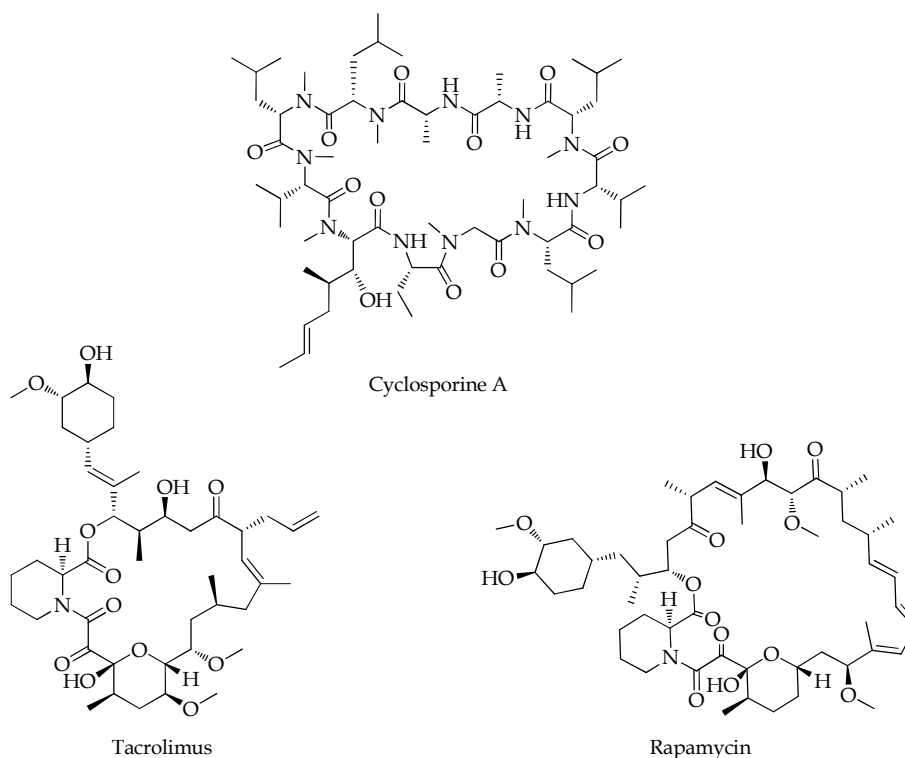


**Figure 3.** Chemical structures of the fungal metabolite cyclosporin A and the bacterial metabolites tacrolimus and rapamycin.

Cyclosporin A was discovered in the 1970s and is produced by *Tolypocladium inflatum*.<sup>59</sup> It has been extensively used as an immunosuppressant in heart, kidney and liver transplants for many years, as it was initially the only product available in the market.<sup>59</sup> It is also effective in the treatment of rheumatoid arthritis, psoriatic arthritis and autoimmune eye disease.<sup>56</sup>

Tacrolimus and rapamycin are two structurally related immunosuppressant drugs. Tacrolimus (FK506) is a secondary metabolite of *Streptomyces tsukubaensis* and was found in 1984 by a Japanese pharmaceutical company.<sup>60</sup> Three years later, FK506 proved to be 100 times stronger than cyclosporin A as an immunosuppressant drug, and it was soon introduced successfully in clinical trials.<sup>61</sup> A similar immunosuppressive behavior is observed in rapamycin, a metabolite of *Streptomyces hygroscopicus*.<sup>62</sup> Rapamycin was first isolated from Rapa Nui (Easter Island) in 1975, but despite its demonstrated immunosuppressive activity in animals, it took almost thirty years for this metabolite to be approved for prevention of organ rejection.<sup>61</sup>

MPA was already introduced in the previous section as a mycotoxin. However, MPA is extensively used as an immunosuppressant drug in transplanted patients.<sup>63</sup> The main role of this drug *in vivo* is the inhibition of inosine 5'-monophosphate dehydrogenase, which is an enzyme involved in the *de novo* synthesis of guanine nucleotides.<sup>51,56</sup> Since lymphocytes are crucially dependent on this biosynthetic pathway, they become very selective targets of MPA.<sup>61</sup> Hence, the proliferation of T and B lymphocytes is severely affected in the presence of this drug.<sup>51</sup> In sum, MPA is able to cause a decrease in the synthesis of guanine nucleotides, leading to a decrease of DNA synthesis, as this compound is one of the main components of DNA. This significant plunge originates a decreased lymphocyte proliferation and eventually, a lower production of antibodies that could potentially favor transplanted organ rejection.<sup>51,56</sup>

MPA is administered as mycophenolate mofetil, which is the inactive 2-morpholinoester of MPA. Mycophenolate mofetil is completely hydrolyzed into the active MPA inside the body, and it is mostly found (98%) bound to proteins.<sup>56</sup> The majority of MPA, *circa* 99%, is found in plasma, but most of it is glucuronated into a pharmacologically inactive form, the mycophenolic acid  $\beta$ -D-glucuronide (MPAG) (Figure 4).<sup>64</sup> Mycophenolic acid acyl- $\beta$ -D-glucuronide (Acyl-MPAG) is a minor glucuronide metabolite of MPA which is pharmacologically active (Figure 4).<sup>51</sup> The established MPA range for adequate therapy is comprised between 1 and 3.5  $\mu\text{g mL}^{-1}$ .<sup>65</sup> Hence, MPA is subject of thorough therapeutic drug monitoring, since lower concentrations of MPA could lead to organ rejection, whereas higher concentrations could be prejudicial for patients.

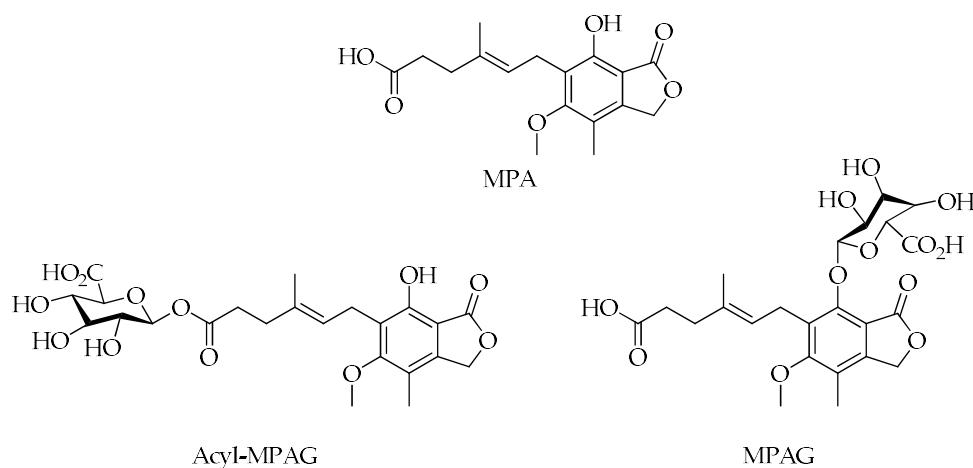


**Figure 4.** Chemical structure of MPA and its two main metabolites, the active form Acyl-MPAG and the inactive form MPAG.

## 1.2. Analytical methods for the analysis of mycotoxins

Mycotoxins are a very heterogeneous group of substances with very diverse properties. This thesis is focused on the analysis of three mycotoxins previously described: MPA, AOH and fumonisin B<sub>1</sub>. However, the former one was analyzed for its role as an immunosuppressant drug. These compounds are of utmost importance in the present days due to their impact on human and animal health, on the food sector and in clinical practices. The great relevance of these secondary metabolites has led to the implementation of sensitive analytical methods for their analysis in different matrices. Regarding mycotoxins, as discussed previously, several international organizations have established maximum regulatory levels for the main ones, and it is expected that the list will be continuously revised in the near future.<sup>66</sup> With reference to immunosuppressant drugs, therapeutic drug monitoring is mandatory due to the imperative need of preserving the therapeutic window of these drugs in transplanted patients.<sup>67</sup>

As previously mentioned, mycotoxins are found in a wide variety of foodstuff, whereas immunosuppressant drugs are routinely analyzed in blood samples. In both cases, the presence of potential interferences in the matrix could hinder the correct analysis of these fungal metabolites. Hence, prior to their analysis, a sample preparation step is usually required.<sup>68,69</sup> Sample preparation generally consists of a extraction step, followed by sample cleanup and pre-concentration before analysis.<sup>68</sup> The extraction is carried out in order to release the analyte from the matrix. This process employs different solvents based on the chemical properties of the analyte and the matrix. Some examples of extraction techniques that have been applied to mycotoxin analysis are pressurized liquid extraction, microwave-assisted extraction, ultrasonic extraction or supercritical fluid extraction.<sup>68</sup> Sample clean up aims for the removal of interferences co-extracted with the analyte, but can also serve as a way to concentrate the sample. In this regard, solid phase extraction, liquid-liquid extraction or immunoaffinity chromatography are commonly used. Nonetheless, depending on the complexity of the matrix and the particularities of the analysis, some of the aforementioned sample treatment procedures can be omitted.

Traditionally, mycotoxins and immunosuppressant drugs have been analyzed by chromatographic methods.<sup>69,70</sup> However, novel immunoassays have also been developed for a fast and cost-effective analysis of these compounds. This chapter includes a brief description the main methods described up to date.

### 1.2.1. Chromatographic methods

Chromatographic methods for the analysis of mycotoxins were initially implemented several decades ago.<sup>71</sup> As previously said, these are low molecular weight compounds, typically soluble in both organic and aqueous solvents, depending on their chemical composition. Therefore, chromatographic techniques are considered a good alternative for their separation and detection.<sup>71</sup> Generally, the three chromatographic techniques most commonly used are thin layer chromatography (TLC), high performance liquid chromatography (HPLC), and gas chromatography (GC). With reference to the detection system, tandem mass detection (MS/MS), ultraviolet (UV) or fluorescence (FLD) are the most widespread techniques.<sup>70</sup>

Even if TLC can be regarded as a rudimentary technique, it was the first one implemented for the analysis of mycotoxins, and it is still currently used for the detection of some of them, such as aflatoxins, in developing countries.<sup>71</sup> Moreover, several TLC-based methods have been approved by the Association of Official Agricultural Chemists (AOAC International) as official methods for the analysis of these compounds.<sup>72</sup>

The applicability of GC for the analysis of fungal metabolites, especially of immunosuppressant drugs, is very limited as most of these compounds require a derivatization step before injection into the GC system.<sup>69,71</sup> However, the analysis of trichothecenes has been extensively carried out with this technique due to their lack of UV absorbance. One of the main advantages of the use of GC is that it enables the simultaneous detection of a variety of trichothecenes due to their similar structure and chemical properties.<sup>71</sup>

The majority of mycotoxins and immunosuppressant drugs are analyzed by HPLC-MS/MS as reference method.<sup>69,71,73,74</sup> However, although MS/MS detection enables a robust, sensitive, and simultaneous quantification of a wide range of analytes, the implementation of this technique into routine analysis is still limited due to its high cost, maintenance and the need of qualified staff. Owing to their absorption or fluorescent properties, some mycotoxins and immunosuppressant drugs can be analyzed by HPLC coupled to an UV or FLD detector. For example, mycophenolate mofetil and their metabolite MPA have been simultaneously analyzed by HPLC-DAD for decades.<sup>75</sup> Additionally, MPA in combination with its two main metabolites, MPAG and Acyl-MPAG, has been successfully analyzed in plasma samples by HPLC-UV.<sup>76</sup> **Table 3** presents a description of the most relevant chromatographic methods found in the literature for the detection of AOH, AME, FB<sub>1</sub>, FB<sub>2</sub>, FB<sub>3</sub> and MPA.

**Table 3.** Analytical characteristics of the most relevant chromatographic methods for the determination of AOH, AME, fumonisins and MPA

Analyte	Matrix	Sample treatment	Analytical technique	LOD/LOQ	Ref
AOH and AME	Poultry feed formula	SLE (MeCN:H <sub>2</sub> O:Ac. Acid 79:20:1)	LC-MS/MS	LOD: 20 µg kg <sup>-1</sup> for AOH and 45 µg kg <sup>-1</sup> for AME	77
AOH and AME	Whole wheat plants	SLE (MeCN:H <sub>2</sub> O 80:20), SPE	LC-MS/MS	LOD: 20 µg kg <sup>-1</sup> for AOH and 1 µg kg <sup>-1</sup> for AME LOQ: 68 µg kg <sup>-1</sup> for AOH and 3 µg kg <sup>-1</sup> for AME	78
AOH and AME	Soya beans	SLE (MeCN:H <sub>2</sub> O:MeOH 45:45:10), SPE	HPLC-DAD	LOD: 8 µg kg <sup>-1</sup> for AOH and 16 µg kg <sup>-1</sup> for AME LOQ: 24 µg kg <sup>-1</sup> for AOH and 48 µg kg <sup>-1</sup> for AME	79
AOH and AME	White wine, red wine, apple juice and other juices	Direct injection, evaporation + reconstitution, SPE and SPE + evaporation + reconstitution	HPLC-DAD	LOD: 2–6 µg kg <sup>-1</sup> for AOH and 0.8–2 µg kg <sup>-1</sup> for AME LOQ: 3.3–10 µg kg <sup>-1</sup> for AOH and 1.4–3.1 µg kg <sup>-1</sup> for AME	80
AOH and AME	Pomegranate and juices	(QuEChERS) SPE (MeCN:H <sub>2</sub> O:Ac. Acid 59:40:1), NaCl + MgSO <sub>4</sub> , d-SPE with PSA + MgSO <sub>4</sub> , evaporation + reconstitution	HPLC-DAD	LOD: 15 µg kg <sup>-1</sup> for AOH and AME LOQ: 50 µg kg <sup>-1</sup> for AOH and AME	81
AOH and AME	Strawberries	LLE (Ethyl ac.), evaporation + reconstitution	LC-MS/MS	LOD: 0.75 µg kg <sup>-1</sup> for AOH and 2 µg kg <sup>-1</sup> for AME LOQ: 1.75 µg kg <sup>-1</sup> for AOH and 3.5 µg kg <sup>-1</sup> for AME	82
AOH	Fruit berry by-products	(QuEChERS) SPE (MeCN:H <sub>2</sub> O:For. acid 50:50:0.1), NaCl + MgSO <sub>4</sub> , evaporation + reconstitution	LC-MS/MS	LOD: 1.5–3 µg kg <sup>-1</sup> for AOH and 3–8 µg kg <sup>-1</sup> for AME LOQ: 5–7 µg kg <sup>-1</sup> for AOH and 9–15 µg kg <sup>-1</sup> for AME	83

Table 3. Cont.

Analyte	Matrix	Sample treatment	Analytical technique	LOD/LOQ	Ref
AOH, AME, FB <sub>1</sub> , FB <sub>2</sub> and MPA	Milk	(QuEChERS) LLE (MeCN:For. Acid 99.5:0.5), NaCl + MgSO <sub>4</sub> , (d-SPE for AME) evaporation + reconstitution	UHPLC-MS/MS	LOD: 0.21 µg kg <sup>-1</sup> for AOH, 0.04 µg kg <sup>-1</sup> for AME, 0.35 µg kg <sup>-1</sup> for FB <sub>1</sub> , 0.31 µg kg <sup>-1</sup> for FB <sub>2</sub> , and 0.04 µg kg <sup>-1</sup> for MPA LOQ: 0.68 µg kg <sup>-1</sup> for AOH, 0.14 µg kg <sup>-1</sup> for AME, 1.15 µg kg <sup>-1</sup> for FB <sub>1</sub> , 1.04 µg kg <sup>-1</sup> for FB <sub>2</sub> , and 0.13 µg kg <sup>-1</sup> for MPA	84
AOH, AME, FB <sub>1</sub> , FB <sub>2</sub> , FB <sub>3</sub> and MPA	Apple puree, hazelnut, maize, and green pepper	SLE (MeCN:H <sub>2</sub> O:Ac. Acid 79:20:1)	LC-MS/MS	LOD: 0.5–9.4 µg kg <sup>-1</sup> for AOH, 0.1–0.5 µg kg <sup>-1</sup> for AME, 2.6–6.5 µg kg <sup>-1</sup> for FB <sub>1</sub> , 1.9–5.7 µg kg <sup>-1</sup> for FB <sub>2</sub> , 2.1–7.4 µg kg <sup>-1</sup> for FB <sub>3</sub> and 2.2–8.7 µg kg <sup>-1</sup> for MPA LOQ: 1.6–31.2 µg kg <sup>-1</sup> for AOH, 0.2–1.7 µg kg <sup>-1</sup> for AME, 8.6–21.6 µg kg <sup>-1</sup> for FB <sub>1</sub> , 6.3–18.9 µg kg <sup>-1</sup> for FB <sub>2</sub> , 6.9–24.6 µg kg <sup>-1</sup> for FB <sub>3</sub> and 7.3–28.9 µg kg <sup>-1</sup> for MPA	85
AOH, AME, FB <sub>1</sub> , FB <sub>2</sub> , FB <sub>3</sub> and MPA	Wine	LLE (MeCN:Ac. Acid 99:1), MgSO <sub>4</sub>	UPLC-MS/MS	LOD: 5–50 µg kg <sup>-1</sup> for all the mycotoxins LOQ: 20–20 µg kg <sup>-1</sup> for all the mycotoxins	86
AOH, AME, FB <sub>1</sub> , FB <sub>2</sub> and FB <sub>3</sub>	Tomato, bell pepper, onion, soft red fruit and derived tomato products	SLE (MeCN:Ethyl ac.:For. acid 60:39:1), evaporation + reconstitution	LC-TOF-MS	LOD: 7.4–17.4 µg kg <sup>-1</sup> for AOH, 4.7–90 µg kg <sup>-1</sup> for AME, 7.8–35 µg kg <sup>-1</sup> for FB <sub>1</sub> , 1.3–20.8 µg kg <sup>-1</sup> for FB <sub>2</sub> and 8.9–23.8 µg kg <sup>-1</sup> for FB <sub>3</sub>	87

Table 3. Cont.

Analyte	Matrix	Sample treatment	Analytical technique	LOD/LOQ	Ref
AOH, AME, FB <sub>1</sub> , FB <sub>2</sub> and FB <sub>3</sub>	Groundnut- and maize-based snacks	SLE (MeCN:H <sub>2</sub> O:Ac. Acid 79:20:1)	LC-MS/MS	LOD: 0.4 µg kg <sup>-1</sup> for AOH, 0.2–0.3 µg kg <sup>-1</sup> for AME, 4–4.5 µg kg <sup>-1</sup> for FB <sub>1</sub> , 2 µg kg <sup>-1</sup> for FB <sub>2</sub> and 3 µg kg <sup>-1</sup> for FB <sub>3</sub>	88
FB <sub>1</sub> and FB <sub>2</sub>	Corn	Ultrasonic extraction MeOH:H <sub>2</sub> O (75:25)	LC-MS/MS	LOD: 3.5 µg kg <sup>-1</sup> for FB <sub>1</sub> and 2.5 µg kg <sup>-1</sup> for FB <sub>2</sub> LOQ: 11.7 µg kg <sup>-1</sup> for FB <sub>1</sub> and 8,3 µg kg <sup>-1</sup> for FB <sub>2</sub>	89
FB <sub>1</sub> and FB <sub>2</sub>	Maize	Matrix solid phase dispersion (Ammonium formate buffer pH 9:THF 70:30)	HPLC-MS/MS	CCα: 514 µg kg <sup>-1</sup> for FB <sub>1</sub> and 176 µg kg <sup>-1</sup> for FB <sub>2</sub> CCβ: 594 µg kg <sup>-1</sup> for FB <sub>1</sub> and 210 µg kg <sup>-1</sup> for FB <sub>2</sub>	90
FB <sub>1</sub> , FB <sub>2</sub> and FB <sub>3</sub>	Maize products	SLE (MeCN:H <sub>2</sub> O 50:50), SAX-SPE, evaporation + reconstitution	HPLC-Corona-CAD	LOD: 20 µg kg <sup>-1</sup> for FB <sub>1</sub> , FB <sub>2</sub> and FB <sub>3</sub> LOQ: 40 µg kg <sup>-1</sup> for FB <sub>1</sub> , FB <sub>2</sub> and FB <sub>3</sub>	91
FB <sub>1</sub> and FB <sub>2</sub>	Maize	SLE (MeOH:H <sub>2</sub> O 80:20), IASPE, evaporation + reconstitution	HPLC-FLD	LOD: 20 µg kg <sup>-1</sup> for FB <sub>1</sub> and 15 µg kg <sup>-1</sup> for FB <sub>2</sub>	92
FB <sub>1</sub> and FB <sub>2</sub>	Feed	SLE (MeOH:MeCN:H <sub>2</sub> O 1:1:2), IASPE	HPLC-FLD	LOD: 30 µg kg <sup>-1</sup> for FB <sub>1</sub> and FB <sub>2</sub> LOQ: 90 µg kg <sup>-1</sup> for FB <sub>1</sub> and 102 µg kg <sup>-1</sup> for FB <sub>2</sub>	93
FB <sub>1</sub> and FB <sub>2</sub>	Chinese rice wine	SAX-SPE, evaporation + reconstitution	HPLC-FLD	LOD: 6 µg kg <sup>-1</sup> for FB <sub>1</sub> and FB <sub>2</sub> LOQ: 90 µg kg <sup>-1</sup> for FB <sub>1</sub> and 102 µg kg <sup>-1</sup> for FB <sub>2</sub>	94
FB <sub>1</sub> and FB <sub>2</sub>	Maize-based baby products	SLE (MeCN-MeOH-phosphate/citrate buffer 1:1:2 pH 4.9), IAC	HPLC-FLD	LOQ: 2.8 µg kg <sup>-1</sup> for FB <sub>1</sub> and 2.2 µg kg <sup>-1</sup> for FB <sub>2</sub>	95



Table 3. Cont.

Analyte	Matrix	Sample treatment	Analytical technique	LOD/LOQ	Ref
FB <sub>1</sub> and FB <sub>2</sub>	Milled Corn Grains	SLE (MeOH-MeCN-H <sub>2</sub> O 1:1:2)	HPLC-MS	LOD: 62 µg kg <sup>-1</sup> for FB <sub>1</sub> and 58.5 µg kg <sup>-1</sup> for FB <sub>2</sub> LOQ: 203 µg kg <sup>-1</sup> for FB <sub>1</sub> and 199 µg kg <sup>-1</sup> for FB <sub>2</sub>	96
FB <sub>2</sub> and MPA	Meat products	SLE (Pentane:H <sub>2</sub> O:MeCN 46:35:19), LLE (Acetone:H <sub>2</sub> O-MeCN phase 72:28), concentration, MMRPAX, evaporation + reconstitution	LC-MS/MS	LOD: 6 µg kg <sup>-1</sup> for FB <sub>2</sub> and 14 µg kg <sup>-1</sup> for MPA LLOQ: 150 µg kg <sup>-1</sup> for FB <sub>2</sub> and 50 µg kg <sup>-1</sup> for MPA	97
FB <sub>1</sub> and MPA	Grape and wine	(QuEChERS) SPE (MeCN:H <sub>2</sub> O:Ac. Acid 66:33:1), NaCl + MgSO <sub>4</sub>	UHPLC-MS/MS	LOD: 1 µg kg <sup>-1</sup> for FB <sub>1</sub> and 0.1 µg kg <sup>-1</sup> for MPA LOQ: 3 µg kg <sup>-1</sup> for FB <sub>1</sub> and 0.3 µg kg <sup>-1</sup> for MPA	53
FB <sub>1</sub> , FB <sub>2</sub> and MPA	Edible insects	SLE (ChCl:urea 1:2)	UHPLC-MS/MS	LOD: 110 µg kg <sup>-1</sup> for FB <sub>1</sub> , 60 µg kg <sup>-1</sup> for FB <sub>2</sub> and 100 µg kg <sup>-1</sup> for MPA LOQ: 370 µg kg <sup>-1</sup> for FB <sub>1</sub> , 220 µg kg <sup>-1</sup> for FB <sub>2</sub> and 330 µg kg <sup>-1</sup> for MPA	98
MPA	Blue and white mould cheese	SLE (MeCN:Hexane 55:45), evaporation + reconstitution	LC-MS/MS	LOD: 0.3 µg kg <sup>-1</sup> LOQ: 0.6 µg kg <sup>-1</sup>	99
MPA	Blue cheese	SPME (carbowax/templated resin)	HPLC-UV/DAD	LOD: 50-100 µg kg <sup>-1</sup>	100
MPA	Plasma	Ultrafiltration (Centrifree® Micropartition system)	LC-MS/MS	LLOQ: 0.5 µg L <sup>-1</sup> for free MPA and 50 µg L <sup>-1</sup> for total MPA	101

Table 3. Cont.

Analyte	Matrix	Sample treatment	Analytical technique	LOD/LOQ	Ref
MPA	Meat products	SLE (NaHCO <sub>3</sub> pH 8.8: Pentane: MeCN 44:33:23), MMRPAX, evaporation + reconstitution	LC-HRMS	LOD: 4–6 µg kg <sup>-1</sup> LOQ: 100 µg kg <sup>-1</sup>	102
MPA	Human plasma	LLE (MeCN)	LC-TOF-MS	LLOQ: 10 µg L <sup>-1</sup>	103
MPA, MPAG and Acyl-MPAG	Human plasma	SPE (Isolute C2)	UPLC-DAD	LOD: 20 µg L <sup>-1</sup> for MPA, 50 µg L <sup>-1</sup> for Acyl-MPAG and 100 µg L <sup>-1</sup> for MPAG LLOQ: 100 µg L <sup>-1</sup> for MPA and Acyl-MPA and 1000 µg L <sup>-1</sup> for MPAG	104
MPA	Breast milk	LLE (MeCN:MeOH 50:50)	LC-MS/MS	LLOQ: 2 µg L <sup>-1</sup>	105
MPA and MPAG	Plasma and saliva	LLE (MeCN), evaporation + reconstitution	LC-MS/MS	LOD: 0.07–1 µg L <sup>-1</sup> for MPA and 0.8–3 µg L <sup>-1</sup> for MPAG LLOQ: 1.6–2 µg L <sup>-1</sup> for MPA and 5–9 µg L <sup>-1</sup> for MPAG	106

SLE: solid-liquid extraction; SPE: solid phase extraction; d-SPE: dispersive solid phase extraction; LLE: liquid-liquid extraction; SAX-SPE: strong anion exchange; IASPE: immunoaffinity solid phase extraction; MMRPAX: mixed mode reverse phase anion exchange; LC: liquid chromatography; HPLC: high performance liquid chromatography; UHPLC (also UPLC): ultra-high performance liquid chromatography; MS: mass spectrometry; MS/MS: tandem mass spectrometry; DAD: diode array detection; TOF: time of flight; Corona-CAD: corona-charged aerosol detector; FLD: fluorescence detection; LOD: limit of detection; LOQ: limit of quantification; CC $\alpha$ : decision limit; CC $\beta$ : detection capability; LLOQ: lower limit of quantification;

In general, the use of chromatographic methods requires high-skilled personnel as well as time consuming sample preparation methods. An alternative for the fast and sensitive detection of mycotoxins is the use of immunoassays or biosensors.

### 1.2.2. Non-chromatographic methods

Over the last decades, a plethora of immunoassays have been developed for the quantitative, semiquantitative or qualitative detection of mycotoxins and immunosuppressant drugs in different matrixes.<sup>107</sup> The general principle of all immunoassays is the interaction between a selective antibody and its corresponding antigen for the quantitation of the analyte.<sup>108</sup>

Immunoassays present a series of advantages in comparison to chromatographic methods, such as their higher simplicity, speed in operation, ease of portability and automation as well as a high reliability of determinations.<sup>109</sup> They are also very versatile regarding the assay formats, as many different types of immunoassays can be found in the literature, such as enzyme-linked immunosorbent assay (ELISA), radioimmunoassay (RAI), chemiluminescent enzyme immunoassay (CLEIA), bioluminescent enzyme immunoassay (BLEIA) chemiluminescent microparticle immunoassay (CMIA), enzyme multiplied immunoassay (EMIT), fluorescent polarization immunoassay (FPIA), particle-enhanced turbidimetric inhibition immunoassay (PETINIA), cloned enzyme donor immunoassay (CEDIA), microparticle enzyme immunoassay (MEIA) or antibody conjugated magnetic immunoassay (ACMIA).<sup>69,110,111</sup> Among the different immunoassays mentioned, ELISA is the most widely used method. ELISAs can be divided into four main different types, direct, indirect, sandwich and competitive ELISAs, depending on the particularities of the assay (**Figure 5**).<sup>112</sup> However, all these assays include an immobilization step, of either the antibody or the antigen of interest, a blocking step to avoid non-specific binding, a detection step and the final readout of the analytical signal.

Direct ELISAs are the simplest ones, consisting of the antigen immobilization onto a 96-well plate and a detection with a primary antibody conjugated to an enzyme. In the presence of its substrate, the enzyme is able to give the analytical signal, which generally involves a color formation or a color change.<sup>112</sup> The indirect assay has a similar format, but in this case, the primary antibody is not labelled. Hence, a labelled secondary antibody is introduced to give the analytical signal. Sandwich assays received that name because the antigen is kept in between two different antibodies. In this case, a primary antibody is coated onto the well plates, then, the sample containing the antigen is added, allowing it to bind to the primary antibody. Next, a secondary antibody is added that either recognizes the antigen, or the primary antibody-antigen complex. Finally, a labelled antibody is added to detect the secondary antibody and give the analytical signal. Competitive ELISAs establish a previous incubation between the antibody and a sample containing the antigen. Then, the mixture is added to antigen-coated wells, where a competition is established. Those samples with fewer antigens would have more available antibodies binding to the immobilized antigen on the plate. After a washing step to remove all the unbound antibodies and antigens, a labelled secondary antibody is added to give the analytical signal.<sup>112</sup>

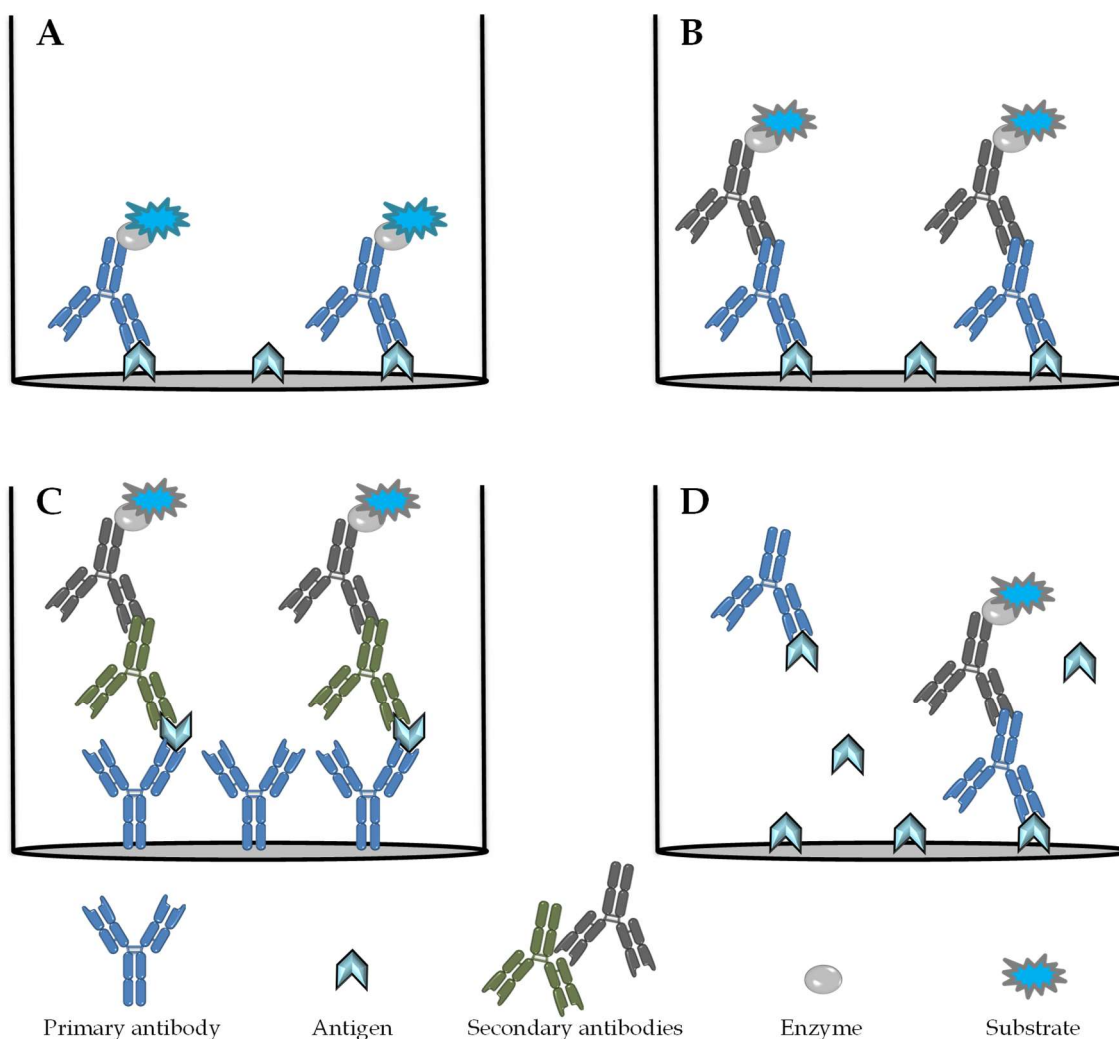


**Figure 5.** Schematic representation of different types of ELISAs. A. Direct ELISA, based on the interaction between an immobilized antigen and a labelled antibody. B. Indirect ELISA, based on the same interaction as the direct ELISA, but using an unlabeled antibody for the interaction with the antigen. A labelled secondary antibody is required to detect the first antibody. C. Sandwich ELISA, based on the immobilization of an antibody on the surface. The antigen interacts with the immobilized antibody and then a secondary antibody interacts either with the antigen-antibody complex or with the antigen alone. If needed, a labelled antibody selective for the secondary antibody is added to obtain the analytical signal. D. Competitive ELISA, based on the initial interaction of the antibody with a solution containing the antigen and then adding the mixture to antigen-coated wells. Already-bound antibodies would be washed away, whereas the rest of antibodies would interact with the bound antigens on the plate. A labelled secondary antibody selective for the first antibody is added to provide the analytical signal.

These previous ELISAs are included in the category of heterogeneous immunoassays since they require a solid surface, commonly a plate or beads, to immobilize either the antibody or the antigen. Heterogeneous immunoassays are considered 'reagent excess' systems. They are typically fast assays and of very high precision, but subject to some errors. For instance, if the binding between the antibody and the antigen is weak, it could potentially be disrupted due to the washing steps, causing a decrease in the sensitivity of the immunoassay.<sup>113</sup>

Homogeneous immunoassays, on the contrary, are based on the antigen-antibody interaction in solution, without the need of a solid support. Therefore, these immunoassays only require the mixing of two different solutions containing the antigen and the antibody respectively to provide an analytical signal. Homogeneous immunoassays are believed to be simpler and more sensitive than heterogeneous immunoassays, but they can be prone to more nonspecific interactions, since the components of the matrix are not washed away.<sup>113</sup>

Immunoassays have become essential tools in clinical diagnostics, biopharmaceutical analysis and food testing, among others.<sup>107</sup> A common example of the applicability of immunoassays in point of care testing is the HIV test. It consists of an indirect assay in which HIV antibodies are detected by immobilizing the antigen onto a stick. A labelled secondary anti-human antibody is used to give the analytical signal. This test only takes a few minutes to be performed, and it provides precise results.<sup>112</sup> With reference to mycotoxins, there are a wide variety of immunoassays developed, and even some commercial kits, some of which also target immunosuppressant drugs. Particularly, in the case of MPA, commercial kits are available from Siemens, Roche or Thermo Scientific.<sup>114-116</sup> Moreover, other immunoassay formats such as EMIT, PETINIA and FPIA have been published in the literature.<sup>117-119</sup> However, in most cases, conjugation of the drug to a carrier protein is needed for assay development. This conjugation can be particularly challenging or require expensive or potentially toxic reagents that can pose a risk to the user. One of the aims of this doctoral thesis has been the development of a novel analytical methodology for the detection of MPA and fumonisin B1 that overcomes those aforementioned drawbacks.

### 1.3. Biosensors for analytical applications

Biosensors have revolutionized many different analytical fields over the last decades including clinical analysis, industrial and chemical processing, environmental monitoring or even in the tactic supervision of chemical warfare.<sup>120</sup> Furthermore, biosensors will experience a major outbreak into our daily lives in the near future, as their implementation within the megatrend of the Internet of Things seems inevitable.<sup>121</sup>

Regardless of the enormous potential of biosensors in society, there are still many misconceptions with reference to what biosensors truly represent. This chapter is focused on giving a basic understanding of the general concept of biosensors, and more in particular, of optical biosensors.

#### 1.3.1. Principles of biosensors: definitions and concepts

The first example ever of a biosensor was published in 1962 by Clark and Lyons.<sup>122</sup> They described an electrochemical biosensor to detect glucose measuring the  $pO_2$  of a solution. To this end, they attached the glucose-oxidase enzyme to an amperometric electrode sensitive to  $O_2$  concentration. When glucose was present in the solution, it was quickly transformed into gluconic acid and hydrogen peroxide with the help of the enzyme. The more glucose present in the solution, the more oxygen was consumed, and therefore, a bigger decay in its concentration was observed. Despite this early approach, it was not until the late 1970s when the term 'biosensor' started appearing in the literature.<sup>123</sup>

'Biosensor' has been a misleading concept for many years, and some controversies have aroused on whether or not to call biosensor to a specific assay platform or probe.<sup>124</sup> Back in the 1980s, biosensors were defined as "a device incorporating a biological sensing element either intimately connected to or integrated within a transducer".<sup>125</sup> A few years later, the International Union of Pure and Applied Chemistry (IUPAC) published a glossary of terms used in biochemistry. In this glossary, the definition of biosensor was "a device that uses specific biochemical reactions mediated by isolated enzymes, immunosystems, tissues, organelles or whole cells to detect chemical compounds usually by electrical, thermal or optical signals".<sup>126</sup> Regardless of the exact definition, the two main components that all biosensors must have are a biological recognition element, also known as receptor, and a transducer. The biological receptor is responsible for analyte recognition, which can either be qualitative or quantitative, and it is frequently based on a binding process or a biocatalytic reaction.<sup>123</sup> This process needs to grant any kind of analytical information, for example a change in the properties of the solution or a product formation, which is subsequently gathered by the transducer and converted into an electrical signal.<sup>124</sup> There are several approaches for the mode of transduction, such as optical, electrochemical, thermal or piezoelectrical.<sup>123</sup> In particular, this doctoral thesis is focused on the application of optical transduction, which will be discussed in the following section.

### 1.3.2. Optical biosensors

Optical biosensors rely on the development or modification of an optical phenomena such as absorption, emission, reflectance, chemiluminescence, bioluminescence or surface plasmon resonance, during analyte biorecognitions.<sup>124,125</sup> The first examples of optical biosensors trace back to the decade of the 1980s, with the use of cumbersome optical equipments.<sup>127</sup> Since then, the exponential technological growth has allowed the current implementation of optical biosensors in badges, wristbands or even contact lenses for noninvasive analytical detections.<sup>121</sup> Optical biosensors present high sensitivity, robustness, reliability, and can be easily integrated on a lab-on-a-chip devices.<sup>124,128</sup> These biosensors can be classified into two different groups: label based and label free devices.

#### 1.3.2.1. Label based and label free biosensors

The main differences between these two types of biosensors is that label based devices require the use of external labels, such as, fluorescent dyes, enzymes or nanoparticles, to monitor the biorecognition event.<sup>129</sup> On the other hand, label free biosensors generate the analytical signal directly based on the sole interaction of the analyte with the biorecognition element.<sup>130</sup>

Label-free biosensors present several advantages over label-based devices, for instance, their simplicity, the reduced assay cost or the swiftness in the analysis time, and most of them allow real time monitoring of the binding interaction.<sup>129</sup> Moreover, these biosensors avoid potential alterations in the binding properties that antigen or antibody conjugates can suffer, leading to systematic errors in the biosensing platform.<sup>130</sup>

Surface plasmon resonance (SPR) stands out as the most widespread label-free optical detection technique. Its application began in the 1980s, and it is considered one of the most powerful tools for real-time measurements and interaction studies.<sup>128,131,132</sup> SPR is based on the refractive index variations of a metal-dielectric surface motivated by molecular interactions occurring in the vicinity of the surface layer (**Figure 6**).<sup>133</sup> To track these variations, p-polarized light (or light with an electric field parallel to the surface layer) is propagated until it reaches the metal-dielectric interface where, under certain conditions, generates surface plasmons. At a specific angle, the p-polarized light resonates with these surface plasmons generating a decrease in the intensity of the reflected light. This angle varies depending on the refractive index of the metal layer that can slightly change whenever molecular interactions occur on that layer.<sup>134</sup> For a better understanding of this complex principle, some lectures are recommended.<sup>134,135</sup> SPR platforms based on antibody-antigen interactions have been successfully applied for the detection of a plethora of mycotoxins, for instance fumonisins, nivalenol or deoxynivalenol.<sup>136-138</sup>

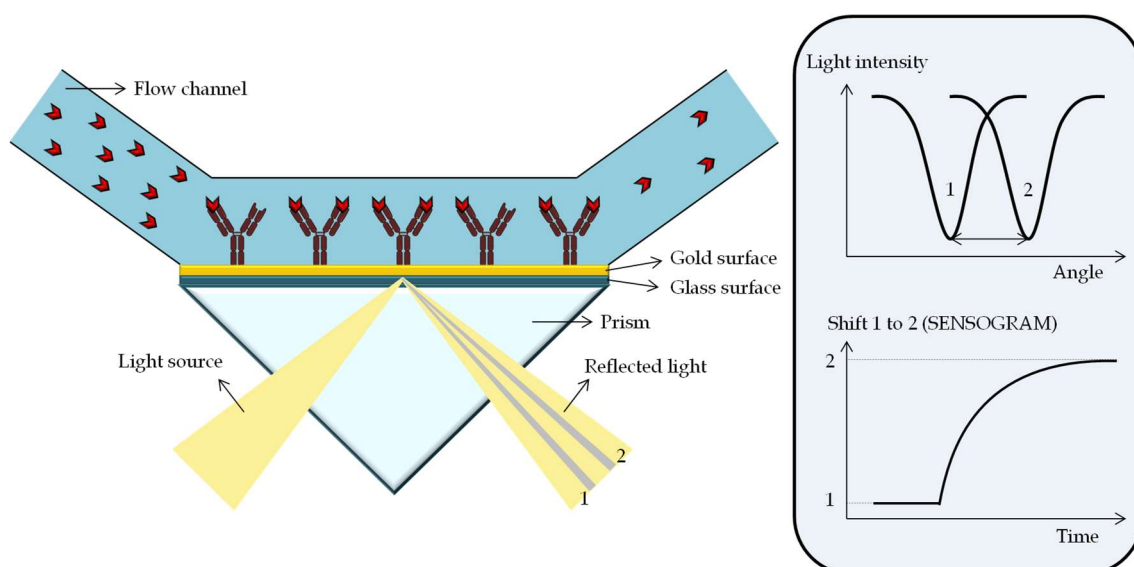


**Figure 6.** Schematic representation of the SPR principle. Molecular interactions are monitored on a gold surface. In this representation, IgG antibodies are coupled to the gold surface, and the analyte is delivered there through a microfluidic system. The sensor consists of a glass surface with a thin gold layer on top in which the antibody is attached. Polarized p-light is propagated generally over a prism until it reaches the gold surface, where it generates a plasmon and it is reflected. At a specific angle, the incident light resonates with the plasmon, producing a decay in the light intensity (beam 1). When the analyte interacts with the antibody, the refractive index slightly changes, causing a shift in the light angle that resonates with the plasmon generated on the gold surface (beam 2). The representation of the shift between the first angle that produces the decay in the light intensity and the second angle *versus* the time is called sensogram.

Besides SPR, other label-free optical biosensors are based on surface-enhanced Raman spectroscopy (SERS) or interferometry.<sup>129</sup> Despite their potential the application of label-free biosensors for the analysis of mycotoxins is still scarce.

Label-based optical sensors employ an optical label or probe to give the analytical signal. Even if they are generally more sensitive than the aforementioned, they require a conjugation step that can be challenging, however, this enables a huge versatility in the measurable wavelength.<sup>124</sup> Bioconjugation consists on the coupling of two molecules in which, at least, one is of biological origin.<sup>139</sup> It is an essential step for most label-based optical sensors, and it is extensively applied in current research. The bioconjugate molecule is meant to present the properties of every constituent; however, if the reaction is not properly controlled, undesirable results, such as the loss of biological recognition, can be obtained.<sup>139-141</sup> The bioconjugation process needs to be planned according to the final purpose of the complex. Some typical bioconjugates used for a wide variety of applications include the formation of enzyme-streptavidin (neutravidin or avidin) conjugates, oligo probes with fluorescent dyes, antibody-enzyme conjugates, fluorescently labeled antibodies or protein-enzyme conjugates.<sup>139</sup> The following section includes a description of several optical labels commonly used for biosensing purposes.

### 1.3.2.2. Chemical and biological-derived optical labels

Optical labels can be classified, according to their nature, into two distinct categories: chemical and biological. Common chemical labels include fluorescent dyes



and nanoparticles while biological labels generally comprise enzymes and luminescent proteins.

Fluorescent dyes are widely applied in many different fields, from cell imaging to environmental analysis, since they allow highly sensitive determinations, up to single molecule detection.<sup>142</sup> Fluorescent molecules are generally characterized by a large conjugated electron system that absorbs photons of a specific wavelength and eventually release the excess of energy by emitting photons from the lowest excited state.<sup>142</sup> Two important characteristics of fluorescent molecules for assay development are their emission quantum yield and the Stokes shift. The quantum yield can be defined as the ratio of the photons emitted as fluorescence to the total number of photons absorbed (by the molecule during an identical time or per unit time).<sup>141</sup> Considering that definition, it is desired that fluorophores show a quantum yield of 1, the maximum value, since that means that all the absorbed photons would be emitted as fluorescence. The Stokes shift is defined as the separation of the maximum absorption wavelength and the maximum emission wavelength. In this case, a greater Stokes shift leads to a better signal isolation, reducing the background noise and Rayleigh scattering interferences.<sup>142</sup> Fluorescent molecules may be sensitive to pH, solvent polarity and oxygen concentration, which can potentially produce a severe quenching effect, therefore the assay conditions must be thoroughly controlled. Some of the most widely applied fluorescent dyes are fluorescein derivatives, rhodamine derivatives, coumarin derivatives, boron dipyrromethene (BODIPY) derivatives and pyrene derivatives.

Over the last years, the enormous breakthrough in nanotechnology has provided a wide variety of nanoparticles with diverse optical properties that has paved the way to the production of novel and powerful bioanalytical tools. Nanoparticles offer a huge versatility in terms of size, shape and composition, which help surmounting some of the classical chemical and spectral limitations of fluorescent molecules.<sup>143</sup> Noble metal nanoparticles, particularly gold nanoparticles, are among the most frequently used for optical sensing. They offer a great scope of optical properties based on their size and shape. Moreover, they are easily synthesized and modified and present high biological compatibility, as well as long term stability.<sup>144,145</sup> The typical shape of gold nanoparticles is spherical; however, they can be synthesized with the form of triangles, cages, stars or rods, among others. Silver nanoparticles also possess excellent optical properties, but are less commonly used due to their oxygen sensitivity, that decreases their stability.<sup>146,147</sup> An elegant example of the application of noble metal nanoparticles to the analysis of mycotoxins is the determination of FB<sub>1</sub> using a homogeneous quenching immunoassay and gold nanoparticles as quenchers. To this aim, an anti-fumonisin antibody was coupled to protein G-coated AuNPs. In the absence of the toxin, a fumonisin mimopeptide fused to a yellow fluorescent protein (YFP) was bound to the antibody and the emission of light was quenched. In the presence of FB<sub>1</sub>, the amount of YFP-mimotope bound to the antibody decreases with increasing target concentrations and the fluorescence is recovered due to the larger distance from the AuNPs.<sup>148</sup>

Quantum dots are inorganic nanocrystals made of semiconductor materials like CdSe, CdS or CdTe. They present spherical shapes of varying sizes, typically between 2 and 10 nm, with tunable luminescent properties.<sup>145,149</sup> Quantum dots present high quantum yields, high resistance to photobleaching as well as low chemical degradation, therefore, they are among the preferred options for optical labelling.<sup>143</sup> Nevertheless, their application for *in vivo* experiments has diminished over the last years owing to the

potential cytotoxic effects of heavy metals such as Cd.<sup>150</sup> One of the most prominent uses of quantum dots is as energy donors in Foster resonance energy transfer (FRET) assays.<sup>151</sup> Furthermore, their size-dependent optical properties enable their application in multiplexing applications, for example, OTA, ZEA and FB<sub>1</sub> have been simultaneously determined in corn samples using this strategy.<sup>152</sup>

Other successful luminescent nanomaterials frequently used are lanthanide-doped up-conversion nanoparticles (UCNPs) and carbon dots (CDs). The former ones are able to convert low energy excitations, generally in the IR or NIR, into a wide variety of different wavelengths in the UV, Vis and NIR, also known as an anti-Stokes emission.<sup>143,153</sup> CDs are being considered as substitutes for quantum dots due to their lower toxicity and high photoluminescence, and have shown to be good alternatives in applications like fluorescence imaging or as nanocarriers for drug delivery.<sup>143,154</sup>

Fluorescent proteins are currently one of the most utilized tools for all kinds of luminescent applications, including fluorescent imaging and immunoassays.<sup>155,156</sup> Green fluorescent protein (GFP), whose discovery and application as a tagging agent in bioscience deserved the Nobel Prize award in Chemistry in 2008,<sup>157</sup> was first isolated as a naturally-produced substance from the jellyfish *Aequorea victoria* back in 1962.<sup>158</sup> Over the last decades, GFP has become one of the most investigated and applied proteins in biochemistry and cell biology, as it can be easily co-expressed as a heterologous fusion with other proteins or antibodies.<sup>159,160</sup> Moreover, it has been reported that mutations in the amino acid sequence of GFP give rise to a modification in its inherent fluorescence, yielding a beautiful spectrum of different derived-fluorescent proteins.<sup>160</sup> Fluorescent proteins have also been applied to the analysis of mycotoxins and immunosuppressant drugs.<sup>161-164</sup>

Even though all the aforementioned optical labels are of great importance, enzymes are currently reigning in the field of sensing as the most widely used labels. Their principle is remarkably simple, as they serve as catalyzers for a colored, fluorescent, or luminescent reaction. Moreover, it is estimated that a single enzyme molecule can convert up to 10<sup>7</sup> substrate molecules per minute thus, sensitive results can be obtained even using low enzyme concentrations.<sup>113</sup> However, the principal drawbacks of the use of enzymes is their sensitivity to pH, ionic strength or temperature changes, the presence of potential inhibitors as well as their short shelf-life.<sup>113,165</sup> Regardless of their high susceptibility and rather low stability, enzymes offer an impressive versatility in terms of applicability in a wide range of immunoassays and biosensors with a tasteful palette of substrates. Some of the most commonly used enzymes are horse-radish peroxidase (HRP), alkaline phosphatase (AP) and  $\beta$ -galactosidase.<sup>165</sup> The optical signal generated solely depends on the substrate added to the reaction. Whereas colorimetric reactions offer simplicity in terms of signal measurement and are ideal for qualitative determinations, they tend to be the least sensitive ones.<sup>113</sup> 3,3',5,5'-Tetramethylbenzidine (TMB), 2,2'-azino-bis(ethylbenzothiazoline-6-sulfonate) (ABTS), and *o*-phenylenediamine (OPD) are some of the most frequently used colorimetric substrates.<sup>113,165</sup> On the other hand, fluorescent substrates provide higher sensitivities but rely on the use of a fluorometer or microplate reader to monitor the quantitative signal. Among ordinary fluorescent substrates, 4-methylumbelliferyl phosphate (4-MUP) and 10-acetyl-3,7-dihydroxyphenoxazine (Amplex<sup>TM</sup> Red) have been used.<sup>113,166</sup>

Some of the enzymes that are gaining an important recognition over the last years are luciferases. They are responsible for the catalysis of luminescent reactions

(bioluminescence) which are utilized for *in vivo* and *in vitro* studies in diagnostics, food testing, drug screening and biomedical research among others.<sup>167</sup> Bioluminescence can be described as the emission of light by living organisms without the need of an excitation source. This phenomenon is extensively found in marine ecosystems, in some fungi and several insects, with fireflies being probably the most typical example of bioluminescence.<sup>167</sup> It is important not to mistake this term with chemiluminescence, which is the emission of light due to a chemical reaction.<sup>168</sup> Luciferases, also known as luciferins, can be classified according to their substrates or to their expression mechanism in cells.<sup>169</sup> *Renilla luciferase*, *Gaussia luciferase* and *Firefly luciferase* are among the most studied luciferases, with a plethora of different applications already described in the literature.<sup>170</sup> This thesis has focused in the application of one of the most novel luciferases: the *Nanoluc luciferase* (NanoLuc). NanoLuc is a luciferase found in the deep sea shrimp *Oplophorus gracilirostris*, and it is one of the smallest luciferases described in the literature, with a molecular weight of only 19 kDa.<sup>167,171</sup> Despite its small size, it is one of the most efficient and brightest bioluminescent systems in combination to its substrate, furimazine.<sup>172</sup> NanoLuc is an exceptionally versatile tool, used in protein-protein or protein-ligand interactions, gene regulation studies, BRET-based assays, bioluminescent imaging, and photouncaging.<sup>171,173</sup> Another luciferase with a similar size as NanoLuc is *Gaussia luciferase* (GLuc), which was first isolated from the marine copepod *Gaussia princeps* in 1999.<sup>174</sup> With a size as small as 19.9 kDa, this luciferase has attracted the attention of many due to its strong bioluminescence at 480 nm in the presence of their substrate, coelenterazine.<sup>175,176</sup> In this thesis, a comparison between the properties of NanoLuc and GLuc was performed for the development of an optimized bioluminescent immunoassay for FB<sub>1</sub>.

As can be seen, the list of optical labels is broad, and the selection of the label will surely influence the success and sensitivity of the method.

## 1.4. Recognition elements in biosensors and bioassays

Biomolecular recognition can be described as the process in which biomolecules bind to and discern their molecular targets from the rest of the substances present in the sample with high specificity, affinity and in a reversible way.<sup>177</sup> This process is influenced by the contribution of several physical phenomena, including van der Waals interactions, hydrogen bonding, and electrostatic interactions as well as entropic contributions like modifications in the configurational disorder and in the solvation of hydrophilic and hydrophobic groups upon complex formation.<sup>178</sup>

Naturally produced biomolecules, such as enzymes or antibodies paved the way to the development of the earliest biosensors. However, biomimetic recognition elements like recombinant antibodies, aptamers, nanozymes or molecularly imprinted polymers (MIPs) are becoming of significant importance for biosensor development since they can surmount some of the limitations of the traditional biorecognition elements.<sup>177</sup> In this chapter, both natural and biomimetic recognition elements will be thoroughly described and their advantages and disadvantages will be compared.

### 1.4.1. Biorecognition elements

As described in **Section 1.3** of this chapter, enzymes represented the first example of biorecognition elements implemented in biosensors.

Enzymes are globular proteins which are primarily constituted of the 20 naturally occurring amino acids, with molecular weights ranging from 10 kDa up to 1000 kDa.<sup>177,179</sup> The unique 3D conformation of these macromolecules is responsible for the enzyme's catalytic activity as well as for its specificity to a particular substrate.<sup>180</sup> One of the main advantages of enzymes is that they can repeatedly catalyze the same reactions as long as their active sites are not modified, resulting in a continuous signal in the presence of the substrate. However, some enzymes need the "help" of an additional component, which can be of either organic or inorganic nature, to generate their catalytic activities.<sup>177</sup> These necessary components are known as cofactors, and they can range from small metal ions such as  $Mn^{2+}$  or  $Cu^+$ , to more complex organic molecules as adenosine triphosphate (ATP).<sup>180</sup> Some of the most common enzymes are oxidases and peroxidases, which catalyze an oxidation-reduction reaction with  $O_2$  or  $H_2O_2$ , respectively. Other examples of well-known enzymes are phosphatases, used to remove phosphate groups; proteases, which catalyze the hydrolysis of peptide bonds in a polypeptidic chain; or DNA polymerases, involved in the synthesis of DNA molecules from dinucleotides.<sup>180</sup> Needless to say, enzymes present a huge impact in current research, and there are a myriad applications of enzyme-based biosensors for the detection of pesticides, heavy metals or even mycotoxins.<sup>181,182</sup> For example, it has been proven that AFB<sub>1</sub> inhibits acetylcholinesterase, an enzyme responsible for the hydrolysis of acetylcholine (AChE).<sup>183</sup> By using this principle, a method was developed for the detection of this mycotoxin in which the resulting enzymatic activity of acetylcholinesterase was measured in a colorimetric assay, obtaining a linear range from 10 to 60 ng mL<sup>-1</sup>. Furthermore, the excellent selectivity of the biosensor was demonstrated by testing the cross-reactivity of other aflatoxins.<sup>184</sup>

The basis of the use of oligonucleotides (small DNA sequences of less than fifty base pairs) as biorecognition elements relies on the detection of specific segments of nucleic

acids by complementary probes.<sup>177</sup> To this aim, firstly, the target DNA sequence needs to be identified. Then, a complementary DNA strand, used as the biorecognition element, is designed and immobilized onto the biosensor platform. These devices are known as genosensors<sup>185</sup> and they are characterized by their extremely high selectivity.<sup>185,186</sup>

Whole cells and tissues can also be used as biorecognition elements. Contrary to oligonucleotides, cells can detect a much broader number of substances, and can provide physiological information that molecular probes are unable to do. Hence they can be applied in fields such as environmental toxicity monitoring or in the study of pharmaceutical effects, such as those of immunosuppressant drugs.<sup>187-189</sup> However, some of the shortcomings of using whole cells or tissues are the lack of sensitivity and selectivity in molecular recognition, as well as the short cells' lifetimes.<sup>188</sup>

Antibodies are an invaluable and probably the most widely used biorecognition tool over the last decades, serving as an inspiration for the development of novel detection technologies.<sup>177</sup> Antibodies, or immunoglobulins (Ig), are globular proteins secreted by B-cells as an immune response to an antigen.<sup>190</sup> Immunoglobulins generally consists of two differentiated regions: a constant region (C), which can only take a few distinguishable forms, and a variable region (V), which can virtually have any form, and it is generally responsible for antigen recognition.<sup>190</sup> Besides constant and variable regions, antibodies are composed of two heavy chains (H) and two light chains (L). Depending on the constant region of the heavy chains, five different antibody isotypes are found, namely IgG, IgM, IgA, IgD and IgE, with the former one being the most abundant in humans (**Figure 7**).<sup>191,192</sup>

The antigen-antibody interactions generally occur between the paratope, which is the binding site of the antibody that recognizes the antigen, and the epitope, that is the part of the antigen that interacts with the antibody paratope.<sup>192</sup> There are mainly three different types of antibodies used for biosensing applications: polyclonal, monoclonal and recombinant antibodies. Polyclonal antibodies are comprised of a mixture of different immunoglobulins that target the same analyte. They are produced after the injection of an antigen into an animal, and subsequently collected from the animal's sera.<sup>177,193</sup> Small antigens must be chemically conjugated with immunogenic carrier proteins, such as keyhole limpet hemocyanin (KLH), to elicit the immune response. Polyclonal antibodies present some limitations, such as batch-to-batch variations, which may hinder their use in biosensing strategies. In this way, monoclonal antibodies, produced by hybridoma cells, are usually the preferred option since they always present the same paratope. Monoclonal antibodies generally offer more confidence in terms of specificity for the target analyte, as well as fewer cross reactivity with other molecules.<sup>177,190</sup> However, their production is a tedious and time consuming process, and slight modifications of the epitope could lead to dramatic decreases in the antibody's binding capacity.<sup>177</sup>

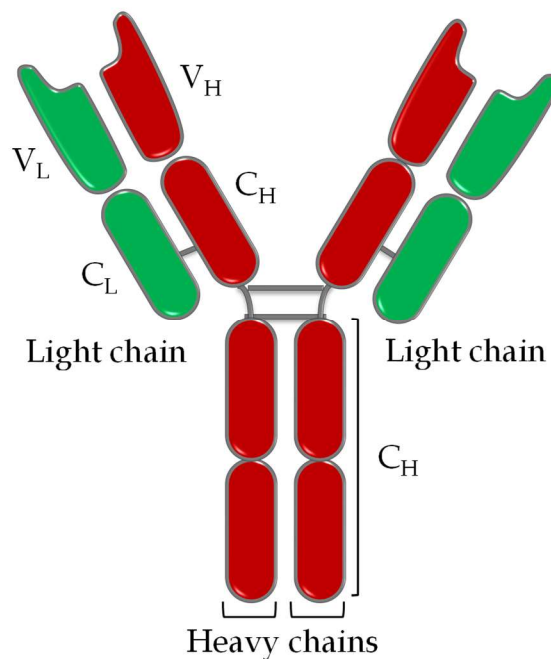
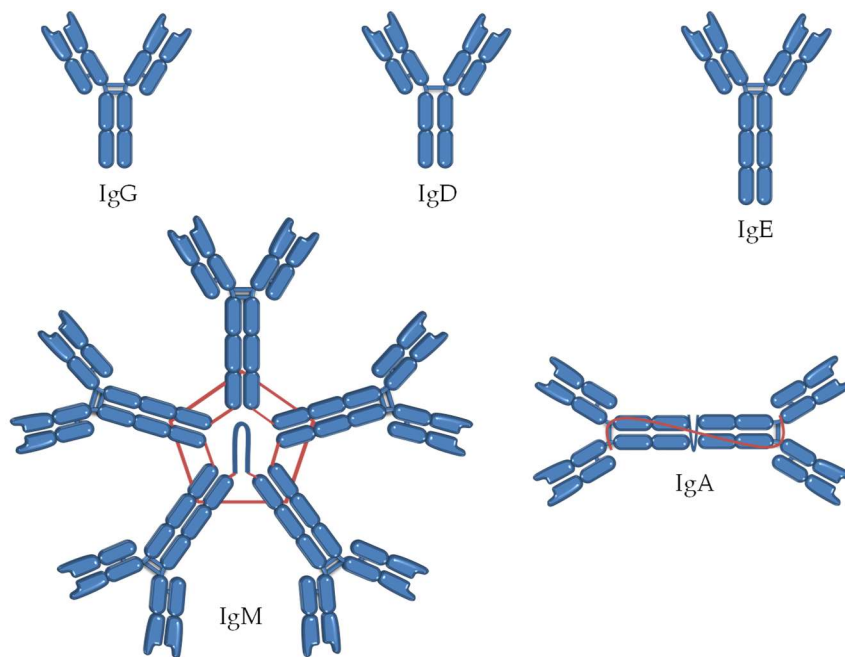


**Figure 7.** Top: Schematic representation of the five antibody isotypes found in humans. Bottom: Scheme of the different parts of an IgG antibody. IgGs are “Y” shaped proteins composed of two heavy chains (marked in red) and two light chains (marked in green). Each heavy chain consists of a variable domain ( $V_H$ ) and three constant domains ( $C_H$ ), whereas the light chains are made of one variable ( $V_L$ ) and one constant ( $C_L$ ) domain. The recognition normally takes place in the variable regions of the light and/or heavy chains.

Polyclonal and especially monoclonal antibodies have been extensively applied for the detection of all kinds of mycotoxins over the last decades.<sup>69,194</sup> Regardless of their widespread implementation, they present some limitations with reference to overall stability as well as non-specific binding.<sup>177,195</sup> On top of that, the production of polyclonal

and monoclonal antibodies entails animal immunization, which is an expensive and time-consuming method, and lately subject of some controversies.<sup>196</sup> Therefore, new strategies for the development of biomimetic recognition elements that can surmount these limitations have been designed.

#### 1.4.2. Biomimetic recognition elements

Since the 1990s, different approaches for the introduction of biomimetic or bioinspired recognition elements into biosensing technologies have been attempted. Biomimetic elements try to overcome the limitations shown by biological elements for biosensing purposes and provide a robust and sensitive antigen recognition. Moreover, contrary to biorecognition elements, artificial receptors can virtually target any analyte.<sup>177</sup> Some of the most important bioinspired recognition elements applied to mycotoxin and immunosuppressant analysis (**Table 4**) range from semi-synthetic nature elements as recombinant antibodies, peptides or aptamers to completely artificial tools such as MIPs.

**Table 4.** Analytical characteristics of non-chromatographic methods for the determination of MPA, FB1 and AOH.

Analyte	Matrix	Recognition element	Analytical technique	LOD/LOQ	Ref
MPA and MPM	Plasma and urine	-	Differential pulse voltammetry	LOD: 128 ng mL <sup>-1</sup> for MPA and 390 ng mL <sup>-1</sup> for MPM	197
MPM	Urine and human serum	Molecularly imprinted polymer	Square wave voltammetry	LOD: 3 ng mL <sup>-1</sup>	198
MPA	Plasma	Monoclonal anti-MPA antibody	PETINIA	LOD: 0.29 µg mL <sup>-1</sup>	199
MPA	Serum and plasma	Polyclonal anti-MPA antibody	Fluorescence polarization	LOD: 0.8 µg mL <sup>-1</sup> LOQ: 1.7 µg mL <sup>-1</sup>	119
MPA	Buffer	Recombinant antibody	Absorbance	n.d.	200
AOH	Wheat	Aptamer	Optical waveguide	LOD: 37 ng kg <sup>-1</sup>	201
AOH	Apple and tomato	Monoclonal and polyclonal antibodies	Absorbance	LOD: 1–2 µg kg <sup>-1</sup> in apple and 1–13 µg kg <sup>-1</sup> in tomato	46
FB1	Buffer	Aptamer	Absorbance, light scattering detection	LOD: 0.056 pg mL <sup>-1</sup> to 2 ng mL <sup>-1</sup>	202
FB1	Corn	Recombinant antibody	Absorbance	LOD: 8.32 µg kg <sup>-1</sup>	203
FB1	Maize, feedstuff and wheat	Recombinant antibody/mimetic peptide	Absorbance	LOD: 1.18 ng mL <sup>-1</sup>	204
FB1	Maize, feedstuff and rice	Recombinant antibody/mimetic peptide	Absorbance	LOD: 0.21 ng mL <sup>-1</sup>	205
FB1	Corn	Monoclonal antibody	Cyclic voltammetry	LOD: 4.2 ng kg <sup>-1</sup>	206

Bioinspired recognition elements of fully synthetic nature comprise nanozymes and MIPs. Nanozymes can be described as nanomaterials of diverse origin, such as metal complexes, dendrimers or polymers that are able to mimic the catalytic activities of naturally occurring enzymes.<sup>207</sup> On the other hand, MIPs are described as tailor made material, prepared by molecular imprinting, containing specific recognition cavities printed on a 3D structure with a predetermined selectivity for a specific analyte or group of similar analytes.<sup>208,209</sup> Some of the advantages presented by these nanomaterials are the easy production, chemical and thermal stability, long shelf lifetime, low cost and possible reusability. However, they tend to be subject to high unspecific interactions and, in general, present lower affinities than antibodies for the target molecules.<sup>177</sup>

Recombinant antibodies represent a truly fascinating alternative to natural antibodies. They are derived antibodies, isolated by enzymatic cleavage or found by combinatorial libraries, such as phage display libraries (see **Section 1.5** of the introduction).<sup>195</sup> Some of the best known recombinant antibodies include the fragment antigen binding (Fab) antibody and the single chain fragment variable (scFv) antibody. Fab fragments are composed of the variable heavy and light chains ( $V_L$  and  $V_H$ ) of natural antibodies, responsible for the antigen binding, as well as the constant light chain and one of the constant heavy chain domains ( $C_L$  and  $C_H$ ). The total molecular weight of Fab antibodies is around 55 kDa, three times lower that of an IgG.<sup>210</sup> Fab antibodies generally exhibit fewer non-specific binding effects in comparison to whole IgGs due to the absence of most of the constant heavy chain domains. Similarly, scFv antibodies symbolize an upgrade in the properties of conventional IgGs. The difference between Fab and scFv antibodies is that the latter ones only consist of the variable heavy and light domains ( $V_L$  and  $V_H$ ) bound together by non-covalent interactions or disulfide bridges, with a total molecular weight of, approximately, 28 kDa.<sup>210,211</sup> Furthermore, both Fab and scFv antibodies can be effectively expressed in bacteria, significantly reducing the time and cost of traditional antibody production.<sup>210</sup>

Aptamers are single stranded DNA or RNA fragments with affinities and specificities for target analytes comparable to those of antibodies yet presenting a size five to ten times smaller than them.<sup>211</sup> Aptamers are selected *in vitro* from randomized massive DNA and RNA pools by their affinity towards a non-nucleic acid molecule.<sup>177</sup> This process, known as “systematic evolution of ligands by exponential enrichment” or SELEX, can however take up to several months to be accomplished.<sup>211</sup> Aptamers have proven to be a versatile tool for the selective recognition of small molecules but also for bigger proteins or even whole cells.<sup>177</sup>

Peptide receptors possess several advantages in comparison to conventional antibodies for molecular recognition, as they can be chemically synthesized with ease and genetically modified to incorporate, for instance, affinity or fluorescent tags.<sup>195</sup> Peptides offer good stabilities and excellent solubility in most of the typically used buffers. Moreover, they can be implemented in competitive immunoassays as peptide mimetics, also known as mimotopes or mimopeptides. Peptide mimetics can be described as peptide molecules that mimic the behavior of antigens, binding to the same antibody paratope, hence establishing a competition for their binding sites.<sup>212</sup> These peptide mimetics, as well as the previously described recombinant antibodies, are often selected using the phage display technology. This Nobel Prize-awarded technology will be described in the following chapter as it is one of the most promising techniques for the discovery of new biorecognition elements.



## 1.5. Phage display as an analytical tool for the selection of mimopeptides and recombinant antibodies

### 1.5.1. Introduction to phage display

Throughout world's history, many diverse types of organisms have inhabited our planet. It is impossible to count all the species that have existed on Earth and, needless to say, the current number and kind of specimens is significantly different in comparison to several million years ago. Despite natural disasters, the key point of these changes is evolution. Those species able to replicate and mutate as a way to adapt to new environments and living conditions are the ones who survive and thrive. This Darwinian simile can be applied, to some extent, to the concept of phage display. At a molecular level, for example, certain molecules can withstand certain conditions better than others, and therefore are "selected" from all the different options initially available. Since these small molecules are unable to replicate by themselves, they need the help of an external source, which, in the case of phage display, are viruses that incorporate the proteins' or peptides' coding sequence within its DNA.<sup>213</sup>

The first paper reporting the phage display technology was published in 1985 by George P. Smith.<sup>214</sup> He proved the ability of expressing a foreign peptide in a phage protein without altering its functionality. Furthermore, it was observed that the incorporated randomized fragment was "immunologically accessible" and could be potentially used to obtain recombinant antibodies or antibody-binding peptides.<sup>214</sup>

However, the decade of the 1990s witnessed the actual blooming of phage display. In this period, the first fully randomized peptide libraries that allowed the selection of very specific antibody epitopes were produced.<sup>215,216</sup> Moreover, Sir Gregory P. Winter was the first to ever publish a successful display of a single-chain variable-fragment antibody.<sup>217-219</sup> These major accomplishments were the outbreak of many different applications of phage display technology, and lead the way for both George P. Smith and Sir Gregory P. Winter to receive one half of the 2018 Nobel Prize in Chemistry for their contributions to the "phage display of peptides and antibodies".<sup>220,221</sup>

### 1.5.2. Bacteriophages

The basis of phage display resides in bacteriophages. These organisms can be considered as the means of transportation for phage display technology and are of vital importance for the success of this technique.

Bacteriophages can be described as viruses that infect bacteria. They are ubiquitous in nature, with an estimation of  $10^{31}$ - $10^{32}$  entities residing in the biosphere.<sup>222</sup> Bacteriophages are considered the most abundant living organisms in the world.<sup>223</sup> As abundant as they are, they also present very different properties and shapes among them. The common denominator is that all bacteriophages present a core in which a single unit of nucleic acid resides, either single-stranded or double-stranded DNA or RNA.

According to their morphology different classifications of bacteriophages have been proposed throughout the last decades, as new organisms have been continuously discovered.<sup>223-226</sup> Bacteriophages can be tailed, polyhedral, filamentous and pleomorphic in shape,<sup>223</sup> and several orders and families with different characteristics can be found

within each group (Table 5).<sup>226,227</sup> However, filamentous phages are the most commonly used in phage display.<sup>228</sup>

**Table 5.** Classification of bacteriophages according to their shape and basic properties.<sup>a</sup>

Shape	Nucleic Acid	Virus	Particularities	Example
Tailed	Ds-DNA, L	<i>Myoviridae</i>	Contractile tail	T4
		<i>Siphoviridae</i>	Long tail, non-contractile	$\lambda$
		<i>Podoviridae</i>	Short tail	T7
Polyhedral	Ss-DNA, C	<i>Microviridae</i>	Conspicuous capsomers	$\Phi$ x174
	Ds-DNA, C, S	<i>Corticoviridae</i>	Complex capsid, lipids	PM2
	Ds-DNA, L	<i>Tectiviridae</i>	Inner lipid vesicle, pseudotail	PRD1
	Ds-DNA, L	<i>SH1 group</i> *	Inner lipid vesicle	SH1
	Ds-DNA, C	<i>STVI group</i> *	Turret-shaped protrusions	STIV
	Ss-RNA, L	<i>Leviviridae</i>	Poliovirus-like	MS2
	Ds-RNA, L, seg	<i>Cystoviridae</i>	envelope, lipids	$\phi$ 6
Filamentous	Ss-DNA, C	<i>Inoviridae</i>	Long filaments	fd
	Ds-DNA, L	<i>Lipothrixoviridae</i>	short rods	MVL1
	Ds-DNA, L	<i>Rudoviridae</i>	Envelope, lipids	TTV1
Pleomorphic	Ds-DNA, C, S	<i>Plasmaviridae</i>	Envelope, lipids, no capsid	L2
	Ds-DNA, C, S	<i>Fuselloviridae</i>	Same, lemon-shaped	SSV1
	Ds-DNA, L, S	<i>Salterprovirus</i>	Same, lemon-shaped	His1
	Ds-DNA, C, S	<i>Guttaviridae</i>	Droplet-shaped	SNDV
	Ds-DNA, L	<i>Ampullaviridae</i> *	Bottle-shaped	ABV
	Ds-DNA, C	<i>Bicaudaviridae</i> *	Two-tailed, growth cycle	ATV
	Ds-DNA, L	<i>Globuloviridae</i> *	Paramyxovirus-like	PSV

Ds: Doubled-stranded; Ss: Single-stranded; C: circular; L: Linear; S: superhelical; seg: segmented; \*Awaiting classification. <sup>a</sup>Adapted from reference [227] with permission of Springer Nature (Copyright 2006).

Filamentous bacteriophages (genus *Inovirus*) are a cylinder-shaped group of viruses that consist of a single-stranded DNA sequence encapsulated in a protein capsid.<sup>228</sup> These bacteriophages are able to infect a wide range of bacteria, such as *Escherichia coli* (*E. coli*), *Xanthomonas*, *Thermus*, *Pseudomonas*, *Salmonella* or *Vibrio*.<sup>229</sup> Among all the different classes of filamentous bacteriophages, the Ff class is the most extensively studied. This class comprises phages such as f1, fd and M13 (Figure 8), all of which have a mean diameter of circa 6.5 nm and a total length of 800–930 nm.<sup>228,229</sup> Moreover, sequencing analysis of the genome of these phages proved that they are 97% homologous among them.<sup>230–232</sup> The Ff bacteriophages infect the cells through the tip of the F conjugative pilus found in male *E. coli* cells and have the particularity of not killing their host during infection. These bacteriophages undergo a lysogenic cycle in which they incorporate their genome to the one of the host cells. Once the new phage particles are assembled inside the cell, they are secreted via the cell membranes without harming their host.<sup>229,233</sup>

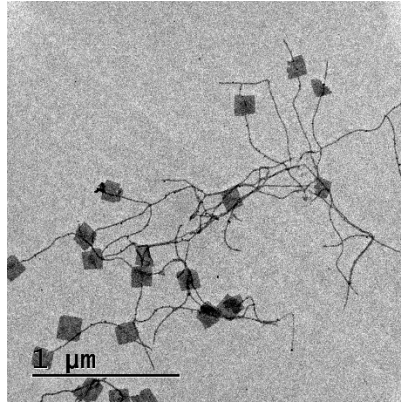


**Figure 8.** Transmission electron micrograph of filamentous phages M13 acquired with negative staining using a JEOL JEM-1400PLUS instrument operating at 120 kV, with a LaB6 electron source and a GATAN US1000 CCD camera.

The Ff class of filamentous bacteriophages is composed of a total of 11 proteins, five of which have a structural function, namely proteins pVIII, pIII, pVI, pVII and pIX (**Figure 9**). Protein pVIII is the major coat protein and it consists of circa 2800 molecules of a 50-amino-acid sequence covering the majority of the phage surface. The other four proteins are found at the ends of the phage. Five molecules of each pVII and pIX proteins are found at one end, and about 5 molecules of proteins pIII and pVI at the other. The remaining six proteins are not included in the outer structure of the phage. Proteins pI, pIV and pXI are responsible for the phage morphogenesis, and proteins pII, pV and pX have a replication function.<sup>228,229</sup>

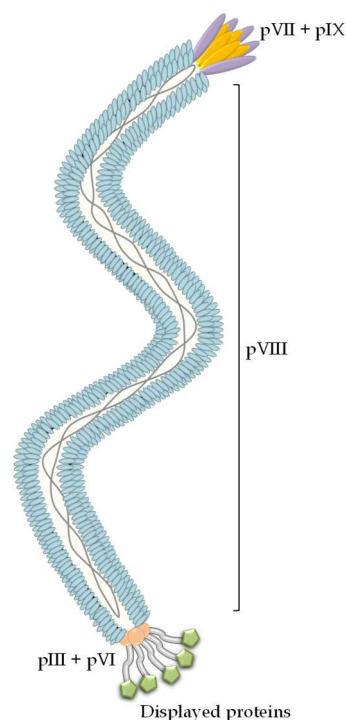


**Figure 9.** Structure of a filamentous Ff phage. M13 phage is illustrated as a representative of the Ff class of filamentous phages. The phage virion consists of five structural proteins, the major coat protein, pVIII (blue), and four minor coat proteins, pIII (grey), pVI (orange), pVII (purple) and pIX (yellow). Phages can be engineered to display different protein sequences in any of the

structural proteins. In this figure, at the end of protein pIII, five copies of a protein (green) are displayed. The phage vector is represented as a grey line in between the major coat protein.

### 1.5.3. Principles and applications of phage display

There are several examples in the literature of successful applications of phage display using different bacteriophages, such as T7 or  $\lambda$ .<sup>234,235</sup> However, as previously mentioned, the most widespread display system is the one using filamentous phages. Back in the 1990s, various examples of peptide and protein displays on pIII,<sup>236</sup> pVIII,<sup>237</sup> pVI,<sup>238</sup> and pVII and pIX,<sup>239</sup> have been published, proving the capability of all structural proteins to display foreign sequences fused to them. A successful display of an extraneous peptide or protein on any coat protein of the phage virion requires the fusion of the DNA sequence of that entity to the gene of the phage protein. Currently, the most typical approaches are those displaying proteins on either the pIII or the pVIII coat proteins.<sup>228</sup>

In order to produce more copies of the phage displaying the foreign peptide or protein of interest, phages need to replicate themselves. For this purpose, filamentous phages infect cells via the F conjugative pilus of male bacteria.<sup>240</sup> As a result of the infection, the phage vector (ssDNA) containing all the genome penetrates the cell and starts the replication process. The ssDNA of the phage first transforms into a dsDNA by a host RNA polymerase. This dsDNA undergoes a rolling-circle replication, with the assistance of proteins pII and pX, producing progeny ssDNA. In the early stages of the infection process, the progeny ssDNA contributes to the synthesis of more dsDNA. In a later infectious stage, the protein pV sequesters most of the progeny ssDNA into a rod-shaped structure, which would eventually acquire all the coat proteins and be subsequently extruded through the cell membrane as a complete virion.<sup>229</sup>

Besides phage vectors, the so-called phagemids can also be used for phage display. Phagemids differ from the phage vectors described above in the fact that they do not contain the genetic information to express all the proteins of the phage particle, yet they can replicate to a very high copy number the sequence of just one of the coat proteins used for display.<sup>229</sup> Despite the ability to maintain itself as a plasmid, the phagemid is unable to generate infectious virions on its own; therefore, a helper phage is needed to complete the whole process.<sup>241</sup> Phagemids carry an antibiotic resistance gene, as well as two replication origins, namely a plasmid replication and a filamentous phage replication origin. The first one allows the phagemid to propagate inside the cell in a high copy number, while, the second remains inactive until the cell harboring the phagemid is infected with the helper phage.<sup>241</sup> It is said that the helper phage “rescues” the phagemid from the cell, as it induces the production and secretion of full infectious virions.<sup>229</sup> If a cell is only infected by a helper phage, the phage DNA is acquired by the cell and it will eventually produce progeny helper phages. On the contrary, if a cell is only infected by a phagemid, the cell will gain the antibiotic resistance from the phagemid, but it will not secrete any phage. Consequently, a cell that has been infected by both the phagemid and the helper phage will acquire the antibiotic resistance capacity and secrete both kinds of phages.

The size and quantity of the target protein to be displayed is what defines the expression strategy. For example, the display on protein pVIII can lead to the expression of thousands of copies of the foreign protein in the phage virion, but it is limited to those

cases expressing short peptides (6–8 amino acids).<sup>237,242</sup> Larger peptides can be expressed, but in fewer amounts, leaving at least 80% of the pVIII proteins as wild type.<sup>228</sup> Opposite to that, protein pIII is only capable of expressing up to five copies of the molecule, although the protein sequence in this case can be larger.<sup>228</sup> One of the drawbacks of expressing longer peptides, or even antibody fragments, is the fact that the infectivity rate of the phage particle decreases.<sup>214</sup> To surmount this problem, the phage can be modified to express only one copy of the larger protein on pIII. Phagemids are preferred when bigger peptides or antibody fragments are expressed, due to their ease of manipulation and propagation inside host cells. Moreover, transformation efficiencies using phagemids are improved in comparison to complex phage vectors.<sup>241</sup>

The general tendency in all display systems is that bigger proteins are expressed in a lower amount than the smaller ones. However, the facility to genetically modify the sequence of a phage vector, or phagemid, has resulted in innumerable applications, from finding new antibody-binding peptide sequences, or peptide-binding antibodies, to the development of diverse biosensing strategies. Among all the different applications, the most prominent one is the construction of phage-display libraries that express either a relatively small peptide sequence or a big antibody fragment for the selection of sensitive and specific binders.

#### 1.5.4. Applications of phage display to the analysis of small molecules

The term small molecule refers to those chemical compounds of low molecular weight, regardless of their origin. There is a plethora of different examples of small molecules with considerably different properties. For example, some molecules are used to cure pathologies whereas others can be very prejudicial for human or animal health, as well as for the environment.<sup>129</sup> The detection of small molecules has been carried out generally by chromatographic methods due to their high sensitivity and selectivity.<sup>129</sup> However, these methods tend to be quite laborious, often require derivatization and clean-up processes and need highly skilled personnel.<sup>243</sup> A solution to this is the implementation of biosensors, described in **Section 1.3.** of this thesis, as they can offer cheaper, faster, sensitive and even on-site analysis of many different targets.<sup>244</sup>

One of the biggest challenges for the development of biosensors for small molecules is the intrinsic nature of these molecules. Their size is not big enough which prevents the immune system from generating antibodies against them. In order to provide an immune response, they need to be bound to a large protein, with the risk of generating responses against the unwanted target.

Phage display offers an alternative path of finding, for example, recombinant antibodies or peptide mimetics for many kinds of small molecules. Antibodies that can recognize practically any target can be selected from phage display libraries.<sup>245</sup> Moreover, anti-immune complex peptide sequences, which recognize the complex between the antigen and the antibody of interest, have also been found.<sup>246–248</sup> As a consequence, the myriad of possibilities and applications that recombinant antibodies offer has led to a vast increase in the number of antibody libraries over the last decades.<sup>249</sup> In addition to this, phage display serves as a way of finding peptide mimetics, also known as mimopeptides.<sup>250</sup> These peptide mimetics, although presenting a completely different structure, are able to mimic the behavior of the target molecule. They are able to bind to the same antibody paratope as the target analyte and therefore establish a competition with the target compound for the antibody binding site.

The scope of phage display sets no limits when targeting small molecules. This is the reason why there have been very diverse biosensing applications for a very wide variety of analytes such as, fungicides and herbicides like benthothiostrobin<sup>251</sup> or clomazone,<sup>252</sup> antioxidants such as resveratrol,<sup>253</sup> medicinal drugs like paracetamol,<sup>254</sup> colorants as malachite green,<sup>255</sup> or mycotoxins such as fumonisin B<sub>1</sub><sup>256</sup> or zearalenone<sup>257</sup> are a few examples of the huge potential of phage display as a very efficient tool for biosensing of small molecules.

## 1.6. Bibliography

- (1) Conly, J.; Johnston, B. Where Are All the New Antibiotics? The New Antibiotic Paradox. *Can. J. Infect. Dis. Med. Microbiol.* **2005**, *16*, 159–160.
- (2) Ciegler, A.; Bennett, J. W. Mycotoxins and Mycotoxicoses. *BioScience* **1980**, *30* (8), 512–515. <https://doi.org/10.2307/1307970>.
- (3) Aminov, R. I. A Brief History of the Antibiotic Era: Lessons Learned and Challenges for the Future. *Front. Microbiol.* **2010**, *1*. <https://doi.org/10.3389/fmicb.2010.00134>.
- (4) Maggon, K. K.; Gupta, S. K.; Venkitasubramanian, T. A. Biosynthesis of Aflatoxins. *Bacteriol. Rev.* **1977**, *41*, 822–855.
- (5) Dube, H. C. *An Introduction to Fungi, 4th Ed.*; Scientific Publishers, 2013.
- (6) Blackwell, M. The Fungi: 1, 2, 3 ... 5.1 Million Species? *Am. J. Bot.* **2011**, *98*, 426–438. <https://doi.org/10.3732/ajb.1000298>.
- (7) Daley, D. K.; Brown, K. J.; Badal, S. Fungal Metabolites. In *Pharmacognosy*; Elsevier, 2017; pp 413–421. <https://doi.org/10.1016/B978-0-12-802104-0.00020-2>.
- (8) Goyal, S.; Ramawat, K. G.; Mérillon, J.-M. Different Shades of Fungal Metabolites: An Overview. In *Fungal Metabolites*; Mérillon, J.-M., Ramawat, K. G., Eds.; Reference Series in Phytochemistry; Springer International Publishing: Cham, 2017; pp 1–29. [https://doi.org/10.1007/978-3-319-25001-4\\_34](https://doi.org/10.1007/978-3-319-25001-4_34).
- (9) Thirumurugan, D.; Cholarajan, A.; Vijayakumar, S. S. S. R. and R. *An Introductory Chapter: Secondary Metabolites*; IntechOpen, 2018. <https://doi.org/10.5772/intechopen.79766>.
- (10) Dufossé, L.; Fouillaud, M.; Caro, Y.; Mapari, S. A.; Sutthiwong, N. Filamentous Fungi Are Large-Scale Producers of Pigments and Colorants for the Food Industry. *Curr. Opin. Biotech.* **2014**, *26*, 56–61. <https://doi.org/10.1016/j.copbio.2013.09.007>.
- (11) Beekman, A. M.; Barrow, R. A.; Beekman, A. M.; Barrow, R. A. Fungal Metabolites as Pharmaceuticals. *Aust. J. Chem.* **2014**, *67*, 827–843. <https://doi.org/10.1071/CH13639>.
- (12) Demain, A. L. Valuable Secondary Metabolites from Fungi. In *Biosynthesis and Molecular Genetics of Fungal Secondary Metabolites*; Martín, J.-F., García-Estrada, C., Zeilinger, S., Eds.; Fungal Biology; Springer: New York, NY, 2014; pp 1–15. [https://doi.org/10.1007/978-1-4939-1191-2\\_1](https://doi.org/10.1007/978-1-4939-1191-2_1).
- (13) Bräse, S.; Encinas, A.; Keck, J.; Nising, C. F. Chemistry and Biology of Mycotoxins and Related Fungal Metabolites. *Chem. Rev.* **2009**, *109*, 3903–3990. <https://doi.org/10.1021/cr050001f>.
- (14) Bennett, J. W.; Klich, M. Mycotoxins. *Clin. Microbiol. Rev.* **2003**, *16*, 497–516. <https://doi.org/10.1128/CMR.16.3.497-516.2003>.
- (15) D’Mello, J. P. F.; Macdonald, A. M. C. Mycotoxins. *Anim. Feed Sci. Technol.* **1997**, *69*, 155–166. [https://doi.org/10.1016/S0377-8401\(97\)81630-6](https://doi.org/10.1016/S0377-8401(97)81630-6).
- (16) Bryden, W. L. Mycotoxin Contamination of the Feed Supply Chain: Implications for Animal Productivity and Feed Security. *Anim. Feed Sci. Technol.* **2012**, *173*, 134–158. <https://doi.org/10.1016/j.anifeedsci.2011.12.014>.
- (17) Eskola, M.; Altieri, A.; Galobart, J. Overview of the Activities of the European Food Safety Authority on Mycotoxins in Food and Feed. *World Mycotoxin J.* **2018**, *11*, 277–289. <https://doi.org/10.3920/WMJ2017.2270>.
- (18) Krska, R.; Schubert-Ullrich, P.; Molinelli, A.; Sulyok, M.; MacDonald, S.; Crews, C. Mycotoxin Analysis: An Update. *Food Addit. Contam. - Chem. Anal. Control Expo. Risk Assess.* **2008**, *25*, 152–163. <https://doi.org/10.1080/02652030701765723>.

- (19) Eskola, M.; Kos, G.; Elliott, C. T.; Hajšlová, J.; Mayar, S.; Krska, R. Worldwide Contamination of Food-Crops with Mycotoxins: Validity of the Widely Cited 'FAO Estimate' of 25%. *Crit. Rev. Food. Sci. Nutr* **2019**, 1–17. <https://doi.org/10.1080/10408398.2019.1658570>.
- (20) EUR-Lex - 02006R1881-20201014 - EN - EUR-Lex <https://eur-lex.europa.eu/legal-content/EN/TXT/?uri=CELEX%3A02006R1881-20201014> (accessed 2021 -06 -23).
- (21) Blount, W. P. Turkey "X" Disease. *Turkeys* **1961**, 9, 52–61.
- (22) Kensler, T. W.; Roebuck, B. D.; Wogan, G. N.; Groopman, J. D. Aflatoxin: A 50-Year Odyssey of Mechanistic and Translational Toxicology. *Toxicol. Sci.* **2011**, 120 (Suppl 1), S28–S48. <https://doi.org/10.1093/toxsci/kfq283>.
- (23) Kumar, P.; Mahato, D. K.; Kamle, M.; Mohanta, T. K.; Kang, S. G. Aflatoxins: A Global Concern for Food Safety, Human Health and Their Management. *Front. Microbiol.* **2017**, 7, 2170. <https://doi.org/10.3389/fmicb.2016.02170>.
- (24) Squire, R. A. Ranking Animal Carcinogens: A Proposed Regulatory Approach. *Science* **1981**, 214, 877–880. <https://doi.org/10.1126/science.7302565>.
- (25) Van Der Merwe, K. J.; Steyn, P. S.; Fourie, L.; Scott, D. B.; Theron, J. J. Ochratoxin A, a Toxic Metabolite Produced by *Aspergillus Ochraceus* Wilh. *Nature* **1965**, 205, 1112–1113. <https://doi.org/10.1038/2051112a0>.
- (26) Al-Anati, L.; Petzinger, E. Immunotoxic Activity of Ochratoxin A. *J. Vet. Pharmacol. Ther.* **2006**, 29, 79–90. <https://doi.org/10.1111/j.1365-2885.2006.00718.x>.
- (27) Bui-Klimke, T. R.; Wu, F. Ochratoxin A and Human Health Risk: A Review of the Evidence. *Crit. Rev. Food Sci. Nutr.* **2015**, 55, 1860–1869. <https://doi.org/10.1080/10408398.2012.724480>.
- (28) Saleh, I.; Goktepe, I. The Characteristics, Occurrence, and Toxicological Effects of Patulin. *Food Chem. Toxicol.* **2019**, 129, 301–311. <https://doi.org/10.1016/j.fct.2019.04.036>.
- (29) *Trichothecene Mycotoxicosis: Pathophysiologic Effects: Volume II*; Beasley, V. R., Ed.; CRC Press: Boca Raton, 2017. <https://doi.org/10.1201/9781315121260>.
- (30) Meng-Reiterer, J.; Bueschl, C.; Rechthaler, J.; Berthiller, F.; Lemmens, M.; Schuhmacher, R. Metabolism of HT-2 Toxin and T-2 Toxin in Oats. *Toxins (Basel)* **2016**, 8, 364. <https://doi.org/10.3390/toxins8120364>.
- (31) Edwards, S.; Barrier-Guillot, B.; Clasen, P.-E.; Hietaniemi, V.; Pettersson, H. Emerging Issues of HT-2 and T-2 Toxins in European Cereal Production. *World Mycotoxin J.* **2009**, 2, 173–179. <https://doi.org/10.3920/WMJ2008.1126>.
- (32) Marin, S.; Ramos, A. J.; Cano-Sancho, G.; Sanchis, V. Mycotoxins: Occurrence, Toxicology, and Exposure Assessment. *Food Chem. Toxicol.* **2013**, 60, 218–237. <https://doi.org/10.1016/j.fct.2013.07.047>.
- (33) Gelderblom, W. C.; Jaskiewicz, K.; Marasas, W. F.; Thiel, P. G.; Horak, R. M.; Vleggaar, R.; Kriek, N. P. Fumonisin--Novel Mycotoxins with Cancer-Promoting Activity Produced by *Fusarium Moniliforme*. *Appl. Environ. Microbiol.* **1988**, 54, 1806–1811.
- (34) Bezuidenhout, S. C.; Gelderblom, W. C. A.; Gorst-Allman, C. P.; Horak, R. M.; Marasas, W. F. O.; Spiteller, G.; Vleggaar, R. Structure Elucidation of the Fumonisin, Mycotoxins from *Fusarium Moniliforme*. *J. Chem. Soc., Chem. Commun.* **1988**, 11, 743–745. <https://doi.org/10.1039/C39880000743>.
- (35) Hetherington, A. C.; Raistrick, H. Studies in the Biochemistry of Micro-Organisms. Part XIV. —On the Production and Chemical Constitution of a New Yellow Colouring Mater, Citrinin, Produced from Glucose by *Penicillium*. *Philosophical*



*Transactions of the Royal Society of London. Series B, Containing Papers of a Biological Character* **1931**, 220, 269–295. <https://doi.org/10.1098/rstb.1931.0025>.

(36) Pan, T.-M.; Hsu, W.-H. Monascus-Fermented Products. In *Encyclopedia of Food Microbiology (Second Edition)*; Batt, C. A., Tortorello, M. L., Eds.; Academic Press: Oxford, 2014; pp 815–825. <https://doi.org/10.1016/B978-0-12-384730-0.00226-3>.

(37) Bennett, J. W.; Bentley, R. Pride and Prejudice: The Story of Ergot. *Perspect. Biol. Med.* **1999**, 42, 333–355. <https://doi.org/10.1353/pbm.1999.0026>.

(38) Arcella, D.; Ruiz, J. Á. G.; Innocenti, M. L.; Roldán, R. Human and Animal Dietary Exposure to Ergot Alkaloids. *EFSA J.* **2017**, 15, e04902. <https://doi.org/10.2903/j.efsa.2017.4902>.

(39) Jestoi, M. Emerging Fusarium-Mycotoxins Fusaproliferin, Beauvericin, Enniatins, and Moniliformin: A Review. *Crit. Rev. Food Sci. Nutr.* **2008**, 48, 21–49. <https://doi.org/10.1080/10408390601062021>.

(40) Gruber-Dorninger, C.; Novak, B.; Nagl, V.; Berthiller, F. Emerging Mycotoxins: Beyond Traditionally Determined Food Contaminants. *J. Agric. Food Chem.* **2017**, 65, 7052–7070. <https://doi.org/10.1021/acs.jafc.6b03413>.

(41) Kolf-Clauw, M.; Sassahara, M.; Luciola, J.; Rubira-Gerez, J.; Alassane-Kpembi, I.; Lyazhri, F.; Borin, C.; Oswald, I. P. The Emerging Mycotoxin, Enniatin B1, down-Modulates the Gastrointestinal Toxicity of T-2 Toxin in Vitro on Intestinal Epithelial Cells and Ex Vivo on Intestinal Explants. *Arch. Toxicol.* **2013**, 87, 2233–2241. <https://doi.org/10.1007/s00204-013-1067-8>.

(42) Bianchini, A.; Bullerman, L. B. MYCOTOXINS | Classification. In *Encyclopedia of Food Microbiology (Second Edition)*; Batt, C. A., Tortorello, M. L., Eds.; Academic Press: Oxford, 2014; pp 854–861. <https://doi.org/10.1016/B978-0-12-384730-0.00230-5>.

(43) Raistrick, H.; Stickings, C. E.; Thomas, R. Studies in the Biochemistry of Micro-Organisms. 90. Alternariol and Alternariol Monomethyl Ether, Metabolic Products of *Alternaria Tenuis*. *Biochem J.* **1953**, 55, 421–433.

(44) Ostry, V. *Alternaria* Mycotoxins: An Overview of Chemical Characterization, Producers, Toxicity, Analysis and Occurrence in Foodstuffs. *World Mycotoxin J.* **2008**, 1, 175–188. <https://doi.org/10.3920/WMJ2008.x013>.

(45) Scientific Opinion on the Risks for Animal and Public Health Related to the Presence of *Alternaria* Toxins in Feed and Food. *EFSA J.* **2011**, 9, 2407. <https://doi.org/10.2903/j.efsa.2011.2407>.

(46) Ackermann, Y.; Curtui, V.; Dietrich, R.; Gross, M.; Latif, H.; Märtilbauer, E.; Usleber, E. Widespread Occurrence of Low Levels of Alternariol in Apple and Tomato Products, as Determined by Comparative Immunochemical Assessment Using Monoclonal and Polyclonal Antibodies. *J. Agric. Food Chem.* **2011**, 59, 6360–6368. <https://doi.org/10.1021/jf201516f>.

(47) Hickert, S.; Bergmann, M.; Ersen, S.; Cramer, B.; Humpf, H.-U. Survey of *Alternaria* Toxin Contamination in Food from the German Market, Using a Rapid HPLC-MS/MS Approach. *Mycotoxin Res* **2016**, 32, 7–18. <https://doi.org/10.1007/s12550-015-0233-7>.

(48) Dall'Asta, C.; Cirilini, M.; Falavigna, C. Chapter Three - Mycotoxins from *Alternaria*: Toxicological Implications. In *Advances in Molecular Toxicology*; Fishbein, J. C., Heilman, J. M., Eds.; Elsevier, 2014; Vol. 8, pp 107–121. <https://doi.org/10.1016/B978-0-444-63406-1.00003-9>.

(49) Pollock, G. A.; DiSabatino, C. E.; Heimsch, R. C.; Coulombe, R. A. The Distribution, Elimination, and Metabolism of <sup>14</sup>C-alternariol Monomethyl Ether. *J. Environ. Sci. Health, Part B* **1982**, 17, 109–124. <https://doi.org/10.1080/03601238209372306>.

- (50) Frisvad, J. C.; Thrane, U.; Samson, R. A.; Pitt, J. I. Important Mycotoxins and the Fungi Which Produce Them. In *Advances in Food Mycology*; Hocking, A. D., Pitt, J. I., Samson, R. A., Thrane, U., Eds.; Advances in Experimental Medicine and Biology; Springer US: Boston, MA, 2006; pp 3–31. [https://doi.org/10.1007/0-387-28391-9\\_1](https://doi.org/10.1007/0-387-28391-9_1).
- (51) Bentley, R. Mycophenolic Acid: A One Hundred Year Odyssey from Antibiotic to Immunosuppressant. *Chem. Rev.* **2000**, *100*, 3801–3826. <https://doi.org/10.1021/cr990097b>.
- (52) Engel, G.; von Milczewski, K. E.; Prokopek, D.; Teuber, M. Strain-Specific Synthesis of Mycophenolic Acid by *Penicillium Roqueforti* in Blue-Veined Cheese. *Appl. Environ. Microbiol.* **1982**, *43*, 1034–1040. <https://doi.org/10.1128/AEM.43.5.1034-1040.1982>.
- (53) Zhang, B.; Chen, X.; Han, S.-Y.; Li, M.; Ma, T.-Z.; Sheng, W.-J.; Zhu, X. Simultaneous Analysis of 20 Mycotoxins in Grapes and Wines from Hexi Corridor Region (China): Based on a QuEChERS-UHPLC-MS/MS Method. *Molecules* **2018**, *23*, 1926. <https://doi.org/10.3390/molecules23081926>.
- (54) OVERY, D. P.; FRISVAD, J. C. Mycotoxin Production and Postharvest Storage Rot of Ginger (*Zingiber Officinale*) by *Penicillium Brevicompactum*. *J. Food Prot.* **2005**, *68*, 607–609. <https://doi.org/10.4315/0362-028X-68.3.607>.
- (55) Brent, L. 2 - The Immunologic Basis of Allograft Rejection. In *A History of Transplantation Immunology*; Brent, L., Ed.; Academic Press: London, 1997; pp 56–115. <https://doi.org/10.1016/B978-012131770-6/50022-5>.
- (56) Van Laar, J. M. Chapter 62 - Immunosuppressive Drugs. In *Kelley and Firestein's Textbook of Rheumatology (Tenth Edition)*; Firestein, G. S., Budd, R. C., Gabriel, S. E., McInnes, I. B., O'Dell, J. R., Eds.; Elsevier, 2017; pp 983–998.e4. <https://doi.org/10.1016/B978-0-323-31696-5.00062-0>.
- (57) Schwartz, R.; Dameshek, W.; Donovan, J. The effects of 6-Mercaptopurine on homograft reactions. *J. Clin. Invest.* **1960**, *39*, 952–958.
- (58) Suthanthiran, M.; Morris, R. E.; Strom, T. B. Immunosuppressants: Cellular and Molecular Mechanisms of Action. *Am. J. Kidney Dis.* **1996**, *28*, 159–172. [https://doi.org/10.1016/S0272-6386\(96\)90297-8](https://doi.org/10.1016/S0272-6386(96)90297-8).
- (59) Demain, A. L. Pharmaceutically Active Secondary Metabolites of Microorganisms. *Appl. Microbiol. Biotechnol.* **1999**, *52*, 455–463. <https://doi.org/10.1007/s002530051546>.
- (60) Ordóñez-Robles, M.; Santos-Beneit, F.; Martín, J. F. Unraveling Nutritional Regulation of Tacrolimus Biosynthesis in *Streptomyces Tsukubaensis* through Omic Approaches. *Antibiotics (Basel)* **2018**, *7*, 39. <https://doi.org/10.3390/antibiotics7020039>.
- (61) Hackstein, H.; Thomson, A. W. Dendritic Cells: Emerging Pharmacological Targets of Immunosuppressive Drugs. *Nat. Rev. Immunol.* **2004**, *4*, 24–34. <https://doi.org/10.1038/nri1256>.
- (62) Wong, G. K.; Griffith, S.; Kojima, I.; Demain, A. L. Antifungal Activities of Rapamycin and Its Derivatives, Prolylrapamycin, 32-Desmethylrapamycin, and 32-Desmethoxyrapamycin. *J. Antibiot.* **1998**, *51*, 487–491. <https://doi.org/10.7164/antibiotics.51.487>.
- (63) Shaw, L. M.; Nawrocki, A.; Korecka, M.; Solari, S.; Kang, J. Using Established Immunosuppressant Therapy Effectively: Lessons from the Measurement of Mycophenolic Acid Plasma Concentrations. *Ther. Drug Monit.* **2004**, *26*, 347–351.
- (64) Bullingham, R. E. S.; Nicholls, A. J.; Kamm, B. R. Clinical Pharmacokinetics of Mycophenolate Mofetil. *Clin. Pharmacokinet.* **1998**, *34*, 429–455. <https://doi.org/10.2165/00003088-199834060-00002>.
- (65) Tredger, J. M.; Brown, N. W.; Adams, J.; Gonde, C. E.; Dhawan, A.; Rela, M.; Heaton, N. Monitoring Mycophenolate in Liver Transplant Recipients: Toward a

- Therapeutic Range. *Liver Transplant*. **2004**, *10*, 492–502. <https://doi.org/10.1002/lt.20124>.
- (66) Cheli, F.; Battaglia, D.; Gallo, R.; Dell'Orto, V. EU Legislation on Cereal Safety: An Update with a Focus on Mycotoxins. *Food Control* **2014**, *37*, 315–325. <https://doi.org/10.1016/j.foodcont.2013.09.059>.
- (67) Kahan, B. D.; Keown, P.; Levy, G. A.; Johnston, A. Therapeutic Drug Monitoring of Immunosuppressant Drugs in Clinical Practice. *Clinical Therapeutics* **2002**, *24* (3), 330–350. [https://doi.org/10.1016/S0149-2918\(02\)85038-X](https://doi.org/10.1016/S0149-2918(02)85038-X).
- (68) Razzazi-Fazeli, E.; Reiter, E. V. 2 - Sample Preparation and Clean up in Mycotoxin Analysis: Principles, Applications and Recent Developments. In *Determining Mycotoxins and Mycotoxigenic Fungi in Food and Feed*; De Saeger, S., Ed.; Woodhead Publishing Series in Food Science, Technology and Nutrition; Woodhead Publishing, 2011; pp 37–70. <https://doi.org/10.1533/9780857090973.1.37>.
- (69) Mika, A.; Stepnowski, P. Current Methods of the Analysis of Immunosuppressive Agents in Clinical Materials: A Review. *J. Pharm. Biomed. Anal.* **2016**, *127*, 207–231. <https://doi.org/10.1016/j.jpba.2016.01.059>.
- (70) Rahmani, A.; Jinap, S.; Soleimany, F. Qualitative and Quantitative Analysis of Mycotoxins. *Compr. Rev. Food Sci. Food Saf.* **2009**, *8*, 202–251. <https://doi.org/10.1111/j.1541-4337.2009.00079.x>.
- (71) Shephard, G. S. 3 - Chromatographic Separation Techniques for Determination of Mycotoxins in Food and Feed. In *Determining Mycotoxins and Mycotoxigenic Fungi in Food and Feed*; De Saeger, S., Ed.; Woodhead Publishing Series in Food Science, Technology and Nutrition; Woodhead Publishing, 2011; pp 71–89. <https://doi.org/10.1533/9780857090973.1.71>.
- (72) Trucksess, M. W.; Pohland, A. E. Methods and Method Evaluation for Mycotoxins. *Mol. Biotechnol.* **2002**, *22*, 287–292. <https://doi.org/10.1385/MB:22:3:287>.
- (73) Sydenham, E. W.; Shephard, G. S. Chromatographic and Allied Methods of Analysis for Selected Mycotoxins. In *Progress in Food Contaminant Analysis*; Gilbert, J., Ed.; Springer US: Boston, MA, 1996; pp 65–146. [https://doi.org/10.1007/978-1-4613-1117-1\\_3](https://doi.org/10.1007/978-1-4613-1117-1_3).
- (74) Tittlemier, S. a.; Cramer, B.; Dall'Asta, C.; Iha, M. h.; Lattanzio, V. m. t.; Maragos, C.; Solfrizzo, M.; Stranska, M.; Stroka, J.; Sumarah, M. Developments in Mycotoxin Analysis: An Update for 2018-19. *World Mycotoxin J.* **2020**, *13*, 3–24. <https://doi.org/10.3920/WMJ2019.2535>.
- (75) Sugioka, N.; Odani, H.; Ohta, T.; Kishimoto, H.; Yasumura, T.; Takada, K. Determination of a New Immunosuppressant, Mycophenolate Mofetil, and Its Active Metabolite, Mycophenolic Acid, in Rat and Human Body Fluids by High-Performance Liquid Chromatography. *J. Chromatogr. B: Biomed. Appl.* **1994**, *654*, 249–256. [https://doi.org/10.1016/0378-4347\(94\)00006-9](https://doi.org/10.1016/0378-4347(94)00006-9).
- (76) Patel, C. G.; Akhlaghi, F. High-Performance Liquid Chromatography Method for the Determination of Mycophenolic Acid and Its Acyl and Phenol Glucuronide Metabolites in Human Plasma. *Ther. Drug Monit.* **2006**, *28*, 116–122. <https://doi.org/10.1097/01.ftd.0000177664.96726.56>.
- (77) Ezekiel, C. N.; Bandyopadhyay, R.; Sulyok, M.; Warth, B.; Krska, R. Fungal and Bacterial Metabolites in Commercial Poultry Feed from Nigeria. *Food Addit. Contam: Part A* **2012**, *29*, 1288–1299. <https://doi.org/10.1080/19440049.2012.688878>.
- (78) Schenzel, J.; Forrer, H.-R.; Vogelgsang, S.; Bucheli, T. D. Development, Validation and Application of a Multi-Mycotoxin Method for the Analysis of Whole Wheat Plants. *Mycotoxin Res* **2012**, *28* (2), 135–147. <https://doi.org/10.1007/s12550-012-0125-z>.

- (79) Oviedo, M. S.; Barros, G. G.; Chulze, S. N.; Ramirez, M. L. Natural Occurrence of Alternariol and Alternariol Monomethyl Ether in Soya Beans. *Mycotoxin Res.* **2012**, *28*, 169–174. <https://doi.org/10.1007/s12550-012-0132-0>.
- (80) Broggi, L.; Reynoso, C.; Resnik, S.; Martinez, F.; Drunday, V.; Bernal, A. R. Occurrence of Alternariol and Alternariol Monomethyl Ether in Beverages from the Entre Rios Province Market, Argentina. *Mycotoxin Res.* **2013**, *29*, 17–22. <https://doi.org/10.1007/s12550-012-0147-6>.
- (81) Myresiotis, C. K.; Testempasis, S.; Vryzas, Z.; Karaoglanidis, G. S.; Papadopoulou-Mourkidou, E. Determination of Mycotoxins in Pomegranate Fruits and Juices Using a QuEChERS-Based Method. *Food Chem.* **2015**, *182*, 81–88. <https://doi.org/10.1016/j.foodchem.2015.02.141>.
- (82) Juan, C.; Chamari, K.; Oueslati, S.; Mañes, J. Rapid Quantification Method of Three Alternaria Mycotoxins in Strawberries. *Food Anal. Methods* **2015**, *9*. <https://doi.org/10.1007/s12161-015-0338-9>.
- (83) Juan, C.; Mañes, J.; Font, G.; Juan-García, A. Determination of Mycotoxins in Fruit Berry By-Products Using QuEChERS Extraction Method. *LWT - Food Sci. Technol.* **2017**, *86*. <https://doi.org/10.1016/j.lwt.2017.08.020>.
- (84) González-Jartín, J. M.; Rodríguez-Cañás, I.; Alfonso, A.; Sainz, M. J.; Vieytes, M. R.; Gomes, A.; Ramos, I.; Botana, L. M. Multianalyte Method for the Determination of Regulated, Emerging and Modified Mycotoxins in Milk: QuEChERS Extraction Followed by UHPLC-MS/MS Analysis. *Food Chem.* **2021**, *356*, 129647. <https://doi.org/10.1016/j.foodchem.2021.129647>.
- (85) Malachová, A.; Sulyok, M.; Beltrán, E.; Berthiller, F.; Krska, R. Optimization and Validation of a Quantitative Liquid Chromatography-Tandem Mass Spectrometric Method Covering 295 Bacterial and Fungal Metabolites Including All Regulated Mycotoxins in Four Model Food Matrices. *J Chromatogr. A* **2014**, *1362*, 145–156. <https://doi.org/10.1016/j.chroma.2014.08.037>.
- (86) Pizzutti, I. R.; de Kok, A.; Scholten, J.; Righi, L. W.; Cardoso, C. D.; Necchi Rohers, G.; da Silva, R. C. Development, Optimization and Validation of a Multimethod for the Determination of 36 Mycotoxins in Wines by Liquid Chromatography-Tandem Mass Spectrometry. *Talanta* **2014**, *129*, 352–363. <https://doi.org/10.1016/j.talanta.2014.05.017>.
- (87) Perre, E. van de; Deschuyffeleer, N.; Jacxsens, L.; Vekeman, F.; Hauwaert, W. van der; Asam, S.; Rychlik, M.; Devlieghere, F.; Meulenaer, B. de. Screening of Moulds and Mycotoxins in Tomatoes, Bell Peppers, Onions, Soft Red Fruits and Derived Tomato Products. *Food Control* **2014**, *37*, 165–170.
- (88) Kayode, O. F.; Sulyok, M.; Fapohunda, S. O.; Ezekiel, C. N.; Krska, R.; Oguntona, C. R. B. Mycotoxins and Fungal Metabolites in Groundnut- and Maize-Based Snacks from Nigeria. *Food Addit. Contam. Part B* **2013**, *6*, 294–300. <https://doi.org/10.1080/19393210.2013.823626>.
- (89) Li, C.; Wu, Y.-L.; Yang, T.; Huang-Fu, W.-G. Rapid Determination of Fumonisin B1 and B2 in Corn by Liquid Chromatography-Tandem Mass Spectrometry with Ultrasonic Extraction. *J. Chromatogr. Sci* **2012**, *50*, 57–63. <https://doi.org/10.1093/chromsci/bmr009>.
- (90) de Oliveira, G. B.; de Castro Gomes Vieira, C. M.; Orlando, R. M.; Faria, A. F. Simultaneous Determination of Fumonisin B1 and B2 in Different Types of Maize by Matrix Solid Phase Dispersion and HPLC-MS/MS. *Food Chem.* **2017**, *233*, 11–19. <https://doi.org/10.1016/j.foodchem.2017.04.091>.
- (91) Szekeres, A.; Budai, A.; Bencsik, O.; Németh, L.; Bartók, T.; Szécsi, Á.; Mesterházy, Á.; Vágvölgyi, C. Fumonisin Measurement from Maize Samples by High-Performance Liquid Chromatography Coupled with Corona Charged Aerosol Detector. *J. Chromatogr. Sci.* **2014**, *52*, 1181–1185. <https://doi.org/10.1093/chromsci/bmt173>.

- (92) Lino, C. M.; Silva, L. J. G.; Pena, A. L. S.; Silveira, M. I. Determination of Fumonisin B<sub>1</sub> and B<sub>2</sub> in Portuguese Maize and Maize-Based Samples by HPLC with Fluorescence Detection. *Anal. Bioanal. Chem.* **2006**, *384*, 1214–1220. <https://doi.org/10.1007/s00216-005-0295-z>.
- (93) Smith, L. L.; Francis, K. A.; Johnson, J. T.; Gaskill, C. L. Quantitation of Fumonisin B<sub>1</sub> and B<sub>2</sub> in Feed Using FMOC Pre-Column Derivatization with HPLC and Fluorescence Detection. *Food Chem.* **2017**, *234*, 174–179. <https://doi.org/10.1016/j.foodchem.2017.04.142>.
- (94) Ma, L.; Xu, W.; He, X.; Huang, K.; Wang, Y.; Luo, Y. Determination of Fumonisin B<sub>1</sub> and B<sub>2</sub> in Chinese Rice Wine by HPLC Using AQC Precolumn Derivatization. *J. Sci. Food Agric.* **2013**, *93*, 1128–1133. <https://doi.org/10.1002/jsfa.5862>.
- (95) De Girolamo, A.; Fauw, D. P.; Sizoo, E.; van Egmond, H.; Gambacorta, L.; Bouten, K.; Stroka, J.; Visconti, A.; Solfrizzo, M. Determination of Fumonisin B<sub>1</sub> and B<sub>2</sub> in Maize-Based Baby Food Products by HPLC with Fluorimetric Detection after Immunoaffinity Column Clean-Up. *World Mycotoxin J.* **2010**, *3*, 135–146. <https://doi.org/10.3920/WMJ2010.1213>.
- (96) Dohnal, V.; Jezková, A.; Polisenská, I.; Kuca, K. Determination of Fumonisin in Milled Corn Grains Using HPLC-MS. *J. Chromatogr. Sci.* **2010**, *48*, 680–684. <https://doi.org/10.1093/chromsci/48.8.680>.
- (97) Sørensen, L. M.; Mogensen, J.; Nielsen, K. F. Simultaneous Determination of Ochratoxin A, Mycophenolic Acid and Fumonisin B<sub>2</sub> in Meat Products. *Anal. Bioanal. Chem.* **2010**, *398*, 1535–1542. <https://doi.org/10.1007/s00216-010-4059-z>.
- (98) Pradanas-González, F.; Álvarez-Rivera, G.; Benito-Peña, E.; Navarro-Villoslada, F.; Cifuentes, A.; Herrero, M.; Moreno-Bondi, M. C. Mycotoxin Extraction from Edible Insects with Natural Deep Eutectic Solvents: A Green Alternative to Conventional Methods. *J. Chromatogr. A* **2021**, *1648*, 462180. <https://doi.org/10.1016/j.chroma.2021.462180>.
- (99) Kokkonen, M.; Jestoi, M.; Rizzo, A. Determination of Selected Mycotoxins in Mould Cheeses with Liquid Chromatography Coupled to Tandem with Mass Spectrometry. *Food Addit. Contam.* **2005**, *22*, 449–456. <https://doi.org/10.1080/02652030500089861>.
- (100) Zambonin, C. G.; Monaci, L.; Aresta, A. Solid-Phase Microextraction-High Performance Liquid Chromatography and Diode Array Detection for the Determination of Mycophenolic Acid in Cheese. *Food Chem.* **2002**, *78*, 249–254. [https://doi.org/10.1016/S0308-8146\(02\)00108-5](https://doi.org/10.1016/S0308-8146(02)00108-5).
- (101) Streit, F.; Shipkova, M.; Armstrong, V. W.; Oellerich, M. Validation of a Rapid and Sensitive Liquid Chromatography-Tandem Mass Spectrometry Method for Free and Total Mycophenolic Acid. *Clin. Chem.* **2004**, *50*, 152–159. <https://doi.org/10.1373/clinchem.2003.024323>.
- (102) Sørensen, L. M.; Nielsen, K. F.; Jacobsen, T.; Koch, A. G.; Nielsen, P. V.; Frisvad, J. C. Determination of Mycophenolic Acid in Meat Products Using Mixed Mode Reversed Phase-Anion Exchange Clean-up and Liquid Chromatography-High-Resolution Mass Spectrometry. *J. Chromatogr. A* **2008**, *1205*, 103–108. <https://doi.org/10.1016/j.chroma.2008.08.019>.
- (103) Antunes, N. J.; Ince, N.; Raymond, J.; Kipper, K.; Couchman, L.; Holt, D. W.; De Nucci, G.; Johnston, A. Quantification of Mycophenolic Acid in Human Plasma by Liquid Chromatography with Time-of-Flight Mass Spectrometry for Therapeutic Drug Monitoring. *Biomed. Chromatogr.* **2021**, *35*, e5011. <https://doi.org/10.1002/bmc.5011>.
- (104) Musuamba, F. T.; Di Fazio, V.; Vanbinst, R.; Wallemacq, P. A Fast Ultra-Performance Liquid Chromatography Method for Simultaneous Quantification of

- Mycophenolic Acid and Its Phenol- and Acyl-Glucuronides in Human Plasma. *Ther. Drug. Monit.* **2009**, *31*, 110–115. <https://doi.org/10.1097/FTD.0b013e318191897d>.
- (105) Monfort, A.; Jutras, M.; Martin, B.; Boucoiran, I.; Ferreira, E.; Leclair, G. Simultaneous Quantification of 19 Analytes in Breast Milk by Liquid Chromatography-Tandem Mass Spectrometry (LC-MS/MS). *J. Pharm. Biomed.* **2021**, *204*, 114236. <https://doi.org/10.1016/j.jpba.2021.114236>.
- (106) Wiesen, M. H. J.; Farowski, F.; Feldkötter, M.; Hoppe, B.; Müller, C. Liquid Chromatography-Tandem Mass Spectrometry Method for the Quantification of Mycophenolic Acid and Its Phenolic Glucuronide in Saliva and Plasma Using a Standardized Saliva Collection Device. *J. Chromatogr. A* **2012**, *1241*, 52–59. <https://doi.org/10.1016/j.chroma.2012.04.008>.
- (107) Vashist, S. K.; Luong, J. H. T. Chapter 1 - Immunoassays: An Overview. In *Handbook of Immunoassay Technologies*; Vashist, S. K., Luong, J. H. T., Eds.; Academic Press, 2018; pp 1–18. <https://doi.org/10.1016/B978-0-12-811762-0.00001-3>.
- (108) Darwish, I. A. Immunoassay Methods and Their Applications in Pharmaceutical Analysis: Basic Methodology and Recent Advances. *Int. J. Biomed. Sci.* **2006**, *2*, 217–235.
- (109) Goryacheva, I. Y.; De Saeger, S. 5 - Immunochemical Methods for Rapid Mycotoxin Detection in Food and Feed. In *Determining Mycotoxins and Mycotoxigenic Fungi in Food and Feed*; De Saeger, S., Ed.; Woodhead Publishing Series in Food Science, Technology and Nutrition; Woodhead Publishing, 2011; pp 135–167. <https://doi.org/10.1533/9780857090973.1.135>.
- (110) Ohkuma, H.; Abe, K.; Kosaka, Y.; Maeda, M. Detection of Luciferase Having Two Kinds of Luminescent Colour Based on Optical Filter Procedure: Application to an Enzyme Immunoassay. *Luminescence* **2000**, *15*, 21–27. [https://doi.org/10.1002/\(SICI\)1522-7243\(200001/02\)15:1<21::AID-BIO579>3.0.CO;2-8](https://doi.org/10.1002/(SICI)1522-7243(200001/02)15:1<21::AID-BIO579>3.0.CO;2-8).
- (111) Opheim, K. E.; Glick, M. R.; Ou, C. N.; Ryder, K. W.; Hood, L. C.; Ainardi, V.; Collymore, L. A.; DeArmas, W.; Frawley, V. L.; Hutchinson, J. Particle-Enhanced Turbidimetric Inhibition Immunoassay for Theophylline Evaluated with the Du Pont Aca. *Clin. Chem.* **1984**, *30*, 1870–1874.
- (112) Shah, K.; Maghsoudlou, P. Enzyme-Linked Immunosorbent Assay (ELISA): The Basics. *Br. J. Hosp. Med. (Lond.)* **2016**, *77*, C98-101. <https://doi.org/10.12968/hmed.2016.77.7.C98>.
- (113) *The Immunoassay Handbook: Theory and Applications of Ligand Binding, ELISA, and Related Techniques*, 4th ed.; Wild, D., Ed.; Elsevier: Oxford ; Waltham, MA, 2013.
- (114) EMIT 2000 Mycophenolic Acid Assay\* <https://www.siemens-healthineers.com/pe/clinical-specialities/organ-transplant/mycophenolic-acid-assays/emit-2000-mycophenolic> (accessed 2021 -07 -22).
- (115) Therapeutic drug monitoring (TDM) Portfolio <https://diagnostics.roche.com/global/en/products/params/therapeutic-drug-monitoring-tdm.html> (accessed 2021 -07 -22).
- (116) Inmunoensayos, calibradores y controles para ácido micofenólico CEDIA™ <https://www.thermofisher.com/order/catalog/product/100276> (accessed 2021 -07 -22).
- (117) Rebollo, N.; Calvo, M. V.; Martín-Suárez, A.; Domínguez-Gil, A. Modification of the EMIT Immunoassay for the Measurement of Unbound Mycophenolic Acid in Plasma. *Clin. Biochem.* **2011**, *44*, 260–263. <https://doi.org/10.1016/j.clinbiochem.2010.09.025>.
- (118) Dasgupta, A.; Tso, G.; Chow, L. Comparison of Mycophenolic Acid Concentrations Determined by a New PETINIA Assay on the Dimension EXL Analyzer and a HPLC-UV Method. *Clin. Biochem.* **2013**, *46*, 685–687. <https://doi.org/10.1016/j.clinbiochem.2012.11.025>.

- (119) Glahn-Martínez, B.; Benito-Peña, E.; Salis, F.; Descalzo, A. B.; Orellana, G.; Moreno-Bondi, M. C. Sensitive Rapid Fluorescence Polarization Immunoassay for Free Mycophenolic Acid Determination in Human Serum and Plasma. *Anal. Chem.* **2018**, *90*, 5459–5465. <https://doi.org/10.1021/acs.analchem.8b00780>.
- (120) Thompson, M.; Krull, U. J. Biosensors and Bioprobes. *TrAC Trend Anal. Chem.* **1984**, *3*, 173–178. [https://doi.org/10.1016/0165-9936\(84\)87009-0](https://doi.org/10.1016/0165-9936(84)87009-0).
- (121) Mayer, M.; Baeumner, A. J. A Megatrend Challenging Analytical Chemistry: Biosensor and Chemosensor Concepts Ready for the Internet of Things. *Chem. Rev.* **2019**, *119*, 7996–8027. <https://doi.org/10.1021/acs.chemrev.8b00719>.
- (122) Clark, L. C.; Lyons, C. Electrode Systems for Continuous Monitoring in Cardiovascular Surgery. *Annals of the New York Academy of Sciences* **1962**, *102*, 29–45. <https://doi.org/10.1111/j.1749-6632.1962.tb13623.x>.
- (123) D'Orazio, P. Biosensors in Clinical Chemistry. *Clin. Chim. Acta* **2003**, *334*, 41–69. [https://doi.org/10.1016/S0009-8981\(03\)00241-9](https://doi.org/10.1016/S0009-8981(03)00241-9).
- (124) Borisov, S. M.; Wolfbeis, O. S. Optical Biosensors. *Chem. Rev.* **2008**, *108*, 423–461. <https://doi.org/10.1021/cr068105t>.
- (125) Turner, A.; Karube, I.; Wilson, G. S. *Biosensors: Fundamentals and Applications*; Oxford University Press, 1987.
- (126) Nagel, B.; Dellweg, H.; Gierasch, L. M. Glossary for chemists of terms used in biotechnology (IUPAC Recommendations 1992). *Pure Appl. Chem.* **1992**, *64*, 143–168. <https://doi.org/10.1351/pac199264010143>.
- (127) Ligler, F. S. A Perspective on Optical Biosensors and Integrated Sensor Systems. *Anal. Chem.* **2009**, *81*, 519–526. <https://doi.org/10.1021/ac8016289>.
- (128) Chen, C.; Wang, J. Optical Biosensors: An Exhaustive and Comprehensive Review. *Analyst* **2020**, *145*, 1605–1628. <https://doi.org/10.1039/C9AN01998G>.
- (129) Peltomaa, R.; Glahn-Martínez, B.; Benito-Peña, E.; Moreno-Bondi, M. Optical Biosensors for Label-Free Detection of Small Molecules. *Sensors* **2018**, *18*, 4126. <https://doi.org/10.3390/s18124126>.
- (130) Khansili, N.; Rattu, G.; Krishna, P. M. Label-Free Optical Biosensors for Food and Biological Sensor Applications. *Sens. Actuators B: Chem.* **2018**, *265*, 35–49. <https://doi.org/10.1016/j.snb.2018.03.004>.
- (131) Liedberg, B.; Nylander, C.; Lunström, I. Surface Plasmon Resonance for Gas Detection and Biosensing. *Sens. Actuators* **1983**, *4*, 299–304. [https://doi.org/10.1016/0250-6874\(83\)85036-7](https://doi.org/10.1016/0250-6874(83)85036-7).
- (132) Fan, X.; White, I. M.; Shopova, S. I.; Zhu, H.; Suter, J. D.; Sun, Y. Sensitive Optical Biosensors for Unlabeled Targets: A Review. *Anal. Chim. Acta* **2008**, *620*, 8–26. <https://doi.org/10.1016/j.aca.2008.05.022>.
- (133) Cooper, M. A. Optical Biosensors in Drug Discovery. *Nat. Rev. Drug Discov.* **2002**, *1*, 515–528. <https://doi.org/10.1038/nrd838>.
- (134) Markey, F. Principles of Surface Plasmon Resonance. In *Real-Time Analysis of Biomolecular Interactions: Applications of BIACORE*; Nagata, K., Handa, H., Eds.; Springer Japan: Tokyo, 2000; pp 13–22. [https://doi.org/10.1007/978-4-431-66970-8\\_2](https://doi.org/10.1007/978-4-431-66970-8_2).
- (135) Homola, J. Surface Plasmon Resonance Sensors for Detection of Chemical and Biological Species. *Chem. Rev.* **2008**, *108*, 462–493. <https://doi.org/10.1021/cr068107d>.
- (136) Mullett, W.; Lai, E. P.; Yeung, J. M. Immunoassay of Fumonisin by a Surface Plasmon Resonance Biosensor. *Anal. Biochem.* **1998**, *258*, 161–167. <https://doi.org/10.1006/abio.1998.2616>.
- (137) Tüdös, A. J.; Lucas-van den Bos, E. R.; Stigter, E. C. A. Rapid Surface Plasmon Resonance-Based Inhibition Assay of Deoxynivalenol. *J. Agric. Food Chem.* **2003**, *51*, 5843–5848. <https://doi.org/10.1021/jf030244d>.

- (138) Kadota, T.; Takezawa, Y.; Hirano, S.; Tajima, O.; Maragos, C. M.; Nakajima, T.; Tanaka, T.; Kamata, Y.; Sugita-Konishi, Y. Rapid Detection of Nivalenol and Deoxynivalenol in Wheat Using Surface Plasmon Resonance Immunoassay. *Anal. Chim. Acta* **2010**, *673*, 173–178. <https://doi.org/10.1016/j.aca.2010.05.028>.
- (139) Hermanson, G. T. Chapter 1 - Introduction to Bioconjugation. In *Bioconjugate Techniques (Third Edition)*; Hermanson, G. T., Ed.; Academic Press: Boston, 2013; pp 1–125. <https://doi.org/10.1016/B978-0-12-382239-0.00001-7>.
- (140) Kalia, J.; Raines, R. T. Advances in Bioconjugation. *Curr. Org. Chem.* **2010**, *14*, 138–147.
- (141) Demchenko, A. P. *Introduction to Fluorescence Sensing*, 2nd ed.; Springer International Publishing, 2015. <https://doi.org/10.1007/978-3-319-20780-3>.
- (142) Hermanson, G. T. Chapter 10 - Fluorescent Probes. In *Bioconjugate Techniques (Third Edition)*; Hermanson, G. T., Ed.; Academic Press: Boston, 2013; pp 395–463. <https://doi.org/10.1016/B978-0-12-382239-0.00010-8>.
- (143) Coto-García, A. M.; Sotelo-González, E.; Fernández-Argüelles, M. T.; Pereiro, R.; Costa-Fernández, J. M.; Sanz-Medel, A. Nanoparticles as Fluorescent Labels for Optical Imaging and Sensing in Genomics and Proteomics. *Anal. Bioanal. Chem.* **2011**, *399*, 29–42. <https://doi.org/10.1007/s00216-010-4330-3>.
- (144) Holzinger, M.; Le Goff, A.; Cosnier, S. Nanomaterials for Biosensing Applications: A Review. *Front. Chem.* **2014**, *0*. <https://doi.org/10.3389/fchem.2014.00063>.
- (145) Deng, W.; Goldys, E. M. Chemical Sensing with Nanoparticles as Optical Reporters: From Noble Metal Nanoparticles to Quantum Dots and Upconverting Nanoparticles. *Analyst* **2014**, *139*, 5321–5334. <https://doi.org/10.1039/C4AN01272K>.
- (146) Haes, A. J.; Van Duyne, R. P. A Nanoscale Optical Biosensor: Sensitivity and Selectivity of an Approach Based on the Localized Surface Plasmon Resonance Spectroscopy of Triangular Silver Nanoparticles. *J. Am. Chem. Soc.* **2002**, *124*, 10596–10604. <https://doi.org/10.1021/ja020393x>.
- (147) Lok, C.-N.; Ho, C.-M.; Chen, R.; He, Q.-Y.; Yu, W.-Y.; Sun, H.; Tam, P. K.-H.; Chiu, J.-F.; Che, C.-M. Silver Nanoparticles: Partial Oxidation and Antibacterial Activities. *J. Biol. Inorg. Chem.* **2007**, *12*, 527–534. <https://doi.org/10.1007/s00775-007-0208-z>.
- (148) Peltomaa, R.; Amaro-Torres, F.; Carrasco, S.; Orellana, G.; Benito-Peña, E.; Moreno-Bondi, M. C. Homogeneous Quenching Immunoassay for Fumonisin B<sub>1</sub> Based on Gold Nanoparticles and an Epitope-Mimicking Yellow Fluorescent Protein. *ACS Nano* **2018**, *12*, 11333–11342. <https://doi.org/10.1021/acsnano.8b06094>.
- (149) Bruchez, M.; Moronne, M.; Gin, P.; Weiss, S.; Alivisatos, A. P. Semiconductor Nanocrystals as Fluorescent Biological Labels. *Science* **1998**, *281*, 2013–2016. <https://doi.org/10.1126/science.281.5385.2013>.
- (150) Hardman, R. A Toxicologic Review of Quantum Dots: Toxicity Depends on Physicochemical and Environmental Factors. *Environ. Health Perspect.* **2006**, *114*, 165–172. <https://doi.org/10.1289/ehp.8284>.
- (151) Medintz, I. L.; Mattoussi, H. Quantum Dot-Based Resonance Energy Transfer and Its Growing Application in Biology. *Phys. Chem. Chem. Phys.* **2008**, *11*, 17–45. <https://doi.org/10.1039/B813919A>.
- (152) Duan, H.; Li, Y.; Shao, Y.; Huang, X.; Xiong, Y. Multicolor Quantum Dot Nanobeads for Simultaneous Multiplex Immunochromatographic Detection of Mycotoxins in Maize. *Sens. Actuators B: Chem.* **2019**, *291*, 411–417. <https://doi.org/10.1016/j.snb.2019.04.101>.
- (153) Auzel, F. Upconversion and Anti-Stokes Processes with f and d Ions in Solids. *Chem. Rev.* **2004**, *104*, 139–174. <https://doi.org/10.1021/cr020357g>.



- (154) Sagbas, S.; Sahiner, N. 22 - Carbon Dots: Preparation, Properties, and Application. In *Nanocarbon and its Composites*; Khan, A., Jawaid, M., Inamuddin, Asiri, A. M., Eds.; Woodhead Publishing Series in Composites Science and Engineering; Woodhead Publishing, 2019; pp 651–676. <https://doi.org/10.1016/B978-0-08-102509-3.00022-5>.
- (155) Stepanenko, O. V.; Stepanenko, O. V.; Shcherbakova, D. M.; Kuznetsova, I. M.; Turoverov, K. K.; Verkhusha, V. V. Modern fluorescent proteins: from chromophore formation to novel intracellular applications <https://www.future-science.com/doi/abs/10.2144/000113765> (accessed 2021 -08 -05).
- (156) Sakamoto, S.; Shoyama, Y.; Tanaka, H.; Morimoto, S. Application of Green Fluorescent Protein in Immunoassays. *Adv. Biosci. Biotechnol.* **2014**, *5*, 557–563. <https://doi.org/10.4236/abb.2014.56065>.
- (157) The Nobel Prize in Chemistry 2008 <https://www.nobelprize.org/prizes/chemistry/2008/advanced-information/> (accessed 2021 -08 -05).
- (158) Shimomura, O.; Johnson, F. H.; Saiga, Y. Extraction, Purification and Properties of Aequorin, a Bioluminescent Protein from the Luminous Hydromedusan, Aequorea. *J. Cell. Physiol.* **1962**, *59*, 223–239. <https://doi.org/10.1002/jcp.1030590302>.
- (159) Tsien, R. Y. The Green Fluorescent Protein. *Annu. Rev. Biochem.* **1998**, *67*, 509–544. <https://doi.org/10.1146/annurev.biochem.67.1.509>.
- (160) Chudakov, D. M.; Matz, M. V.; Lukyanov, S.; Lukyanov, K. A. Fluorescent Proteins and Their Applications in Imaging Living Cells and Tissues. *Physiol. Rev.* **2010**, *90*, 1103–1163. <https://doi.org/10.1152/physrev.00038.2009>.
- (161) Peltomaa, R.; Agudo-Maestro, I.; Más, V.; Barderas, R.; Benito-Peña, E.; Moreno-Bondi, M. C. Development and Comparison of Mimotope-Based Immunoassays for the Analysis of Fumonisin B1. *Anal. Bioanal. Chem.* **2019**, *411*, 6801–6811. <https://doi.org/10.1007/s00216-019-02068-7>.
- (162) Arcas, J. M.; González, A.; Gers-Barlag, K.; González-González, O.; Bech, F.; Demirkhanyan, L.; Zakharian, E.; Belmonte, C.; Gomis, A.; Viana, F. The Immunosuppressant Macrolide Tacrolimus Activates Cold-Sensing TRPM8 Channels. *J. Neurosci.* **2019**, *39*, 949–969. <https://doi.org/10.1523/JNEUROSCI.1726-18.2018>.
- (163) Huang, R.; Baranov, P.; Lai, K.; Zhang, X.; Ge, J.; Young, M. J. Functional and Morphological Analysis of the Subretinal Injection of Human Retinal Progenitor Cells under Cyclosporin A Treatment. *Mol. Vis.* **2014**, *20*, 1271–1280.
- (164) Rajasekaran, K.; Cary, J. W.; Cotty, P. J.; Cleveland, T. E. Development of a GFP-Expressing *Aspergillus Flavus* Strain to Study Fungal Invasion, Colonization, and Resistance in Cottonseed. *Mycopathologia* **2008**, *165*, 89–97. <https://doi.org/10.1007/s11046-007-9085-9>.
- (165) Blake, C.; Gould, B. J. Use of Enzymes in Immunoassay Techniques. A Review. *Analyst* **1984**, *109*, 533–547. <https://doi.org/10.1039/AN9840900533>.
- (166) Amplex™ Red Reagent <https://www.thermofisher.com/order/catalog/product/A12222> (accessed 2021 -08 -07).
- (167) Fleiss, A.; Sarkisyan, K. S. A Brief Review of Bioluminescent Systems (2019). *Curr. Genet.* **2019**, *65*, 877–882. <https://doi.org/10.1007/s00294-019-00951-5>.
- (168) Yan, Y.; Shi, P.; Song, W.; Bi, S. Chemiluminescence and Bioluminescence Imaging for Biosensing and Therapy: In Vitro and In Vivo Perspectives. *Theranostics* **2019**, *9*, 4047–4065. <https://doi.org/10.7150/thno.33228>.
- (169) Thorne, N.; Inglese, J.; Auld, D. S. Illuminating Insights into Firefly Luciferase and Other Bioluminescent Reporters Used in Chemical Biology. *Chem. Biol.* **2010**, *17*, 646–657. <https://doi.org/10.1016/j.chembiol.2010.05.012>.

- (170) Kirkpatrick, A.; Xu, T.; Ripp, S.; Sayler, G.; Close, D. *Biotechnological Advances in Luciferase Enzymes*; IntechOpen, 2019. <https://doi.org/10.5772/intechopen.85313>.
- (171) England, C. G.; Ehlerding, E. B.; Cai, W. NanoLuc: A Small Luciferase Is Brightening Up the Field of Bioluminescence. *Bioconjug. Chem.* **2016**, *27*, 1175–1187. <https://doi.org/10.1021/acs.bioconjchem.6b00112>.
- (172) NanoLuc® Luciferase: One Enzyme, Endless Capabilities <https://www.promega.es/resources/technologies/nanoluc-luciferase-enzyme/> (accessed 2021 -01 -25).
- (173) Chang, D.; Lindberg, E.; Feng, S.; Angerani, S.; Riezman, H.; Winssinger, N. Luciferase-Induced Photouncaging: Bioluminolysis. *Angew. Chem. Int. Ed.* **2019**, *58*, 16033–16037. <https://doi.org/10.1002/anie.201907734>.
- (174) Bryan, B. J.; Szent-Gyorgyi, C. Luciferases, Fluorescent Proteins, Nucleic Acids Encoding the Luciferases and Fluorescent Proteins and the Use Thereof in Diagnostics, High Throughput Screening and Novelty Items. CA2324648A1, September 30, 1999.
- (175) Wu, N.; Rathnayaka, T.; Kuroda, Y. Bacterial Expression and Re-Engineering of *Gaussia Princeps* Luciferase and Its Use as a Reporter Protein. *Biochim. Biophys. Acta* **2015**, *1854*, 1392–1399. <https://doi.org/10.1016/j.bbapap.2015.05.008>.
- (176) Rathnayaka, T.; Tawa, M.; Sohya, S.; Yohda, M.; Kuroda, Y. Biophysical Characterization of Highly Active Recombinant *Gaussia* Luciferase Expressed in *Escherichia Coli*. *Biochim. Biophys. Acta* **2010**, *1804*, 1902–1907. <https://doi.org/10.1016/j.bbapap.2010.04.014>.
- (177) *Recognition Receptors in Biosensors*; Zourob, M., Ed.; Springer New York: New York, NY, 2010. <https://doi.org/10.1007/978-1-4419-0919-0>.
- (178) Olsson, T. S. G.; Williams, M. A.; Pitt, W. R.; Ladbury, J. E. The Thermodynamics of Protein–Ligand Interaction and Solvation: Insights for Ligand Design. *J. Mol. Biol.* **2008**, *384*, 1002–1017. <https://doi.org/10.1016/j.jmb.2008.09.073>.
- (179) Zhu, Y.-C.; Mei, L.-P.; Ruan, Y.-F.; Zhang, N.; Zhao, W.-W.; Xu, J.-J.; Chen, H.-Y. Chapter 8 - Enzyme-Based Biosensors and Their Applications. In *Advances in Enzyme Technology*; Singh, R. S., Singhania, R. R., Pandey, A., Larroche, C., Eds.; Biomass, Biofuels, Biochemicals; Elsevier, 2019; pp 201–223. <https://doi.org/10.1016/B978-0-444-64114-4.00008-X>.
- (180) Zhao, W.-W.; Xu, J.-J.; Chen, H.-Y. Photoelectrochemical Enzymatic Biosensors. *Biosens. Bioelectron.* **2017**, *92*, 294–304. <https://doi.org/10.1016/j.bios.2016.11.009>.
- (181) Amine, A.; Mohammadi, H.; Bourais, I.; Palleschi, G. Enzyme Inhibition-Based Biosensors for Food Safety and Environmental Monitoring. *Biosens. Bioelectron.* **2006**, *21*, 1405–1423. <https://doi.org/10.1016/j.bios.2005.07.012>.
- (182) Patel, P. D. (Bio)Sensors for Measurement of Analytes Implicated in Food Safety: A Review. *TrAC Trend. Anal. Chem.* **2002**, *21*, 96–115. [https://doi.org/10.1016/S0165-9936\(01\)00136-4](https://doi.org/10.1016/S0165-9936(01)00136-4).
- (183) Arduini, F.; Amine, A.; Moscone, D.; Palleschi, G. Biosensors Based on Cholinesterase Inhibition for Insecticides, Nerve Agents and Aflatoxin B1 Detection (Review). *Microchim. Acta* **2010**, *170*, 193–214. <https://doi.org/10.1007/s00604-010-0317-1>.
- (184) Arduini, F.; Errico, I.; Amine, A.; Micheli, L.; Palleschi, G.; Moscone, D. Enzymatic Spectrophotometric Method for Aflatoxin B Detection Based on Acetylcholinesterase Inhibition. *Anal. Chem.* **2007**, *79*, 3409–3415. <https://doi.org/10.1021/ac061819j>.
- (185) Morales, M. A.; Mark Halpern, J. Guide to Selecting a Biorecognition Element for Biosensors. *Bioconjug. Chem.* **2018**, *29*, 3231–3239. <https://doi.org/10.1021/acs.bioconjchem.8b00592>.

- (186) Odenthal, K. J.; Gooding, J. J. An Introduction to Electrochemical DNA Biosensors. *Analyst* **2007**, *132*, 603–610. <https://doi.org/10.1039/B701816A>.
- (187) Gui, Q.; Lawson, T.; Shan, S.; Yan, L.; Liu, Y. The Application of Whole Cell-Based Biosensors for Use in Environmental Analysis and in Medical Diagnostics. *Sensors (Basel)* **2017**, *17*, 1623. <https://doi.org/10.3390/s17071623>.
- (188) Liu, Q.; Wu, C.; Cai, H.; Hu, N.; Zhou, J.; Wang, P. Cell-Based Biosensors and Their Application in Biomedicine. *Chem. Rev.* **2014**, *114*, 6423–6461. <https://doi.org/10.1021/cr2003129>.
- (189) Dambrin, C.; Klupp, J.; Morris, R. E. Pharmacodynamics of Immunosuppressive Drugs. *Curr. Opin. Immunol.* **2000**, *12*, 557–562. [https://doi.org/10.1016/S0952-7915\(00\)00138-2](https://doi.org/10.1016/S0952-7915(00)00138-2).
- (190) Jr, C. A. J.; Travers, P.; Walport, M.; Shlomchik, M. J.; Jr, C. A. J.; Travers, P.; Walport, M.; Shlomchik, M. J. *Immunobiology*, 5th ed.; Garland Science, 2001.
- (191) Vidarsson, G.; Dekkers, G.; Rispen, T. IgG Subclasses and Allotypes: From Structure to Effector Functions. *Front. Immunol.* **2014**, *5*, 520. <https://doi.org/10.3389/fimmu.2014.00520>.
- (192) Schroeder, H. W.; Cavacini, L. Structure and Function of Immunoglobulins. *J Allergy Clin. Immunol.* **2010**, *125*, S41–S52. <https://doi.org/10.1016/j.jaci.2009.09.046>.
- (193) Cooper, H. M.; Paterson, Y. Production of Polyclonal Antisera. *Curr Protoc Neurosci* **2009**, Chapter 5, Unit 5.5. <https://doi.org/10.1002/0471142301.ns0505s48>.
- (194) Zhou, S.; Xu, L.; Kuang, H.; Xiao, J.; Xu, C. Immunoassays for Rapid Mycotoxin Detection: State of the Art. *Analyst* **2020**, *145*, 7088–7102. <https://doi.org/10.1039/D0AN01408G>.
- (195) Bazin, I.; Tria, S. A.; Hayat, A.; Marty, J.-L. New Biorecognition Molecules in Biosensors for the Detection of Toxins. *Biosens. Bioelectron.* **2017**, *87*, 285–298. <https://doi.org/10.1016/j.bios.2016.06.083>.
- (196) National Research Council (US) Committee on Methods of Producing Monoclonal Antibodies. *Monoclonal Antibody Production*; The National Academies Collection: Reports funded by National Institutes of Health; National Academies Press (US): Washington (DC), 1999.
- (197) Madrakian, T.; Soleimani, M.; Afkhami, A. Simultaneous Determination of Mycophenolate Mofetil and Its Active Metabolite, Mycophenolic Acid, by Differential Pulse Voltammetry Using Multi-Walled Carbon Nanotubes Modified Glassy Carbon Electrode. *Mater. Sci. Eng. C. Mater. Biol. Appl.* **2014**, *42*, 38–45. <https://doi.org/10.1016/j.msec.2014.05.012>.
- (198) Hossein Momeneh; Mohammad Bagher Gholivand. Mycophenolate Mofetil Sensor Based on Molecularly Imprinted Polymer/Multi-Walled Carbon Nanotubes Modified Carbon Paste Electrode. *Anal. biochem.* **2018**, *557*, 97–103. <https://doi.org/10.1016/j.ab.2018.07.014>.
- (199) Vergara Chozas, J. M.; Sáez-Benito Godino, A.; Zopeque García, N.; García Pinteño, S.; Joumady, I.; Carrasco García, C.; Vara Gil, F. Analytical Validation of a Homogeneous Immunoassay for Determination of Mycophenolic Acid in Human Plasma. *Transplant. Proc.* **2012**, *44*, 2669–2672. <https://doi.org/10.1016/j.transproceed.2012.09.063>.
- (200) Antti Tullila; Tarja Nevanen. Utilization of Multi-Immunization and Multiple Selection Strategies for Isolation of Hapten-Specific Antibodies from Recombinant Antibody Phage Display Libraries. *IJMS* **2017**, *18*, 1169. <https://doi.org/10.3390/ijms18061169>.
- (201) Wang, S.; Gao, H.; Wei, Z.; Zhou, J.; Ren, S.; He, J.; Luan, Y.; Lou, X. Shortened and Multivalent Aptamers for Ultrasensitive and Rapid Detection of Alternariol in

- Wheat Using Optical Waveguide Sensors. *Biosens. Bioelectron.* **2022**, *196*, 113702. <https://doi.org/10.1016/j.bios.2021.113702>.
- (202) Mirón-Mérida, V. A.; González-Espinosa, Y.; Collado-González, M.; Gong, Y. Y.; Guo, Y.; Goycoolea, F. M. Aptamer-Target-Gold Nanoparticle Conjugates for the Quantification of Fumonisin B<sub>1</sub>. *Biosensors* **2021**, *11*, 18. <https://doi.org/10.3390/bios11010018>.
- (203) Zou, L.; Xu, Y.; Li, Y.; He, Q.; Chen, B.; Wang, D. Development of a Single-Chain Variable Fragment Antibody-Based Enzyme-Linked Immunosorbent Assay for Determination of Fumonisin B<sub>1</sub> in Corn Samples. *J. Sci. Food Agric.* **2014**, *94*, 1865–1871. <https://doi.org/10.1002/jsfa.6505>.
- (204) Liu, X.; Xu, Y.; He, Q.; He, Z.; Xiong, Z. Application of Mimotope Peptides of Fumonisin B<sub>1</sub> in Peptide ELISA. *J. Agric. Food Chem.* **2013**, *61*, 4765–4770. <https://doi.org/10.1021/jf400056p>.
- (205) Xu, Y.; Chen, B.; He, Q.; Qiu, Y.-L.; Liu, X.; He, Z.; Xiong, Z. New Approach for Development of Sensitive and Environmentally Friendly Immunoassay for Mycotoxin Fumonisin B<sub>1</sub> Based on Using Peptide-MBP Fusion Protein as Substitute for Coating Antigen. *Anal. Chem.* **2014**, *86*, 8433–8440. <https://doi.org/10.1021/ac502037w>.
- (206) Lu, L.; Seenivasan, R.; Wang, Y.-C.; Yu, J.-H.; Gunasekaran, S. An Electrochemical Immunosensor for Rapid and Sensitive Detection of Mycotoxins Fumonisin B<sub>1</sub> and Deoxynivalenol. *Electrochim. Acta* **2016**, *213*, 89–97. <https://doi.org/10.1016/j.electacta.2016.07.096>.
- (207) Wei, H.; Wang, E. Nanomaterials with Enzyme-like Characteristics (Nanozymes): Next-Generation Artificial Enzymes. *Chem. Soc. Rev.* **2013**, *42*, 6060–6093. <https://doi.org/10.1039/C3CS35486E>.
- (208) BelBruno, J. J. Molecularly Imprinted Polymers. *Chem. Rev.* **2019**, *119*, 94–119. <https://doi.org/10.1021/acs.chemrev.8b00171>.
- (209) Haupt, K.; Medina Rangel, P. X.; Bui, B. T. S. Molecularly Imprinted Polymers: Antibody Mimics for Bioimaging and Therapy. *Chem. Rev.* **2020**, *120*, 9554–9582. <https://doi.org/10.1021/acs.chemrev.0c00428>.
- (210) Holliger, P.; Hudson, P. J. Engineered Antibody Fragments and the Rise of Single Domains. *Nat. Biotechnol.* **2005**, *23*, 1126–1136. <https://doi.org/10.1038/nbt1142>.
- (211) Crivianu-Gaita, V.; Thompson, M. Aptamers, Antibody ScFv, and Antibody Fab' Fragments: An Overview and Comparison of Three of the Most Versatile Biosensor Biorecognition Elements. *Biosens. Bioelectron.* **2016**, *85*, 32–45. <https://doi.org/10.1016/j.bios.2016.04.091>.
- (212) Zhao, F.; Shi, R.; Liu, R.; Tian, Y.; Yang, Z. Application of Phage-Display Developed Antibody and Antigen Substitutes in Immunoassays for Small Molecule Contaminants Analysis: A Mini-Review. *Food Chem.* **2021**, *339*, 128084. <https://doi.org/10.1016/j.foodchem.2020.128084>.
- (213) Smith, G. P.; Petrenko, V. A. Phage Display. *Chem. Rev.* **1997**, *97*, 391–410. <https://doi.org/10.1021/cr960065d>.
- (214) Smith, G. P. Filamentous Fusion Phage: Novel Expression Vectors That Display Cloned Antigens on the Virion Surface. *Science* **1985**, *228*, 1315–1317. <https://doi.org/10.1126/science.4001944>.
- (215) Scott, J. K.; Smith, G. P. Searching for Peptide Ligands with an Epitope Library. *Science* **1990**, *249*, 386–390. <https://doi.org/10.1126/science.1696028>.
- (216) Devlin, J. J.; Panganiban, L. C.; Devlin, P. E. Random Peptide Libraries: A Source of Specific Protein Binding Molecules. *Science* **1990**, *249*, 404–406. <https://doi.org/10.1126/science.2143033>.

- (217) McCafferty, J.; Griffiths, A. D.; Winter, G.; Chiswell, D. J. Phage Antibodies: Filamentous Phage Displaying Antibody Variable Domains. *Nature* **1990**, *348*, 552–554. <https://doi.org/10.1038/348552a0>.
- (218) Winter, G.; Griffiths, A. D.; Hawkins, R. E.; Hoogenboom, H. R. Making Antibodies by Phage Display Technology. *Annu. Rev. Immunol.* **1994**, *12*, 433–455. <https://doi.org/10.1146/annurev.iy.12.040194.002245>.
- (219) Hoogenboom, H. R.; Griffiths, A. D.; Johnson, K. S.; Chiswell, D. J.; Hudson, P.; Winter, G. Multi-Subunit Proteins on the Surface of Filamentous Phage: Methodologies for Displaying Antibody (Fab) Heavy and Light Chains. *Nucleic Acids Res.* **1991**, *19*, 4133–4137.
- (220) The Nobel Prize in Chemistry 2018 <https://www.nobelprize.org/prizes/chemistry/2018/summary/> (accessed 2021 -04 -11).
- (221) Barderas, R.; Benito-Peña, E. The 2018 Nobel Prize in Chemistry: Phage Display of Peptides and Antibodies. *Anal. Bioanal. Chem.* **2019**, *411*, 2475–2479. <https://doi.org/10.1007/s00216-019-01714-4>.
- (222) Domingo-Calap, P.; Delgado-Martínez, J. Bacteriophages: Protagonists of a Post-Antibiotic Era. **2018**, *16*.
- (223) *Bacteriophages: Biology and Applications*; Kutter, E., Sulakvelidze, A., Eds.; CRC Press: Boca Raton, FL, 2005.
- (224) Bradley, D. E. Ultrastructure of Bacteriophages and Bacteriocins. *BACTERIOL. REV.* **85**.
- (225) Rohwer, F.; Edwards, R. The Phage Proteomic Tree: A Genome-Based Taxonomy for Phage. *J. BACTERIOL.* **2002**, *184*, 7.
- (226) Ackermann, H.-W. Bacteriophage Observations and Evolution. *Res. Microbiol.* **2003**, *154*, 245–251. [https://doi.org/10.1016/S0923-2508\(03\)00067-6](https://doi.org/10.1016/S0923-2508(03)00067-6).
- (227) Ackermann, H.-W. 5500 Phages Examined in the Electron Microscope. *Arch. Virol.* **2007**, *152*, 227–243. <https://doi.org/10.1007/s00705-006-0849-1>.
- (228) Barbas, C. F.; Burton, D. R.; Silverman, G. J. *Phage Display: A Laboratory Manual*; CSHL Press, 2004.
- (229) Sidhu, S. S.; Geyer, C. R. *Phage Display In Biotechnology and Drug Discovery*; CRC Press, 2015.
- (230) Beck, E.; Sommer, R.; Auerswald, E. A.; Kurz, Ch.; Zink, B.; Osterburg, G.; Schaller, H.; Sugimoto, K.; Sugisaki, H.; Okamoto, T.; Takanami, M. Nucleotide Sequence of Bacteriophage Fd DNA. *Nucleic Acids Res.* **1978**, *5*, 4495–4504. <https://doi.org/10.1093/nar/5.12.4495>.
- (231) van Wezenbeek, P. M.; Hulsebos, T. J.; Schoenmakers, J. G. Nucleotide Sequence of the Filamentous Bacteriophage M13 DNA Genome: Comparison with Phage Fd. *Gene* **1980**, *11*, 129–148. [https://doi.org/10.1016/0378-1119\(80\)90093-1](https://doi.org/10.1016/0378-1119(80)90093-1).
- (232) Beck, E.; Zink, B. Nucleotide Sequence and Genome Organisation of Filamentous Bacteriophages Fl and Fd. *Gene* **1981**, *16*, 35–58. [https://doi.org/10.1016/0378-1119\(81\)90059-7](https://doi.org/10.1016/0378-1119(81)90059-7).
- (233) Marvin, D. A.; Hohn, B. Filamentous Bacterial Viruses. *Bacteriol. Rev.* **1969**, *33*, 172–209.
- (234) Houshmand, H.; Fröman, G.; Magnusson, G. Use of Bacteriophage T7 Displayed Peptides for Determination of Monoclonal Antibody Specificity and Biosensor Analysis of the Binding Reaction. *Anal. Biochem.* **1999**, *268*, 363–370. <https://doi.org/10.1006/abio.1998.3076>.
- (235) Ansuini, H.; Cicchini, C.; Nicosia, A.; Tripodi, M.; Cortese, R.; Luzzago, A. Biotin-tagged cDNA Expression Libraries Displayed on Lambda Phage: A New Tool for the

- Selection of Natural Protein Ligands. *Nucleic Acids Res.* **2002**, *30*, e78–e78. <https://doi.org/10.1093/nar/gnf077>.
- (236) Clackson, T.; Wells, J. A. In Vitro Selection from Protein and Peptide Libraries. *Trend. Biotechnol.* **1994**, *12*, 173–184. [https://doi.org/10.1016/0167-7799\(94\)90079-5](https://doi.org/10.1016/0167-7799(94)90079-5).
- (237) Iannolo, G.; Minenkova, O.; Petruzzelli, R.; Cesareni, G. Modifying Filamentous Phage Capsid: Limits in the Size of the Major Capsid Protein. *J. Mol. Biol.* **1995**, *248*, 835–844. <https://doi.org/10.1006/jmbi.1995.0264>.
- (238) Jespers, L. S.; Messens, J. H.; Keyser, A. D.; Eeckhout, D.; Brande, I. V. D.; Gansemans, Y. G.; Lauwereys, M. J.; Vlasuk, G. P.; Stanssens, P. E. Surface Expression and Ligand-Based Selection of cDNAs Fused to Filamentous Phage Gene VI. *Bio/Technology* **1995**, *13*, 378–382. <https://doi.org/10.1038/nbt0495-378>.
- (239) Gao, C.; Mao, S.; Lo, C.-H. L.; Wirsching, P.; Lerner, R. A.; Janda, K. D. Making Artificial Antibodies: A Format for Phage Display of Combinatorial Heterodimeric Arrays. *Proc. Natl. Acad. Sci. U.S.A.* **1999**, *96*, 6025–6030.
- (240) Jacobson, A. Role of F Pili in the Penetration of Bacteriophage Fl. *J. Virol.* **1972**, *10*, 835–843.
- (241) Smith, G. P.; Scott, J. K. [15] Libraries of Peptides and Proteins Displayed on Filamentous Phage. In *Methods in Enzymology; Recombinant DNA Part H*; Academic Press, 1993; Vol. 217, pp 228–257. [https://doi.org/10.1016/0076-6879\(93\)17065-D](https://doi.org/10.1016/0076-6879(93)17065-D).
- (242) Malik, P.; Terry, T. D.; Gowda, L. R.; Langara, A.; Petukhov, S. A.; Symmons, M. F.; Welsh, L. C.; Marvin, D. A.; Perham, R. N. Role of Capsid Structure and Membrane Protein Processing in Determining the Size and Copy Number of Peptides Displayed on the Major Coat Protein of Filamentous Bacteriophage. *J. Mol. Biol.* **1996**, *260*, 9–21. <https://doi.org/10.1006/jmbi.1996.0378>.
- (243) Wang, X.-H.; Wang, S. Sensors and Biosensors for the Determination of Small Molecule Biological Toxins. *Sensors (Basel)* **2008**, *8*, 6045–6054. <https://doi.org/10.3390/s8096045>.
- (244) Peltomaa, R.; Benito-Peña, E.; Barderas, R.; Moreno-Bondi, M. C. Phage Display in the Quest for New Selective Recognition Elements for Biosensors. *ACS Omega* **2019**, *4*, 11569–11580. <https://doi.org/10.1021/acsomega.9b01206>.
- (245) Alfaleh, M. A.; Alsaab, H. O.; Mahmoud, A. B.; Alkayyal, A. A.; Jones, M. L.; Mahler, S. M.; Hashem, A. M. Phage Display Derived Monoclonal Antibodies: From Bench to Bedside. *Front. Immunol.* **2020**, *11*. <https://doi.org/10.3389/fimmu.2020.01986>.
- (246) Leivo, J.; Kivimäki, L.; Juntunen, E.; Pettersson, K.; Lamminmäki, U. Development of Anti-Immuno-complex Specific Antibodies and Non-Competitive Time-Resolved Fluorescence Immunoassay for the Detection of Estradiol. *Anal. Bioanal. Chem.* **2019**, *411*, 5633–5639. <https://doi.org/10.1007/s00216-019-01952-6>.
- (247) Hua, X.; Zhou, L.; Feng, L.; Ding, Y.; Shi, H.; Wang, L.; Gee, S. J.; Hammock, B. D.; Wang, M. Competitive and Noncompetitive Phage Immunoassays for the Determination of Benzothiostrubin. *Anal. Chim. Acta* **2015**, *890*, 150–156. <https://doi.org/10.1016/j.aca.2015.07.056>.
- (248) Kim, H.-J.; Rossotti, M. A.; Ahn, K. C.; González-Sapienza, G. G.; Gee, S. J.; Musker, R.; Hammock, B. D. Development of a Noncompetitive Phage Anti-Immuno-complex Assay for Brominated Diphenyl Ether 47. *Anal. Biochem.* **2010**, *401*, 38–46. <https://doi.org/10.1016/j.ab.2010.01.040>.
- (249) Persson, H.; Lantto, J.; Ohlin, M. A Focused Antibody Library for Improved Hapten Recognition. *J. Mol. Biol.* **2006**, *357*, 607–620. <https://doi.org/10.1016/j.jmb.2006.01.004>.
- (250) Stephen, C. W.; Helminen, P.; Lane, D. P. Characterisation of Epitopes on Human P53 Using Phage-Displayed Peptide Libraries: Insights into Antibody-Peptide Interactions. *J. Mol. Biol.* **1995**, *248*, 58–78. <https://doi.org/10.1006/jmbi.1995.0202>.

- (251) Chen, H.; Yang, Q.; Ding, Y.; Vasylieva, N.; Bever, C. S.; Hua, X.; Wang, M.; Hammock, B. D. Competitive and Noncompetitive Immunoassays for the Detection of Benzothiostrubin Using Magnetic Nanoparticles and Fluorescein Isothiocyanate-Labeled Peptides. *Anal. Bioanal. Chem.* **2019**, *411*, 527–535. <https://doi.org/10.1007/s00216-018-1478-8>.
- (252) Rossotti, M. A.; Carlomagno, M.; González-Techera, A.; Hammock, B. D.; Last, J.; González-Sapienza, G. Phage Anti-Immunoassay for Clomazone: Two-Site Recognition Increasing Assay Specificity and Facilitating Adaptation into an On-Site Format. *Anal. Chem.* **2010**, *82*, 8838–8843. <https://doi.org/10.1021/ac101476f>.
- (253) Feng, L.; Jin, J.; Zhang, L.-F.; Yan, T.; Tao, W.-Y. Analysis of the Resveratrol-Binding Protein Using Phage-Displayed Random Peptide Library. *Acta Biochim. Biophys. Sin.* **2006**, *38*, 342–348. <https://doi.org/10.1111/j.1745-7270.2006.00163.x>.
- (254) Smith, M. W.; Smith, J. W.; Harris, C.; Brancale, A.; Allender, C. J.; Gumbleton, M. Phage Display Identification of Functional Binding Peptides against 4-Acetamidophenol (Paracetamol): An Exemplified Approach to Target Low Molecular Weight Organic Molecules. *Biochem. Biophys. Res. Com.* **2007**, *358*, 285–291. <https://doi.org/10.1016/j.bbrc.2007.04.122>.
- (255) Dong, J.-X.; Xu, C.; Wang, H.; Xiao, Z.-L.; Gee, S. J.; Li, Z.-F.; Wang, F.; Wu, W.-J.; Shen, Y.-D.; Yang, J.-Y.; Sun, Y.-M.; Hammock, B. D. Enhanced Sensitive Immunoassay: Noncompetitive Phage Anti-Immune Complex Assay for the Determination of Malachite Green and Leucomalachite Green. *J. Agric. Food Chem.* **2014**, *7*.
- (256) Peltomaa, R.; Benito-Peña, E.; Barderas, R.; Sauer, U.; González Andrade, M.; Moreno-Bondi, M. C. Microarray-Based Immunoassay with Synthetic Mimotopes for the Detection of Fumonisin B<sub>1</sub>. *Anal. Chem.* **2017**, *89*, 6216–6223. <https://doi.org/10.1021/acs.analchem.7b01178>.
- (257) Peltomaa, R.; Fikacek, S.; Benito-Peña, E.; Barderas, R.; Head, T.; Deo, S.; Daunert, S.; Moreno-Bondi, M. C. Bioluminescent Detection of Zearalenone Using Recombinant Peptidomimetic Gaussia Luciferase Fusion Protein. *Microchim. Acta* **2020**, *187*, 547. <https://doi.org/10.1007/s00604-020-04538-7>.





## 2. AIMS OF THE STUDY

The main objective for this thesis was the selection and design of novel molecular recognition elements for the development of optical biosensors. For this aim, the selection and characterization of novel mimopeptides, used as recognition elements, for a series of mycotoxins was described applying the phage display technology. These selected recognition elements needed to fit the requirements of high sensitivity and selectivity in order to be considered competent for the development of optical biosensors. Then, they were used in a variety of assay formats to develop sensitive biosensors for several mycotoxins with a focus on both clinical and food quality fields. The aims of this thesis are listed below:

- Selection and characterization of novel mimopeptides for mycophenolic acid, ochratoxin A and alternariol by phage display technology.
  - Development of a variety of panning strategies for the selection of mimopeptides.
  - Selection of individual phage clones and evaluation of their sensitivity by competitive phage-based ELISAs.
  - Sequencing and characterization of the best competitors for each mycotoxin.
- Development of an immunoassay for the sensitive detection of mycophenolic acid in blood samples of transplanted patients.
  - Analysis of the binding kinetics of the mycophenolic acid mimopeptide by SPR and NMR characterization of the mimopeptide's disulfide bond.
  - Construction and characterization of NanoLuc-based fusion proteins.
  - Development and optimization of a sensitive immunoassay on magnetic beads with the bioluminescent fusion proteins.
  - Analysis of free MPA in blood samples from transplanted patients and method validation.
- Conduct a comparative study of the performance of two luciferases for the development of an immunoassay to detect fumonisin in wheat samples.
  - Construction of two different fusion proteins using *Gaussia* luciferase and NanoLuc luciferase in combination with a fumonisin mimopeptide.
  - Expression and purification of both fusion proteins.
  - Development and optimization of immunoassays for the analysis of fumonisin in wheat samples.
  - Analysis of spiked wheat samples, a wheat reference material and real wheat samples, as well as a validation of the method by HPLC-MS/MS.



### **3. SELECTION OF MIMOPEPTIDES BY PHAGE DISPLAY**

#### **3.1. Introduction**

##### 3.1.1. Phage-display libraries

###### *3.1.1.1. Antibody libraries*

###### *3.1.1.2. Peptide libraries*

##### 3.1.2. Selection of mimopeptides by phage display

#### **3.2. Objectives**

#### **3.3. Experimental part**

##### 3.3.1. Reagents and solutions

##### 3.3.2. Analytical instrumentation and materials

##### 3.3.3. Experimental procedures

###### *3.3.3.1. Antibody coupling to magnetic beads*

###### *3.3.3.2. Neutravidin coupling to magnetic beads*

###### *3.3.3.3. Antibody biotinylation*

###### *3.3.3.4. Panning rounds*

###### *3.3.3.5. Phage amplification*

###### *3.3.3.6. Phage titering*

###### *3.3.3.7. Selection of monoclonal phages*

###### *3.3.3.8. Phage-based ELISAs*

###### *3.3.3.9. Confirmatory bead-based phage-ELISA*

###### *3.3.3.10. DNA amplification and purification of phage clones*

#### **3.4. Results and discussion**

##### 3.4.1. Selection of mimopeptides for mycophenolic acid

###### *3.4.1.1. Panning strategies*

###### *3.4.1.2. Selection of MPA mimopeptides by phage-based ELISA*

###### *3.4.1.3. Sequence and structural analysis of MPA mimopeptide*

##### 3.4.2. Selection of mimopeptides for ochratoxin A

###### *3.4.2.1. Panning strategies*

###### *3.4.2.2. Selection of OTA mimopeptides by phage-based ELISA*

### 3.4.3. Selection of mimopeptides for alternariol

#### 3.4.3.1. *Panning strategies*

#### 3.4.3.2. *Selection of AOH mimopeptides by phage-based ELISA*

#### 3.4.3.3. *Sequence and structural analysis of AOH mimopeptides*

### **3.5. Conclusions**

### **3.6. Bibliography**

## 3.1. Introduction

### 3.1.1. Phage-display libraries

As described in **Chapter 1**, phages can be genetically modified to express a foreign sequence on one of their coat proteins. The heterogeneous mixture of a plethora of DNA-modified phages expressing different sequences is known as a phage-display library.<sup>1</sup> Currently, commercial libraries include up to several billions of different phage clones. Both antibody and peptide libraries are of great interest for the discovery of new binders to nearly any molecule and will be discussed below.

#### 3.1.1.1. Antibody libraries

The discovery of new recombinant antibodies is considered one of the biggest breakthroughs of the phage display technology. One of the main reasons behind the popularity of this technique is the versatility of phage display libraries.<sup>31</sup> Theoretically, many different antibodies for almost any antigen could be obtained with the use of just one library. Even if the production of full-length IgG antibodies has been reported previously.<sup>32</sup> Phage display libraries mainly consist of antibody fragments such as Fab, scFv, VHH (camel heavy chain variable domain) and dAbs (domain antibodies/human heavy chain variable domain).<sup>33–37</sup>

Phage display antibody libraries can be of various kinds. On the one hand, immune libraries can be manufactured from the variable (V) genes of antibodies extracted from previously immunized species.<sup>38</sup> This approach is more oriented to medical applications as these libraries are already biased towards a specific antigen, therefore, antibodies for that specific target could be easily obtained.<sup>33</sup> On the other hand, synthetic, semisynthetic and naive libraries represent a more versatile alternative for antibody selection.<sup>33</sup> They are frequently referred to as “single-pot” libraries, as they provide non-biased antibody fragments that could potentially bind to any target.<sup>39</sup> Synthetic libraries are completely designed *in vitro*. They use oligonucleotides to provide more diversity to the hypervariable complementarity determining regions (CDRs) of one or more V genes of an immunoglobulin. Contrary to the *in vivo* designed libraries, the synthetic ones avoid any kind of bias thanks to the possible control over the V genes.<sup>40</sup> Naive, or nonimmunized libraries are crafted from rearranged V genes coming from B cells of species that have not been immunized before.<sup>33</sup> Semi-synthetic libraries are typically a combination of the two libraries described previously and they provide both, the natural as well as the functional diversity of naive and synthetic libraries.<sup>40</sup>

The size of the library can be of great importance when selecting antibodies.<sup>39</sup> It has been proven that smaller antibody libraries, of about  $10^7$  different clones, can provide antibodies with affinities in the micromolar range. Nonetheless, if the size of the library is increased up to  $10^9$ – $10^{10}$  different clones, the affinities of the antibodies obtained can be in the nanomolar range.<sup>41</sup> One of the best examples of the applicability of antibody phage display is the possibility to obtain therapeutic antibodies. For example, Humira is a well-known recombinant antibody found in a human phage display library that targets human tumor necrosis factor (TNF). This antibody was approved by the US Food and Drug Administration almost twenty years ago for therapeutic use, and it is currently applied to treat illnesses such as rheumatoid arthritis and Crohn’s disease.<sup>42–44</sup>

### 3.1.1.2. Peptide libraries

Despite the fact that antibody phage display is considered the most outstanding application, peptide libraries were the starting point of phage display. The main purpose of peptide libraries is to find binders that mimic the behavior of a native ligand to its binding site, which can either be a receptor, an antibody, an enzyme or even another peptide.<sup>16</sup> The first examples of peptide libraries arose a few years after G. Smith published the first paper on phage display.<sup>2</sup> These first examples targeted binders for different proteins, such as the protein myohemerythrin,<sup>3</sup> streptavidin,<sup>4</sup> and  $\beta$ -endorphin,<sup>45</sup> using libraries with 6 to 15-residue peptide sequences. In fact, peptide libraries can be of varying length and morphology (**Figure 10**).<sup>1</sup> Besides linear-displayed sequences, it is common to find libraries that contain disulfide bonds displaying a loop-shaped sequence,<sup>46</sup> or others, with typical residues found in  $\alpha$ -helices.<sup>47</sup> Regarding length, numerous examples were reported of the display of different peptide sizes, mainly on pIII and pVIII, in which the number of randomized residues can result as low as 4,<sup>48</sup> or high as 40.<sup>49</sup> However, even when large peptide sequences are displayed, it is believed that only a small number of these residues interact with the target molecule.<sup>16</sup>

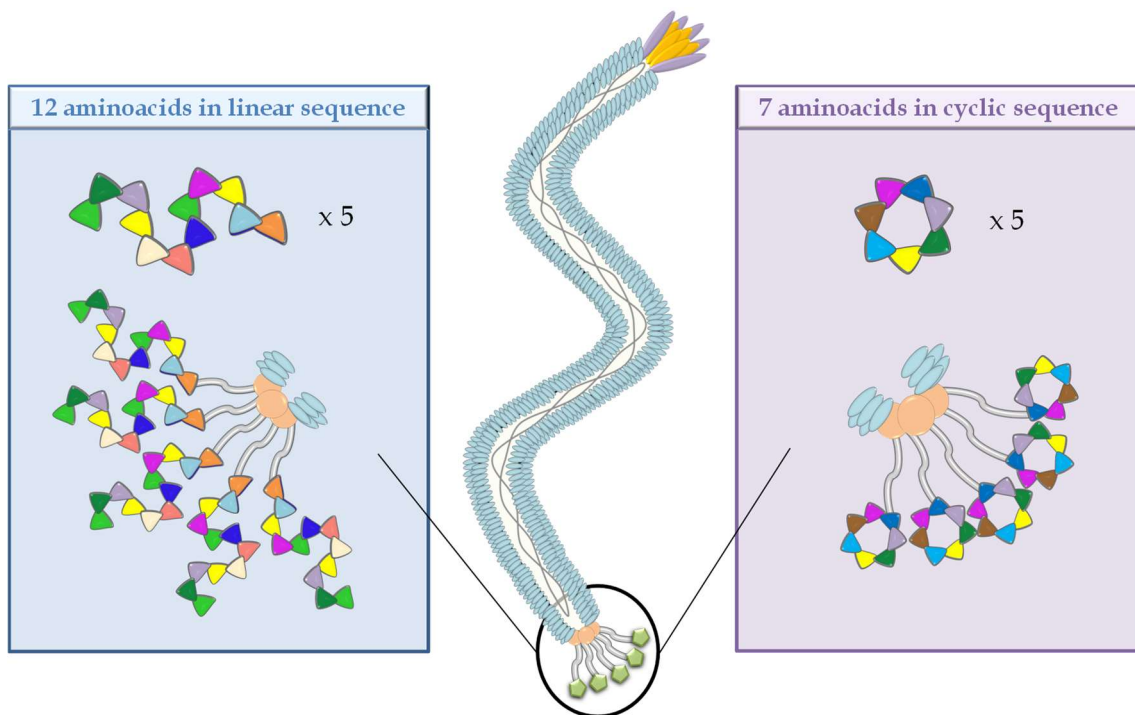


**Figure 10.** Two different examples of phage-displayed peptide libraries. On both cases, the sequences are displayed on pIII of an M13 phage. On the left hand, a pentavalent display of a 12-amino acid linear sequence is portrayed, whereas on the right hand, a sequence of 7 amino acids forming a loop-shaped peptide is depicted.

The libraries described previously use oligonucleotides that have been modified in order to include a randomized peptide sequence into the phage or phagemid genome. Every randomized residue is generally encoded by a NNK or NNS codon, in which N refers to any nucleotide, adenine (A), thymine (T), cytosine (C) or guanine (G); K stands for G and T; and S for G and C.<sup>16</sup> Both combinations can code all of the 20 amino acids and a stop codon. The main reason these NNK and NNS combinations are used is because a fully randomized combination (NNN) would bias those amino acids that are

encoded by more than one codon. However, it would be ideal to produce a library in which every amino acid could be encoded by just one codon, in order to remove all possible biases. Depending on the number of randomized residues that one would desire in a peptide library, a full representation of all the possible amino acid combinations would be conceivable or not.<sup>1</sup> For example, if a peptide library consists of peptides with only 5 randomized residues, regardless of the total peptide length, 3,200,000 different clones are needed to cover all the possible combinations. This would be a plausible approach for random phage display libraries, which mainly consist of  $10^7$ – $10^9$  different clones. Nevertheless, for peptides with more than 9 randomized residues, the possible combinations rise to over  $5 \cdot 10^{11}$ , and a full representation of all the different options would be almost impossible, although this is not necessarily a major drawback. In the end, the efficiency of a peptide (or antibody) library is determined by the number of selective and high-affinity binders obtained once the selection of biorecognition elements is carried out. Even though it is generally expected that libraries with a larger representation of different clones would provide better results, libraries containing fewer combinations can potentially be equally or even more efficient than larger ones.

### 3.1.2. Selection of mimopeptides by phage display

The interest in phage display lies in the discovery of new biorecognition elements for specific targets. The key to achieve that goal is to conduct an efficient selection and screening of the phage library. Initially, the library consists of a pool of *circa*  $10^7$ – $10^{10}$  different phage clones and ideally each clone should be repeated between 100 and 1000 times to carry out the selection.<sup>17</sup> Due to the unfeasibility of testing every single clone of the library individually, selection rounds are carried out in order to select the clones with the best affinity to the target out of the whole pool. Those phages showing a high affinity to the target are expected to move forward in the selection rounds, be amplified, and therefore easily discriminated. However, there are few considerations to bear in mind to accomplish that goal:

- The target concentration is critical, especially in the initial round.<sup>17</sup> As previously mentioned, the number of copies of a certain clone in the initial round is extremely low in comparison to the total number of phages. Consequently, low target concentrations could lead to an irrevocable loss of good binders. The efficiency of the selection in the first round could be increased both with higher target concentrations as well as longer incubation times.<sup>17</sup>
- The type of display plays an important role when selecting the size of the initial phage pool.<sup>17</sup> A monovalent display would demand a higher representation of each clone, in comparison to a polyvalent display, in which several copies of the ligand are expressed on the phage virion.
- The selection stringency presents a high variability and is pivotal to determine the efficiency of the selection. The stringency is considered as a set of conditions in which the rate of high affinity phages obtained would be favored over those with lower affinities. One would expect that higher stringency is always desired, but higher stringencies lead to lower yields. As a result, a balance between stringency and yield is desired, particularly in the first round of selection.<sup>1</sup>

Notwithstanding the aforementioned considerations, the selections are always flawed in practice, and background-binding phages would always be carried through all the rounds.<sup>1</sup> As a way to reduce nonspecific phage binding, blocking agents can be employed to coat the surface and avoid the amplification of phages bound to them. This approach presents the risk of amplifying phages that bind to the blocking agents. Therefore, to reduce that probability, blocking agents can be switched after every round.

The selection process of phage display libraries is often referred to as panning. Pannings consist of four main steps (**Figure 11A**), namely an incubation step in which the pool of phages interacts with the target, followed by a washing step to remove all the unbound phages. Then, an elution step is carried out, to release those phages bound to the target, and finally, the amplification of these selectively bound phages takes place in bacterial cells.<sup>16</sup> Prior to the incubation step, some protocols include a “negative panning” in which the pool of phages first interacts with the surface without the target, typically a plate or beads, to remove phage clones that interact nonspecifically.<sup>16</sup> Pannings are normally carried out between three to five times, observing a subsequent enrichment output of phages.

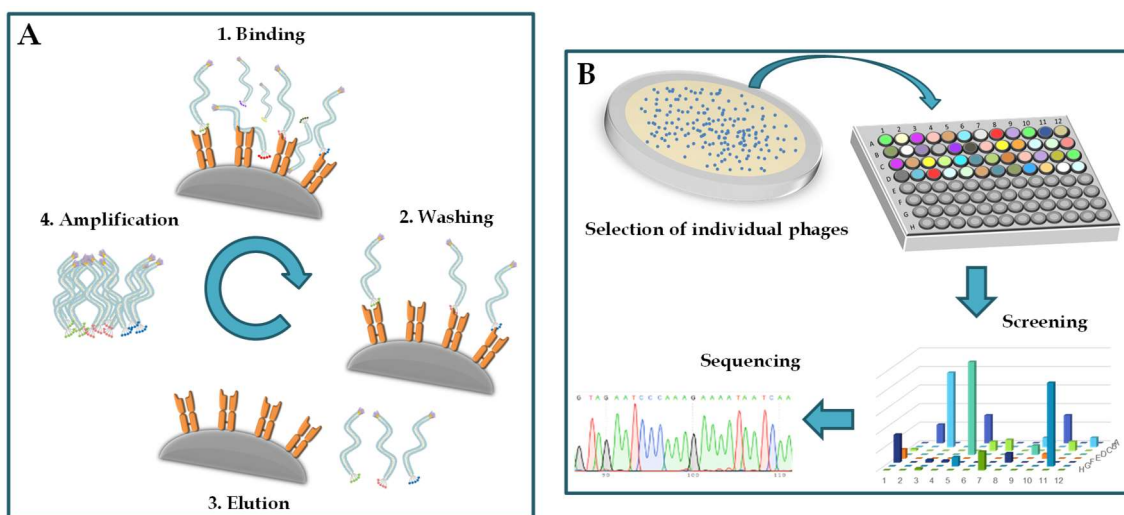


**Figure 11.** Selection of biorecognition elements by phage display. A. Schematic representation of panning rounds. First, a binding step from the whole pool of phages to the target antibody or peptide is required. Second, a washing step removes all the unbound phages. Next, an elution of the phages that interact with the target is carried out. The fourth and last step of the panning is an amplification of the selectively eluted phages. This process is generally repeated between three to five times. B. Selection and characterization of individual clones. Phage clones are picked from fresh agar plates after the panning rounds. These selected clones are screened, typically by phage-based ELISAs and the best clones are sequenced for further characterization.

Pannings are generally performed using microtiter plates or magnetic beads. The target is usually anchored to either the wells of the plate or to the surface of beads to simplify the separation of phages interacting with the target from the whole pool.<sup>17</sup> Other formats, for example, perform the incubation in solution, using a biotinylated target that is later captured with streptavidin beads.<sup>17</sup> Washing steps need to be thoroughly controlled in order to obtain the best recovery in every round.<sup>17</sup> Initially, the pool of phages contains a majority of background or plate-binder phages.<sup>16</sup> Only a small percentage can either present low affinity or high affinity for the target. If the washing



step is very stringent in the first round, the probability to lose those high-affinity binders is very high. However, it is desired to increase the stringency in later rounds of the panning, as more copies of the high-affinity binders would be present in the pool of phages. The basis of the elution step is to break the interaction between the phages and the target. Generally, a pH alteration, either acidic or basic, is enough to disrupt the binding. However, in some cases the addition of a competitor to displace the phage from the binding sites of the target is a successful option.<sup>17</sup> In this case, the concentration of the competitor, as well as the incubation time to accomplish the displacement, need to be optimized. There are also some works in the literature that include a redox elution step.<sup>50</sup>

The amplification of the eluted phages leads to the production of more copies of these phages, and it is essential for the continuation of the panning rounds. To put things under perspective, the phages eluted in the first round are normally in the range of  $10^2$ – $10^4$  clones, although this number can vary depending on the conditions of every experiment. With the amplification step, phages are multiplied to circa  $10^{12}$  clones, allowing the continuation of the panning process. It is important to point out the fact that not all phage clones would be amplified in the same way, as some phages are naturally better-expressing clones than others.

Once the panning rounds are finished, it is of great relevance to monitor the efficiency of the selection process (**Figure 11B**). Prior to the selection of individual clones (or monoclonal phages), a phage ELISA with polyclonal phages is carried out after every round to have a hint of the success of the panning rounds. Phage-based ELISAs are an excellent tool to determine whether the selected phages are able to bind to the target or not. It is expected that the initial rounds would present worse results than the latter ones, regardless of what is being assessed. If the results of the ELISA with polyclonal phages seem promising, individual clones are selected from the latest panning rounds and screened, generally through phage-based ELISAs. Those clones that present the desired behavior can be DNA-sequenced, although alternatively DNA sequencing can also be conducted before phage-based ELISAs. The sequencing results can unveil interesting information, for example, if the sequenced clones present identical residues or some conserved motifs. Ultimately, what matters is to obtain at least a clone with the properties that were sought in the beginning.<sup>17</sup>

### 3.2. Objectives

The main objective of this chapter was the selection and characterization of novel mimopeptides for a series of mycotoxins applying the phage display technique. To this aim, the first approach was the development of different panning protocols for the selection of mimopeptides for MPA, AOH and OTA, using either a magnetic bead-based or a plate-based approach. Once the panning rounds were conducted, individual clones were selected and evaluated in phage-based ELISAs, with the purpose of selecting the best competitors for the different antibodies of the aforementioned mycotoxins. Those phages presenting good competition with the mycotoxin for the binding sites of their respective antibody were sequenced to obtain the amino acid sequences corresponding to the displayed peptides. The objectives of this chapter are summarized below:

- Development of different panning strategies for the selection of mimopeptides for MPA, OTA and AOH.
- Selection of individual phage clones by phage-based ELISA and evaluation of their sensitivity for the antibody of interest in competitive immunoassays.
- Sequencing and characterization of the best competitors for each mycotoxin.

### 3.3. Experimental part

#### 3.3.1. Reagents and solutions

##### Cell culture and molecular biology

- LB broth, Lennox (**Thermo Fisher Scientific**)
- Tetracycline (Tet) (**Sigma-Aldrich**)
- LB Agar (**NZYtech**)
- Agar Granulated (**NZYtech**)
- *E. coli* K12 ER2738 (**New England Biolabs**)
- Ph.D.-C7C Phage Display Peptide Library Kit (**New England Biolabs**)
- Ph.D.-12 Phage Display Peptide Library Kit (**New England Biolabs**)
- Phusion Hot Start II DNA Polymerase (**Thermo Fisher Scientific**)
- High-fidelity DNA Polymerase (**Thermo Fisher Scientific**)
- PCR Nucleotide Mix (**Roche Diagnostics**)
- Agarose D1 Low EEO (**Conda**)
- Red Nucleic acid gel stain (**Thermo Fisher Scientific**)
- GelPilot Loading dye (**Qiagen**)
- GeneRuler 1 kb DNA Ladder (**Thermo Scientific**)

##### Antibodies

- HRP-conjugated anti-M13 monoclonal antibody (**GE Healthcare**)
- Polyclonal sheep anti-MPA IgG antibody (**Randox**)
- Monoclonal Anti-MPA antibody, kindly donated by Dr. Erwin Märtlbauer from Ludwig-Maximilians-Universität München, Germany.
- Monoclonal anti-alternariol (anti-AOH), provided by Dr. Antonio Abad and Dr. Josep Mercader from Instituto de Agroquímica y Tecnología de Alimentos (IATA) in Valencia, Spain, in the frame of a Material Transfer Agreement.
- The recombinant anti-MPA Fab and the recombinant anti-OTA Fab were obtained from a phage display library proprietary of VTT, Finland, and produced as described previously.<sup>50</sup>

##### Mycotoxins

- Alternariol (AOH) (**TRC**)
- Ochratoxin A (OTA) (**Fermentek**)
- Mycophenolic acid (MPA) (**Alfa Aesar**)

##### Chemical reagents

- Phosphate buffer saline (PBS) pH 7.4 (**Sigma-Aldrich**)
- Sodium carbonate anhydrous (for analysis) (**Riedel-deHaën**)
- Sodium hydrogen carbonate (puriss. p.a.) (**Riedel-deHaën**)
- Sodium phosphate monobasic monohydrate (≥98%) (**Sigma-Aldrich**)
- Sodium phosphate dibasic dehydrate (puriss. p.a.) (**Fluka**)
- Sodium chloride (**Quimipur**)
- Tris base (**Fisher Bioreagents**)
- Cobalt (II) chloride hexahydrate (for analysis) (**Merck**)

- Citric acid anhydrous (**Sigma-Aldrich**)
- BupH™ MES [2-(N-morpholino)ethanesulfonic acid] buffered saline pack (**Thermo Scientific**)
- Acetic acid glacial (**Carlo Erba Reagents**)
- Ethylenediaminetetraacetic acid disodium salt dihydrate (EDTA) (**Sigma-Aldrich**)
- Dimethyl sulfoxide (≥ 99.5%) (**Sigma-Aldrich**)
- Dimethyl formamide over molecular sieves (≥ 99.5%) (**Sigma Aldrich**)
- Triethylamine (99%) (**Alfa Aesar**)
- Diethanolamine (**Sigma-Aldrich**)
- Hydrochloric acid (36.5–38%) (**Scharlau**)
- Sulfuric acid (95–98%) (**Scharlau**)
- Hydrogen peroxide 30% (**Merck**)
- Amplex UltraRed reagent (**Thermo Fisher Scientific**)
- 1-Step™ Ultra TMB-ELISA (**Thermo Scientific**)
- (4-Nitrophenyl phosphate disodium salt hexahydrate (≥99%) (PNPP) (**Sigma**)
- Diethanolamine-MgCl<sub>2</sub> buffer (**Reagenia**)
- 2,2'-azino-di-(3-ethylbenzthiazoline sulfonic acid) (ABTS) (**Roche Diagnostics**)
- 1-(3-Dimethylaminopropyl)-3-ethylcarbodiimide hydrochloride (EDC) (**FluoroChem**)
- N-Hydroxysulfosuccinimide sodium salt (Sulfo-NHS) (**FluoroChem**)
- Glycine (**Fisher BioReagents**)
- Isopropyl-β-d-thiogalactopyranoside (IPTG) (**Sigma-Aldrich**)
- 5-Bromo-4-chloro-3-indolyl β-D-galactopyranoside (X-gal) (**Sigma-Aldrich**)
- Tween 20 (**Sigma-Aldrich**)
- Albumin Bovine Fraction V (BSA) (**NZYtech**)
- Casein (**Thermo Fisher Scientific**)
- Protein free (**Thermo Fisher Scientific**)
- Super Block (**Thermo Fisher Scientific**)
- Poly(ethylene glycol (PEG) average Mw 6000 (**Aldrich**)
- Glycerol (**Fisher Scientific**)
- EZ-Link Sulfo-NHS-LC-Biotin, No-Weigh Format (**Thermo Fisher Scientific**)
- Biotinylated peptide A(CEGLYAHWC)GGGSK(Bio)-NH<sub>2</sub> (**Peptide Synthetics**)
- NeutrAvidin Biotin-Binding Protein (**Thermo Scientific**)

### PCR Primers

Primers for phage DNA amplification:

- gIII forward primer: 5'-TTA TTC GCA ATT CCT TTA GTG-3' (**Integrated DNA technologies**)

- 96 gIII reverse primer: 5'-CCC TCA TAG TTA GCG TAA CG-3' (**Integrated DNA technologies**)

**Other reagents**

- BcMag Iminodiacetic acid (IDA)-modified beads (1 $\mu$ m) (**Bioclone**)
- LodeStars™ 2.7 Carboxyl (**Agilent Technologies**)
- Streptavidin microtiter plates (**Kaivogen**)

**Commercial kit**

- QIAquick® PCR & Gel Cleanup Kit (**Qiagen**)

**Plates**

**LB-IPTG-Xgal plates** (for 20 plates approximately): 16 g of LB agar were dissolved in 400 mL of MQ water. The solution was autoclaved and after cooled at a temperature lower than 70 °C, 400  $\mu$ L IPTG/X-gal were added. The solution (around 20-25 mL) was immediately poured into a plate and left to stand until the mixture was solidified. Plates were stored at 4 °C in the dark.

**LB/Tet plates** (for 20 plates approximately): 16 g of LB agar were dissolved in 400 mL of MQ water at a temperature below 70 °C, followed by the addition of 400  $\mu$ L tetracycline. The solution was immediately poured into a plate (around 20-25 mL) and left to stand until solidification. Plates were stored at 4 °C in the dark.

**Solutions and buffers:**

**Top Agar:** 2 g of LB broth and 0.7 g of Bacto-Agar were dissolved in 100 mL of MQ water. The solution was autoclaved and while it was still liquid, dispensed into 3 mL aliquots. The autoclaved mixture was stored solid at room temperature, and it was melted in a water bath when needed.

**PBS 10x:** one pouch of PBS was dissolved in deionized water. The pH was adjusted to 7.4 in a final volume of 100 mL. The solution was sterilized by autoclaving and stored at room temperature.

**PBS 1x:** the solution was prepared by diluting 10 times in autoclaved water the PBS 10x solution. The final concentration was 0.01 mol L<sup>-1</sup> PBS, pH 7.4.

**Tween-20 solution 10% (v/v):** 10 mL of Tween® 20 were diluted with 90 mL deionized water. The solution was sterilized by autoclaving and stored at room temperature.

**BSA 3%:** 3 g BSA were dissolved in 100 mL PBS 1x pH 7.4. The solution was filtered-sterilized and stored at 4 °C in the dark.

**PBS-0.1% T20:** 10x PBS stock was diluted 10 times and Tween 20 10% (v/v) was diluted 100 times with autoclaved water. For 10 mL, 1 mL PBS and 100  $\mu$ L Tween 20 10% (v/v) were dissolved in 8.9 mL autoclaved water.

**PBS-0.05% T20 + (0.1% BSA):** 10x PBS stock was diluted 10 times and Tween 20 10% (v/v) was diluted 200 times with autoclaved water. Whenever BSA was added to the mixture, it was diluted 30 times from the 3% BSA stock.

**Coating buffer pH 9.6 (0.05 mol L<sup>-1</sup> NaHCO<sub>3</sub>/Na<sub>2</sub>HCO<sub>3</sub> buffer):** 288 mg NaHCO<sub>3</sub> and 167 mg Na<sub>2</sub>HCO<sub>3</sub> were dissolved in deionized water. The pH was adjusted to 9.6 in a final volume of 100 mL. The solution was filtered-sterilized and stored at room temperature.

**Coating buffer pH 8.6 (0.1 mol L<sup>-1</sup> NaHCO<sub>3</sub> buffer):** 840 mg NaHCO<sub>3</sub> were dissolved in deionized water. The pH was adjusted to 8.6 for a final volume of 100 mL. The solution was filtered-sterilized and stored at room temperature.

**Elution buffer acid (0.2 mol L<sup>-1</sup> Glycine-HCl pH 2.2) (+ 1mg mL<sup>-1</sup> BSA):** 750 mg glycine were dissolved in deionized water and the pH was adjusted to 2.2 with HCl in a final volume of 100 mL. The solution was autoclaved and stored at 4 °C in the dark. BSA was added to the mixture, after the solution was autoclaved, from the 3% BSA stock solution, to a final BSA concentration of 1 mg mL<sup>-1</sup>.

**Elution buffer basic (100 µL 0.1 mol L<sup>-1</sup> triethylamine pH 11.2):** 1.4 mL triethylamine were dissolved in deionized water and the pH was adjusted to 11.2 for a final volume of 100 mL. The solution was autoclaved and stored at room temperature.

**Elution solution (mycotoxins):** the mycotoxin solutions used for phage elution were prepared fresh from the concentrated mycotoxin stocks and dissolved in PBS-0.05% T20 at the desired concentration, typically 100 ng mL<sup>-1</sup> or 10 ng mL<sup>-1</sup>.

**Neutralization buffer basic (1 mol L<sup>-1</sup> Tris-HCl pH 9.1):** 6.06 g Tris were dissolved in deionized water. The pH was adjusted to 9.1 with HCl for a final volume of 50 mL. The solution was autoclaved and stored at room temperature.

**Neutralization buffer acid (1 mol L<sup>-1</sup> Tris-HCl pH 6.8):** 6.06 g Tris were dissolved in deionized water. The pH was adjusted to 6.8 with HCl for a final volume of 50 mL. The solution was autoclaved and stored at room temperature.

**Precipitation buffer (20% PEG, 2.5 mol L<sup>-1</sup> NaCl):** 20 g PEG and 14.6 g NaCl were dissolved in 100 mL deionized water. The solution was autoclaved, and the two phases were mixed while the solution was still warm. The solution was stored at room temperature.

**Storage buffer (20 mmol L<sup>-1</sup> Na<sub>2</sub>HPO<sub>4</sub>/NaH<sub>2</sub>PO<sub>4</sub>, 1 mol L<sup>-1</sup> NaCl, pH 7.0):** 0.712 g sodium dihydrogen phosphate dihydrate and 0.552 g sodium dihydrogen phosphate monohydrate were each dissolved in 180 mL deionized water. 20 mL of NaCl 0.5 mol L<sup>-1</sup> were added to each solution and the volumes were combined. The pH was adjusted to 7.0 and the solution was stored at room temperature.

**Suspension buffer (100 mmol L<sup>-1</sup> Na<sub>2</sub>HPO<sub>4</sub>/NaH<sub>2</sub>PO<sub>4</sub>, 1 mol L<sup>-1</sup> NaCl, 20 % EtOH, pH 6,8):** 3.56 g sodium dihydrogen phosphate dihydrate and 2.76 g sodium dihydrogen phosphate monohydrate were each dissolved in 160 mL deionized water. 20 mL of NaCl 0.5 mol L<sup>-1</sup> were added to each solution, the volumes were then combined, and 40 mL of absolute ethanol were added to the mixture. The pH was adjusted to 6.8 and the solution was stored at room temperature.

**Coupling buffer A (MES 0.1 mol L<sup>-1</sup>, 0.9% NaCl + 0.01% SDS, pH 5.7):** one pack of MES powder was dissolved in 500 mL deionized water. Then, 5 mL of the MES solution was added together with 50 µL of 10% SDS solution to 40 mL deionized water. The pH was adjusted to 5.7 in a final volume of 50 mL. The solution was stored at 4 °C in the dark.

**Coupling buffer B (PBS 1x + 0.01% SDS, pH 7.4):** 5 mL of PBS 10x and 50 µL of 10% SDS solution were added to 40 mL deionized water. The pH was adjusted to 7.4 in a final volume of 50 mL. The solution was stored at 4 °C in the dark.

**TAE 50x electrophoresis buffer (2 mol L<sup>-1</sup> Tris base, 1 mol L<sup>-1</sup> acetic acid, 1 mol L<sup>-1</sup> EDTA, pH 8.6):** 242 g Tris base, 18.61 g disodium EDTA and 59.95 g acetic acid were dissolved in 800 mL deionized water. Once dissolved, more deionized water was added

for a total volume of 1 L. The pH was not adjusted. The solution was stored at room temperature.

**TAE 1x electrophoresis buffer:** The solution was prepared by diluting the 50x TAE solution 50 times in deionized water.

### 3.3.2. Analytical instrumentation and materials

- CLARIOstar microplate reader (**BMG Labtech**)
- Varioksan plate reader (**Thermo Scientific**)
- Nanodrop 1000 spectrophotometer (**Thermo Scientific**)
- Spectrophotometer DS-11 FX (**DeNovix**)
- Analytical balance with 0.01 mg sensitivity (**Sartorius**)
- pH Meter GLP 21 (**Crison**)
- Automatic magnetic bead processor, KingFisher™ (**Thermo Fisher Scientific**)
- Eppendorf centrifuge 5430R (**Eppendorf**)
- Eppendorf miniSpin (**Eppendorf**)
- Eppendorf centrifuge 5804 R (**Eppendorf**)
- Shaker incubator innova 40 (**New Brunswick Scientific**)
- Shaker incubator KS 4000 i control (**IKA**)
- Autoclave (**Selecta**)
- Thermostatic eppendorf shaker (**Thermo Scientific**)
- Vortex shaker (**Fisher brand**)
- PowerPac™ Basic power supply for gel electrophoresis (**Bio-Rad**)
- Thermocycler SureCycler 8800 (**Agilent Technologies**)
- Automatic plate washer hydro flex (**Tecan**)
- Analytical material of contrasted quality

### 3.3.3. Experimental procedures

#### 3.3.3.1. Antibody coupling to magnetic beads

Recombinant anti-MPA Fab and anti-OTA Fab, previously described by Tullila and Nevanen,<sup>50</sup> were conjugated to carboxylated paramagnetic beads to carry out the panning rounds using an automatic magnetic bead processor. Briefly, 4.5 mg of beads were added to 150  $\mu$ L suspension buffer and vortexed. Then, the beads were washed twice with deionized water and resuspended in 750  $\mu$ L of 100 mmol L<sup>-1</sup> CoCl<sub>2</sub>. The mixture was incubated for 30 min at room temperature with slow shaking and the beads were subsequently washed five times with storage buffer. Next, the beads solution was mixed with the antibody (either anti-MPA Fab or anti-OTA Fab) in a proportion of 1 mg of antibody per 2 mg of beads in a total volume of 1 mL PBS 1 $\times$ , and the resulting solution was incubated overnight at 4 °C under rotation. The antibody-coupled beads were collected with a magnet and the buffer was aspirated. Then, 1 mL of 0.03% H<sub>2</sub>O<sub>2</sub> in deionized water was added to the beads and incubated for 4 h at room temperature under rotation. Finally, the beads were washed two times with the storage buffer and reserved at +4 °C in the same buffer.

To confirm antibody immobilization onto the magnetic beads, MPA-alkaline phosphatase and OTA-alkaline phosphatase enzyme conjugates were incubated for one hour in 10 mmol L<sup>-1</sup> Tris-HCl pH 8.0, together with anti-MPA or anti-OTA Fab

functionalized beads, respectively. After washing the beads thrice with PBS-0.05% T20, 500  $\mu\text{L}$  of 2 mg  $\text{mL}^{-1}$  *p*-nitrophenylphosphate in diethanolamine were added and the solution was incubated for 10 min. The solution was transferred to a microplate well and the absorbance at 405 nm was measured using a Varioksan microplate reader.

### 3.3.3.2. Neutravidin coupling to magnetic beads

LodeStars™ 2.7 Carboxylated beads were thoroughly resuspended for 30 min and 1 mg (33.5  $\mu\text{L}$ ) was transferred to a 1.5 mL microcentrifuge tube. The beads were then activated by two washes with 250  $\mu\text{L}$  aliquots of 0.01 mol  $\text{L}^{-1}$  NaOH, followed by three washes with cold deionized water and one final wash with coupling buffer A. Next, the beads were resuspended in 350  $\mu\text{L}$  coupling buffer A and 75  $\mu\text{L}$  of 0.75 mol  $\text{L}^{-1}$  EDC in coupling buffer A and 75  $\mu\text{L}$  of 0.525 mol  $\text{L}^{-1}$  NHS in coupling buffer A were immediately added. The reaction was incubated during 2 h at room temperature with an Eppendorf shaker at 1000 rpm. Next, the tube was placed on a magnetic rack to aspirate the supernatant and the beads were washed thrice with 250  $\mu\text{L}$  of cold coupling buffer B and resuspended in 100  $\mu\text{L}$  of the same buffer. Then, 16.5  $\mu\text{L}$  of 5 mg  $\text{mL}^{-1}$  NeutrAvidin and 148.5  $\mu\text{L}$  coupling buffer B were added to the bead suspension and incubated for 4 h at room temperature at 1000 rpm. The beads were consequently rinsed with 250  $\mu\text{L}$  SuperBlock and blocked with the same buffer for 1 h. Finally, the beads were washed three times with SuperBlock and resuspended in 100  $\mu\text{L}$  SuperBlock, for a final bead concentration of 10 mg  $\text{mL}^{-1}$ .

### 3.3.3.3. Antibody biotinylation

Anti-MPA Fab antibody and anti-OTA Fab antibody, previously described by Tullila and Nevanen,<sup>50</sup> were biotinylated using EZ-Link Sulfo-NHS-LC-Biotin, according to the manufacturer's instructions.<sup>67</sup> A molar excess of Sulfo-NHS-LC-Biotin three times greater than the antibody was employed. Illustra NAP-5 columns were used for purification following to the manufacturer's instructions.

### 3.3.3.4. Panning rounds

#### a) Plate-based protocol

Linear or cyclic peptides that specifically bind to anti-MPA or anti-AOH antibodies were selected from commercial phage-display peptide libraries (Ph.D.-12 and Ph.D.-C7C). In this case, the antibody solutions in coating buffer, pH 9.6 or pH 8.6, were added to microwell plates and were incubated overnight at 4 °C. Then, the coating solution was discarded, and the wells were covered with 250  $\mu\text{L}$  blocking buffer (BSA, Protein Free or SuperBlock) for 2 h at room temperature with slow shaking. Next, the wells were washed 3 times with PBS-0.1% T20 and the phage library, diluted in PBS-0.05% T20 for a total of  $2.0 \times 10^{11}$  phages, was added to the wells. After incubation at room temperature and slow shaking for varying time, typically 1 h or 1.5 h, the unbound phages were discarded by pouring off the solution contained on the wells. The plates were then washed several times, from 6 to 15 times with PBS-0.1% T20 and the bound phages were eluted with either the elution buffer acid for 10 min or the mycotoxin elution solution for 30 min. In the case of the elution with the acidic buffer, the eluted phages were



immediately neutralized with a basic neutralization buffer. The resulting solutions were stored at 4 °C for several weeks.

b) Magnetic bead-based protocol

Cyclic peptides that specifically bind to anti-MPA or anti-OTA Fab antibodies were selected from a commercial phage-display peptide library (Ph.D.-C7C). For this aim, an automatic magnetic bead processor was employed. The antibodies of interest were coupled to magnetic beads (see antibody coupling to magnetic beads) prior to the start of the panning rounds. Briefly, 50 µg of the antibody-coupled magnetic beads were incubated on KingFisher™ Plastics with a 96 deep-well format with the phage library (containing always  $2.0 \times 10^{11}$  phages as the input value) in a total volume of 505 µL PBS-0.05% T20 for 2 h at room temperature. Then, the beads were washed two times with PBS-0.1% T20 for 30 s, and the bound phages were subsequently eluted with 100 µL of basic elution buffer for 30 min. The eluted phages were immediately neutralized with an acid neutralization buffer and the resulting solution was stored at 4 °C for several weeks.

### 3.3.3.5. Phage amplification

To amplify the phages, 70 µL of the eluted (and neutralized where applicable) phage solution were added to a 40 mL early-log phase (with an OD<sub>600</sub> of ~0.05) *E. coli* ER2738 culture. The solution was incubated at 37 °C for 4.5 h and then centrifuged for 10 min at 12,000 g and 4 °C collecting the supernatant containing the amplified phages. The supernatant was centrifuged again under the same conditions and then, 1/6 volume of precipitation buffer was added, and the phages were let to precipitate overnight at 4 °C. The next day, the phages were harvested by centrifugation during 15 min at 12,000 g at 4 °C and the supernatant was discarded. The phage pellet was resuspended in 3 mL PBS 1× and centrifuged again for 15 min at 12,000 g and 4 °C to remove any remaining cell debris. The supernatant was precipitated again with 1/6 volume of precipitation buffer and left for 1 h on ice, followed by another centrifugation for 15 min at 12000 g and 4 °C. Finally, the phage pellet was resuspended in 500 µL PBS 1× and the solution was stored at 4 °C for several weeks. The amplified phage stock was used for the following panning round.

### 3.3.3.6. Phage titering

To estimate the phage concentration on both the eluted fractions as well as the amplified fractions, a phage titering was carried out. To this aim, *E. coli* ER2738 bacterial cultures were inoculated from single colonies and grown in 10 mL LB supplemented with 200 µg mL<sup>-1</sup> tetracycline at 37 °C with vigorous shaking. When the cell culture reached the mid-log phase (OD<sub>600</sub> of ~0.5), the solution was kept on ice until used. While the cells were growing, top agar aliquots of 3 mL were melted on a water bath and kept at 45 °C until use, and LB-IPTG-Xgal plates were pre-warmed at 37 °C. Additionally, serial phage dilutions of the eluate or the amplified fractions were prepared on LB. When the 10 mL ER2738 culture reached mid-log phase (OD<sub>600</sub> of ~0.5), 200 µL were dispensed into microcentrifuge tubes, one for each phage dilution. To conduct the infection, 10 µL of each phage dilution was dispensed in each tube and incubated at room temperature for 1–5 min. The infected cells were transferred to culture tubes containing the 3 mL top agar aliquots. The solution was quickly vortexed, and the culture was immediately

poured gently onto a pre-warmed LB-IPTG-Xgal plate. The plates were allowed to cool down for 5 min, and they were incubated overnight at 37 °C. Blue plaques were counted the day after from each plate and the concentration of the phage eluate, or the amplified fraction, was estimated considering the dilution made.

### 3.3.3.7. Selection of monoclonal phages

Fresh titering plates of phage eluates from each round were used to select monoclonal phages. Briefly, 80 µL of *E. coli* ER2738 bacterial culture in the early-log phase (OD<sub>600</sub> of ~0.05) were dispensed in autoclaved round bottom 96-well plates. Single phage plaques were selected from fresh titering plates and transferred each to one well containing the bacterial culture, and the monoclonal phages were incubated for 2.5 h at +37 °C with vigorous shaking. Then, monoclonal phages were streaked out and grown overnight on IPTG-X-Gal plates at 37 °C. Individual clones were subsequently inoculated from the IPTG-Xgal plates on 500 µL of LB and grown for 6 h at +37 °C with vigorous shaking. Finally, the phage solutions were centrifuged for 5 min at 10,000 g, and 4 °C to harvest the cells, transferring the supernatant to a fresh tube. The concentration of the amplified individual clones, determined by titering, typically ranged from 10<sup>11</sup> to 10<sup>12</sup> pfu mL<sup>-1</sup>.

### 3.3.3.8. Phage-based ELISAs

After each selection round the amplified phages, or the selected monoclonal phage solutions, were screened in an ELISA test to evaluate their binding performances towards immobilized MPA, AOH or OTA antibodies. Two different protocols were followed, depending on the antibodies employed in the assays. First, anti-MPA Fab and anti-OTA Fab were previously biotinylated following the protocol described above. Then, 100 µL of 5 µg mL<sup>-1</sup> dilutions were immobilized on streptavidin-coated wells for 30 min using SuperBlock blocking buffer supplemented with 0.05% T20, followed by three washes with PBS-0.1% T20. The wells were then blocked with 280 µL of SuperBlock with 0.05% T20 for 30 min and washed again three times with PBS-0.1% T20. Then, 100 µL of concentrations between 10<sup>10</sup> and 10<sup>11</sup> pfu mL<sup>-1</sup> of the amplified phage stock or the monoclonal phage stock were added to the wells in SuperBlock with 0.05% T20 and incubated for 1 h with slow shaking. The wells were consequently washed as described above and 100 µL of a 1:5000 dilution of the HRP-conjugated anti-M13 monoclonal antibody in SuperBlock with 0.05% T20 was added to the wells and incubated for 1 h. Finally, the plate was washed again three times and 100 µL of a 0.22 mg mL<sup>-1</sup> solution of ABTS in 0.05 mol L<sup>-1</sup> citric acid containing 0.05% H<sub>2</sub>O<sub>2</sub> were added to the wells. After 5 min, absorbance at 405 nm was measured in a Varioksan plate reader.

On the other hand, 60 µL of 3.33 µg mL<sup>-1</sup> dilutions of polyclonal or monoclonal antibodies were immobilized on microplate wells using coating buffer pH 8.6 (for MPA antibody) or pH 9.6 (for AOH antibody) Next, the wells were blocked with SuperBlock with 0.05% T20 for MPA or BSA 3% in PBS 1× pH 7.4 for AOH for 2 h and washed three times with PBS-0.1% T20. Then, 100 µL of concentrations between 10<sup>10</sup> and 10<sup>11</sup> pfu mL<sup>-1</sup> of the amplified phage stock or the monoclonal phage stock was added to the wells in PBS-0.05% T20 and incubated for 1 h with slow shaking. After washing the wells thrice with PBS-0.1% T20, 60 µL of a 1:5000 dilution of the HRP-conjugated anti-M13 monoclonal antibody in PBS-0.05% T20 was added to the wells and incubated for 1 h.

Finally, the plate was washed three times with PBS-0.1% T20 and 60  $\mu\text{L}$  of TMB were added to the wells and incubated until a blue color starts developing (typically from 1 min until 15 min). The absorbance at 450 nm was measured in a CLARIOstar plate reader.

In both protocols, the phages were also tested in background wells, which did not contain the antibody, to confirm the absence of nonspecific binding. Those monoclonal phage clones that showed specific binding to the antibody were assessed in an analogous way in the presence of 100  $\text{ng mL}^{-1}$  of free mycotoxin, added at the same time as the phage clones, in order to establish a competition between the mycotoxin and the phage clone for the binding sites of the antibody. Additionally, a calibrate with varying mycotoxin concentrations was conducted for those clones that presented competition with the mycotoxin in the same conditions as described above.

### **3.3.3.9. Confirmatory bead-based phage ELISA**

A bead-based assay with the phage that provided the highest sensitivity in the plate-based assay was developed. Briefly, a black microtiter plate was blocked with 280  $\mu\text{L}$  of SuperBlock with 0.05% T20 for 1 h at room temperature and slow shaking. The plate was washed three times with PBS-0.1% T20 and then, 60  $\mu\text{L}$  of 1.2  $\mu\text{g mL}^{-1}$  biotinylated anti-MPA and 20  $\mu\text{L}$  of 125  $\mu\text{g mL}^{-1}$  neutravidin-coated magnetic beads functionalized as described above were added to the wells in SuperBlock with 0.05% T20 and incubated for 30 min at room temperature and slow shaking. Then, the beads were washed three times with PBS-0.1% T20 using a plate washer with a magnetic support. Different concentration of MPA in SuperBlock with 0.05% T20 together with the phage clone at a final concentration of  $10^{11}$  pfu  $\text{mL}^{-1}$ , for a total volume of 60  $\mu\text{L}$ , were added to the wells and incubated for 30 min at room temperature and slow shaking. The beads were washed again in the same conditions as described above and then, 80  $\mu\text{L}$  of a 1:5000 dilution of the HRP-conjugated anti-M13 monoclonal antibody in PBS-0.05% T20 was added to the wells and incubated for 30 min at room temperature and slow shaking. Finally, after washing three times as described above, 80  $\mu\text{L}$  of Amplex UltraRed solution was added to the wells and the fluorescence was measured with a CLARIOstar microplate reader ( $\lambda_{\text{ex}} = 530 \text{ nm}$ ,  $\lambda_{\text{em}} = 590 \text{ nm}$ ).

### **3.3.3.10. DNA amplification and purification of phage clones**

The phage DNA of positive clones was PCR-amplified according to the following protocol. First, a mastermix was prepared containing 1 $\times$  Phusion HS Buffer, 0.2  $\text{mmol L}^{-1}$  dNTPs, 0.5  $\mu\text{mol L}^{-1}$  of gIII forward primer and -96 gIII reverse primer, and 0.2 U  $\mu\text{L}^{-1}$  Phusion Hot Start II DNA polymerase in autoclaved deionized water. Then, 15  $\mu\text{L}$  of the mastermix was mixed with 5  $\mu\text{L}$  of the phage solution. The PCR was conducted with an initial denaturation at 98  $^{\circ}\text{C}$  for 30 s, followed by 30 cycles of denaturation at 98  $^{\circ}\text{C}$  for 10 s, annealing at 58  $^{\circ}\text{C}$  for 30 s and extension at 72  $^{\circ}\text{C}$  for 30 s. Finally, another extension at 72  $^{\circ}\text{C}$  was performed for 10 min.

Amplification of the phage DNA was confirmed with a 1% agarose gel. To prepare the agarose gel, 500 mg agarose were mixed with 50 mL TAE 1x. The mixture was heated over 100  $^{\circ}\text{C}$  to dissolve the agarose but avoiding excessive boiling. Once the agarose was dissolved, the mixture was cooled below 70  $^{\circ}\text{C}$  and 2  $\mu\text{L}$  nucleic acid gel stain was added, and the mixture was then poured onto a container to form the gel. A comb was place

before the mixture solidified to generate holes. To run the gel, a mixture of 6  $\mu$ L autoclaved deionized water, 2  $\mu$ L loading dye and 2  $\mu$ L amplified phage DNA was added to each of the channels of the agarose gel. The gel was then covered in TAE 1x buffer and connected to the power supply to start the electrophoresis.

DNA purification was performed using a NucleoSpin Gel and PCR Clean-up according to the manufacturer's instructions. The concentration of the purified DNA was measured at 280 nm on a Nanodrop, and the samples were sequenced at the C.A.I. Genómica y Proteómica facility of Universidad Complutense de Madrid.

### 3.4. Results and discussion

Phage display has proven to be a very useful technique for the discovery of novel antibodies against different compounds or of mimopeptides from numerous analytes throughout the last decades. Mimopeptides have become a very useful tool in competitive assays since they can be easily and cost-effectively produced in combination with enzymes or fluorescent proteins, for example. Thus, tedious and expensive conjugation processes of the analyte of interest to different tags are avoided. However, up to now, phage display has only been employed for the selection of mimopeptides for some of the most common legislated mycotoxins.

One of the goals of this doctoral thesis was the selection of mimopeptides for some unlegislated, mycophenolic acid, alternariol, and one regulated mycotoxin, ochratoxin A, using different panning strategies.

Some of the results described in the present PhD thesis work for the selection of mimopeptides for mycophenolic acid and ochratoxin were obtained during a predoctoral research stage at VTT research center, Finland, under the supervision of Dr. Tarja Nevanen. Her research group is internationally known for their contributions to the selection of novel recombinant antibodies by phage display and have focused on mycotoxin research during the last years. Hence, the recombinant anti-MPA and anti-OTA Fab antibodies employed in this doctoral thesis were previously isolated by her group using proprietary phage display libraries.

During the research stage, the bead-based panning protocols were carried out using a KingFisher™ automatic magnetic bead processor.

#### 3.4.1. Selection of mimopeptides for mycophenolic acid

Mycophenolic acid is a well-known mycotoxin with a characteristic immunosuppressive behavior that is commonly administered to transplanted patients to prevent organ rejection.<sup>68</sup> The selection of an MPA mimopeptide by phage display allows the development of competitive immunoassays without the need of conjugating the mycotoxin to any other label. To the best of our knowledge, there were no mimopeptides for MPA previously described in the literature; therefore, it was of great interest to achieve the selection of the first mimopeptide for MPA applying phage display technology.

##### 3.4.1.1. Panning strategies

The first panning strategy for the selection of MPA mimopeptides was a plate-based method, using a polyclonal sheep anti-MPA IgG antibody and a Ph.D.-12 phage display library. This library consists of 12 randomized amino acids in a linear sequence expressed at the N-terminus of protein pIII. A pre-selection step, also known as a negative panning, was carried out to remove binders that could be attached to the plate, or the blocking agent before the actual panning in the presence of the antibody. In the first panning, BSA was used as the blocking agent; therefore, the negative panning was conducted against a plate blocked with BSA. After the phages were incubated on the negative panning wells, they were transferred to the positive panning wells and incubated during the same time as described in the protocol. Furthermore, in order to increase the stringency of the selection rounds, the second and third round were carried

out with lower antibody concentrations in the coating step, lower incubation times and a greater number of washes. The detailed conditions of all the rounds for the first panning strategy are described in **Table 6**.

**Table 6.** Experimental conditions of the first panning strategy for the selection of MPA mimopeptides.

<b>Anti-MPA polyclonal antibody, Ph.D.-12 library</b>		
1st round	Negative selection Blocking Target selection Washing Elution	1.5 h BSA 3% in PBS 1×, 2 h 3 wells with 10 $\mu\text{g mL}^{-1}$ of Ab, 1.5 h 6 times with PBS + 0.1 % T20 Gly-HCl pH 2.2, 10 min
2nd round	Negative selection Blocking Target selection Washing Elution	1 h BSA 3% in PBS 1×, 2 h 2 wells with 5 $\mu\text{g mL}^{-1}$ of Ab, 1 h 10 times with PBS + 0.1 % T20 100 $\text{ng mL}^{-1}$ MPA, 30 min
3rd round	Negative selection Blocking Target selection Washing Elution	1 h BSA 3% in PBS 1×, 2h 1 well with 2.5 $\mu\text{g mL}^{-1}$ of Ab, 1 h 12 times with PBS + 0.1 % T20 10 $\text{ng mL}^{-1}$ MPA, 30 min

As can be seen in **Table 6**, the first elution was performed with Gly-HCl, at pH 2.2 for 10 min, to break down the interactions of the phages with the antibody. The second and third elution rounds were conducted by adding a solution of MPA at different concentrations, 100  $\text{ng mL}^{-1}$  for the second round and 10  $\text{ng mL}^{-1}$  for the third round, with an incubation time of 30 min. Another important feature of the conditions described in **Table 6** is the fact that the number of wells decreased for the target selection. By using a greater number of wells, the surface area is larger, thus allowing more phages to interact with the target antibody. With a lesser number of wells, it is expected that only those phages presenting a higher affinity for the antibody would establish an interaction.

It is also important to point out the fact that the same input of phages was added in all the rounds. According to the manufacturer's instructions, the size of the Ph.D.-12 library is approximately  $10^9$  unique clones.<sup>69</sup> For the selections, it is desired to have at least 100 copies of each individual clone, therefore, the phage input in every round was set for  $2 \cdot 10^{11}$  phages in total.

The phage output, determined by the phage titering protocol described in the experimental section, is the total number of phages that are eluted in every round. It is expected that the phage output would increase as rounds advance, since those phages that show some binding for the target antibody are enriched among the phage population. However, if the selection conditions are varied from one round to another, *i.e.*, the elution method or the number of washes, monitoring the phage output is not as straightforward, and the phage output could even decrease in successive rounds. **Figure**

12 shows the phage output of the three rounds for the panning described above. As can be observed, the first round had a slightly higher phage output than the second one. This can be due to the fact that for the first round, Gly-HCl was employed, whereas for the second round the elution method was a displacement with MPA. The third round, on the other hand, presented a significantly higher output than the two other rounds.

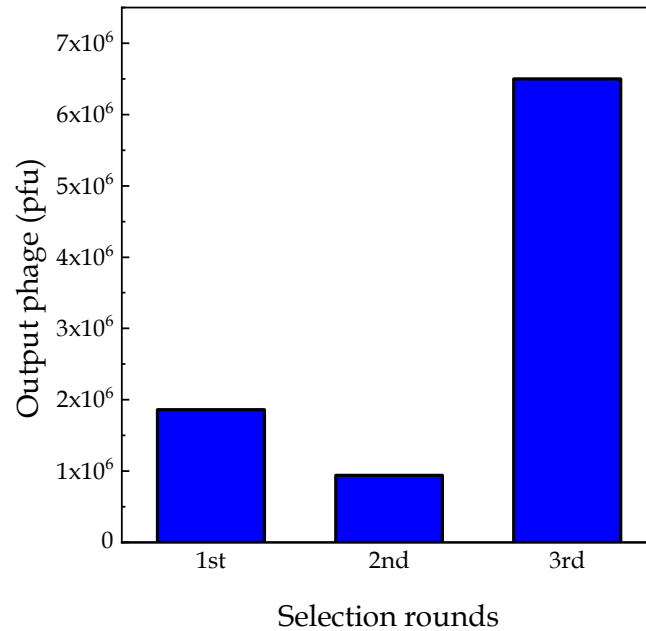


**Figure 12.** Phage output obtained from the eluates of the three selection rounds.

The amplified eluates from each round were consequently tested in a phage-based ELISA (from now on referred to as ELISA with polyclonal phages) to observe the binding behavior of each pool of the amplified phages. For the ELISA with polyclonal phages, background wells (without antibody but with blocking buffer) and target wells (with antibody and with blocking buffer) were tested. The expected optimal behavior of the ELISA with polyclonal phages would lead to a high signal in the target wells and no signal in the background wells, proving an effecting binding of the pool of amplified phages for the antibody. Moreover, it is also expected that the third round would present a higher absorbance value than the other two rounds due to the enrichment of phages during the selection rounds. The results of the ELISA with polyclonal phages for the first panning strategy are shown in **Figure 13**.

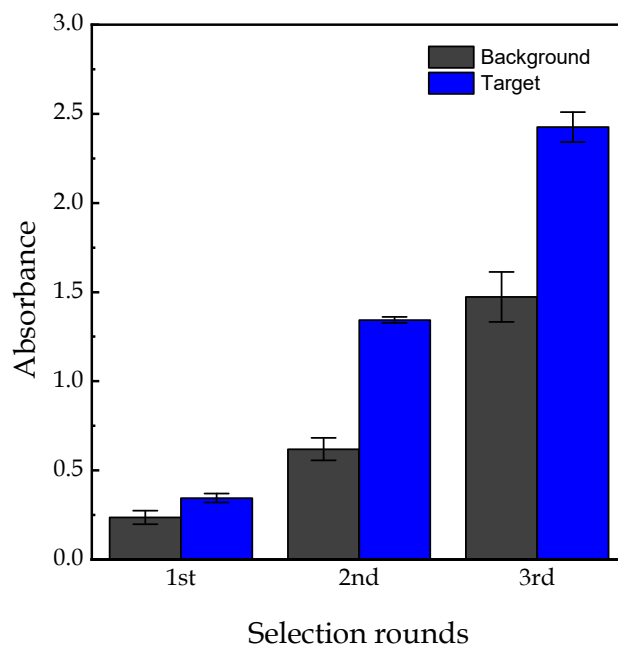


**Figure 13.** ELISA with polyclonal phages for the first panning strategy for MPA. The three rounds showed binding to the target wells (blue bars) but also high nonspecific binding to the background wells (grey). The phage concentration tested was  $10^{10}$  pfu  $\text{mL}^{-1}$ . The results are shown as the mean values of the absorbance  $\pm$  the standard deviation of the mean ( $n = 3$ ).

As can be observed, the absorbance of the background wells is very high, proving that many of the eluted and amplified phages presented affinity for the BSA coating rather than for the antibody. In fact, it has been previously described that MPA shows very high affinity for lipoproteins. As an example, it has been observed that free MPA was 70% higher in transplanted patients with low albumin levels.<sup>70</sup> On top of that, the use of polyclonal antibodies for panning selections could hinder the process of finding good mimopeptides, but the polyclonal anti-MPA used was the only MPA antibody commercially available. Since polyclonal antibodies present different paratopes, the selected phages may present excellent binding to some of them. However, other antibodies present in the mixture could still bind freely to MPA; therefore, the sensitivity of the assay could be substantially reduced. Consequently, a new panning strategy was conducted, using a monoclonal MPA antibody as well as varying the blocking agent from BSA to Protein Free blocking buffer, which has proved no unspecific binding towards MPA in previous works.<sup>71</sup> In **Table 7** the conditions for the second panning strategy are reflected.



**Table 7.** Experimental conditions of the second panning strategy for the selection of MPA mimopeptides.

<b>Anti-MPA monoclonal antibody, Ph.D.-12 and Ph.D.-C7C libraries</b>		
1st round	Negative selection Blocking Target selection Washing Elution	No Protein Free, 2h 3 wells with 10 $\mu\text{g mL}^{-1}$ of Ab, 1.5 h 6 times with PBS + 0.1 % T20 Gly-HCl pH 2.2, 10 min
2nd round	Negative selection Blocking Target selection Washing Elution	No Protein Free, 2h 2 wells with 5 $\mu\text{g mL}^{-1}$ of Ab, 1 h 10 times with PBS + 0.1 % T20 100 $\text{ng mL}^{-1}$ MPA, 30 min
3rd round	Negative selection Blocking Target selection Washing Elution	1 h Protein Free, 2h 1 well with 2.5 $\mu\text{g mL}^{-1}$ of Ab, 1 h 12 times with PBS + 0.1 % T20 10 $\text{ng mL}^{-1}$ MPA, 30 min

Besides the antibody and blocking agent, another variation introduced in the second panning strategy was the absence of negative selection on the first two rounds. The first selection rounds are normally the most important ones, as any bias or loss of diversity would be amplified in subsequent rounds. Negative panning is a useful tool to discard undesired phages from the initial pool. Nevertheless, on the first round there could be a risk of losing potential mimopeptides due to the small number of copies for each individual phage clone. Finally, instead of only using the Ph.D.-12 library, the protocol was also applied for another library, the Ph.D.-C7C library, in order to increase the chances of finding a good mimopeptide. This library consists of a sequence of 7 amino acids that present a disulfide constrained loop generated by two cysteines flanking the randomized sequence. In a similar way as the Ph.D.-12 library, the Ph.D.-C7C expresses the randomized sequence at the N-terminus of pIII.

**Figure 14** shows the output of the eluted phages for both libraries. It can be observed that there was a huge increase in the output from the first round to the second round in both libraries. However, the Ph.D.-12 library presented a slight increase in the output between the second and the third round whereas in the Ph.D.-C7C library the output severely decreased. Interestingly, a negative selection was introduced in the third round, in which phages were previously incubated in wells coated with the blocking agent in the absence of antibody. Therefore, the drop in the phage output of the third round for the Ph.D.-C7C library could indicate that a great number of phages would be binding to either the plate or the blocking agent.

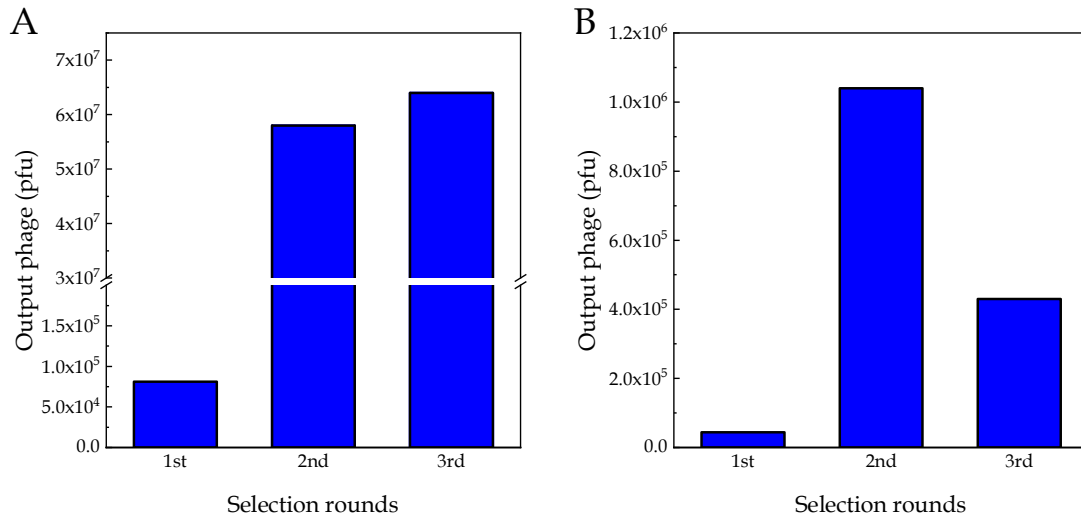


**Figure 14.** Phage output obtained from the eluates of the three selection rounds. A. Output for the Ph.D.-12 library and B. Output for the Ph.D.-C7C library.

The ELISA with polyclonal phages conducted for the amplified phages of the three rounds of both libraries (**Figure 15**) confirmed the hypothesis. It can be observed that the amplified fractions of the Ph.D.-12 library show affinity for the antibody-coated wells and negligible binding for the background wells, whereas the amplified fractions of the Ph.D.-C7C library present even a higher signal for the background wells.

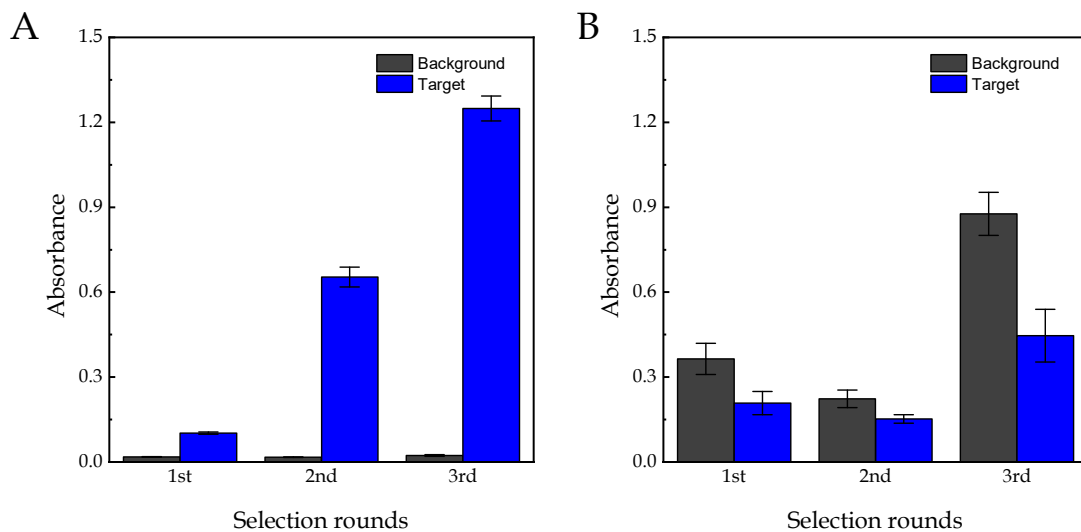


**Figure 15.** ELISA with polyclonal phages for the second panning strategy for MPA. A. Results obtained for the Ph.D.-12 amplified fractions, in which phages have high specificity for target wells (blue) and negligible signal in background wells (grey) and B. Results for the Ph.D.-C7C amplified fractions, showing high nonspecific binding for background wells. In both cases, the phage concentration tested was  $5 \cdot 10^9$  pfu mL<sup>-1</sup>. The results are shown as the mean values of the absorbance  $\pm$  the standard deviation of the mean ( $n = 3$ ).

The results obtained led to the discard of the amplified elutions of the Ph.D.-C7C library, carrying out the selection of individual clones only from the Ph.D.-12 library.

The final panning strategy followed for MPA was performed during the research stage at VTT Research center, Finland, using a magnetic bead-based protocol. In this case, a recombinant anti-MPA Fab antibody (from now on referred to as anti-MPA), previously selected from a phage display library,<sup>50</sup> was utilized for the selection rounds. Moreover, the phage display library employed for the mimopeptide selection was the Ph.D.-C7C library due to its commercial availability. The anti-MPA was first immobilized onto magnetic beads following the 'antibody coupling to magnetic beads' protocol described in the experimental section. The three selection rounds were carried out with no major modifications of the protocol described. The only modification for the second and third round was introducing an additional 30 s wash with PBS-0.1% T20. In this strategy, individual clones were selected directly from fresh titrating plates without carrying out an ELISA with polyclonal phages.

#### ***3.4.1.2. Selection of MPA mimopeptides by phage-based ELISA***

According to the results discussed before, individual phage clones were selected from the second and third panning strategies following the 'selection of monoclonal phages' protocol described in the experimental procedures. Regarding the second plate-based panning strategy with the Ph.D.-12 library, a total of 32 individual clones were selected from fresh titrating plates of the second and third round. Eight clones (1 to 8) were from the second round and the remaining twenty-four clones (9 to 32) were from the third round. The amplified 32 individual clones were initially screened in a phage-based ELISA (from now on referred to as ELISA with monoclonal phages) with background wells (without antibody but with blocking buffer) and target wells (with antibody and blocking buffer). The results, presented in **Figure 16**, proved that more than half of the individual phages selected showed specific binding towards the monoclonal MPA antibody. Only clone 26 presented higher affinity for the background than for the target well. These results confirmed the previous ones obtained in the ELISA with polyclonal phages, in which it was observed an almost negligible nonspecific interaction with background wells.

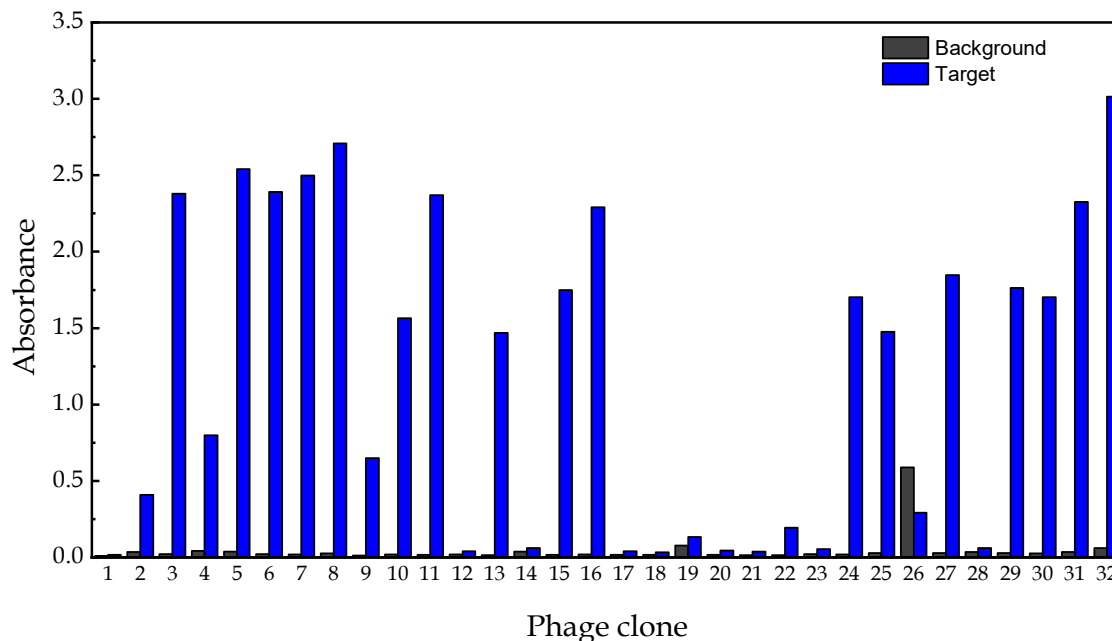


**Figure 16.** ELISA with monoclonal phages of the 32 clones selected from the second plate-based panning strategy with the Ph.D.-12 library for MPA. Only one clone showed significant affinity towards background wells (grey), whereas more than half selectively bound to the target wells containing the monoclonal antibody (blue). The results show the absorbance value for each clone ( $n=1$ ).

The 16 clones that showed the highest affinity for the antibody were tested in an ELISA with monoclonal phages with the same conditions as the previous one but introducing free MPA in some wells to test the competition. Therefore, three different types of wells were used in the new ELISA with monoclonal phages: background wells, target wells and competition wells (wells with antibody, blocking buffer and  $1 \mu\text{g mL}^{-1}$  free MPA to compete against the phages for the binding sites of the antibody). The free MPA was added at the same time as the phages in the ELISA.

**Figure 17** shows the results for the competitive ELISA with the 16 clones that presented the best binding. As can be observed, none of the clones competed with the free MPA for the binding sites of the antibody. Therefore, it can be concluded that the individual phages were selective for the monoclonal antibody but bound to a different antibody paratope than MPA and did not show competition with the mycotoxin.

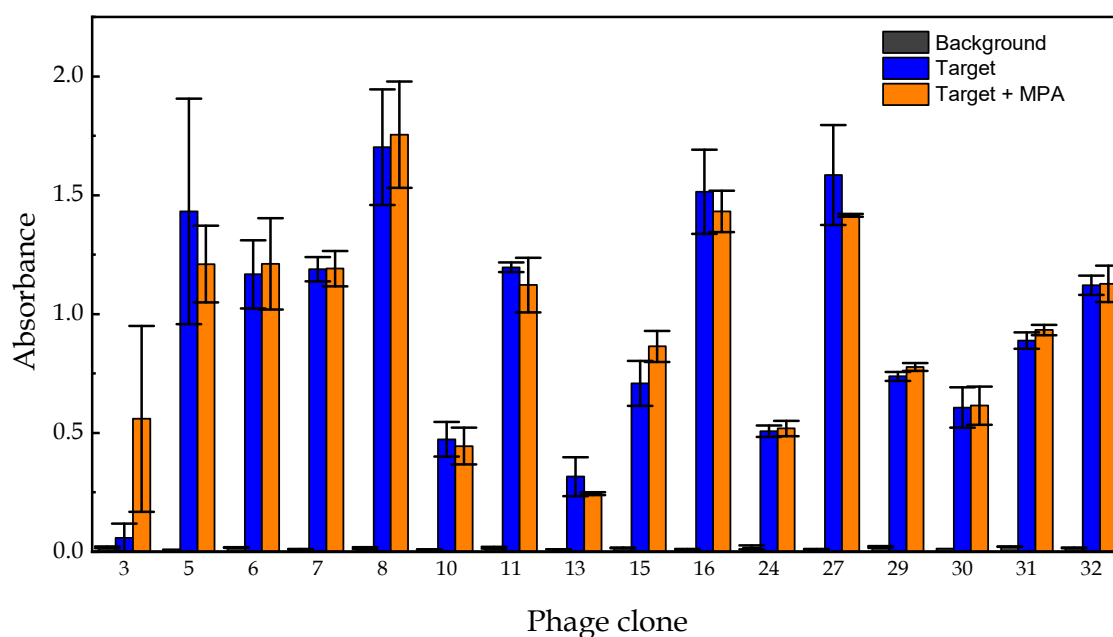


**Figure 17.** Competitive ELISA with monoclonal phages for the 16 clones with the highest affinity for the antibody. Not a single clone presented affinity for the background wells (grey), and most of them bound to the target wells containing the monoclonal antibody (blue). However, none of the clones showed competition when  $1 \mu\text{g mL}^{-1}$  free MPA was added to the wells (orange). The results are shown as the average absorbance value  $\pm$  the standard deviation of the mean ( $n = 2$ ).

With reference to the magnetic bead-based panning strategy, eight clones were selected from fresh titrating plates of the second and third round and were tested in a phage ELISA. Contrary to the direct coating of the antibody used before, streptavidin plates were used in this case. Therefore, the anti-MPA Fab antibody was previously biotinylated following the 'antibody biotinylation' protocol described in the experimental procedures. It can be observed in **Figure 18** that only one of the clones tested showed specific binding towards the anti-MPA Fab antibody. The remaining clones proved negligible signal for both background and target wells, similarly to the signal provided in the absence of phage clones (shown in the figure as 'Blank').

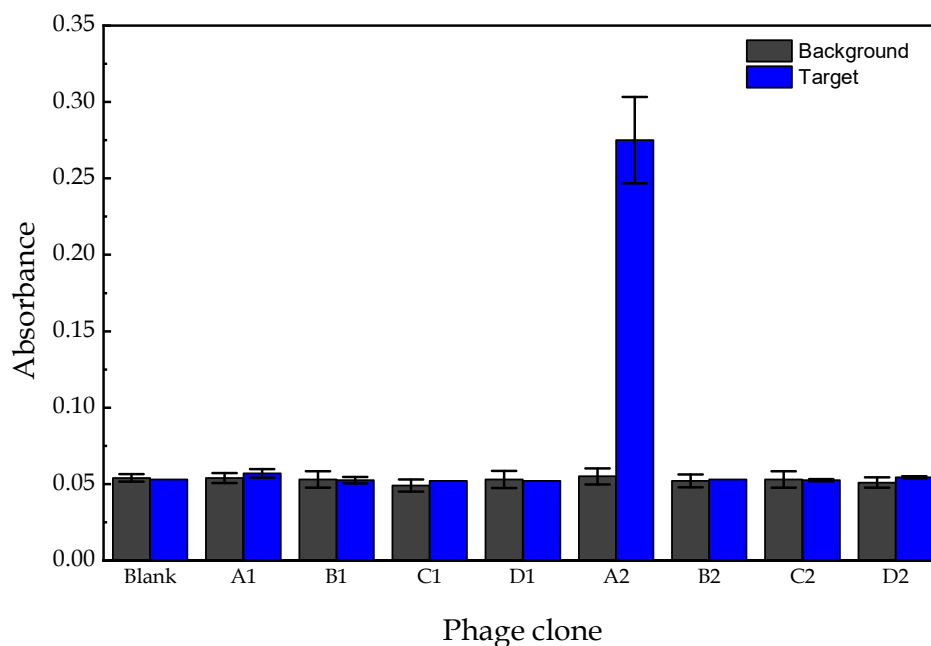


**Figure 18.** ELISA with monoclonal phages for the eight clones selected from the second and third round of the magnetic bead-based panning strategy for MPA. Phage clones did not show any background signal (grey) and only one of the clones, clone A2, presented affinity for the target antibody (blue). Additionally, background and target wells in the absence of phage (Blank) were tested, providing the similar signal as those phages that showed no interaction with the anti-MPA Fab antibody. The results are shown as the average absorbance value  $\pm$  the standard deviation of the mean ( $n = 3$ ).

Since only one of the clones showed competition, a competitive plate-based ELISA with monoclonal phages was carried out in the same conditions as the previous assay with several free MPA concentrations, ranging from  $0 \text{ ng mL}^{-1}$  to  $3200 \text{ ng mL}^{-1}$ . The results shown on **Figure 19** reflect a clear competition between the free MPA and the A2 phage clone for the anti-MPA Fab antibody. However, in order to confirm these results, a bead-based phage ELISA was conducted. In this ELISA, the biotinylated anti-MPA Fab was coupled to neutravidin-conjugated magnetic beads. Then, the phage clone A2 and ranging concentrations of free MPA were added simultaneously. The results of the confirmatory phage ELISA appear on **Figure 20**. It can be confirmed that clone A2 showed a competition in the nanomolar range with free MPA for the anti-MPA Fab antibody. The calibration curve presented an  $\text{IC}_{50}$  of  $2.1 \text{ ng mL}^{-1}$  ( $6.6 \text{ nmol L}^{-1}$ ) and a limit of detection, calculated as the 10% inhibition of the maximum signal,<sup>72</sup> of  $0.61 \text{ ng mL}^{-1}$  ( $20.6 \text{ nmol L}^{-1}$ ).

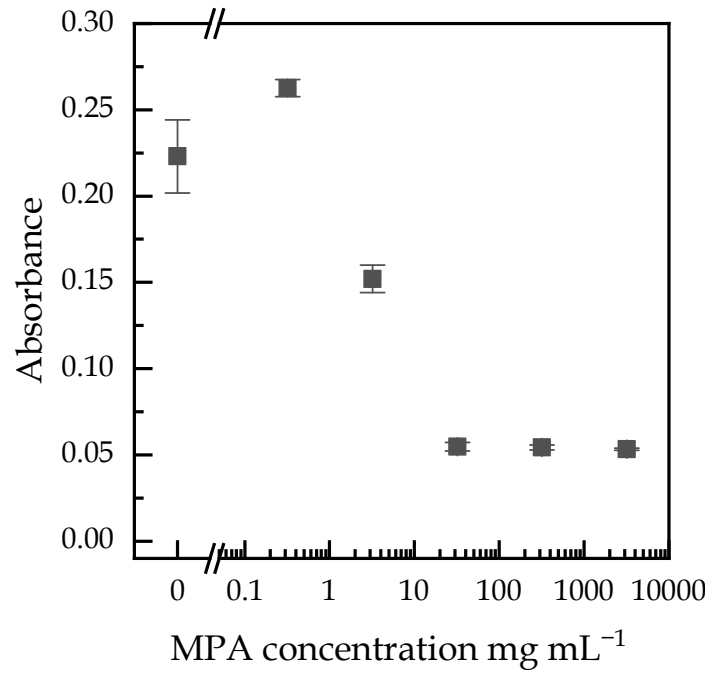


**Figure 19.** Competitive phage-based ELISA for clone A2 with increasing free MPA concentrations ranging from 0 ng mL<sup>-1</sup> to 3200 ng mL<sup>-1</sup>. The results represent the average absorbance values  $\pm$  the standard error of the mean ( $n = 3$ ).

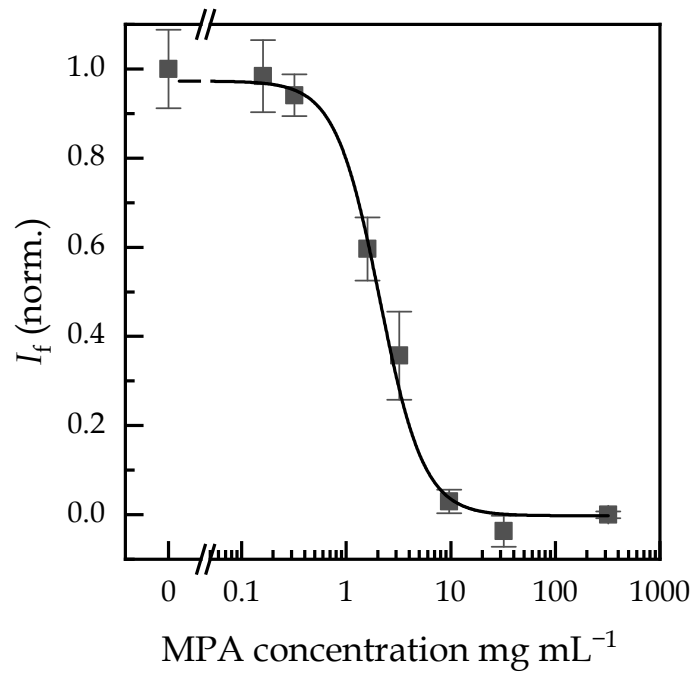


**Figure 20.** Confirmatory bead-based phage ELISA for clone A2. The phage clone A2 was incubated together with different MPA concentrations, ranging from 0 ng mL<sup>-1</sup> to 3200 ng mL<sup>-1</sup>. The results show the mean fluorescence intensity values  $\pm$  the standard error of the mean ( $n = 3$ ).

### **3.4.1.3. Sequence and structural analysis of MPA mimopeptide**

After the third panning for MPA, using the magnetic bead-based strategy, a phage clone that proved selectivity for the anti-MPA Fab antibody and competition with free MPA was isolated. The results revealed that the peptide sequence of the phage clone A2 was ACEGLYAHWC, with a disulfide bond between the two underlined cysteines. This sequence proved to be a unique sequence never found as a mimopeptide in the literature. Out of the seven amino acids composing the loop, together with the two cysteines, three of them (G, L and A) were nonpolar, aliphatic amino acids, two amino acids were aromatic (Y and W), one amino acid was positively charged (H) and the remaining amino acid was negatively charged (E). In total, four amino acids were nonpolar (G, L, A and W) and three of them were polar (Y, E and H).

### **3.4.2. Selection of mimopeptides for ochratoxin A**

Ochratoxin A is a very hazardous mycotoxin present in a wide variety of foodstuff, including cereals, wine and coffee. It can present adverse health effects such as nephrotoxicity and other renal diseases.<sup>73</sup> Similarly to MPA, to the best of our knowledge, no OTA mimopeptide has been described before. Therefore, one panning strategy was attempted to aim for the selection of the first OTA mimopeptide.

#### **3.4.2.1. Panning strategies**

The selection of OTA mimopeptides was also carried out during the research stage at VTT Research Center, Finland. Only one panning strategy was tested, using the magnetic bead-based strategy that resulted successful in the search of the MPA mimopeptide. The panning protocol was performed under the same conditions as for MPA, but this time the anti-OTA Fab antibody was coupled to the magnetic beads.

#### **3.4.2.2. Selection of OTA mimopeptides by Phage-based ELISA**

A total of 47 clones were selected from the second round (24 clones) and the third round (23 clones) and tested in an ELISA with monoclonal phages, with the same conditions as described above. The results shown in **Figure 21** refer to the screening of the clones from the second round, whereas the results of the clones from the third round appear in **Figure 22**. As can be seen, a positive control with A2 clone and anti-MPA Fab was added in both cases. The results prove that none of the individual clones selected presented any specificity for the anti-OTA Fab antibody. Therefore, the panning for the search of OTA mimopeptides was not successful.



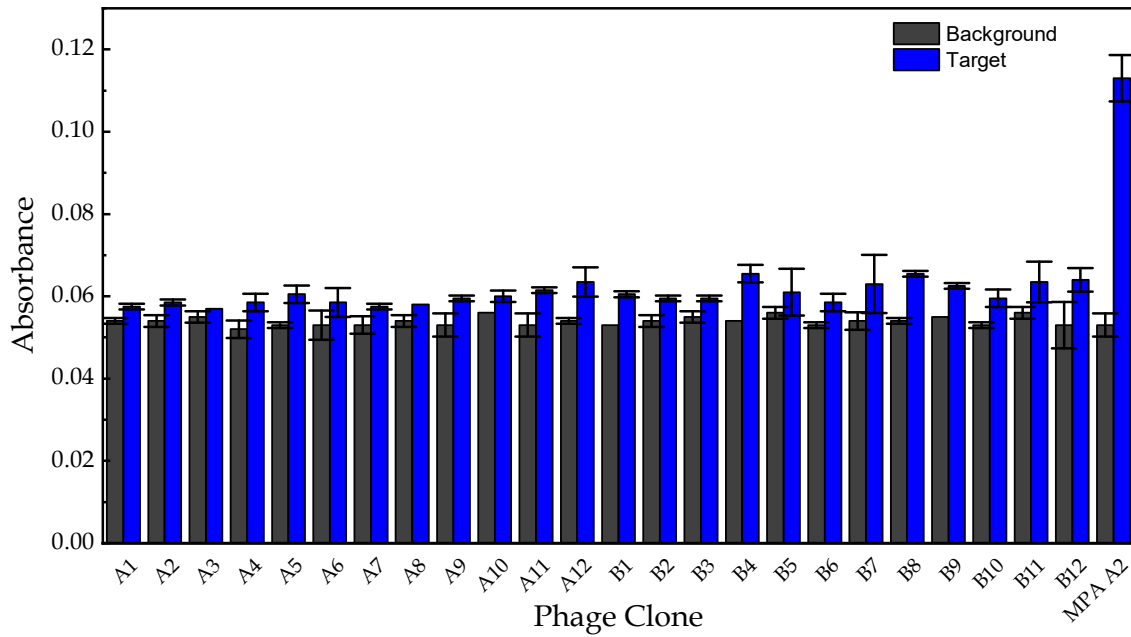


**Figure 21.** ELISA with monoclonal phages for the 24 individual clones selected from the second round of the magnetic bead-based panning for OTA. A positive control (MPA clone A2 for anti-MPA Fab antibody) was also tested. The clones showed a similar behavior for the background (grey) and the target wells with anti-OTA Fab (blue). The results show the average absorbance values  $\pm$  the standard deviation of the mean ( $n = 2$ ).

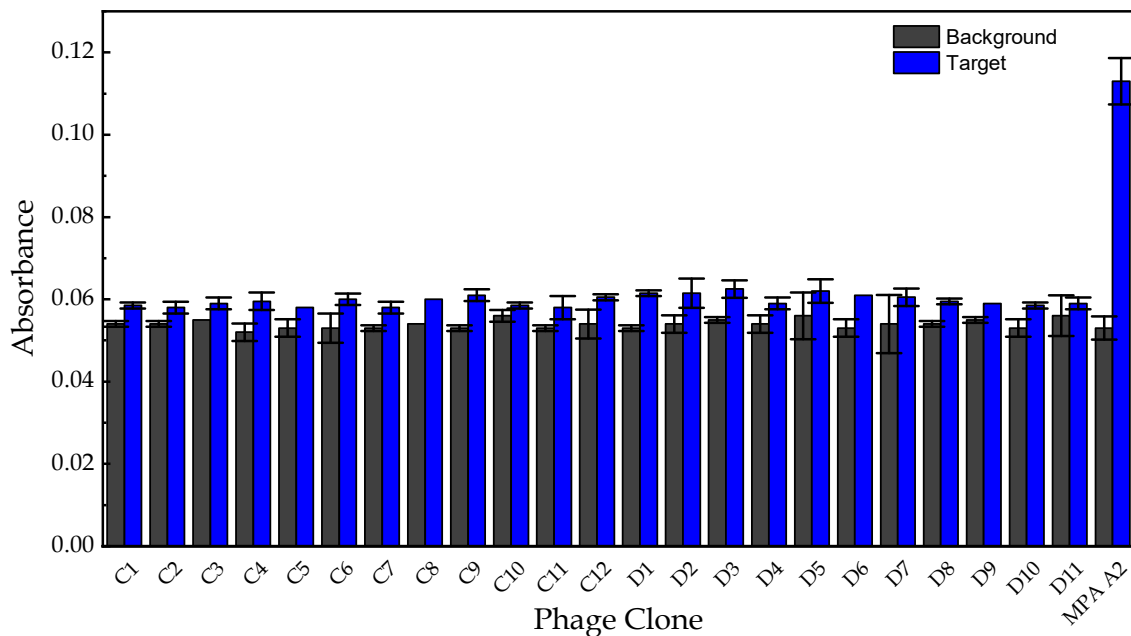


**Figure 22.** ELISA with monoclonal phages for the 23 individual clones selected from the third round of the magnetic bead-based panning for OTA. In the same way as the ELISA for the clones of the second round, the same positive control (MPA clone A2 for anti-MPA Fab) was tested. None of the clones tested showed any remarkable difference between the background (grey) and target

wells with anti-OTA Fab (blue). The results show the average absorbance values  $\pm$  the standard deviation of the mean ( $n = 2$ ).

### 3.4.3. Selection of mimopeptides for alternariol (AOH)

Alternariol was the third and last mycotoxin targeted for the selection of mimopeptides. This non-legislated mycotoxin is one of the most prominent mycotoxin from *Alternaria* species typically found in fruits and vegetables.<sup>74</sup> Similar to MPA and OTA, there has not been described yet any mimopeptide for AOH.

#### 3.4.3.1. Panning strategies

A total of five different panning strategies were conducted for AOH, all of them following the plate-based method described in the experimental part. In order to carry out all the pannings, a monoclonal anti-AOH antibody, provided in the frame of a Material Transfer agreement by Dr. Antonio Abad and Dr. Josep Mercader from Instituto de Agroquímica y Tecnología de Alimentos (IATA) in Valencia, Spain, was used for the assays. **Table 8** reflects the conditions for the first panning strategy (used for both libraries, Ph.D.-12 and Ph.D.-C7C).

**Table 8.** Experimental conditions of the first panning strategy for the selection of AOH mimopeptides.

Anti-AOH monoclonal antibody, Ph.D.-12 and Ph.D.-C7C libraries		
1st round	Negative selection	No
	Blocking	No
	Target selection	3 wells with 10 $\mu\text{g mL}^{-1}$ of Ab, 1.5 h
	Washing	6 times with 150 $\text{mmol L}^{-1}$ NaCl + 0.05% T20
	Elution	Gly-HCl pH 2.2, 10 min
2nd round	Negative selection	No
	Blocking	No
	Target selection	2 wells with 5 $\mu\text{g mL}^{-1}$ of Ab, 1 h
	Washing	10 times with 150 $\text{mmol L}^{-1}$ NaCl + 0.05% T20
	Elution	Gly-HCl pH 2.2, 10 min
3rd round	Negative selection	No
	Blocking	No
	Target selection	2 wells with 2.5 $\mu\text{g mL}^{-1}$ of Ab, 1 h
	Washing	12 times with 150 $\text{mmol L}^{-1}$ NaCl + 0.05% T20
	Elution	100 $\text{ng mL}^{-1}$ AOH, 30 min
4th round	Negative selection	No
	Blocking	No
	Target selection	1 well with 2.5 $\mu\text{g mL}^{-1}$ of Ab, 1 h
	Washing	15 times with 150 $\text{mmol L}^{-1}$ NaCl + 0.05% T20
	Elution	10 $\text{ng mL}^{-1}$ AOH, 30 min

The initial strategy consisted of eliminating the blocking and the negative selection to avoid any loss of diversity from the initial phage pool and allow the interaction of all the phages with the wells coated with the monoclonal anti-AOH antibody. By removing the blocking agent in the panning rounds, it was expected to obtain phages with no affinity for any blocking buffer later used in the ELISAs, although it could be expected to observe background binding to the wells. Moreover, these two selection rounds, one for each phage library, consisted of 4 rounds, in which the first two rounds were eluted with Gly-HCl and the last two rounds by displacement with free AOH. Following the recommendations of Dr. Antonio Abad and Dr. Josep Mercader, the washing buffer was also changed from PBS 1× + 0.1% T20 to 150 mmol L<sup>-1</sup> NaCl + 0.05% T20.

The output results from the two pannings using the strategy aforementioned can be seen in **Figure 23**. A considerable enrichment in the eluted phage output can be observed for both libraries between the first and the third round. However, the output phages drop in the fourth round for both cases, with a more dramatic decrease in the case of the Ph.D.-C7C library.

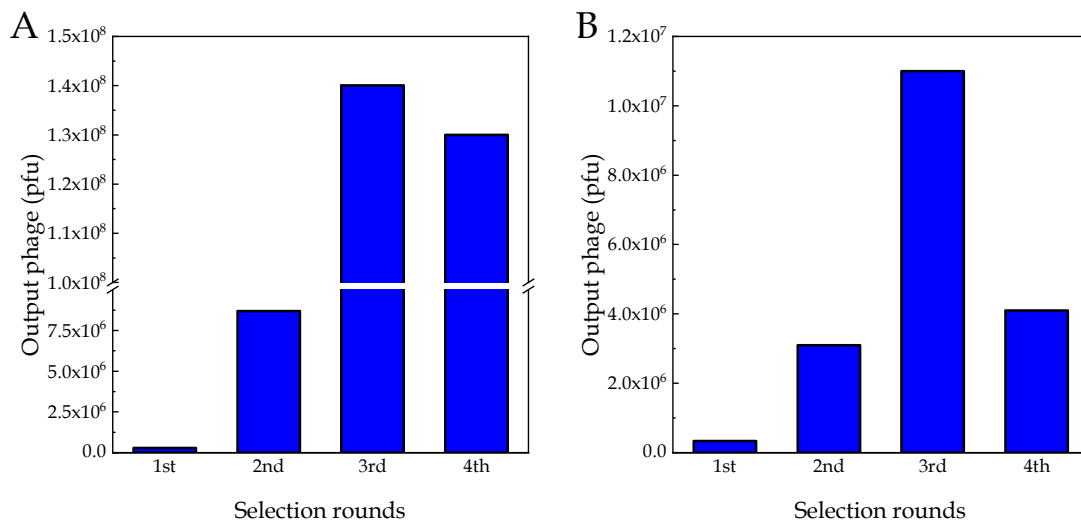


**Figure 23.** Phage output obtained from the eluates of the four selection rounds from the first panning strategy for AOH mimopeptides. A. Output for the Ph.D.-12 library and B. Output for the Ph.D.-C7C library.

The amplified phages of the four rounds of both libraries were consequently tested in an ELISA with polyclonal phages and the results can be seen in **Figure 24**. For these ELISAs, the wells were previously blocked with BSA 3% for two hours. It was expected that the phage pools would present low nonspecific binding after introducing a blocking buffer that was not previously used during the selection rounds. However, the results proved that the amplified fractions of the Ph.D.-12 library showed high nonspecific binding, whereas the fractions from the third and fourth round of the Ph.D.-C7C library presented specificity for the target wells coated with the antibody. Therefore, the selection of individual clones was carried out only from the third and fourth rounds of the Ph.D.-C7C library.

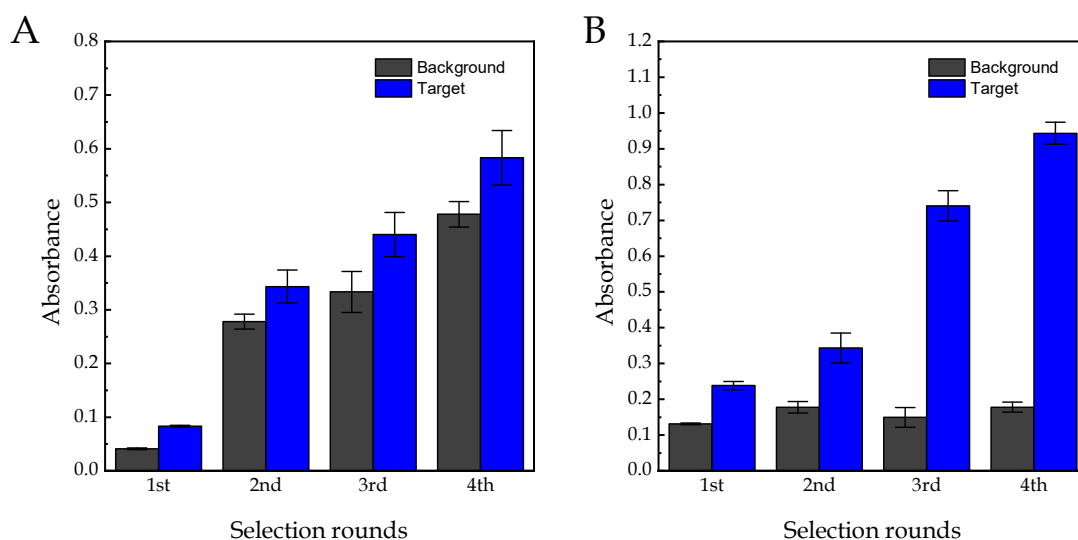


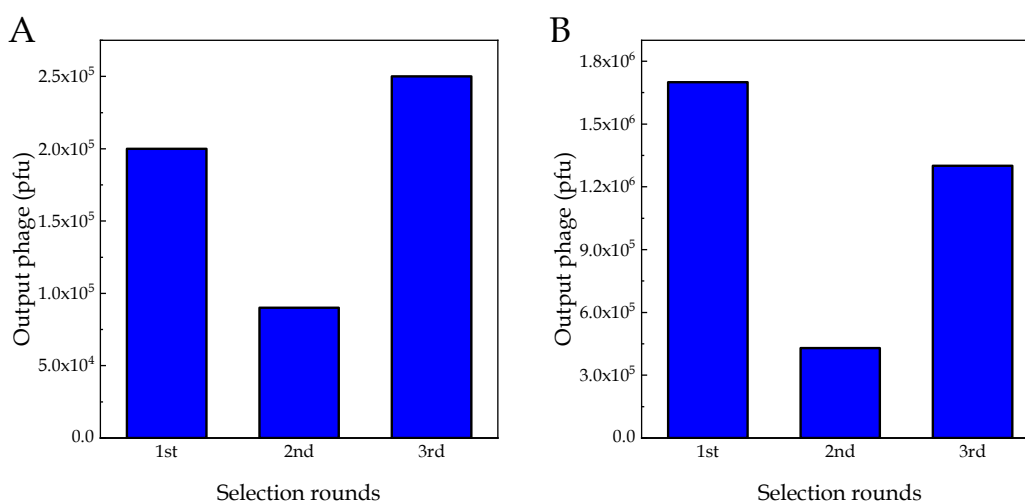
**Figure 24.** ELISA with polyclonal phages for the first two panning for AOH mimopeptides. A. Results obtained for the Ph.D.-12 amplified fractions, in which phages have similar specificity for target wells (blue) and background wells (grey) and B. Results for the Ph.D.-C7C amplified fractions, showing high specificity for target wells and little binding for background wells. In both cases, the phage concentration tested was  $5 \cdot 10^9$  pfu mL<sup>-1</sup>. The results are shown as the mean values of the absorbance  $\pm$  the standard deviation of the mean ( $n = 3$ ).

**Table 9** presents the conditions of the second panning strategy for AOH mimopeptides. In this case, it was decided that the negative selections and the plate blocking would not still be introduced. However, the number of rounds, as well as the washing and the elution conditions were modified. Taking into account the results from the first panning strategy, the fourth round seemed to be ineffective in terms of phage enrichment, therefore, it was decided to proceed with only three selection rounds. Moreover, the washing conditions were switched to the original conditions described for the selections of MPA mimopeptides, but with a higher number of washes than before. This increase in the number of washes was implemented in order to reduce the nonspecific binding of the phages in the wells. Nevertheless, the most drastic change was introduced in the elution conditions. For the second and the third round, a double elution was conducted in order to remove more nonspecific interactions. For the second round, a first elution was carried out with  $100 \text{ ng mL}^{-1}$  AOH for 30 min, followed by another elution under the same conditions. With reference to the third round, the first elution was performed with Gly-HCl pH 2.2 for 10 min, to remove more nonspecific phages, and the second elution was with  $100 \text{ ng mL}^{-1}$  AOH for 30 min. In both cases, only the second elutions were kept and amplified.

**Table 9.** Experimental conditions of the second panning strategy for the selection of AOH mimopeptides.

Anti-AOH monoclonal antibody, Ph.D.-12 and Ph.D.-C7C libraries		
1st round	Negative selection Blocking Target selection Washing Elution	No No 3 wells with $10 \mu\text{g mL}^{-1}$ of Ab, 1.5 h 8 times with PBS + 0.1 % T20 Gly-HCl pH 2.2, 10 min
2nd round	Negative selection Blocking Target selection Washing Elution	No No 2 wells with $5 \mu\text{g mL}^{-1}$ of Ab, 1 h 15 times with PBS + 0.1 % T20 First elution with $100 \text{ ng mL}^{-1}$ AOH, 30 min Second elution with $100 \text{ ng mL}^{-1}$ AOH, 30 min
3rd round	Negative selection Blocking Target selection Washing Elution	No No 1 well with $2.5 \mu\text{g mL}^{-1}$ of Ab, 1 h 15 times with PBS + 0.1 % T20 First elution with Gly-HCl pH 2.2, 10 min Second elution with $100 \text{ ng mL}^{-1}$ AOH, 30 min

The phage output results for the second panning strategy are shown in **Figure 25**. Phage output obtained from the eluates of the three selection rounds from the second panning strategy for AOH mimopeptides. A. Output for the Ph.D.-12 library and B. Output for the Ph.D.-C7C library. In this case, both libraries experience a similar and expected behavior. Since a double elution was introduced in the second round, the phage output severely decreases with both libraries. The third round in both cases, even with a double elution, recovers the values obtained in the first elution, confirming an enrichment of the phages eluted from the second to the third round.

**Figure 25.** Phage output obtained from the eluates of the three selection rounds from the second panning strategy for AOH mimopeptides. A. Output for the Ph.D.-12 library and B. Output for the Ph.D.-C7C library.

The results of the ELISAs with polyclonal phages for both libraries are displayed in **Figure 26**. Whereas the Ph.D.-C7C library maintains a good specificity for the target wells throughout the three rounds, this specificity is lost in the third round of the Ph.D.-12 library. Again, these results lead to the selection of individual clones only from the second and third round of the Ph.D.-C7C library.

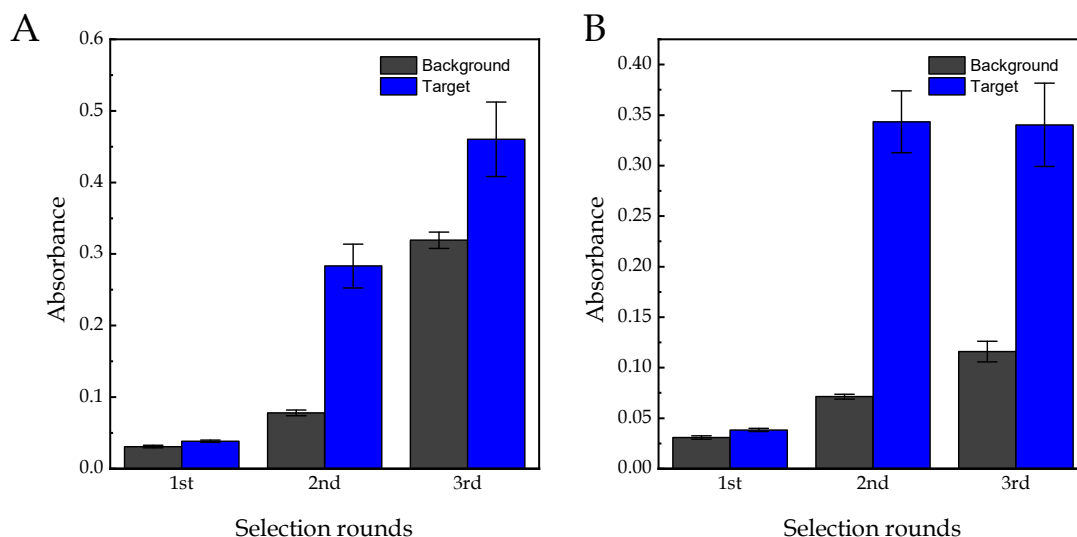


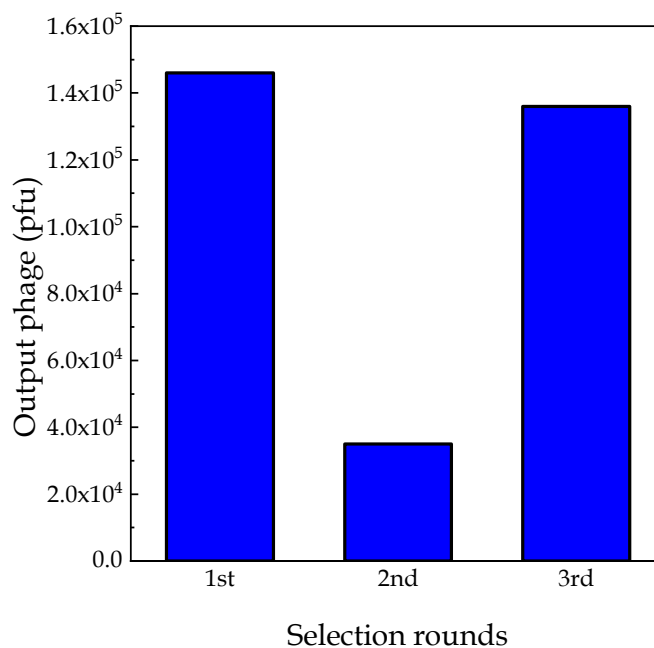
**Figure 26.** ELISA with polyclonal phages for the second panning strategy for AOH mimopeptides. A. Results obtained for the Ph.D.-12 amplified fractions, in which phages gain specificity for target wells (blue), maintaining a negligible signal in background wells (grey) until the third round, in which the non-specificity was amplified and, B. Results for the Ph.D.-C7C amplified fractions, showing high specific binding for target wells since the second round in comparison to background wells. In both cases, the phage concentration tested was  $5 \cdot 10^9$  pfu mL<sup>-1</sup>. The results are shown as the mean values of the absorbance  $\pm$  the standard deviation of the mean ( $n = 3$ ).

The experimental conditions of the last panning are detailed in **Table 10**. In this case, both negative selections and blocking steps were introduced, in a similar manner as the ones detailed for the first panning strategy for MPA mimopeptides. The rest of the protocol followed similar experimental conditions as for the first MPA protocol described previously. Only three rounds were carried out, with decreasing number of target wells for the selection and a progressive number of washes after the phage incubation. The first elution was conducted with Gly-HCl, whereas the second and third rounds were eluted only once by a displacement with 100 ng mL<sup>-1</sup> AOH and 10 ng mL<sup>-1</sup> AOH, respectively. Moreover, due to the dissatisfactory results obtained previously with the Ph.D.-12 library, it was decided to carry out the panning with the Ph.D.-C7C library.

**Table 10.** Experimental conditions of the third panning strategy for the selection of AOH mimopeptides.

Anti-AOH monoclonal antibody, Ph.D.-C7C library		
1st round	Negative selection Blocking Target selection Washing Elution	1.5 h BSA 3% in PBS 1×, 2 h 3 wells with 10 µg mL <sup>-1</sup> of Ab, 1.5 h 6 times with PBS + 0.1 % T20 Gly-HCl pH 2.2, 10 min
2nd round	Negative selection Blocking Target selection Washing Elution	1 h BSA 3% in PBS 1×, 2 h 2 wells with 5 µg mL <sup>-1</sup> of Ab, 1 h 10 times with PBS + 0.1 % T20 100 ng mL <sup>-1</sup> AOH, 30 min
3rd round	Negative selection Blocking Target selection Washing Elution	1 h BSA 3% in PBS 1×, 2 h 1 well with 2.5 µg mL <sup>-1</sup> of Ab, 1 h 12 times with PBS + 0.1 % T20 10 ng mL <sup>-1</sup> AOH, 30 min

The results of the phage output in **Figure 27** show that there was a decrease in the phage output from the first round to the second of one order of magnitude. This dramatic drop can be attributed to the modification of the elution method between these two rounds. This variation has been observed in some of the panning described previously.

**Figure 27.** Phage output obtained from the eluates of the three selection rounds from the last panning strategy for AOH mimopeptides.

According to the results of the ELISA with polyclonal phages (**Figure 28**), the first two rounds did not show significant binding for the target antibody. However, the third round proved considerably affinity towards the antibody, with negligible binding to the background wells containing with the same blocking buffer employed in the selection rounds. Therefore, the selection of monoclonal phages was carried out from the eluted fraction of phages of the third round

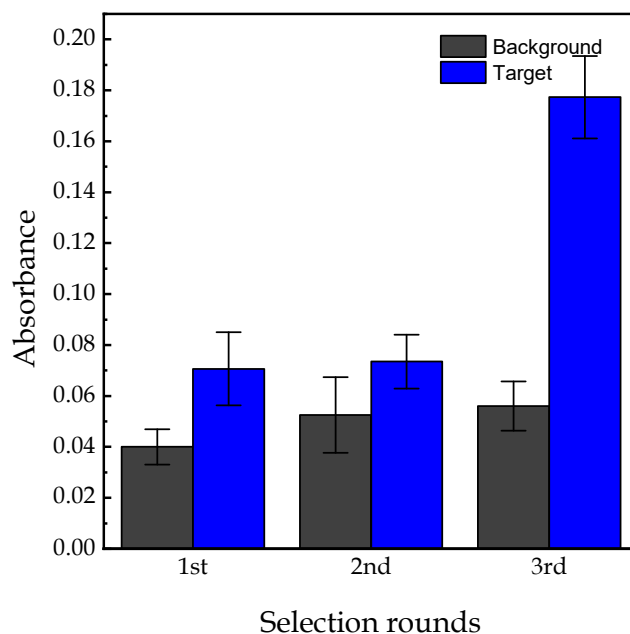


**Figure 28.** ELISA with polyclonal phages for the last panning strategy for AOH mimopeptides. High specificity for target wells (blue) is achieved only in the third round. The other two rounds present very low affinity for both target and background (grey) wells. The phage concentration tested was  $5 \cdot 10^9$  pfu mL<sup>-1</sup>. The results are shown as the mean values of the absorbance  $\pm$  the standard deviation of the mean ( $n = 3$ ).

#### 3.4.3.2. Selection of AOH mimopeptides by phage-based ELISA

More than one hundred clones from the different selection rounds were picked and tested in ELISAs with monoclonal phages, carried out in a similar way as described before. Clones were only selected from the Ph.D.-C7C library due to the dissatisfactory results obtained in the selection rounds with the Ph.D.-12 library. The clones that presented a significant affinity towards the antibody and negligible background signal were consequently tested in a similar ELISA with competition with free AOH. With reference to the first panning strategy, a total of 47 different clones were selected and tested. The results of the first ELISA with monoclonal phages appear in **Figure 29**. It can be observed that nearly half of the clones presented affinity towards the monoclonal antibody and only a few of them bound to the wells nonspecifically.



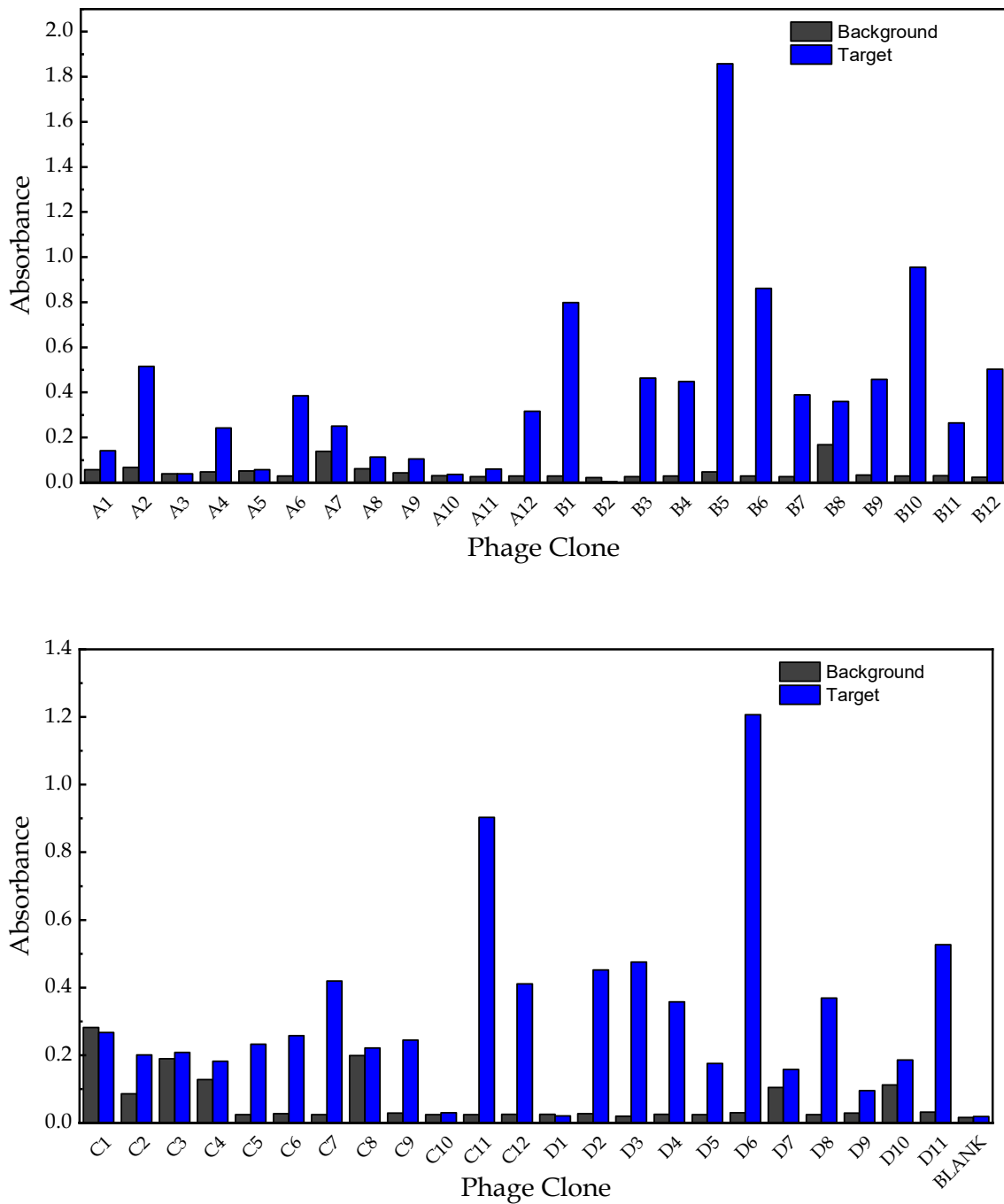


**Figure 29.** ELISA with monoclonal phages for the 47 individual clones selected from the third (top) and fourth (bottom) rounds of the first panning strategy with the Ph.D.-C7C library for AOH. Nearly half of the clones presented specificity for the target wells (blue) and negligible signal for background wells (grey). The results show the absorbance value for each clone ( $n=1$ ).

The 20 clones that presented the highest signal were tested in a second ELISA, in with the presence of  $100 \text{ ng mL}^{-1}$  AOH. The results, shown in **Figure 30**, prove that all of the clones, except one, were selective for the target antibody, but none of them presented competition with the free AOH added. Therefore, it is believed that the

amplified phages bound to a different antibody paratope than AOH, resulting in an unsuccessful panning.

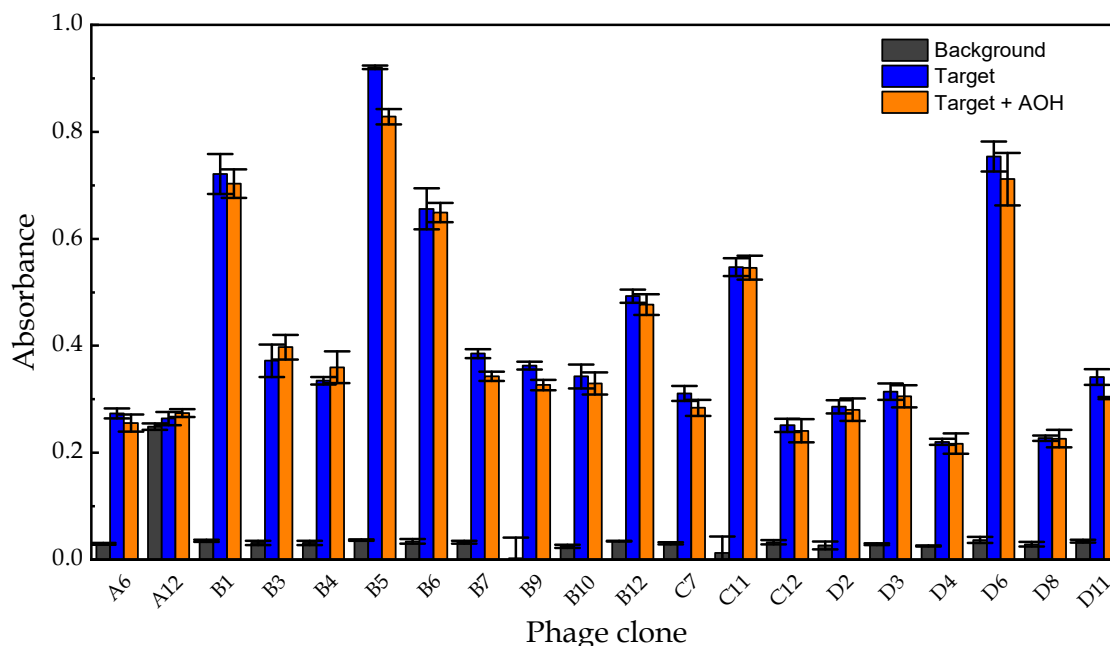


**Figure 30.** Competitive ELISA with monoclonal phages for the 20 clones with the highest affinity for the antibody. Only one clone presented affinity for the background wells (grey), and all of them bound to the target wells containing the monoclonal antibody (blue). However, none of the clones showed exceptional competition when  $100 \text{ ng mL}^{-1}$  free AOH was added to the wells (orange). The results are shown as the average absorbance value  $\pm$  the standard deviation of the mean ( $n = 3$ ).

Regarding the second panning strategy, a total of 48 clones were picked from the second and third selection rounds of the panning with the Ph.D.-C7C library. The results displayed in **Figure 31** proved a rather high nonspecific binding for those phages selected from the second round, whereas the phages from the third round presented in general very low affinity for both background and target wells. Nevertheless, some of the clones selected from both rounds were selective for the monoclonal antibody and were consequently tested in a competitive ELISA with  $100 \text{ ng mL}^{-1}$  free AOH. The results for the competitive ELISA with monoclonal phages are shown in **Figure 32**. The poor results from the previous ELISA were confirmed in the competitive ELISA, with none of the clones showing competition with AOH for the binding sites of the antibody.

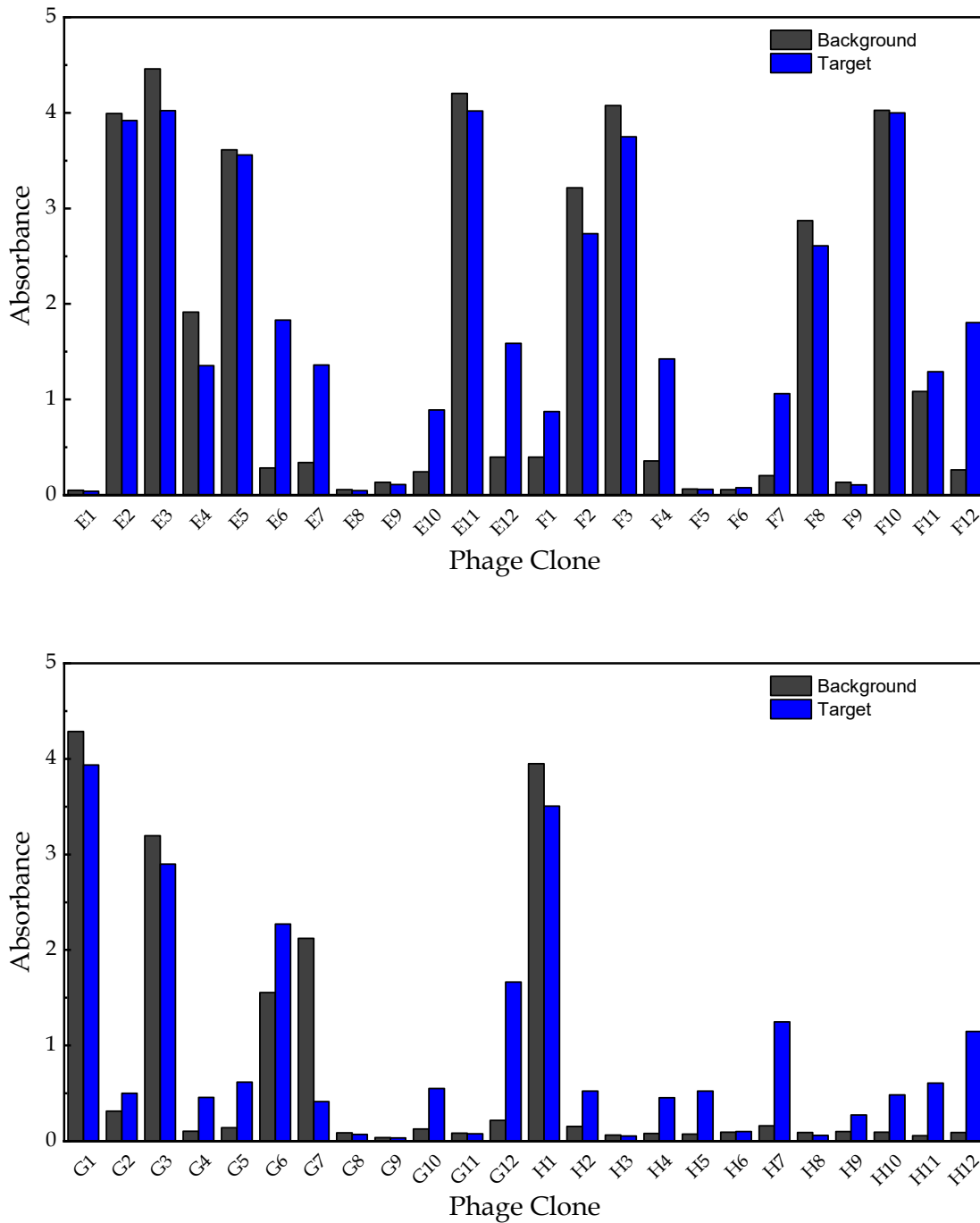


**Figure 31.** ELISA with monoclonal phages for the 48 individual clones selected from the second (top) and third (bottom) rounds of the second panning strategy with the Ph.D.-C7C library for AOH. Nearly a third of the clones presented specificity for the background wells (grey) and only a few clones showed specificity for target wells (blue). The results show the absorbance value for each clone ( $n=1$ ).

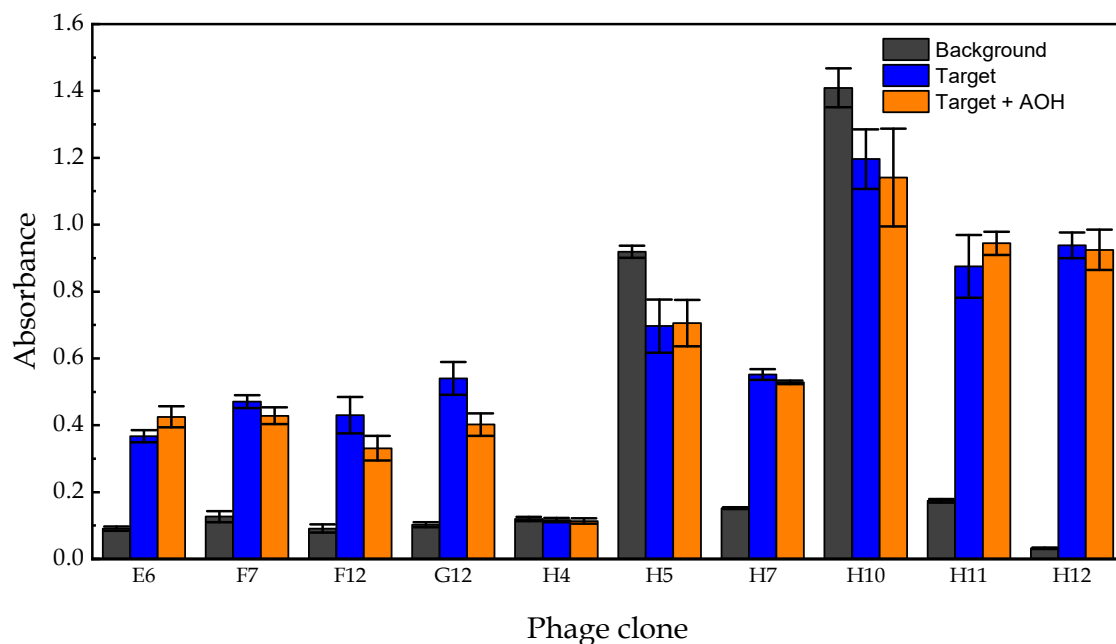


**Figure 32.** Competitive ELISA with monoclonal phages for the 10 clones with the highest affinity for the antibody. Two of the clones presented affinity for the background wells (grey), and seven of them bound selectively to the target wells containing the monoclonal antibody (blue). However, none of the clones showed exceptional competition when  $100 \text{ ng mL}^{-1}$  free AOH was added to the wells (orange). The results are shown as the average absorbance value  $\pm$  the standard deviation of the mean ( $n = 3$ ).

For the final panning strategy described and considering the results of the ELISA with polyclonal phages previously reported, a total of 24 clones were selected and tested in an ELISA with monoclonal phages. The results can be observed in **Figure 33**. The majority of the clones selected showed negligible affinity for background and target wells. However, some of the clones (especially clone I2) presented high affinity for the target wells. The 10 clones with the highest signal to background difference were tested in a competitive ELISA with  $100 \text{ ng mL}^{-1}$  free AOH (**Figure 34**). It can be observed that clone J5 showed a slight competition with AOH for the binding sites. However, when the clone was tested in a similar ELISA with varying concentrations of AOH, it showed negligible competition. Therefore, it can be concluded that some of the clones selected as potential AOH mimopeptides were good antibody binders, but none of them competed effectively with free AOH for the binding sites of the monoclonal antibody.

Future work related to the search of AOH mimopeptides will be focused on a different panning strategy, such as the bead-based strategy that proved good results in the quest of MPA mimopeptides. Moreover, IgG antibodies always presents more potential binding sites compared to Fab antibodies. This could increase the chances of finding selective binders for the antibody which fail to compete for the binding sites of AOH. In addition to that, a different phage display library may be tested in the quest of AOH mimopeptides due to the dissatisfactory results obtained with both Ph.D.-12 and Ph.D.C7C libraries.

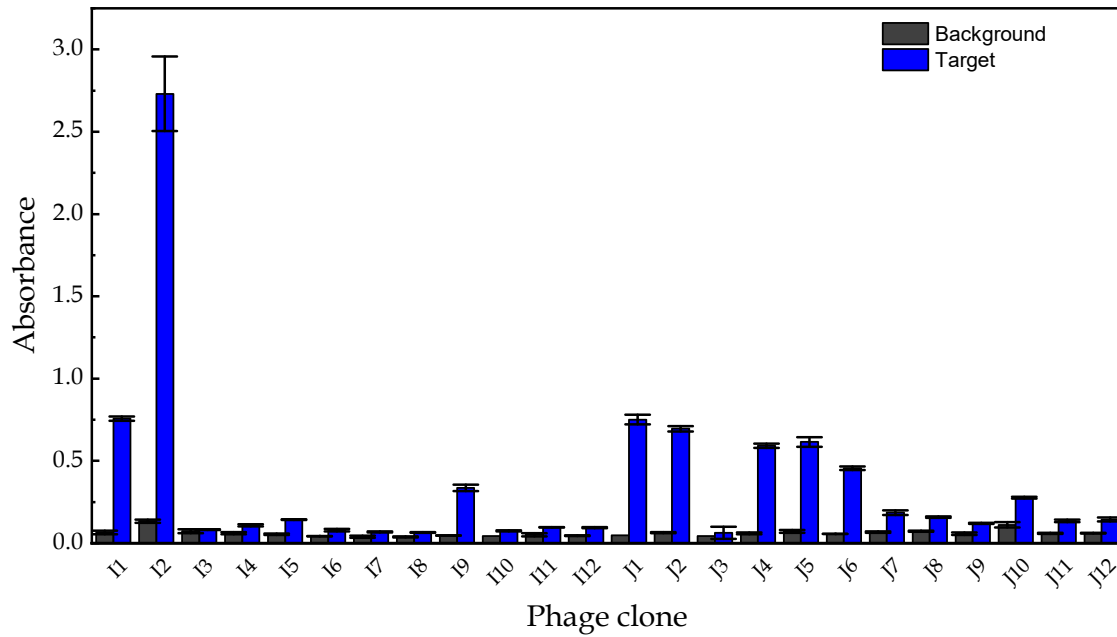


**Figure 33.** ELISA with monoclonal phages for the 24 individual clones selected from the third round of the last panning strategy with the Ph.D.-C7C library for AOH. None of the clones presented specificity for the background wells (grey) and roughly half of the clones showed specificity for target wells (blue). The results are shown as the average absorbance value  $\pm$  the standard deviation of the mean ( $n = 2$ ).

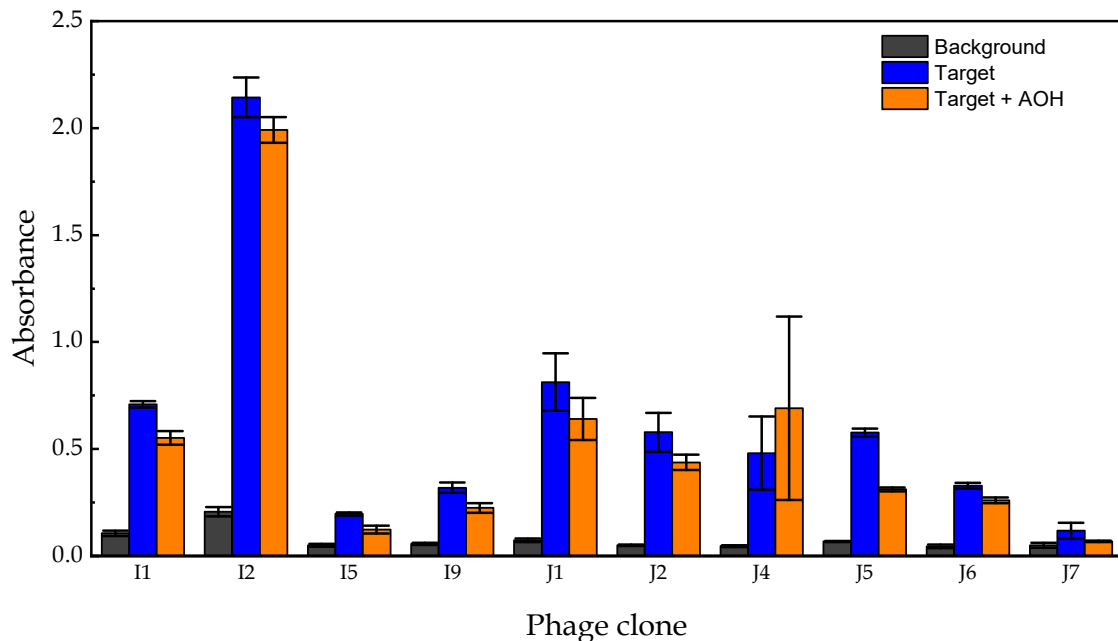


**Figure 34.** Competitive ELISA with monoclonal phages for the 10 clones with the highest affinity for the antibody. None of the clones presented affinity for the background wells (grey), and eight of them bound selectively to the target wells containing the monoclonal antibody (blue). Some of the clones showed a slight competition when  $100 \text{ ng mL}^{-1}$  free AOH was added to the wells

(orange). The results are shown as the average absorbance value  $\pm$  the standard deviation of the mean ( $n = 3$ ).

### 3.4.3.3. Sequence and structural analysis of AOH mimopeptides

Some of the clones that selectively bound to the antibody were sequenced to possibly identify any amino acid pattern between the phage clones. Some similarities between the sequenced phage clones can be observed (**Table 11**). All of the clones contained the WY pattern, and three of them presented it in the same position. Furthermore, two of the clones displayed the same sequence, whereas the third one had 4 of the amino acids in the same position. The repeated amino acid sequence, GNQWYNE, consisted of two nonpolar amino acids, G and W, four polar amino acids, Y, Q and two Ns, and one negatively charged amino acid, E. Therefore, the amino acid sequence proved to be highly polar. Moreover, two of the three aromatic amino acids, W and Y, were present in all of the sequences. Consequently, it is believed that the aromatic rings of the amino acids can effectively contribute to the specific binding towards the antibody.

**Table 11.** Identified amino acid sequences from the AOH panning. The conserved amino acid sequences between the different clones are reflected in bold.

Clone name	Amino acid sequence
B5	--ACGLHWYNWC-
B7	--ACGNQWYNEC-
B9	--ACGNQWYNEC-
D11	-ACEDVPWYKC--

### 3.5. Conclusions

Phage display has proven to be a useful technique for the selection of MPA mimopeptides from a commercial phage display library, Ph.D.-C7C. This commercial library consists of a sequence of 7 randomized amino acids that is flanked by a disulfide constrained loop generated by two cysteines.

The plate-based method described in this chapter has given dissatisfactory results in the quest of novel mimopeptides for MPA and AOH. In this method, the antibody is coated onto the wells in a non-oriented way. However, the bead-based method, in which the antibody paratope is always oriented, has proven excellent results for the selection of an MPA mimopeptide.

The selected MPA mimopeptide, clone A2, expressing the amino acid sequence ACEGLYAHWC (with a disulfide bond between the two Cs) showed an excellent competition with free MPA in the nanomolar range, with an  $IC_{50}$  of  $2.1 \text{ ng mL}^{-1}$  and a limit of detection of  $0.61 \text{ ng mL}^{-1}$ .

The sequenced phage clones selective for the anti-AOH antibody revealed a conserved WY motif in all of them, determining that the presence of aromatic rings seemed mandatory to establish a tight affinity for some binding sites of the antibody.

Future work related to the search of AOH mimopeptides should be focused on a bead-based strategy and the use of a different antibodies. Moreover, due to the dissatisfactory results obtained with the Ph.D.-12 and Ph.D.-C7C libraries, a different phage display library could be tested in the quest of AOH mimopeptides

### 3.6. Bibliography

- (1) Smith, G. P.; Petrenko, V. A. Phage Display. *Chem. Rev.* **1997**, *97*, 391–410. <https://doi.org/10.1021/cr960065d>.
- (2) Smith, G. P. Filamentous Fusion Phage: Novel Expression Vectors That Display Cloned Antigens on the Virion Surface. *Science* **1985**, *228*, 1315–1317. <https://doi.org/10.1126/science.4001944>.
- (3) Scott, J. K.; Smith, G. P. Searching for Peptide Ligands with an Epitope Library. *Science* **1990**, *249*, 386–390. <https://doi.org/10.1126/science.1696028>.
- (4) Devlin, J. J.; Panganiban, L. C.; Devlin, P. E. Random Peptide Libraries: A Source of Specific Protein Binding Molecules. *Science* **1990**, *249*, 404–406. <https://doi.org/10.1126/science.2143033>.
- (5) McCafferty, J.; Griffiths, A. D.; Winter, G.; Chiswell, D. J. Phage Antibodies: Filamentous Phage Displaying Antibody Variable Domains. *Nature* **1990**, *348*, 552–554. <https://doi.org/10.1038/348552a0>.
- (6) Winter, G.; Griffiths, A. D.; Hawkins, R. E.; Hoogenboom, H. R. Making Antibodies by Phage Display Technology. *Annu. Rev. Immunol.* **1994**, *12*, 433–455. <https://doi.org/10.1146/annurev.iy.12.040194.002245>.
- (7) Hoogenboom, H. R.; Griffiths, A. D.; Johnson, K. S.; Chiswell, D. J.; Hudson, P.; Winter, G. Multi-Subunit Proteins on the Surface of Filamentous Phage: Methodologies for Displaying Antibody (Fab) Heavy and Light Chains. *Nucleic Acids Res.* **1991**, *19*, 4133–4137.
- (8) The Nobel Prize in Chemistry 2018 <https://www.nobelprize.org/prizes/chemistry/2018/summary/> (accessed 2021 -04 -11).
- (9) Barderas, R.; Benito-Peña, E. The 2018 Nobel Prize in Chemistry: Phage Display of Peptides and Antibodies. *Anal. Bioanal. Chem.* **2019**, *411*, 2475–2479. <https://doi.org/10.1007/s00216-019-01714-4>.
- (10) Domingo-Calap, P.; Delgado-Martínez, J. Bacteriophages: Protagonists of a Post-Antibiotic Era. **2018**, *16*.
- (11) *Bacteriophages: Biology and Applications*; Kutter, E., Sulakvelidze, A., Eds.; CRC Press: Boca Raton, FL, 2005.
- (12) Bradley, D. E. Ultrastructure of Bacteriophages and Bacteriocins. *Bacteriol. Rev.* **85**.
- (13) Rohwer, F.; Edwards, R. The Phage Proteomic Tree: A Genome-Based Taxonomy for Phage. *J. Bacteriol.* **2002**, *184*, 7.
- (14) Ackermann, H.-W. Bacteriophage Observations and Evolution. *Research in Microbiology* **2003**, *154*, 245–251. [https://doi.org/10.1016/S0923-2508\(03\)00067-6](https://doi.org/10.1016/S0923-2508(03)00067-6).
- (15) Ackermann, H.-W. 5500 Phages Examined in the Electron Microscope. *Arch. Virol.* **2007**, *152*, 227–243. <https://doi.org/10.1007/s00705-006-0849-1>.
- (16) Barbas, C. F.; Burton, D. R.; Silverman, G. J. *Phage Display: A Laboratory Manual*; CSHL Press, 2004.
- (17) Sidhu, S. S.; Geyer, C. R. *Phage Display In Biotechnology and Drug Discovery*; CRC Press, 2015.
- (18) Beck, E.; Sommer, R.; Auerswald, E. A.; Kurz, Ch.; Zink, B.; Osterburg, G.; Schaller, H.; Sugimoto, K.; Sugisaki, H.; Okamoto, T.; Takanami, M. Nucleotide Sequence of Bacteriophage Fd DNA. *Nucleic Acids Res.* **1978**, *5*, 4495–4504. <https://doi.org/10.1093/nar/5.12.4495>.



- (19) van Wezenbeek, P. M.; Hulsebos, T. J.; Schoenmakers, J. G. Nucleotide Sequence of the Filamentous Bacteriophage M13 DNA Genome: Comparison with Phage Fd. *Gene* **1980**, *11*, 129–148. [https://doi.org/10.1016/0378-1119\(80\)90093-1](https://doi.org/10.1016/0378-1119(80)90093-1).
- (20) Beck, E.; Zink, B. Nucleotide Sequence and Genome Organisation of Filamentous Bacteriophages Fl and Fd. *Gene* **1981**, *16*, 35–58. [https://doi.org/10.1016/0378-1119\(81\)90059-7](https://doi.org/10.1016/0378-1119(81)90059-7).
- (21) Marvin, D. A.; Hohn, B. Filamentous Bacterial Viruses. *Bacteriol. Rev.* **1969**, *33*, 172–209.
- (22) Houshmand, H.; Fröman, G.; Magnusson, G. Use of Bacteriophage T7 Displayed Peptides for Determination of Monoclonal Antibody Specificity and Biosensor Analysis of the Binding Reaction. *Anal. Biochem.* **1999**, *268*, 363–370. <https://doi.org/10.1006/abio.1998.3076>.
- (23) Ansuini, H.; Cicchini, C.; Nicosia, A.; Tripodi, M.; Cortese, R.; Luzzago, A. Biotin-tagged cDNA Expression Libraries Displayed on Lambda Phage: A New Tool for the Selection of Natural Protein Ligands. *Nucleic Acids Res.* **2002**, *30*, e78–e78. <https://doi.org/10.1093/nar/gnf077>.
- (24) Clackson, T.; Wells, J. A. In Vitro Selection from Protein and Peptide Libraries. *Trend. Biotechnol.* **1994**, *12*, 173–184. [https://doi.org/10.1016/0167-7799\(94\)90079-5](https://doi.org/10.1016/0167-7799(94)90079-5).
- (25) Iannolo, G.; Minenkova, O.; Petruzzelli, R.; Cesareni, G. Modifying Filamentous Phage Capsid: Limits in the Size of the Major Capsid Protein. *J. Mol. Biol.* **1995**, *248*, 835–844. <https://doi.org/10.1006/jmbi.1995.0264>.
- (26) Jespers, L. S.; Messens, J. H.; Keyser, A. D.; Eeckhout, D.; Brande, I. V. D.; Gansemans, Y. G.; Lauwereys, M. J.; Vlasuk, G. P.; Stanssens, P. E. Surface Expression and Ligand-Based Selection of cDNAs Fused to Filamentous Phage Gene VI. *Bio/Technology* **1995**, *13*, 378–382. <https://doi.org/10.1038/nbt0495-378>.
- (27) Gao, C.; Mao, S.; Lo, C.-H. L.; Wirsching, P.; Lerner, R. A.; Janda, K. D. Making Artificial Antibodies: A Format for Phage Display of Combinatorial Heterodimeric Arrays. *Proc. Natl. Acad. Sci. U.S.A.* **1999**, *96*, 6025–6030.
- (28) Jacobson, A. Role of F Pili in the Penetration of Bacteriophage Fl. *J. Virol* **1972**, *10*, 835–843.
- (29) Smith, G. P.; Scott, J. K. [15] Libraries of Peptides and Proteins Displayed on Filamentous Phage. In *Methods in Enzymology; Recombinant DNA Part H*; Academic Press, 1993; Vol. 217, pp 228–257. [https://doi.org/10.1016/0076-6879\(93\)17065-D](https://doi.org/10.1016/0076-6879(93)17065-D).
- (30) Malik, P.; Terry, T. D.; Gowda, L. R.; Langara, A.; Petukhov, S. A.; Symmons, M. F.; Welsh, L. C.; Marvin, D. A.; Perham, R. N. Role of Capsid Structure and Membrane Protein Processing in Determining the Size and Copy Number of Peptides Displayed on the Major Coat Protein of Filamentous Bacteriophage. *J. Mol. Biol.* **1996**, *260*, 9–21. <https://doi.org/10.1006/jmbi.1996.0378>.
- (31) Hammers, C. M.; Stanley, J. R. Antibody Phage Display: Technique and Applications. *J. Investig. Dermatol.* **2014**, *134*, 1–5. <https://doi.org/10.1038/jid.2013.521>.
- (32) Mazor, Y.; Van Blarcom, T.; Mabry, R.; Iverson, B. L.; Georgiou, G. Isolation of Engineered, Full-Length Antibodies from Libraries Expressed in Escherichia Coli. *Nat. Biotechnol.* **2007**, *25*, 563–565. <https://doi.org/10.1038/nbt1296>.
- (33) Frenzel, A.; Kügler, J.; Wilke, S.; Schirrmann, T.; Hust, M. Construction of Human Antibody Gene Libraries and Selection of Antibodies by Phage Display. In *Human Monoclonal Antibodies: Methods and Protocols*; Steinitz, M., Ed.; Methods in Molecular Biology; Humana Press: Totowa, NJ, 2014; pp 215–243. [https://doi.org/10.1007/978-1-62703-586-6\\_12](https://doi.org/10.1007/978-1-62703-586-6_12).
- (34) Brockmann, E.-C. Selection of Stable ScFv Antibodies by Phage Display. In *Antibody Engineering: Methods and Protocols, Second Edition*; Chames, P., Ed.; Methods in

- Molecular Biology; Humana Press: Totowa, NJ, 2012; pp 123–144. [https://doi.org/10.1007/978-1-61779-974-7\\_7](https://doi.org/10.1007/978-1-61779-974-7_7).
- (35) Rader, C. Generation of Human Fab Libraries for Phage Display. In *Antibody Methods and Protocols*; Proetzel, G., Ebersbach, H., Eds.; Methods in Molecular Biology; Humana Press: Totowa, NJ, 2012; pp 53–79. [https://doi.org/10.1007/978-1-61779-931-0\\_4](https://doi.org/10.1007/978-1-61779-931-0_4).
- (36) Holt, L. J.; Herring, C.; Jespers, L. S.; Woolven, B. P.; Tomlinson, I. M. Domain Antibodies: Proteins for Therapy. *Trends Biotechnol.* **2003**, *21*, 484–490. <https://doi.org/10.1016/j.tibtech.2003.08.007>.
- (37) Sellmann, C.; Pekar, L.; Bauer, C.; Ciesielski, E.; Krah, S.; Becker, S.; Toleikis, L.; Kügler, J.; Frenzel, A.; Valldorf, B.; Hust, M.; Zielonka, S. A One-Step Process for the Construction of Phage Display ScFv and VHH Libraries. *Mol. Biotechnol.* **2020**, *62*, 228–239. <https://doi.org/10.1007/s12033-020-00236-0>.
- (38) Clackson, T.; Hoogenboom, H. R.; Griffiths, A. D.; Winter, G. Making Antibody Fragments Using Phage Display Libraries. *Nature* **1991**, *352*, 624–628. <https://doi.org/10.1038/352624a0>.
- (39) Hust, M.; Dübel, S. Mating Antibody Phage Display with Proteomics. *Trends Biotechnol.* **2004**, *22*, 8–14. <https://doi.org/10.1016/j.tibtech.2003.10.011>.
- (40) Hoogenboom, H. R. Selecting and Screening Recombinant Antibody Libraries. *Nat. Biotechnol.* **2005**, *23*, 1105–1116. <https://doi.org/10.1038/nbt1126>.
- (41) Hoogenboom, H. R. Designing and Optimizing Library Selection Strategies for Generating High-Affinity Antibodies. *Trends Biotechnol.* **1997**, *15*, 62–70. [https://doi.org/10.1016/S0167-7799\(97\)84205-9](https://doi.org/10.1016/S0167-7799(97)84205-9).
- (42) Dübel, S. Recombinant Therapeutic Antibodies. *Appl. Microbiol. Biotechnol.* **2007**, *74*, 723–729. <https://doi.org/10.1007/s00253-006-0810-y>.
- (43) Drugs@FDA: FDA-Approved Drugs <https://www.accessdata.fda.gov/scripts/cder/daf/index.cfm?event=overview.process&ApplNo=125057> (accessed 2021 -06 -02).
- (44) HUMIRA® (Adalimumab) Injection, for Subcutaneous Use. 104.
- (45) Cwirla, S. E.; Peters, E. A.; Barrett, R. W.; Dower, W. J. Peptides on Phage: A Vast Library of Peptides for Identifying Ligands. *Proc. Natl. Acad. Sci. U.S.A.* **1990**, *87*, 6378–6382. <https://doi.org/10.1073/pnas.87.16.6378>.
- (46) O’Neil, K. T.; Hoess, R. H.; Jackson, S. A.; Ramachandran, N. S.; Mousa, S. A.; DeGrado, W. F. Identification of Novel Peptide Antagonists for GPIIb/IIIa from a Conformationally Constrained Phage Peptide Library. *Proteins* **1992**, *14*, 509–515. <https://doi.org/10.1002/prot.340140411>.
- (47) Rebar, E. J.; Pabo, C. O. Zinc Finger Phage: Affinity Selection of Fingers with New DNA-Binding Specificities. *Science* **1994**, *263*, 671–673. <https://doi.org/10.1126/science.8303274>.
- (48) Giebel, L. B.; Cass, R. T.; Milligan, D. L.; Young, D. C.; Arze, R.; Johnson, C. R. Screening of Cyclic Peptide Phage Libraries Identifies Ligands That Bind Streptavidin with High Affinities. *Biochemistry* **1995**, *34*, 15430–15435. <https://doi.org/10.1021/bi00047a006>.
- (49) McConnell, S. I.; Uveges, A. J.; Fowlkes, D. M.; Spinella, D. G. Construction and Screening of M13 Phage Libraries Displaying Long Random Peptides. *Mol. Divers.* **1996**, *1*, 165–176. <https://doi.org/10.1007/BF01544954>.
- (50) Antti Tullila; Tarja Nevanen. Utilization of Multi-Immunization and Multiple Selection Strategies for Isolation of Hapten-Specific Antibodies from Recombinant Antibody Phage Display Libraries. *IJMS* **2017**, *18*, 1169. <https://doi.org/10.3390/ijms18061169>.

- (51) Peltomaa, R.; Glahn-Martínez, B.; Benito-Peña, E.; Moreno-Bondi, M. Optical Biosensors for Label-Free Detection of Small Molecules. *Sensors* **2018**, *18*, 4126. <https://doi.org/10.3390/s18124126>.
- (52) Wang, X.-H.; Wang, S. Sensors and Biosensors for the Determination of Small Molecule Biological Toxins. *Sensors (Basel)* **2008**, *8*, 6045–6054. <https://doi.org/10.3390/s8096045>.
- (53) Peltomaa, R.; Benito-Peña, E.; Barderas, R.; Moreno-Bondi, M. C. Phage Display in the Quest for New Selective Recognition Elements for Biosensors. *ACS Omega* **2019**, *4*, 11569–11580. <https://doi.org/10.1021/acsomega.9b01206>.
- (54) Alfaleh, M. A.; Alsaab, H. O.; Mahmoud, A. B.; Alkayyal, A. A.; Jones, M. L.; Mahler, S. M.; Hashem, A. M. Phage Display Derived Monoclonal Antibodies: From Bench to Bedside. *Front. Immunol.* **2020**, *11*. <https://doi.org/10.3389/fimmu.2020.01986>.
- (55) Leivo, J.; Kivimäki, L.; Juntunen, E.; Pettersson, K.; Lamminmäki, U. Development of Anti-Immuno-complex Specific Antibodies and Non-Competitive Time-Resolved Fluorescence Immunoassay for the Detection of Estradiol. *Anal. Bioanal. Chem.* **2019**, *411*, 5633–5639. <https://doi.org/10.1007/s00216-019-01952-6>.
- (56) Hua, X.; Zhou, L.; Feng, L.; Ding, Y.; Shi, H.; Wang, L.; Gee, S. J.; Hammock, B. D.; Wang, M. Competitive and Noncompetitive Phage Immunoassays for the Determination of Benzothiostrubin. *Anal. Chim. Acta* **2015**, *890*, 150–156. <https://doi.org/10.1016/j.aca.2015.07.056>.
- (57) Kim, H.-J.; Rossotti, M. A.; Ahn, K. C.; González-Sapienza, G. G.; Gee, S. J.; Musker, R.; Hammock, B. D. Development of a Noncompetitive Phage Anti-Immuno-complex Assay for Brominated Diphenyl Ether 47. *Anal. Biochem.* **2010**, *401*, 38–46. <https://doi.org/10.1016/j.ab.2010.01.040>.
- (58) Persson, H.; Lantto, J.; Ohlin, M. A Focused Antibody Library for Improved Hapten Recognition. *J. Mol. Biol.* **2006**, *357*, 607–620. <https://doi.org/10.1016/j.jmb.2006.01.004>.
- (59) Stephen, C. W.; Helminen, P.; Lane, D. P. Characterisation of Epitopes on Human P53 Using Phage-Displayed Peptide Libraries: Insights into Antibody-Peptide Interactions. *J. Mol. Biol.* **1995**, *248*, 58–78. <https://doi.org/10.1006/jmbi.1995.0202>.
- (60) Chen, H.; Yang, Q.; Ding, Y.; Vasylieva, N.; Bever, C. S.; Hua, X.; Wang, M.; Hammock, B. D. Competitive and Noncompetitive Immunoassays for the Detection of Benzothiostrubin Using Magnetic Nanoparticles and Fluorescein Isothiocyanate-Labeled Peptides. *Anal. Bioanal. Chem.* **2019**, *411*, 527–535. <https://doi.org/10.1007/s00216-018-1478-8>.
- (61) Rossotti, M. A.; Carlomagno, M.; González-Techera, A.; Hammock, B. D.; Last, J.; González-Sapienza, G. Phage Anti-Immuno-complex Assay for Clomazone: Two-Site Recognition Increasing Assay Specificity and Facilitating Adaptation into an On-Site Format. *Anal. Chem.* **2010**, *82*, 8838–8843. <https://doi.org/10.1021/ac101476f>.
- (62) Feng, L.; Jin, J.; Zhang, L.-F.; Yan, T.; Tao, W.-Y. Analysis of the Resveratrol-Binding Protein Using Phage-Displayed Random Peptide Library. *Acta Biochim. Biophys. Sin.* **2006**, *38*, 342–348. <https://doi.org/10.1111/j.1745-7270.2006.00163.x>.
- (63) Smith, M. W.; Smith, J. W.; Harris, C.; Brancale, A.; Allender, C. J.; Gumbleton, M. Phage Display Identification of Functional Binding Peptides against 4-Acetamidophenol (Paracetamol): An Exemplified Approach to Target Low Molecular Weight Organic Molecules. *Biochem. Biophys. Res. Com.* **2007**, *358*, 285–291. <https://doi.org/10.1016/j.bbrc.2007.04.122>.
- (64) Dong, J.-X.; Xu, C.; Wang, H.; Xiao, Z.-L.; Gee, S. J.; Li, Z.-F.; Wang, F.; Wu, W.-J.; Shen, Y.-D.; Yang, J.-Y.; Sun, Y.-M.; Hammock, B. D. Enhanced Sensitive Immunoassay:

- Noncompetitive Phage Anti- Immune Complex Assay for the Determination of Malachite Green and Leucomalachite Green. *J. Agric. Food Chem.* **2014**, *7*.
- (65) Peltomaa, R.; Benito-Peña, E.; Barderas, R.; Sauer, U.; González Andrade, M.; Moreno-Bondi, M. C. Microarray-Based Immunoassay with Synthetic Mimotopes for the Detection of Fumonisin B<sub>1</sub>. *Anal. Chem.* **2017**, *89*, 6216–6223. <https://doi.org/10.1021/acs.analchem.7b01178>.
- (66) Peltomaa, R.; Fikacek, S.; Benito-Peña, E.; Barderas, R.; Head, T.; Deo, S.; Daunert, S.; Moreno-Bondi, M. C. Bioluminescent Detection of Zearalenone Using Recombinant Peptidomimetic Gaussia Luciferase Fusion Protein. *Microchim. Acta* **2020**, *187*, 547. <https://doi.org/10.1007/s00604-020-04538-7>.
- (67) EZ-Link™ Sulfo-NHS-LC-Biotin, formato No-Weigh™ <https://www.thermofisher.com/order/catalog/product/A39257> (accessed 2021 -01 -25).
- (68) Vardanyan, R.; Hruby, V. Chapter 29 - Immunopharmacological Drugs. In *Synthesis of Best-Seller Drugs*; Vardanyan, R., Hruby, V., Eds.; Academic Press: Boston, 2016; pp 549–572. <https://doi.org/10.1016/B978-0-12-411492-0.00029-8>.
- (69) Ph.D.™-12 Phage Display Peptide Library | NEB <https://international.neb.com/products/e8111-phd-12-phage-display-peptide-library> (accessed 2021 -09 -07).
- (70) Bohnert, T.; Gan, L.-S. Plasma Protein Binding: From Discovery to Development. *J. Pharm. Sci.* **2013**, *102*, 2953–2994. <https://doi.org/10.1002/jps.23614>.
- (71) Glahn-Martínez, B.; Benito-Peña, E.; Salis, F.; Descalzo, A. B.; Orellana, G.; Moreno-Bondi, M. C. Sensitive Rapid Fluorescence Polarization Immunoassay for Free Mycophenolic Acid Determination in Human Serum and Plasma. *Anal. Chem.* **2018**, *90*, 5459–5465. <https://doi.org/10.1021/acs.analchem.8b00780>.
- (72) Masseyeff, R. F.; Albert, W. H. W. (Winfried H. W. ); Staines, N. *Methods of Immunological Analysis*; Weinheim, Germany : VCH Verlagsgesellschaft ; New York, NY (USA) : VCH Publishers, 1992.
- (73) Bui-Klimke, T. R.; Wu, F. Ochratoxin A and Human Health Risk: A Review of the Evidence. *Crit. Rev. Food Sci. Nutr.* **2015**, *55*, 1860–1869. <https://doi.org/10.1080/10408398.2012.724480>.
- (74) Bianchini, A.; Bullerman, L. B. MYCOTOXINS | Classification. In *Encyclopedia of Food Microbiology (Second Edition)*; Batt, C. A., Tortorello, M. L., Eds.; Academic Press: Oxford, 2014; pp 854–861. <https://doi.org/10.1016/B978-0-12-384730-0.00230-5>.

## **4. IMMUNODETECTION OF MYCOPHENOLIC ACID IN BLOOD OF TRANSPLANTED PATIENTS USING A RECOMBINANT PEPTIDE MIMETIC BIOLUMINESCENT TRACER**

### **4.1. Introduction**

### **4.2. Objectives**

### **4.3. Experimental part**

#### 4.3.1. Reagents and solutions

#### 4.3.2. Analytical instrumentation and materials

#### 4.3.3. Experimental procedures

##### *4.3.3.1. Neutravidin coupling to magnetic beads*

##### *4.3.3.2. Synthetic peptide-based ELISA*

##### *4.3.3.3. Analysis of the mimopeptide/antibody interaction by SPR*

##### *4.3.3.4. Construction of the NanoLuc-tagged MPA mimopeptides*

##### *4.3.3.5. Expression and purification of the NanoLuc-tagged fusion proteins*

##### *4.3.3.6. Structural analysis of the mimopeptide and the fusion protein*

##### *4.3.3.7. Bioluminescent bead-based immunoassay for MPA analysis*

##### *4.3.3.8. Sample analysis and treatment of MPA in blood of transplanted patients*

##### *4.3.3.9. RRLC-DAD method*

### **4.4. Results and discussion**

#### 4.4.1. Synthetic peptide-based ELISA

#### 4.4.2. Analysis of the mimopeptide binding kinetics by SPR

#### 4.4.3. Construction of the mimopeptide-NanoLuc fusions

#### 4.4.4. Structural characterization of the mimopeptide and the fusion protein

#### 4.4.5. Optimization of the measuring conditions

#### 4.4.6. Analytical characteristics of the bioluminescent assay

##### *4.4.6.1. Calibration*

##### *4.4.6.2. Cross-reactivity*

##### *4.4.6.3. Long term stability of the NanoLuc-mimopeptide fusion protein*

##### *4.4.6.4. Matrix effect*

4.4.7. Sample analysis

**4.5. Conclusions**

**4.6. Bibliography**

## 4.1. Introduction

Mycophenolic acid (MPA), a mycotoxin produced by a wide variety of *Penicillium* species, holds an important application as an immunosuppressant drug to prevent solid-organ rejection in transplanted patients.<sup>1,2</sup> MPA is a natural non-competitive inhibitor of the inosine monophosphate dehydrogenase enzyme (IMPDH).<sup>3</sup> However, it has also been reported that mycophenolates can be used in combination with other immunosuppressant drugs, such as sirolimus, to tackle calcineurin inhibitors.<sup>4</sup> Moreover, a recent publication revealed the potential of MPA as a chemotherapeutic agent as it is able to inhibit the proliferation of cancer cells.<sup>5</sup>

One of the main drawbacks of mycophenolic acid is its small therapeutic window. High doses of MPA could lead to adverse health effects such as gastrointestinal problems, leukopenia and thrombocytopenia.<sup>6</sup> Therefore, it is of utmost importance to conduct an efficient monitoring of MPA levels inside the human body.<sup>7</sup> Mycophenolic acid is generally found in serum, although the majority of it is bound to proteins and merely 1% of the total administered MPA exists in the free form, which is the pharmacologically active form.<sup>7-9</sup> Consequently, sensitive analytical methods for the determination of mycophenolic acid in serum samples are highly relevant.

Traditionally, MPA has been determined using liquid chromatography methods coupled to ultraviolet or mass spectrometry detection in human plasma, or directly in tissues.<sup>10-14</sup> Nevertheless, chromatographic methods demand skilled personnel, are time-consuming and rather uneconomical. On top of that, in most cases an extensive sample treatment is necessary. Fast screening methods, such as immunoassays, are an alternative to traditional chromatographic methods. The use of antibodies allows the development of a plethora of highly sensitive and selective analyte determinations.<sup>15</sup> Furthermore, immunoassays are outstandingly versatile as they can be easily automatized and integrated into routine laboratory determinations or into point-of-care devices.

With reference to mycophenolic acid, several immunoassays have been currently described in the literature for their determination.<sup>16-18</sup> These previously reported immunoassays either present no comparison with chromatographic-based methods, fail in the determination of free MPA in blood samples, or they grant a poor selectivity when several potential interferences are present in the sample. A homogeneous fluorescence polarization immunoassay was previously developed in our research group for the determination of free MPA in blood samples, offering excellent sensitivity, together with low cross-reactivity against potential interferences and great recovery rates in the analysis of real samples.<sup>19</sup> However, a chemical conjugation of the immunosuppressant drug to a luminescent dye was required for method development.

The analysis of low molecular weight molecules can sometimes turn into a difficult task, owing to some potential disadvantageous properties, such as high toxicity or carcinogenicity. Also, their determinations can be challenging due to their high cost or intricacy of functionalization without altering the interaction of the molecule towards its respective antibody. The use of peptide mimetics, also known as mimotopes or mimopeptides, is considered a practicable solution for those problems. Mimopeptides can be easily functionalized or fused to a wide variety of proteins that could act as a label

cost-effectively. On top of that, they are able to bind and compete for the binding sites of an antibody against the corresponding antigen.<sup>20-22</sup>

Mimopeptides and recombinant antibodies can be identified through phage display technology.<sup>21</sup> In the previous chapter of this thesis, a mimopeptide for MPA has been identified, and a phage-based ELISA was developed. Phage-based immunoassays are generally known for not requiring excessive preparation steps and offering good sensitivities.<sup>23-27</sup> However, previous works have established that the sensitivity of the immunoassay can improve when the mimopeptide is isolated from the phage moiety.<sup>28,29</sup> In order to perform faster and simpler immunoassays, mimopeptides can be fused to a wide range of proteins that act as a label, rather than using secondary antibodies. Genetic modifications tend to be a more homogeneous functionalization process than chemical modification, presenting a well-defined stoichiometry between the protein and the peptide.<sup>30</sup> Among the extensive collection of fluorescent and bioluminescent proteins available, the NanoLuc protein is becoming of great relevance lately due to its excellent properties. It has been reported that NanoLuc presents a hundred times more brightness when compared to other luciferases such as firefly or Renilla, with a molecular weight of only 19 kDa.<sup>31</sup> Therefore, the NanoLuc protein was chosen as a label for the development of a bioluminescent immunoassay to determine free mycophenolic acid in blood samples.



## 4.2. Objectives

This chapter was focused on the development of an immunoassay for the detection of mycophenolic acid in blood samples of transplanted patients. To this aim the mimopeptide sequence previously described in **Chapter 3** was synthesized and tested in a bead-based ELISA to demonstrate the affinity of the mimopeptide towards the anti-MPA Fab. Moreover, an analysis of the binding kinetics of the mimopeptide was conducted by SPR.

In order to develop a sensitive, fast and cost-effective analysis, a construction of a fusion protein containing the mimopeptide's sequence and a bioluminescent protein (NanoLuc) was conducted. After the expression and purification, the bioluminescent protein was characterized, and a bead-based immunoassay was optimized. Finally, the analysis of blood samples from transplanted patients was carried out and the results were compared to those obtained from a chromatographic method. The objectives of this chapter are summarized below:

- Development of an immunoassay with the synthetic MPA mimopeptide selected by phage display as described in **Chapter 3**, analysis of its binding kinetics by SPR and NMR characterization of the mimopeptide's disulfide bond.
- Construction and characterization of NanoLuc-MPA mimopeptide fusion proteins.
- Development and optimization of a sensitive immunoassay with the bioluminescent fusion protein based on magnetic beads.
- Analysis of free MPA in blood samples from transplanted patients and method validation.

## 4.3. Experimental part

### 4.3.1. Reagents and solutions

#### Cell culture and molecular biology

- LB broth, Lennox (**Thermo Fisher Scientific**)
- Tetracycline (Tet) (**Sigma-Aldrich**)
- Ampicillin (Amp) (**Fluka**)
- LB Agar (**NZYtech**)
- *E. coli* K12 ER2738 (**New England Biolabs**)
- NEB 5-alpha competent *E. coli* cells (**New England Biolabs**)
- SHUFFLE competent *E. coli* cells (**New England Biolabs**)
- Phusion Hot Start II DNA Polymerase (**Thermo Scientific**)
- PCR Nucleotide Mix (**Roche Diagnostics**)
- dNTPs (2 mM each) (**Novagen**)
- NEBuilder® HiFi DNA Assembly Master Mix (**New England Biolabs**)
- 5X Phusion HF Buffer (**Thermo Scientific**)
- Betaine (**Sigma Aldrich**)
- Agarose D1 Low EEO (**Conda**)
- Red Nucleic acid gel stain (**Thermo Fisher Scientific**)
- GelPilot Loading dye (**Qiagen**)
- GeneRuler 1 kb DNA Ladder (**Thermo Scientific**)
- PageRuler™ Prestained Protein Ladder, 10 to 180 kDa (**Thermo Scientific**)
- ATG-42 plasmid DNA, containing the NanoLuc gene (**Promega**)
- pMAL-c5X vector (**New England Biolabs**)
- NZY Bacterial Cell Lysis Buffer (**Nzytech**)
- Lysozyme (**Nzytech**)
- DNase I (**Nzytech**)
- Pierce™ Protease Inhibitor Mini Tablets, EDTA-Free (**Thermo Scientific**)

#### Antibodies

- HRP-conjugated anti-M13 monoclonal antibody (**GE Healthcare**)
- Rabbit HRP-conjugated anti-mouse IgG monoclonal antibody (**Jackson Immunoresearch**)
- The recombinant anti-MPA Fab and the recombinant anti-OTA fab were obtained from a phage display library and produced as described previously.<sup>32</sup>

#### Mycotoxins, metabolites and immunosuppressants

- Mycophenolic acid (MPA) (**Alfa Aesar**)
- Mycophenolic acid  $\beta$ -D-glucuronide (MPAG) (**Carbosynth**)
- Mycophenolic acid acyl- $\beta$ -D-glucuronide (Acyl-MPAG) (**Santa Cruz Biotechnology**)
- Cyclosporin A (**Sinoway Industrial**)
- Tacrolimus (**Sinoway Industrial**)

### Chemical reagents

- Phosphate buffer saline (PBS) pH 7.4 (**Sigma-Aldrich**)
- Phosphate buffer saline (PBST) (**Sigma-Aldrich**)
- PBS-P (20 mmol L<sup>-1</sup> phosphate buffer, 2.7 mmol L<sup>-1</sup> KCl, 0.137 mol L<sup>-1</sup> NaCl, 0.05% P20) (**Cytiva**)
- Sodium chloride (**Quimipur**)
- Sodium hydroxide (**Scharlau**)
- Sodium phosphate monobasic monohydrate (≥98%) (**Sigma-Aldrich**)
- Sodium phosphate dibasic dehydrate (puriss. p.a.) (**Fluka**)
- Sodium Dodecyl Sulfate (SDS) (**Sigma**)
- Tris base (**Fisher Bioreagents**)
- BupH™ MES [2-(N-morpholino)ethanesulfonic acid] buffered saline pack (**Thermo Scientific**)
- Dimethyl sulfoxide (≥ 99.5%) (**Sigma-Aldrich**)
- Ethanol Absolute (**Scharlau**)
- Acetonitrile (**Fisher Chemical**)
- Sulfuric acid (95–98%) (**Scharlau**)
- Trifluoroacetic acid (TFA) peptide grade (**Fluorochem**)
- Dithiothreitol (DTT) (**Thermo Scientific**)
- 1-Step™ Ultra TMB-ELISA (**Thermo Scientific**)
- Hydrogen peroxide 30% (**Merck**)
- Amplex UltraRed reagent (**Thermo Fisher Scientific**)
- 1-(3-Dimethylaminopropyl)-3-ethylcarbodiimide hydrochloride (EDC) (**FluoroChem**)
- N-Hydroxysulfosuccinimide sodium salt (Sulfo-NHS) (**FluoroChem**)
- Isopropyl-β-d-thiogalactopyranoside (IPTG) (**Sigma-Aldrich**)
- Tween 20 (T20) (**Sigma-Aldrich**)
- SuperBlock™ Blocking buffer in PBS (SuperBlock) (**Thermo Fisher Scientific**)
- Pierce™ Protein-Free (in PBS) Blocking Buffer (Protein Free) (**Thermo Fisher Scientific**)
- Glycerol (**Fisher Scientific**)
- EZ-Link Sulfo-NHS-LC-Biotin, No-Weigh Format (**Thermo Fisher Scientific**)
- Biotinylated peptide A(CEGLYAHWC)GGGSK(Bio)-NH<sub>2</sub> (**Peptide Synthetics**)
- NeutrAvidin Biotin-Binding Protein (**Thermo Scientific**)
- Imidazole (**Alfa Aesar**)
- NanoGlo® Reagent for Immunoassay (**Promega**)

### PCR Primers

- Primers to amplify pMAL for case A:  
RP037 forward primer: 5'-GAA AAC CTG TAT TTT CAG GGC CAT CAT CAT CAT CAT CAT CAT TAG GGA TC-3' (**Integrated DNA technologies**)  
RP038 reverse primer: 5'-ACC GCA CCA ATG CGC ATA CAG ACC CTC ACA GCC TCC CAT AAT CTA TGG TCC TTG TTG GTC-3' (**Integrated DNA technologies**)
- Primers to amplify pMAL for case B:

RP039 forward primer: 5'-GT TGT GAG GGT CTG TAT GCG CAT TGG TGC GGA GGC TAG Gga tcC GAA TTC CCT-3' (**Integrated DNA technologies**)

RP040 reverse primer: 5'-G AAA ATA CAG GTT TTC ATG ATG ATG ATG ATG CAT AAT CTA TGG TCC TTG TTG G-3' (**Integrated DNA technologies**)

- Primers to amplify NanoLuc for case A:

RP041 forward primer: 5'-T GCG CAT TGG TGC GGT GGC GGC TCT GGA GGT GGC AGT GTC TTC ACA CTC GAA GAT TTC G-3' (**Integrated DNA technologies**)

RP042 reverse primer: 5'-C CTG AAA ATA CAG GTT TTC CGC CAG AAT GCG TTC GC-3' (**Integrated DNA technologies**)

- Primers to amplify NanoLuc for case B:

RP043 forward primer: 5'-GAA AAC CTG TAT TTT CAG GGC GTC TTC ACA CTC GAA GAT TTC G-3' (**Integrated DNA technologies**)

RP044 reverse primer: 5'-ATA CAG ACC CTC ACA ACT GCC ACC TCC AGA GCC GCC ACC CGC CAG AAT GCG TTC GC-3' (**Integrated DNA technologies**)

### **Other reagents**

- LodeStars™ 2.7 Carboxyl (**Agilent Technologies**)
- High Capacity Magne™ Streptavidin Beads (**Promega**)
- Streptavidin microtiter plates (**Kaivogen**)
- Neutravidin-coated clear plates (**Thermo Fisher Scientific**)
- Human serum type AB (**Thermo Fisher Scientific**)
- HisTrap™ FF crude columns (**Cytiva**)
- Sephadex™ G-25 M columns (**Cytiva**)
- Illustra NAP-5 columns (**Cytiva**)
- Carboxymethyl dextran matrix (**Cytiva**)
- Ultrafiltration 3K Amicon Ultra tubes (**Merck**)
- Sensor Chip CM5 with carboxymethylated dextran matrix (**Cytiva**)

### **Commercial kits**

- QIAquick® PCR & Gel Cleanup Kit (**Qiagen**)
- QIAprep® Spin Miniprep Kit (**Qiagen**)

### **Plates**

**LB/Amp plates** (for 20 plates approximately): 16 g of LB agar were dissolved in 400 mL of MQ water after cooled at a temperature lower than 70 °C, 400 µL ampicillin were added. The solution, around 20-25 mL (almost cover all the plate), was immediately poured into a plate and let stand until mixture solidification. Plates were stored at 4 °C in the dark.

### **Solutions and buffers:**

**PBS 10×**: one pouch of PBS was dissolved in deionized water. The pH was adjusted to 7.4 for a final volume of 100 mL. The solution was sterilized by autoclaving and stored at room temperature.

**PBS 1×**: the solution was prepared by diluting 10 times in autoclaved water the PBS 10x solution. The final concentration was 0.01 mol L<sup>-1</sup> PBS, pH 7.4.

**Tween-20 solution 10% (v/v):** 10 mL of Tween® 20 were diluted with 90 mL deionized water. The solution was sterilized by autoclaving and stored at room temperature.

**Coupling buffer A (MES 0.1 mol L<sup>-1</sup>, 0.9% NaCl + 0.01% SDS, pH 5.7):** one pack of MES powder was dissolved in 500 mL deionized water. Then, 5 mL of the MES solution was added together with 50 µL of 10% SDS solution to 40 mL deionized water. The pH was adjusted to 5.7 for a final volume of 50 mL. The solution was stored at 4 °C in the dark.

**Coupling buffer B (PBS 1x + 0.01% SDS, pH 7.4):** 5 mL of PBS 10x and 50 µL of 10% SDS solution were added to 40 mL deionized water. The pH was adjusted to 7.4 for a final volume of 50 mL. The solution was stored at 4 °C in the dark.

**TAE 50× electrophoresis buffer (2 mol L<sup>-1</sup> Tris base, 1 mol L<sup>-1</sup> acetic acid, 1 mol L<sup>-1</sup> EDTA, pH 8.6):** 242 g tris base, 18.61 g disodium EDTA and 59.95 g acetic acid were dissolved in 800 mL deionized water. Once dissolved, more deionized water was added for a total volume of 1 L. The pH was not adjusted. The solution was stored at room temperature.

**TAE 1× electrophoresis buffer:** the solution was prepared by diluting 50 times in deionized water the TAE 50x solution.

**SOC media:** 10 g tryptone, 2.5 g yeast extract, 0.25 g NaCl and 5 mL of a solution of 20 mmol L<sup>-1</sup> KCl were dissolved in 400 mL deionized water. The pH was adjusted to 7.4 for a total volume of 500 mL. The solution was autoclaved and then, 2.5 mL of 2 mol L<sup>-1</sup> MgCl<sub>2</sub> (previously autoclaved) and 10 mL of 1 mol L<sup>-1</sup> glucose were added. The solution was stored at 4 °C in the dark.

**Binding buffer (BB) (20 mmol L<sup>-1</sup> sodium phosphate buffer pH 7.4, 500 mmol L<sup>-1</sup> NaCl and 20 mmol L<sup>-1</sup> imidazole):** 0.55 g Na<sub>2</sub>HPO<sub>4</sub>, 0.16 g NaH<sub>2</sub>PO<sub>4</sub>, 7.31 g NaCl and 0.34 g imidazole were dissolved in 200 mL deionized water. The pH was adjusted to 7.4 for a total volume of 250 mL. The solution was stored at room temperature.

**Elution buffer (EB): (20 mmol L<sup>-1</sup> sodium phosphate buffer pH 7.4, 500 mmol L<sup>-1</sup> sodium chloride and 500 mmol L<sup>-1</sup> imidazole):** 0.14 g Na<sub>2</sub>HPO<sub>4</sub>, 0.04 g NaH<sub>2</sub>PO<sub>4</sub>, 1.83 g NaCl and 1.7 g imidazole were dissolved in 50 mL deionized water. The pH was adjusted to 7.4 for a total volume of 250 mL. The solution was stored at room temperature.

**Assay buffer (SuperBlock supplemented with 0.05% T20):** 200 µL of a solution of 10% T20 were added to 40 mL SuperBlock. The solution was stored at 4 °C in the dark.

**Washing buffer (137 mmol L<sup>-1</sup> NaCl, 2.7 mmol L<sup>-1</sup> KCl, 10 mmol L<sup>-1</sup> Na<sub>2</sub>HPO<sub>4</sub>, 1.8 mmol L<sup>-1</sup> KH<sub>2</sub>PO<sub>4</sub>, 0.05% T20, pH 7.4):** 8 g NaCl, 200 mg KCl, 1.44 g Na<sub>2</sub>HPO<sub>4</sub>, 240 mg KH<sub>2</sub>PO<sub>4</sub> and 500 µL T20 were dissolved in 900 mL deionized water. The pH was adjusted to 7.4 for a total volume of 1 L. The solution was stored at room temperature.

#### 4.3.2. Analytical instrumentation and materials

- CLARIOstar microplate reader (**BMG Labtech**)
- Nanodrop 1000 spectrophotometer (**Thermo Scientific**)
- Analytical balance with 0.01 mg sensitivity (**Sartorius**)
- pH Meter GLP 21 (**Crison**)
- Eppendorf miniSpin (**Eppendorf**)
- Eppendorf centrifuge 5804 R (**Eppendorf**)
- Shaker incubator KS 4000 i control (**IKA**)
- Autoclave (**Selecta**)
- Thermostatic eppendorf shaker (**Thermo Scientific**)
- Vortex shaker (**Fisher brand**)
- PowerPac™ Basic power supply for gel electrophoresis (**Bio-Rad**)
- Thermocycler SureCycler 8800 (**Agilent Technologies**)
- Automatic plate washer hydro flex (**Tecan**)
- VibraCell Ultrasonic Processor 130 W 20 kHz, Ampl 70% (**Sonics & Materials**).
- Biacore T200 instrument (**Cytiva**)
- Analytical material of contrasted quality

#### 4.3.3. Experimental procedures

##### 4.3.3.1. Neutravidin coupling to magnetic beads

The protocol has been described in **Section 3.3.3.2.** of **Chapter 3.**

##### 4.3.3.2. Synthetic Peptide-Based ELISA

The amino acid sequence of clone A2, MPA mimopeptide previously described in **Chapter 3** of this thesis, was identified by DNA sequencing. Consequently, the biotinylated peptide A(CEGLYAHWC)GGGSK(Bio)-NH<sub>2</sub> (referred to as A2-bio from now on) with a disulfide constrained loop between the two C's was synthesized at Peptide Synthetics.

Prior to the synthetic peptide-based ELISA, a checkerboard-type titration was conducted to optimize the A2-bio as well as the anti-MPA concentrations. In short, 100  $\mu\text{L}$  of ranging concentrations of A2-bio, between 0.05 and 5  $\mu\text{g mL}^{-1}$ , diluted in assay buffer were added to neutravidin-coated clear plates previously blocked with SuperBlock. The mixture was incubated for 30 min at room temperature with slow shaking and the plate was subsequently washed thrice with washing buffer. Then, 100  $\mu\text{L}$  of a solution of varying anti-MPA concentrations, from 0.05 to 5  $\mu\text{g mL}^{-1}$  in assay buffer, were added to the wells and incubated for 30 min at room temperature and slow shaking. This step was performed with and without the addition of 16  $\text{ng mL}^{-1}$  free MPA to the anti-MPA solution. For those samples containing free MPA, the mixture was incubated 15 min at room temperature before being added to the wells. After washing the plate three times with washing buffer, 80  $\mu\text{L}$  of a solution of 0.27  $\mu\text{g mL}^{-1}$  rabbit HRP-conjugated anti-mouse IgG monoclonal antibody were added and incubated for 30 min at room temperature and slow shaking. The plate was washed again under the same conditions as described above followed by the addition of 80  $\mu\text{L}$  TMB. The reaction was

stopped after 1 min incubation by adding 80  $\mu\text{L}$  of a solution of 2 mol  $\text{L}^{-1}$   $\text{H}_2\text{SO}_4$ . The absorbance was measured at 450 nm with a CLARIOstar microplate reader.

For the synthetic peptide bead-based ELISA (**Figure 35**), a similar strategy as the bead-based phage ELISA described in **Chapter 3** was followed, with slight modifications. Briefly, black microtiter plates were initially blocked with SuperBlock supplemented with 0.05% T20 for 1 h at room temperature with slow shaking. The plate was subsequently washed thrice with washing buffer and then, 100  $\mu\text{L}$  of a 0.1  $\mu\text{g mL}^{-1}$  solution of A2-bio were incubated with 20  $\mu\text{L}$  of a 125  $\mu\text{g mL}^{-1}$  solution of neutravidin-functionalized magnetic beads for 30 min at room temperature and slow shaking. After the incubation, the wells were washed three times with washing buffer using a plate washer with a magnetic support. Then, 100  $\mu\text{L}$  of a solution of 0.5  $\mu\text{g mL}^{-1}$  of anti-MPA and ranging concentrations of free MPA, incubated beforehand during 10 min, were added to the beads and incubated for 30 min at room temperature and slow shaking. Once the wells were washed in the same conditions as before, 80  $\mu\text{L}$  of a solution of 0.27  $\mu\text{g mL}^{-1}$  rabbit HRP-conjugated anti-mouse IgG monoclonal antibody were added to the wells and incubated for 30 min at room temperature and slow shaking. After a final washing step under the same conditions as described above, 80  $\mu\text{L}$  of Amplex UltraRed solution containing 0.05%  $\text{H}_2\text{O}_2$  were added, and the fluorescent signal was measured with a CLARIOstar microplate reader ( $\lambda_{\text{ex}} = 530 \text{ nm}$ ,  $\lambda_{\text{em}} = 590 \text{ nm}$ ).

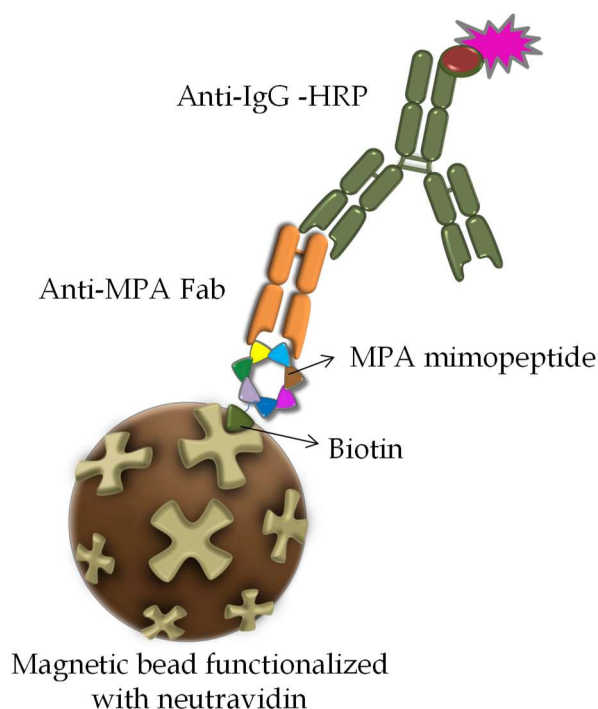


**Figure 35.** Scheme of the synthetic peptide-based ELISA using magnetic beads. The biotinylated MPA mimopeptide is first attached to neutravidin-coupled magnetic beads. Then, the anti-MPA Fab and free MPA are added to the solution and a competition is established between the mimopeptide bound on the beads and free MPA for the anti-MPA Fab binding sites. At low MPA concentrations, more anti-MPA Fab will remain bound to the mimopeptide. A secondary HRP-coupled anti-IgG monoclonal antibody is added to detect the remaining anti-MPA Fab bound to

the beads. After addition of the substrate of the enzyme the fluorescence is measured in a microplate reader.

#### 4.3.3.3. Analysis of the mimopeptide/antibody interaction by SPR

To assess the binding between the mimopeptide and the anti-MPA Fab antibody, a Biacore T200 instrument and a Sensor Chip CM5 with carboxymethylated dextran matrix were utilized. The anti-MPA Fab antibody and the anti-OTA Fab antibody, selected as a control, were immobilized onto the active surfaces of flow channel 2 and flow channel 1 respectively using EDC/NHS chemistry according to the manufacturer's instructions. The running buffer was PBS-P, and all the binding experiments were conducted at 25 °C. Different concentrations of free MPA, or the MPA mimopeptide, namely 0, 0.12, 4.9, 19.5, 78.1, 312.5 and 1250 nmol L<sup>-1</sup>, were injected into the system at a flow rate of 20 µL min<sup>-1</sup> for 2 min. Then, the dissociation phase took place during 5 min, and regeneration was subsequently carried out with 10 mmol L<sup>-1</sup> NaOH supplemented with 0.05% P20 (contact time of 60 s and a flow rate of 30 µL min<sup>-1</sup>). Finally, a stabilization period was conducted for 60 s before injecting the following sample. All samples were assayed in replicates, and the results were analyzed with the Evaluation T200 software using a 1:1 Langmuir binding model.

#### 4.3.3.4. Construction of the NanoLuc-tagged MPA mimopeptides

Two different strategies were planned for the construct of the NanoLuc-tagged MPA mimopeptide. In the first strategy, referred to as case A, the mimopeptide was expressed on the N-terminus of the NanoLuc, whereas in the second strategy, case B, the mimopeptide was expressed on the C-terminus of the NanoLuc. The expression of the MPA mimopeptide fused with the NanoLuc protein was conducted by PCR-amplifying the latter one from the commercial vector ATG 42<sup>33</sup> using the Phusion Hot Start II DNA Polymerase. For case A, the forward primer used to amplify the NanoLuc from the vector ATG-42 was RP041, (5'-T GCG CAT TGG TGC **GGT GGC GGC TCT GGA GGT GGC AGT GTC TTC ACA CTC GAA GAT TTC G-3'**) which hybridized to the 5' end of the NanoLuc and included an overhang (in bold) coding for a 'GGGSGGGS' spacer between the mimopeptide and the NanoLuc. The reverse primer, RP042, (5'-C CTG AAA ATA CAG GTT TTC **CGC CAG AAT GCG TTC GC-3'**) hybridized to the 3' end of the NanoLuc. With reference to case B, the forward primer, RP043, (5'-GAA AAC CTG TAT TTT CAG GGC **GTC TTC ACA CTC GAA GAT TTC G-3'**) hybridized to the 5'-end of the NanoLuc, whereas the reverse primer, RP044, (5'-ATA CAG ACC CTC ACA **ACT GCC ACC TCC AGA GCC GCC ACC CGC CAG AAT GCG TTC GC-3'**) hybridized to the 3'-end and contained an overhang (in bold) that coded for a 'GGGSGGGS' spacer between the NanoLuc and the mimopeptide. In all primers, the hybridizing part of the sequence is underlined. The pMAL vector was utilized to perform the fusion of the cyclic peptide and the NanoLuc for both cases. To amplify the pMAL vector for case A, the forward primer RP037 (5'-GAA AAC CTG TAT TTT CAG GGC CAT CAT CAT CAT CAT CAT TAG GGA TC-3') contained the histidine tag (His-tag) used to purify the product and the reverse primer, RP038, (5'-ACC **GCA CCA ATG CGC ATA CAG ACC CTC ACA GCC TCC CAT AAT CTA TGG TCC TTG TTG GTC-3'**) contained an overhang (in bold) with the DNA sequence encoding for the MPA mimopeptide. For



case B, the forward primer, RP039, (5'-GT TGT GAG GGT CTG TAT GCG CAT TGG TGC GGA GGC TAG GGA TCC GAA TTC CCT-3') presented a 5'-overhang (in bold) for the DNA sequence of the MPA mimopeptide, and the reverse primer, RP040, (5'-G AAA ATA CAG GTT TTC ATG ATG ATG ATG ATG CAT AAT CTA TGG TCC TTG TTG G-3') included a His-tag. To complete the assembly of the mimopeptide and the NanoLuc (Figure 36), the pMAL vector containing the mimopeptide and the NanoLuc insert were incubated for both case A and case B at +50 °C for 15 min with the NEBuilder Master Mix.

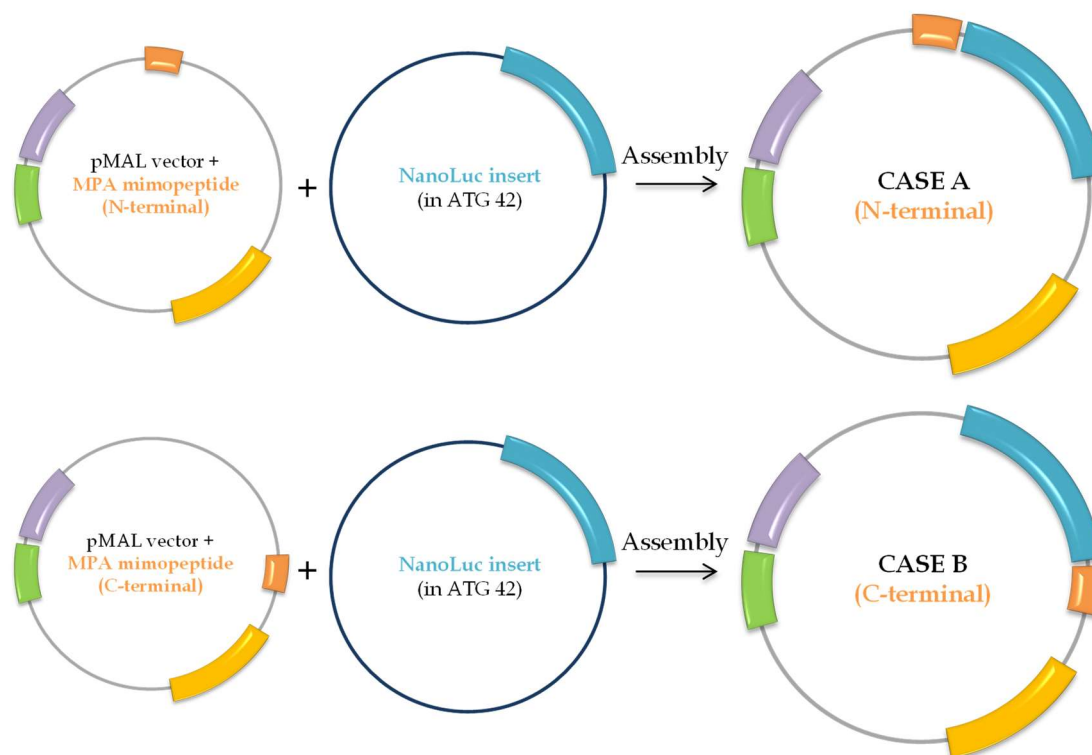


**Figure 36.** Scheme of the assembly process of the MPA mimopeptide (orange) and the NanoLuc (blue) inserts on pMAL vector. PCR-amplified-pMAL vector containing the MPA mimopeptide insert on different sites of the vector is incubated with the PCR-amplified NanoLuc insert to obtain two different products. In case A, the MPA mimopeptide is located on the N-terminus of the NanoLuc sequence, whereas in case B the mimopeptide is on the C-terminus of the NanoLuc.

In order to generate more copies of the assembled products, different NEB 5-alpha competent *E. coli* cells were transformed with the plasmids of case A (N-terminal) and case B (C-terminal). Briefly, 2  $\mu\text{L}$  of the chilled assembled product were added to 100  $\mu\text{L}$  of NEB 5-alpha competent cells previously thawed on ice. The cocktail solution was gently mixed 4–5 times and placed on ice for 30 min. Then, the mixture was transferred to a water bath at 42 °C for 30 s and immediately put back on ice for 2 min. Next, 950  $\mu\text{L}$  of room-temperature SOC media were added to the competent cells and they were subsequently incubated for 1 h under vigorous shaking. After the incubation, a total volume of 100  $\mu\text{L}$  of competent cells was spread over pre-warmed LB/ Amp plates and incubated overnight at 37 °C. The following day, single colonies were picked from the LB/ Amp plates and were grown in 5 mL LB supplemented with 100  $\mu\text{g mL}^{-1}$  ampicillin for 20 h at 37 °C and 180 rpm. The cells were then pelleted and the plasmid was extracted

using the QIAprep® Spin Miniprep Kit according to the manufacturer's instructions.<sup>34</sup> The extracted plasmids were stored in water at  $-20\text{ }^{\circ}\text{C}$  and the success of the cloning was demonstrated by DNA sequencing analysis.

#### **4.3.3.5. Expression and purification of the NanoLuc-tagged fusion proteins**

To carry out the expression of the NanoLuc-tagged mimopeptides, the purified plasmids N-terminal and C-terminal were introduced in SHUFFLE competent *E. coli* cells, which have an oxidizing cytoplasm to enable the formation of the disulfide bond included in the mimopeptide, following the same protocol described for the NEB 5-alpha cells' transformation. Following that, a single colony was picked from LB/Amp plates and grown on 15 mL LB supplemented with  $100\text{ }\mu\text{g mL}^{-1}$  ampicillin overnight. An aliquot from the overnight preculture was transferred the next day to a 200 mL LB culture supplemented with  $100\text{ }\mu\text{g mL}^{-1}$  ampicillin. The solution was incubated at  $37\text{ }^{\circ}\text{C}$  and 180 rpm until the  $\text{OD}_{600}$  (optical density at 600 nm) reached 0.6 units.

To conduct the protein expression, IPTG at a final concentration of  $0.4\text{ mmol L}^{-1}$  was added to the culture with the  $\text{OD}_{600}$  of 0.6, and the expression was allowed to continue for 4 h at  $37\text{ }^{\circ}\text{C}$  and 180 rpm. To stop the cell growth, the culture was placed on an ice bath for 10 min and then, the cells were centrifuged at  $5000\text{ g}$  for 10 min and  $4\text{ }^{\circ}\text{C}$ . The cell pellet was resuspended in NZY Bacterial Cell Lysis Buffer supplemented with protease inhibitor cocktail, lysozyme and DNase I. For 1 g of cell paste, 5 mL of lysis buffer, half tablet of protease inhibitor cocktail,  $10\text{ }\mu\text{L}$  Lysozyme and  $10\text{ }\mu\text{L}$  DNase I are needed. The cells were lysed by sonication using a VibraCell Ultrasonic Processor at 130 W, 20 kHz and Amplitude 70% for 10 s 5 times with 30 s breaks to avoid excessive heating. The resulting solution was centrifuged at  $15000\text{ g}$  for 15 min and  $4\text{ }^{\circ}\text{C}$ , and the insoluble cell debris was discarded.

The supernatant containing the expression product was purified using HisTrap™ purification columns according to the following protocol. The cell lysates were initially diluted 1:3 in binding buffer (BB) (for 10 mL of sample, 20 mL of BB were used). The HisTrap column was first washed with 5 mL of deionized water and then equilibrated with 10 mL BB at a  $1\text{ mL min}^{-1}$  flow rate. The diluted cell lysate was subsequently introduced in the column with a pump at a  $1\text{ mL min}^{-1}$  flow rate and the flow-through was collected. The column was washed with 30 mL BB and the eluted sample of the washing solution was collected as well. Finally, the product was eluted in 1 mL fractions using 10 mL elution buffer (EB). The column was regenerated with 30 mL BB, 30 mL deionized water and it was stored in 20% EtOH. The buffer was exchanged to PBS 1× using Sephadex™ G-25 M columns according to the manufacturer's instructions.<sup>35</sup> The size and purity of the products was confirmed by running an SDS-PAGE according to the manufacturer's instructions.<sup>36</sup> The purified products were stored at  $-20\text{ }^{\circ}\text{C}$  until further use.

#### **4.3.3.6. Structural analysis of the mimopeptide and the fusion protein**

NMR analysis of the mimopeptide was carried out with a Bruker AVIII 700 MHz equipped with a cryoprobe. NMR analysis of the fusion protein was performed with a Bruker AV 600 MHz with a cryoprobe.

For the simulation, the Assisted Model Building with Energy Refinement (AMBER) software was initially employed to obtain all the possible molecular conformations. The minimization was performed with the MAESTRO software (Mestrelab Research).

#### 4.3.3.7. Bioluminescent bead-based immunoassay for MPA analysis

To perform the detection of MPA with the fusion proteins N-terminal and C-terminal, a bead-based assay was conducted on black microtiter well plates following the scheme presented in **Figure 37**. Briefly, black microtiter wells were initially blocked with assay buffer for 1 h. Then, 60  $\mu\text{L}$  of the biotinylated anti-MPA Fab at a concentration of 5  $\mu\text{g mL}^{-1}$ , together with 20  $\mu\text{L}$  of streptavidin beads at a 1:50 dilution from the stock were added to the wells and subsequently incubated for 30 min at room temperature and slow shaking. Once the wells were washed 3 times with PBS 1 $\times$  supplemented with 0.05% T20 using a magnetic support, varying concentrations of free MPA and the NanoLuc-MPA (at a final concentration of 77  $\mu\text{g mL}^{-1}$  in 60  $\mu\text{L}$ ) were simultaneously added to the wells and incubated during 30 min at room temperature and slow shaking. After washing the wells under the same conditions as described above, 60  $\mu\text{L}$  of the NanoGlo<sup>®</sup> substrate diluted in PBS 1 $\times$  was added to the wells and the emerging bioluminescence was monitored at 470 nm with a bandwidth of 80 nm after a 2-min incubation time using a CLARIOstar microplate reader.

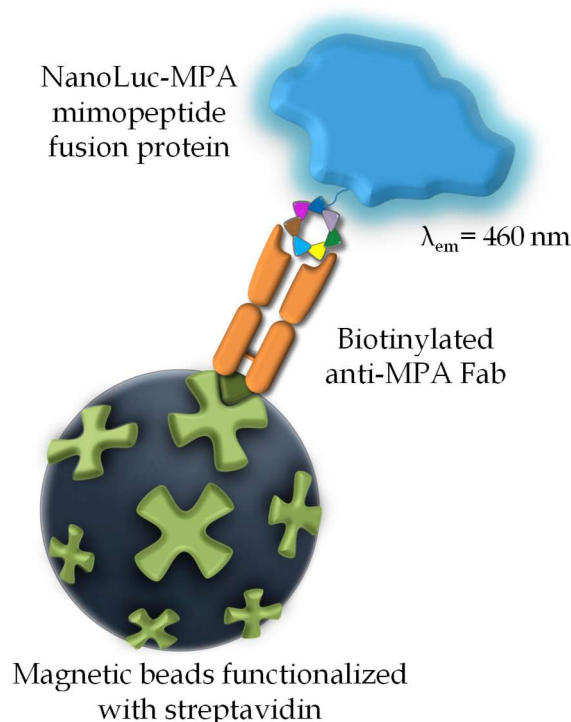


**Figure 37.** Scheme of the bioluminescent bead-based immunoassay for MPA detection. Streptavidin-coated magnetic beads were incubated with the biotinylated anti-MPA Fab. Then, the NanoLuc-MPA mimopeptide fusion protein and varying concentrations of free MPA were simultaneously added and incubated. Finally, the substrate for NanoLuc was added to the wells and the bioluminescence was monitored with a CLARIOstar microplate reader.

#### 4.3.3.8. *Sample analysis and treatment of MPA in blood of transplanted patients*

With permission from the Ethics Committee of Hospital Clínico Universitario de Valladolid, Spain (no. PI 21-2245), whole blood samples were extracted from transplanted patients and healthy individuals. The blood samples were kept at 4 °C during transport and stored at -20 °C in the lab. The donated samples, composed of five transplanted patients under different treatments (T1-T5) and three healthy individuals (H1-H3) were treated according to a procedure previously described.<sup>19</sup> Briefly, 1 mL blood sample was centrifuged at 2000 g for 15 min at room temperature. Then, 500 µL of the supernatant was transferred to ultrafiltration 3K Amicon Ultra tubes, previously rinsed with PBS 1× supplemented with 0.05% T20, and centrifuged at 12045 g for 30 min. The ultrafiltered samples were stored at -20 °C until further analysis.

For the bioluminescent bead-based immunoassay, plasma samples were diluted 1:8 with SuperBlock supplemented with 0.05% T20. For the chromatographic analysis, 1000 µL acetonitrile were added to 200 µL of the ultrafiltered samples and vortexed vigorously at 1,000 rpm for 10 min. After centrifuging the plasma samples at 12,045 g for 10 min and the supernatant was transferred to a new tube. The samples were evaporated to a volume of circa 30 µL and reconstituted in a final volume of 150 µL using PBS 1× supplemented with 0.05% T20 and acidified with TFA to a final concentration of 0.4% (v/v).

#### 4.3.3.9. *RRLC-DAD method*

The separation of MPA and its two metabolites, MPAG and Acyl-MPAG was carried out using a gradient elution mode, with a mixture of deionized water supplemented with 0.1% TFA and acetonitrile supplemented with 0.1% TFA as mobile phase. The flow rate was 0.6 mL min<sup>-1</sup>, the column temperature was kept constant at 45 °C and the injection volume was 100 µL. MPA, MPAG and Acyl-MPAG were quantified by an internal standard calibration model using a derivatized form of MPA, MPA-LuciferYellow. The nine-point calibration curve was conducted for MPA at a concentration range of 0.5-80 ng mL<sup>-1</sup>, 50-15000 ng mL<sup>-1</sup> for MPAG and 12-250 ng mL<sup>-1</sup> for Acyl-MPAG. The R<sup>2</sup> > 0.99 in all cases.

## 4.4. Results and discussion

### 4.4.1. Synthetic peptide-based ELISA

As previously described in the experimental part of this chapter, the biotinylated peptide A(CEGLYAHWC)GGGSK(Bio)-NH<sub>2</sub> with a disulfide constrained loop between the two C's was synthesized at Peptide Synthetics. The GGG sequence was included in the peptide as a linker due to the fact that it also appeared in the phage of origin. Moreover, a biotin (Bio) was added in the C-terminal lysine residue to allow an easier coupling on different surfaces.

The first aim with the synthesized biotinylated mimopeptide was to develop an immunoassay in similar conditions as the phage-based immunoassay on magnetic beads described in **Chapter 3** of this thesis. This immunoassay was conducted to verify that the mimopeptide was responsible for the competition with the free MPA for the binding sites of the anti-MPA Fab, rather than any other part of the phage. Prior to the development of the immunoassay, the concentrations of the synthetic peptide, as well as the anti-MPA Fab, were optimized by performing a checkerboard titration. The peptide and the anti-MPA Fab amounts were varied, from 0.005 µg to 0.5 µg for the A2-bio mimopeptide and 0.05 µg to 0.25 µg for the anti-MPA Fab, in the presence and the absence of free MPA in solution. The results are displayed in (**Figure 38**). It can be observed that higher peptide and antibody quantities in the assay lead to a higher signal in the immunoassay. The use of lower mimopeptide concentrations resulted in considerably higher differences in the presence and the absence of free MPA in solution.

**Table 12** shows the ratios observed between the signal in the presence and in the absence of free MPA for every peptide-antibody combination tested. It can be seen that the MPA mimopeptide plays an important role when establishing the differences in the signal with and without free MPA. For those experiments with the same amount of peptide, the ratios are nearly equal for all the antibody amounts tested. However, in the presence of the same amount of antibody, the ratios vastly differ when varying the peptide concentration in solution. It would be expected that the antibody-mimopeptide amounts presenting the highest ratio would be selected to carry out the bead-based immunoassay. Nevertheless, due to the negligible signal observed with 0.005 µg of A2-bio mimopeptide, it was decided that the optimal combination for the immunoassay would be using 0.01 µg A2-bio mimopeptide and 0.05 µg of anti-MPA Fab.

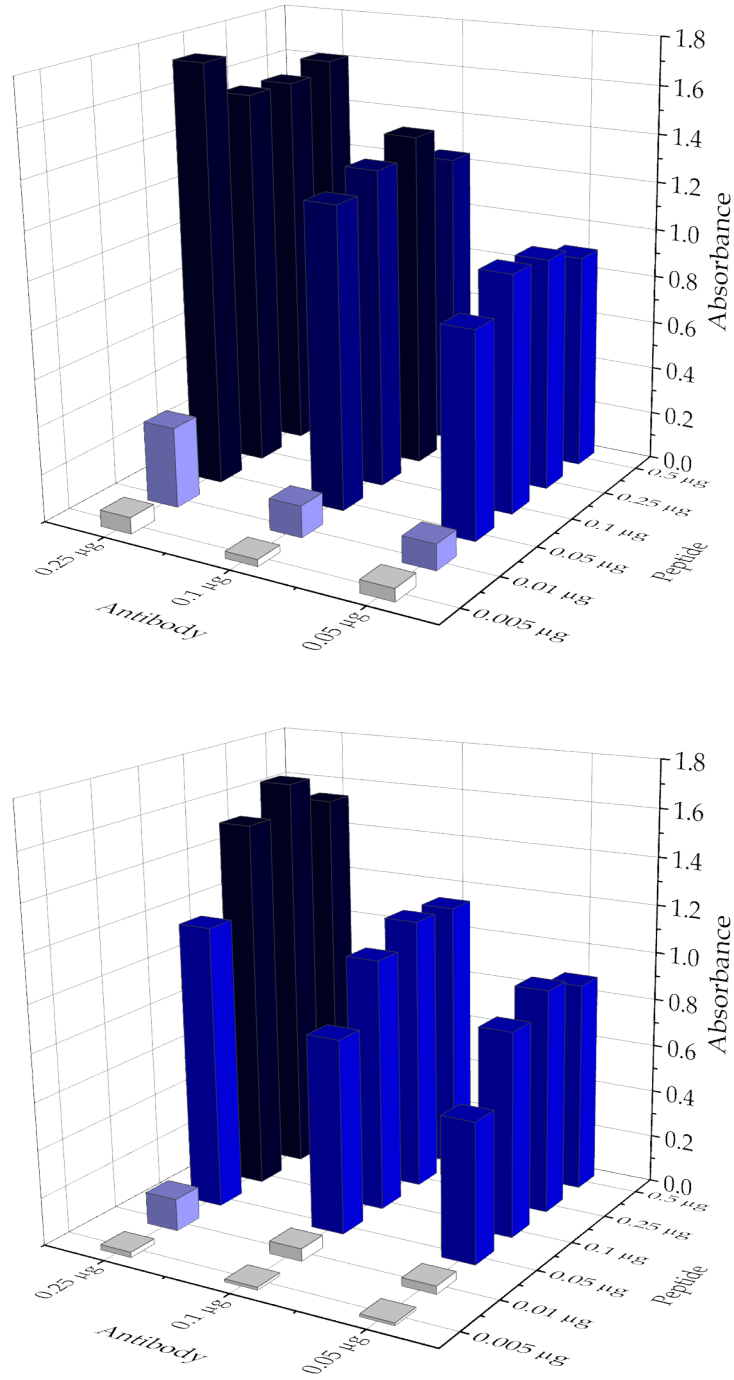


**Figure 38.** Checkerboard titration for the optimization of the mimopeptide and antibody concentrations of the synthetic peptide-based ELISA in the absence (top) and presence (bottom) of 16 ng mL<sup>-1</sup> free MPA (RSD < 16.5%).

**Table 12.** Ratios between the signals obtained in the checkerboard titration in the presence and the absence of free MPA in solution for every peptide and antibody amount tested. The optimal combination selected is shown in bold (RSD < 13.1%).

		Antibody		
		0.25 $\mu\text{g}$	0.10 $\mu\text{g}$	0.05 $\mu\text{g}$
Peptide	0.50 $\mu\text{g}$	1.05	1.10	1.02
	0.25 $\mu\text{g}$	0.94	1.22	1.03
	0.10 $\mu\text{g}$	1.02	1.26	1.16
	0.05 $\mu\text{g}$	1.48	1.55	1.47
	0.01 $\mu\text{g}$	2.51	2.53	<b>3.17</b>
	0.005 $\mu\text{g}$	3.06	2.39	4.71

Once the best composition for the assay was determined, the synthetic peptide-based ELISA was carried out in a similar way as the phage ELISA with slight modifications. In this case, the biotinylated mimopeptide was bound to the neutravidin-coupled magnetic instead of the biotinylated anti-MPA Fab used in the phage assay. Moreover, the anti-MPA Fab used in the peptide-based ELISA was not biotinylated. The secondary antibody also differed from the previous immunoassay. An anti-M13 coupled to HRP was used for the phage-based ELISA, whereas an HRP-coupled anti-IgG antibody was employed for the peptide-based ELISA.

**Figure 39** shows the comparison of the peptide-based and the phage-based immunoassays. It can be observed that the biotinylated mimopeptide presented competition with free MPA for the binding sites of the antibody in the peptide-based ELISA, confirming that the peptide sequence obtained from phage display was an outstanding mimetic of MPA. When comparing both immunoassays, the phage-based ELISA presented more sensitivity, with a limit of detection, calculated as the 10% inhibition,<sup>37</sup> of 0.69 ng mL<sup>-1</sup> and an IC<sub>50</sub> of 2.1 ng mL<sup>-1</sup>. The peptide-based ELISA showed a limit of detection of 0.94 ng mL<sup>-1</sup> and an IC<sub>50</sub> of 9.1 ng mL<sup>-1</sup>. However, the phage-based ELISA showed a considerably narrower dynamic range, taken as the 20–80% inhibition,<sup>38</sup> (2.4–60 ng mL<sup>-1</sup>) in comparison to the peptide-based immunoassay (1.0–4.1 ng mL<sup>-1</sup>).

One of the main differences between the phage-based and the peptide-based ELISAs is the immobilized moiety onto the magnetic beads. On the phage-based ELISA, as stated before, the biotinylated anti-MPA Fab was bound to the neutravidin-coated magnetic beads. However, in the case of the peptide-based ELISA, it was the biotinylated peptide that was immobilized onto the neutravidin-coated magnetic beads. This variation could lead to the differences observed in terms of sensitivity in both immunoassays. The assay time resulted the same for both immunoassays, and the detection was performed adding Amplex UltraRed as substrate.

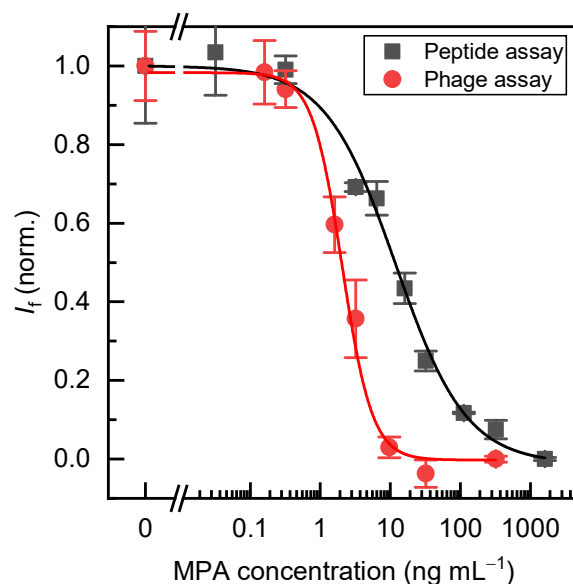


**Figure 39.** Comparison of the bead-based ELISAs with the MPA synthetic mimopeptide (black) and the phage clone A2 (red). The fluorescence emission ( $\lambda_{\text{ex}} = 530 \text{ nm}$ ,  $\lambda_{\text{em}} = 590 \text{ nm}$ ) was measured immediately after the addition of the Amplex UltraRed as substrate. The results represent the normalized mean values  $\pm$  the standard error of the mean ( $n = 3$ ) with a logistic fit (OriginPro 2019).

After proving the capability of the bio-A2 mimopeptide to mimic the behavior of free MPA and compete against it for the binding sites of the anti-MPA Fab antibody, a new approach was tackled. The new aim was to simplify the immunoassay, reduce the number of steps, as well as the total time of the assay. Therefore, the construction of a fusion protein, composed of a luciferase in combination with the mimopeptide sequence, was conducted. In this approach, the luciferase would act as a label for the immunoassay, avoiding the use of a secondary antibody and conveniently reducing the assay time and cost.

#### 4.4.2. Analysis of the mimopeptide binding kinetics by SPR

Label-free surface plasmon resonance (SPR) technology was utilized to compare the binding properties of mycophenolic acid and the synthesized biotinylated mimopeptide towards the anti-MPA Fab antibody. It was described in previous binding experiments that the produced and purified anti-MPA and anti-OTA Fab antibodies were able to recognize free MPA and OTA, respectively.<sup>32</sup> Therefore, these two antibodies were used as the target (anti-MPA) and the control (anti-OTA), and were consequently immobilized onto sensor chip surfaces. The experimental conditions used to study the binding properties of free MPA and the mimopeptide were the same for both and were described in the experimental section. The results are presented in **Figure 40** and **Figure 41**. It can be observed that mycophenolic acid and the MPA mimopeptide presented binding to the anti-MPA Fab, with binding responses increasing in a concentration-dependent manner.



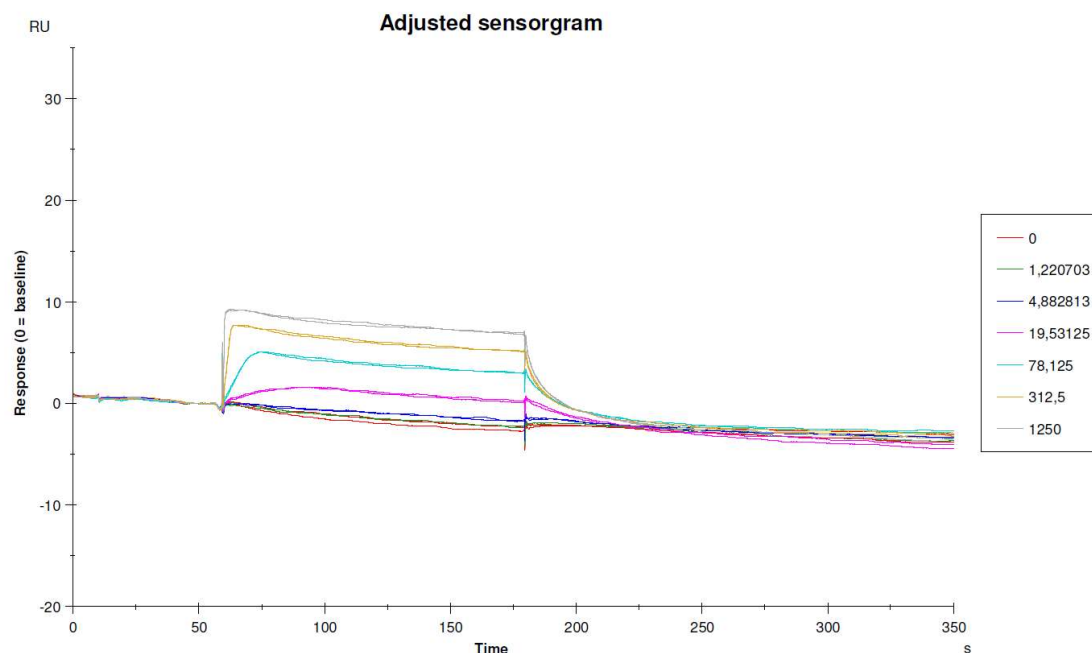


**Figure 40.** SPR sensorgrams of the interaction between free MPA and the anti-MPA Fab antibody using Biacore T200. The colors observed refer to the different nanomolar concentrations of MPA added.

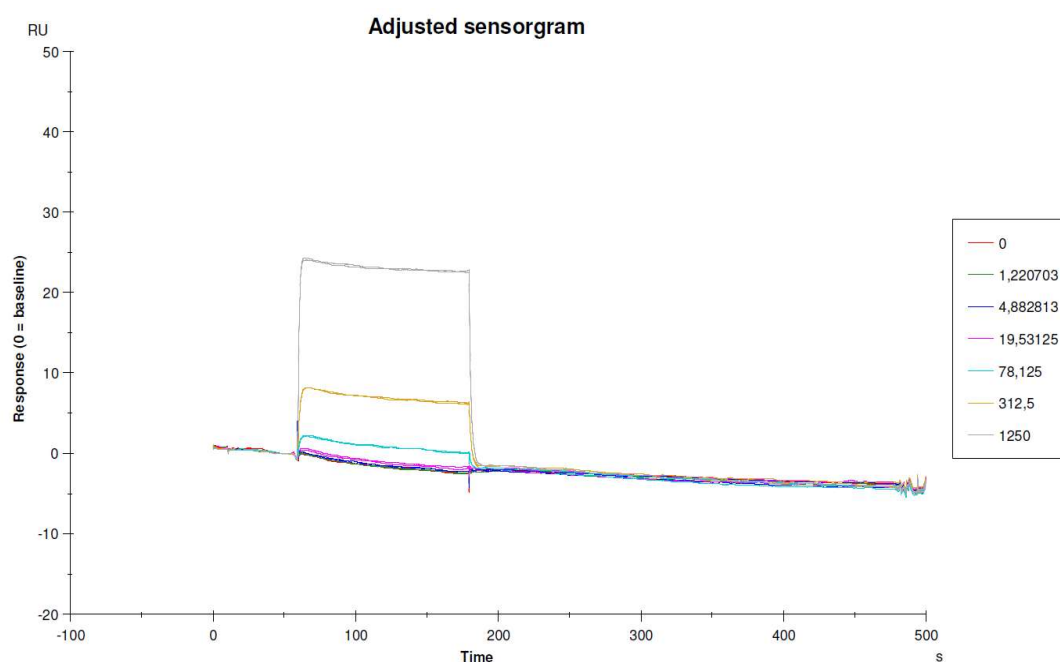


**Figure 41.** SPR sensorgrams of the interaction between the mimopeptide and the anti-MPA Fab antibody using Biacore T200. The colors observed refer to the different nanomolar concentrations of the mimopeptide added.

**Table 13** summarizes the results obtained from the SPR experiments. The affinity constant for the MPA and anti-MPA Fab interaction, in agreement with previous results reported,<sup>32</sup> was  $\sim 40 \text{ nmol L}^{-1}$ . This affinity constant differed two orders of magnitude from the affinity constant of the interaction between the mimopeptide and the anti-MPA

Fab, which resulted to be  $\sim 14 \mu\text{mol L}^{-1}$ . The weaker interaction between the mimopeptide and the anti-MPA Fab is due to the slower association and faster dissociation of the complex, compared to the values obtained for the interaction between the MPA and the anti-MPA Fab. Nevertheless, these results confirm the binding affinity of the MPA mimopeptide for the anti-MPA Fab.

**Table 13.** Kinetic constants determined for the interaction of the anti-MPA Fab with free MPA and the mimopeptide using Biacore T200. The values are shown as the average  $\pm$  the standard error of seven different analyte concentrations.

	Association rate constant $k_a$ (1/Ms)	Dissociation rate constant $k_d$ (1/s)	Affinity constant $K_D$ (M)
MPA	$(1.846 \pm 0.009) \times 10^6$	$0.0741 \pm 0.0004$	$4.016 \times 10^{-8}$
Mimopeptide	$(4.06 \pm 0.02) \times 10^5$	$0.583 \pm 0.001$	$1.434 \times 10^{-6}$

#### 4.4.3. Construction of the mimopeptide-NanoLuc fusions

The construction of protein fusions always offers endless possibilities, as DNA vectors can be altered in many different ways to produce a wide variety of protein combinations. For the construction of the mimopeptide-NanoLuc fusion protein, two different constructions were carried out. On one hand, the first combination was designed to express the mimopeptide on the N-terminus of the NanoLuc protein (referred to as N-terminal product). It is important to point out that a 'GGSGGGS' linker was introduced between the mimopeptide and the NanoLuc to prevent the mimopeptide from being concealed by the NanoLuc. On the other hand, the second combination was designed to express the mimopeptide on the C-terminus of the NanoLuc protein (referred to as C-terminal fusion). Again, the same linker was inserted in between the NanoLuc and the mimopeptide to allow a better binding with the anti-MPA Fab antibody.

Two clones for each N-terminal and C-terminal fusions that showed a successful alignment after the transformation on NEB 5-alpha were expressed and purified according to the protocols described in the experimental section. In order to test whether or not the NanoLuc was correctly expressed, 90  $\mu\text{L}$  of each purified product were added to black microtiter plates and 10  $\mu\text{L}$  of the substrate dilution, composed of 2  $\mu\text{L}$  of the NanoGlo substrate in 100  $\mu\text{L}$  of PBS buffer, were added to each well and the bioluminescence was measured immediately with a CLARIOstar microplate reader. The results of the expression test are reflected in **Figure 42** and confirm the correct expression of the NanoLuc protein in the four products tested due to the bioluminescence observed after the addition of the substrate. However, it can be observed that both of the C-terminal fusions showed a brighter bioluminescence than the N-terminal fusions. According to these results, the N-terminal product 1 and the C-terminal fusion 1 were chosen for further tests due to the brighter bioluminescence in comparison to their homologous N-terminal 2 and C-terminal 2, respectively.

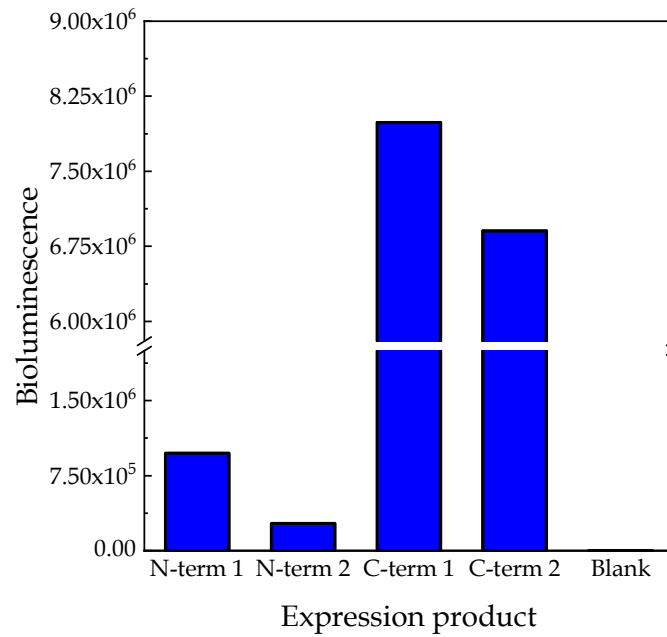


**Figure 42.** Expression test with the four clones that showed successful alignment after the transformation of NEB 5-alpha cells and a blank. The results show the bioluminescence of each product (n = 1).

The size and purity of both fusion proteins, N-terminal 1 and C-terminal 1 (referred to as N-terminal and C-terminal from now on) was confirmed by SDS-PAGE. As a reference, **Figure 43** shows the SDS-PAGE analysis of the C-terminal fusion.

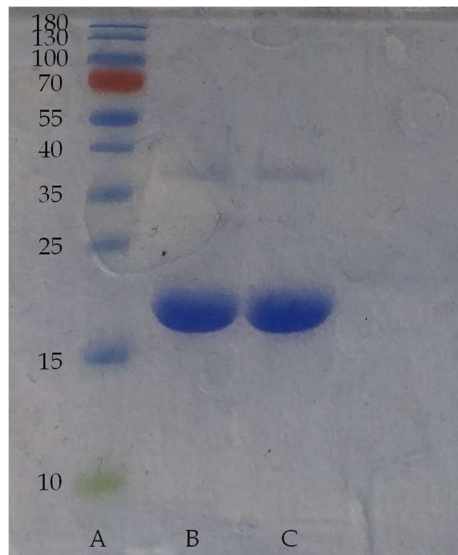


**Figure 43.** SDS-PAGE analysis for the C-terminal fusion protein with Coomassie brilliant blue protein staining: lane A, molecular marker (Thermo Scientific™ PageRuler™ Prestained Protein

Ladder, 10 to 180 kDa), B, C-terminal fusion , C, C-terminal fusion with a 5 min boiling step at 95 °C.

#### 4.4.4. Structural characterization of the mimopeptide and the fusion protein

A Total Correlation Spectroscopy (TOCSY)  $^1\text{H}$ - $^1\text{H}$  bidimensional spectrum was performed to determine the amino acids of the synthesized biotinylated mimopeptide A(CEGLYAHWC)GGGSK(Bio)-NH<sub>2</sub>. The study was carried out in collaboration with Prof. M<sup>a</sup> Ángeles Herranz Astudillo from the Dpmt. Organic Chemistry at UCM. The bidimensional spectrum and the assignment of the amino acids are shown in **Figure 44**. As can be observed, three of the amino acids that compose the mimopeptide were not identified in the spectrum. It is believed that the G that was not assigned is overlapping in the spectrum with the other two Gs close to each other. Additionally, it is also considered as normal that the first amino acid of the peptide (in this case, A) do not appear in the spectrum. The C that is not assigned might not present enough resolution in the spectrum or could overlap with the other C. The remaining amino acids were correctly assigned in the spectrum by relating the signals observed with NMR charts.

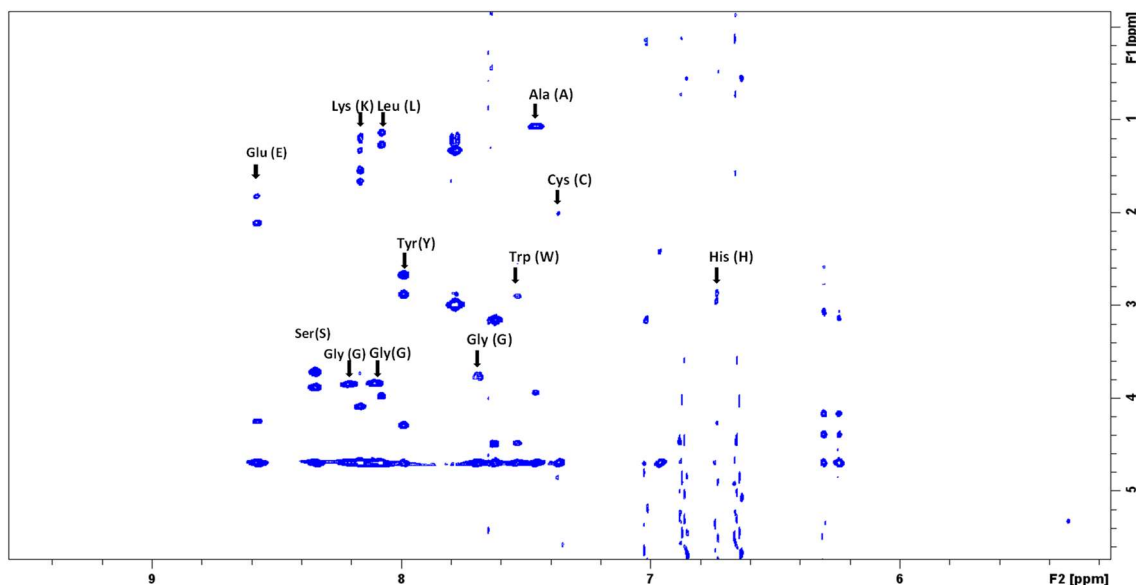


**Figure 44.**  $^1\text{H}$ - $^1\text{H}$  TOCSY bidimensional spectrum of the MPA mimopeptide A(CEGLYAHWC)GGGSK(Bio)-NH<sub>2</sub>. The amino acids were assigned in the spectrum according to NMR charts.

In order to test the possible existence of the disulfide constrained loop in the synthesized mimopeptide, another NMR experiment was carried out, in which a few drops of dithiothreitol (DTT), a well-known reducing agent for disulfide bonds,<sup>39,40</sup> were added to the dissolved mimopeptide. The comparison of both monodimensional spectra, with and without the addition of DTT, is shown in **Figure 45**. A structural change can be observed in the spectra that contains DTT from the original one without DTT. This structural change is vastly observed in the anomeric region between 9 and 6 ppm. Therefore, it can be concluded that the mimopeptide structure was severely affected after the addition of DTT, confirming the existence of the second Cysteine that was not observed in the TOCSY  $^1\text{H}$ - $^1\text{H}$  bidimensional spectrum, as well as the disulfide bond in the original structure.

The structural simulation of the mimopeptide (**Figure 46**) was carried out by submitting the mimopeptide's linear sequence, A(CEGLYAHWC)GGGSK(Bio)-NH<sub>2</sub>, in the AMBER program. Different feasible combinations of the linear sequence were obtained from the software, and the mimopeptide structure, presenting the disulfide constrained loop between the two cysteines was observed as an alternative. The mimopeptide's sequence was then submitted in the MAESTRO software, in which after an automatic minimization presented the structural combination shown in **Figure 46**. Therefore, the structural simulation verified the possibility of presenting a disulfide constrained loop between the two cysteines in the mimopeptide.

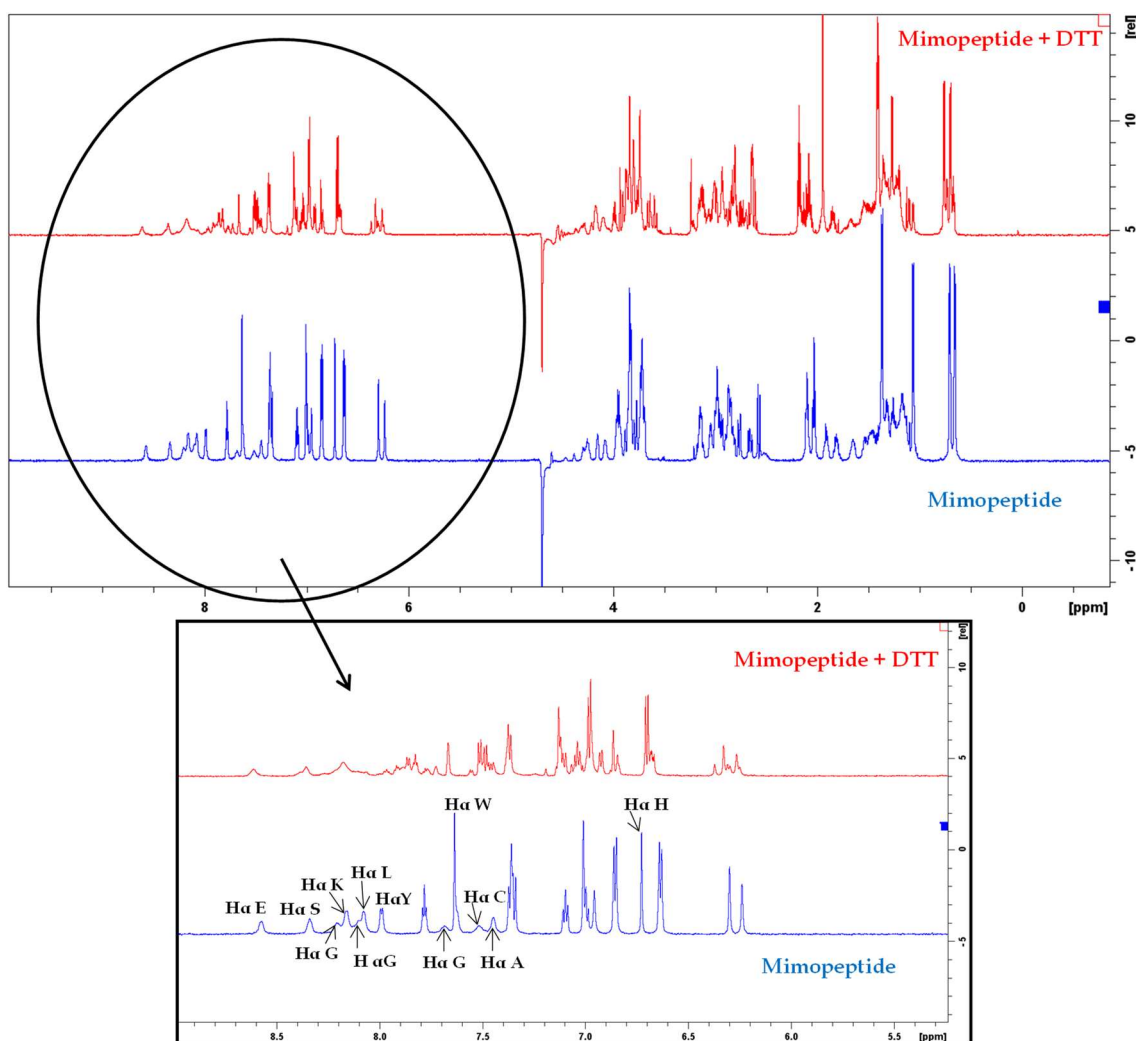


**Figure 45.** <sup>1</sup>H-NMR spectra of the MPA mimopeptide in the presence (red) and the absence (blue) of a few drops of DTT. The structural change is observed in the anomeric region between 9 and 5 ppm of the amplified spectra. The H $\alpha$  assignment of the amino acids can be observed in the amplified spectrum of the mimopeptide in the absence of DTT.

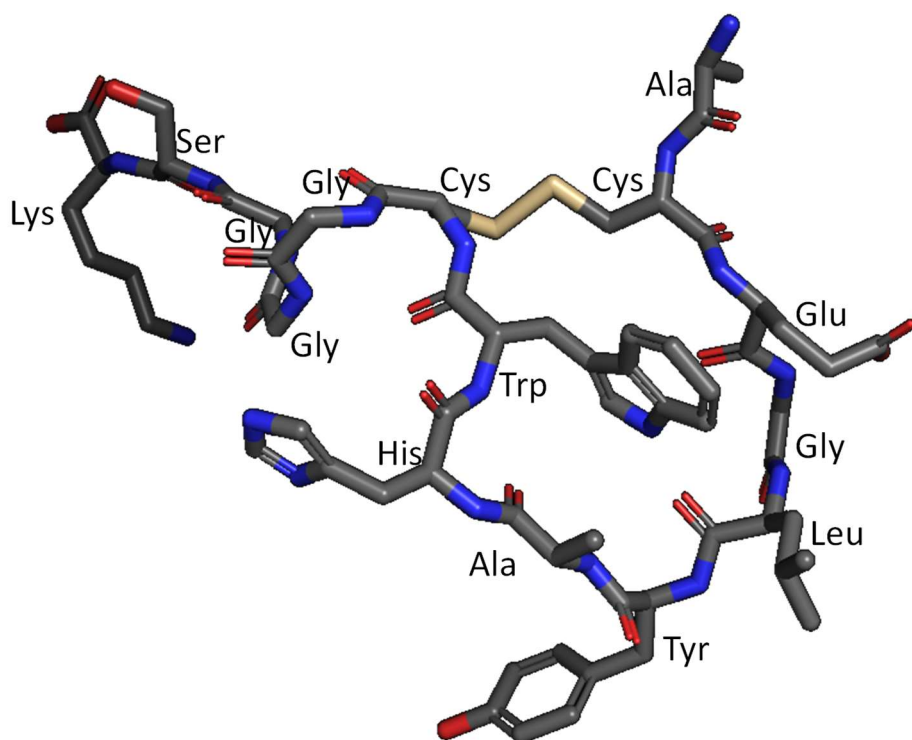


**Figure 46.** Structural simulation of the MPA mimopeptide with MAESTRO software.

Finally, an H-N Heteronuclear Single Quantum Coherence (HSQC) bidimensional spectrum of the NanoLuc-mimopeptide fusion protein was conducted (**Figure 47**). According to the spectrum, it can be deduced that the protein presents a stable conformation and a good folding, as the signals are dispersed throughout the spectrum.

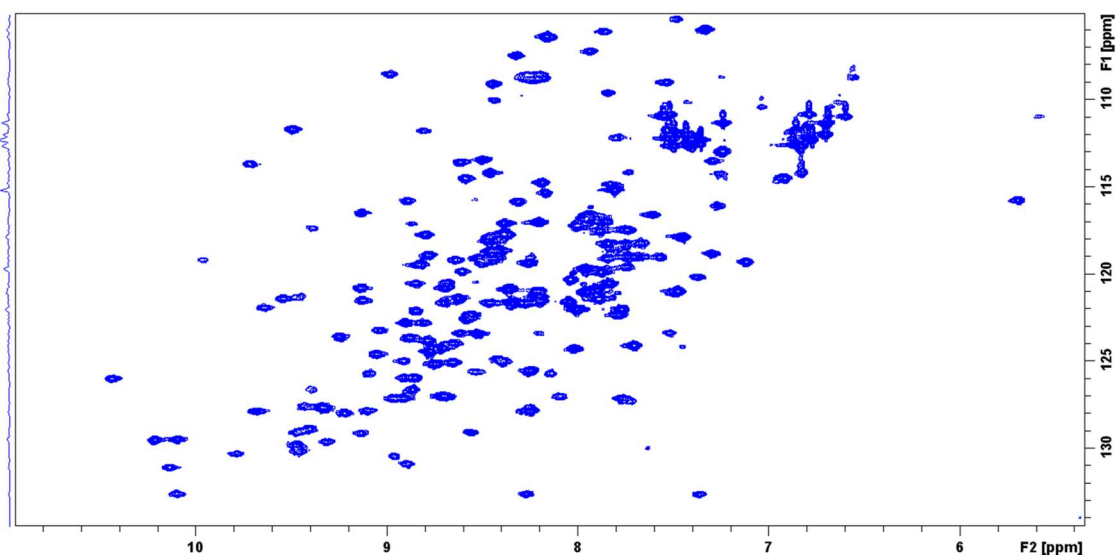


**Figure 47.**  $^1\text{H}$ - $^{15}\text{N}$  HSQC spectrum of the NanoLuc-mimopeptide fusion protein.

#### 4.4.5. Optimization of the measuring conditions

The first attempt for the development of the immunoassay using the NanoLuc-mimopeptide fusion proteins was to immobilize the anti-MPA Fab onto neutravidin-coated plates. After washing to remove the unbound antibody, a 1:50 dilution of each of the fusion proteins was added to the wells and incubated for 30 min. After another washing step, the NanoLuc substrate was added, and the bioluminescence was measured in a CLARIOstar microplate reader. The results are shown in **Figure 48**. As can be observed, both fusion products presented very high nonspecific binding for the plate when the NanoLuc was incubated in wells without the anti-MPA Fab. This nonspecific binding was particularly high for the N-terminal product, in which the bioluminescent signal was considerably higher in the wells without the antibody than in those containing the antibody.

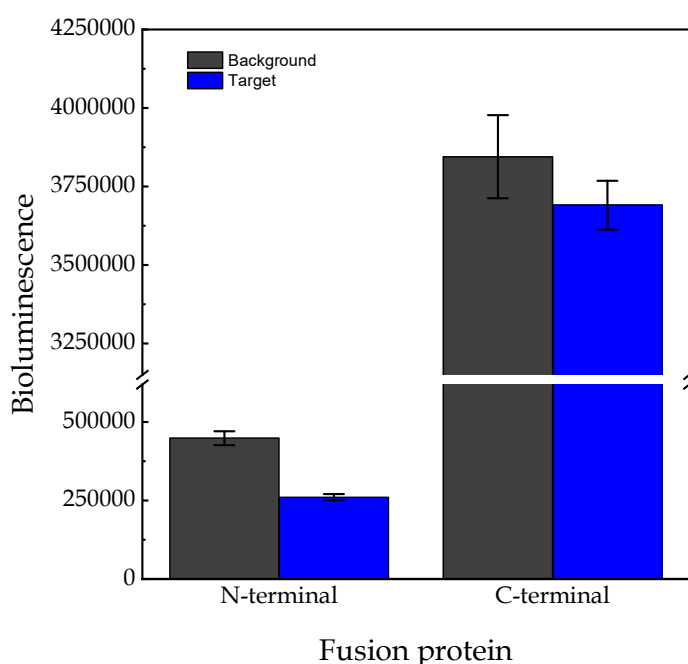


**Figure 48.** Binding test of the NanoLuc-mimopeptide fusion proteins on neutravidin-coated wells. Both products present very high nonspecific interaction for background wells (grey) in comparison to the signal obtained in the target wells with the anti-MPA Fab (blue). The results are shown as the mean values of the bioluminescence signal  $\pm$  the standard deviation of the mean ( $n = 3$ ).

Due to the high nonspecific binding observed, a blocking step was introduced before adding the fusion protein to the wells. Two different blocking buffers were tested: SuperBlock and Protein Free buffer, owing to the high affinity of MPA to proteins such as BSA or casein, previously discussed in the third chapter of this thesis. Furthermore, a 1:250 dilution of the protein fusions was added to the wells, instead of the 1:50 dilution previously added, to avoid excessive concentration of the NanoLuc-tagged mimopeptide. The results of the binding test introducing the blocking step are shown in **Figure 49**. Regardless of the blocking agent added, a very high nonspecific binding was

observed in those wells without anti-MPA Fab antibody, similar to the previous binding test for both the N-terminal and the C-terminal fusions.

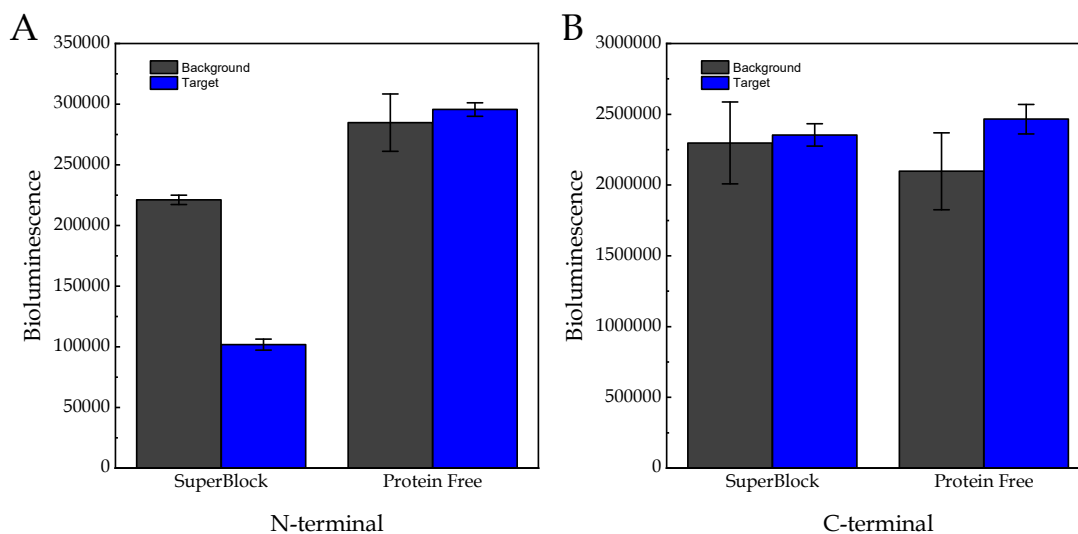


**Figure 49.** Binding test of the NanoLuc-mimopeptide fusion proteins on neutravidin-coated wells previously blocked. Both fusion proteins, N-terminal (A) and C-terminal (B) present very high nonspecific interactions with both of the blocking agents for background wells (grey) in comparison to the signal obtained in the target wells with the anti-MPA Fab (blue). The results are shown as the mean values of the bioluminescence signal  $\pm$  the standard deviation of the mean ( $n = 3$ ).

The plate-format assay was discarded owing to the very high nonspecific interactions observed, even after including a blocking step with either SuperBlock or Protein Free buffer. Therefore, a new strategy using neutravidin-coupled magnetic beads was developed. In this case, black microtiter wells were initially blocked with either superblock supplemented with 0.05% T20 or Protein Free buffer for 1 h at room temperature. After washing three times with washing buffer, 60  $\mu\text{L}$  of a solution of 0.5  $\mu\text{g mL}^{-1}$  anti-MPA Fab and 20  $\mu\text{L}$  of 100  $\mu\text{g mL}^{-1}$  neutravidin coated beads were added and incubated for 30 min at room temperature and slow shaking. The plate was subsequently washed thrice and then 60  $\mu\text{L}$  of the fusion protein in different dilutions (1:10, 1:50, 1:250 and 1:1250) from the original stock were added and incubated for 30 min at room temperature and slow shaking. Finally, after washing the plate three times, the substrate was added, and the bioluminescence was measured. The assay was also performed without anti-MPA Fab, magnetic beads and fusion protein to test nonspecific binding. The results with the C-terminal fusion (**Figure 50** and **Figure 51**) show that a very high signal was obtained when the anti-MPA Fab was not present in the assay for both blocking buffer tested. The negative controls without beads and without the fusion protein presented considerably low bioluminescence. Therefore, it could be concluded that the fusion protein bound nonspecifically to the neutravidin-coated magnetic beads, regardless of the dilution and the blocking buffer used.



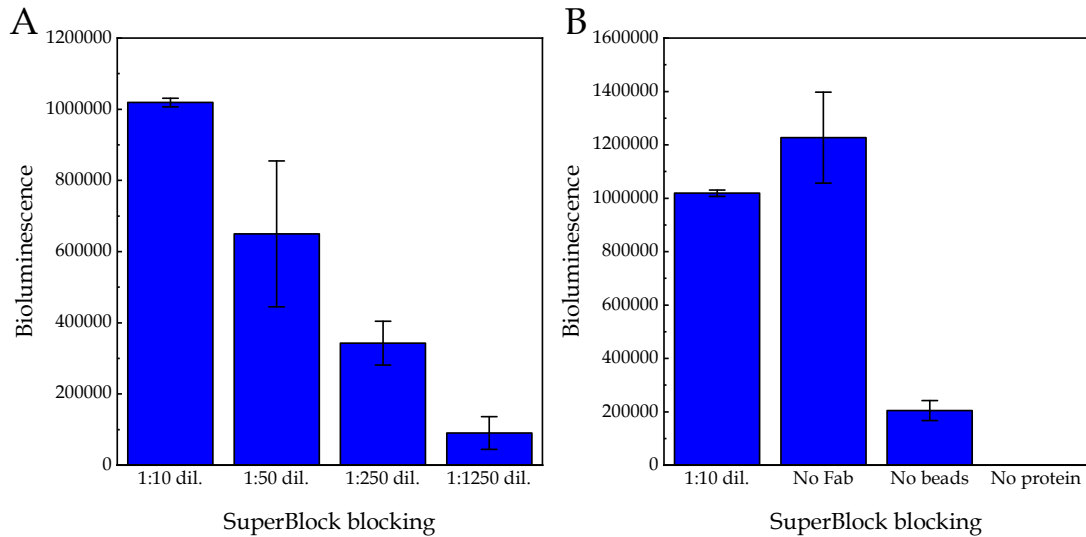


**Figure 50.** Neutravidin bead-based assay with SuperBlock blocking buffer supplemented with 0.05% T20. A. Bioluminescence observed with different dilutions of the fusion protein in the assay. B. Comparison of the signal obtained with a 1:10 dilution of the fusion protein with three negative controls, in which the assay was reproduced in the same conditions but in the absence of anti-MPA Fab (no Fab), neutravidin-coated magnetic beads (no beads) and the NanoLuc-MPA mimopeptide fusion protein (no protein). The results are shown as the average bioluminescence values  $\pm$  the standard deviation of the mean ( $n=3$ ).

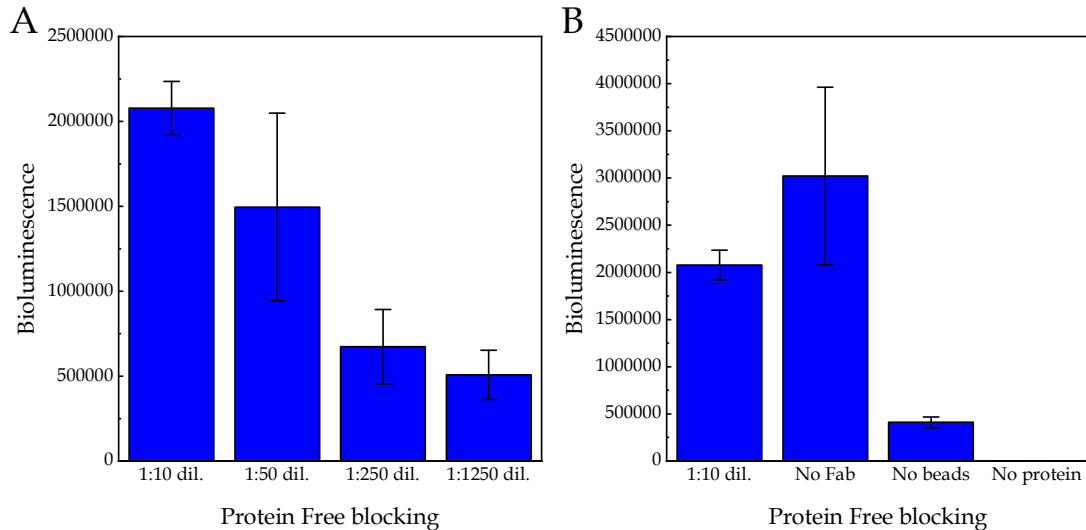


**Figure 51.** Neutravidin bead-based assay with Protein Free blocking buffer supplemented with 0.05% T20. A. Bioluminescence observed with different dilutions of the fusion protein in the assay. B. Comparison of the signal obtained with a 1:10 dilution of the fusion protein with three negative controls, in which the assay was reproduced in the same conditions but in the absence of anti-MPA Fab (no Fab), neutravidin-coated magnetic beads (no beads) and the NanoLuc-MPA mimopeptide fusion protein (no protein). The results are shown as the average bioluminescence values  $\pm$  the standard deviation of the mean ( $n=3$ ).

Due to the persistent nonspecific binding problems, we tested the application of iron-encapsulated microporous cellulose beads for the assay. These beads were already functionalized with streptavidin for direct coupling to biotinylated proteins.<sup>41</sup> In this case, the same protocol described for the neutravidin-coupled magnetic beads was conducted. SuperBlock was chosen as blocking agent owing to the lower dispersity observed in the previous assays. Additionally, the experiments were conducted in the presence and the absence of  $32 \text{ ng mL}^{-1}$  MPA, incubated simultaneously with the fusion protein. Both fusion products, N-terminal and C-terminal were tested, but only with two dilutions each, the 1:10 dilution and 1:50 dilution. As negative controls, the assay was reproduced for the 1:10 dilution of each fusion protein in the absence of anti-MPA Fab on the one hand and on the other hand in the absence of streptavidin magnetic beads. The results are shown in **Figure 52** and **Figure 53**. It can be seen that with these beads, the nonspecific interactions were extensively reduced in comparison to the previous assays. The total bioluminescence observed was substantially lower than the previous experiments, even with the same concentrations employed before, which might be a proof of the high nonspecific binding observed previously. Competition with free MPA was clearly observed for both fusion proteins, confirming the correct expression of the mimopeptide in the N-terminal and the C-terminal products. However, the C-terminal fusion showed a slightly better signal to background ratio than the N-terminal product, as well as a higher bioluminescence signal. This could lead to the idea that the mimopeptide presents less steric hindrances when it is expressed as the C-terminal fusion of the NanoLuc rather than as the N-terminal product.

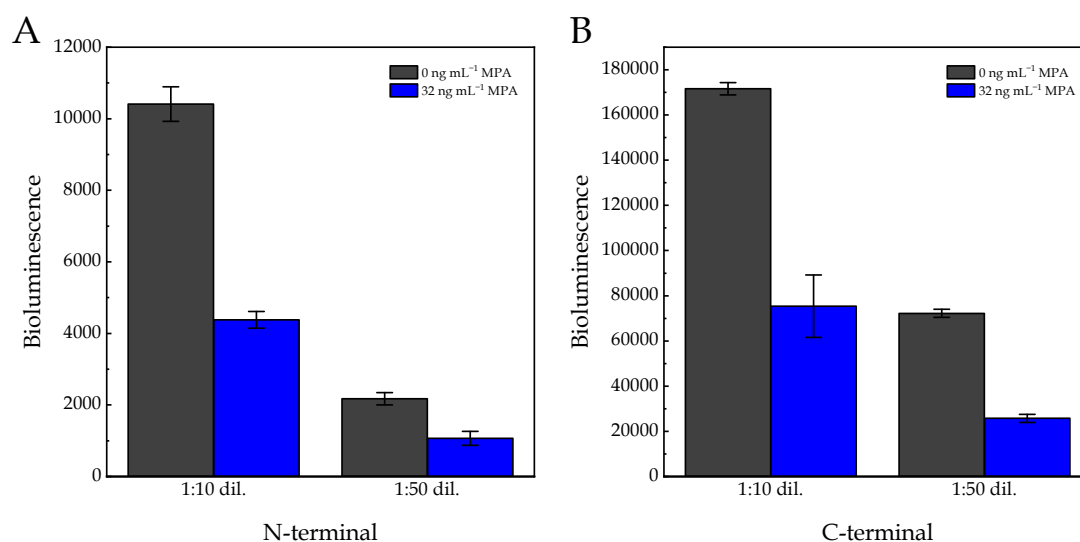


**Figure 52.** Streptavidin cellulose bead-based assay for (A) the N-terminal and (B) the C-terminal fusions at two different dilution factors, in the presence (blue) and absence (grey) of  $32 \text{ ng mL}^{-1}$  MPA. Under the same conditions, the C-terminal fusion shows ten times higher bioluminescence than the N-terminal product. The results are shown as the average bioluminescence values  $\pm$  the standard deviation of the mean ( $n=3$ ).

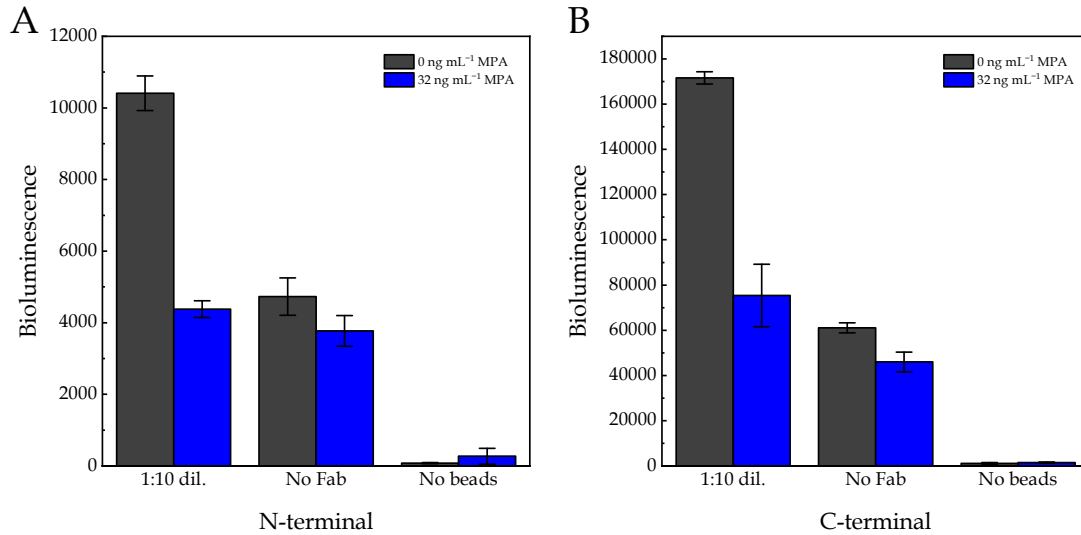


**Figure 53.** Streptavidin cellulose bead-based assay for (A) the N-terminal and (B) the C-terminal fusions in the presence (blue) and absence (grey) of 32 ng mL<sup>-1</sup> MPA with two different negative controls: the absence of anti-MPA Fab and the absence of streptavidin beads. Under the same assay conditions, the C-terminal fusion shows slightly better signal to background ratio than the N-terminal product. The results are shown as the average bioluminescence values  $\pm$  the standard deviation of the mean ( $n=3$ ).

As a way to summarize all the different assay formats tested, **Figure 54** shows a scheme of the three formats tested.

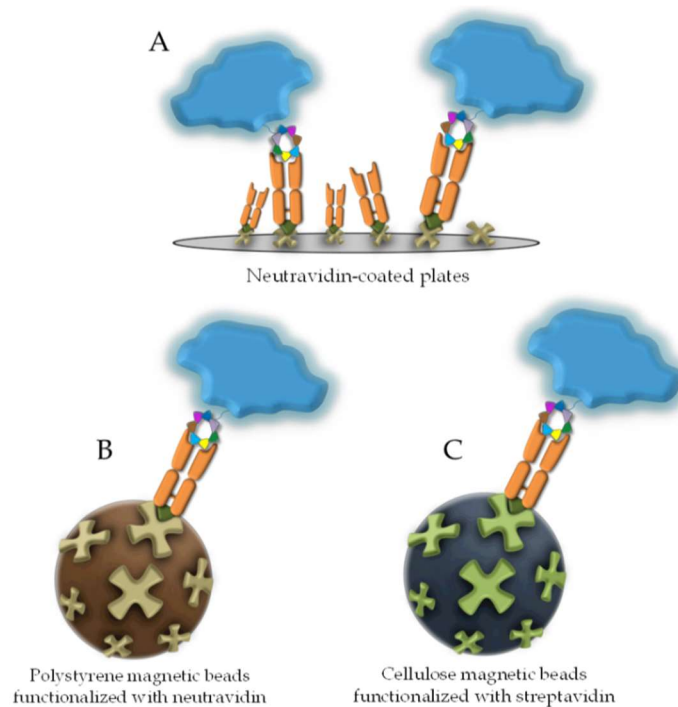


**Figure 54.** Scheme of the developed assays for NanoLuc fusion proteins. A. Plate-based method. B. Neutravidin beads-based method. C. Streptavidin beads-based method.

After proving the low nonspecific binding of the NanoLuc-mimopeptide fusion protein to the cellulose magnetic beads functionalized with streptavidin, a checkerboard titration was carried out to optimize the bead and the antibody concentrations in the assay. Four different dilutions of the streptavidin beads were tested, 1 in 500, 5 in 500, 10 in 500 and 20 in 500 v/v from the original stock. Regarding the anti-MPA Fab concentrations, 0.1, 0.5, 1 and 5  $\mu\text{g mL}^{-1}$  anti-MPA Fab were assayed. Due to the higher bioluminescence, the C-terminal fusion was chosen for this optimization. The checkerboard was carried out in the presence and the absence of 32  $\text{ng mL}^{-1}$  MPA. The results are shown in **Table 14** and **Figure 55**. The ratios between the bioluminescence in the absence and the presence of free MPA show that a higher antibody concentration generally gives a better ratio. However, regarding the streptavidin beads dilutions, better results are obtained with intermediate dilutions. It can be clearly observed that the best ratio was obtained with an antibody concentration of 5.0  $\mu\text{g mL}^{-1}$  and a bead dilution of 10 in 500 v/v. This value is surprisingly much higher than any of the other values observed; therefore, these concentrations were consequently used for the development of the immunoassay.

**Table 14.** Ratios between the signals obtained in the checkerboard titration in the presence and the absence of free MPA in solution for every antibody and magnetic bead concentration tested. The optimal combination selected is shown in bold (RSD < 14.8%).

		Beads (v/v)			
		1 in 500	5 in 500	10 in 500	20 in 500
Antibody	5.0 $\mu\text{g mL}^{-1}$	1.76	1.33	<b>4.29</b>	2.73
	1.0 $\mu\text{g mL}^{-1}$	1.35	1.29	1.77	1.43
	0.50 $\mu\text{g mL}^{-1}$	0.90	1.32	0.89	1.67
	0.10 $\mu\text{g mL}^{-1}$	0.78	1.38	1.06	1.56

With the optimized antibody and streptavidin beads concentrations, the bioluminescent immunoassay was conducted with both fusion proteins, the N-terminal and the C-terminal fusion. The results (**Figure 56**) prove that both products can recognize the anti-MPA Fab as well as compete against free MPA at very low concentrations (nanograms per milliliter interval) for the binding sites of the antibody. Nevertheless, the C-terminal fusion proved a wider dynamic range and a lower dispersity, especially at low concentrations, in comparison to the N-terminal product. Therefore, the C-terminal fusion was selected for subsequent experiments.

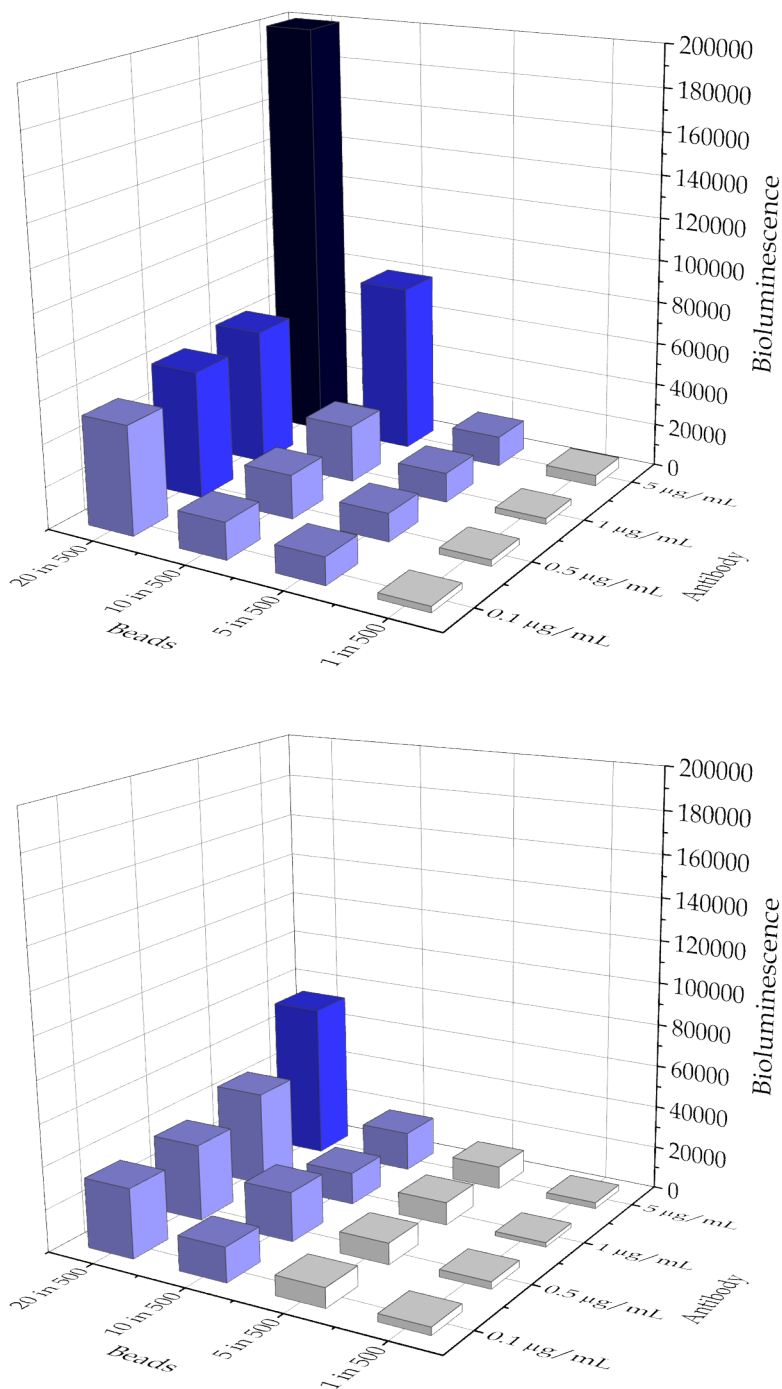


**Figure 55.** Checkerboard titration for the optimization of the antibody and magnetic bead concentrations for the immunoassay with the NanoLuc-mimopeptide fusion protein in the absence (top) and presence (bottom) of 32 ng mL<sup>-1</sup> free MPA (RSD < 17.5%).

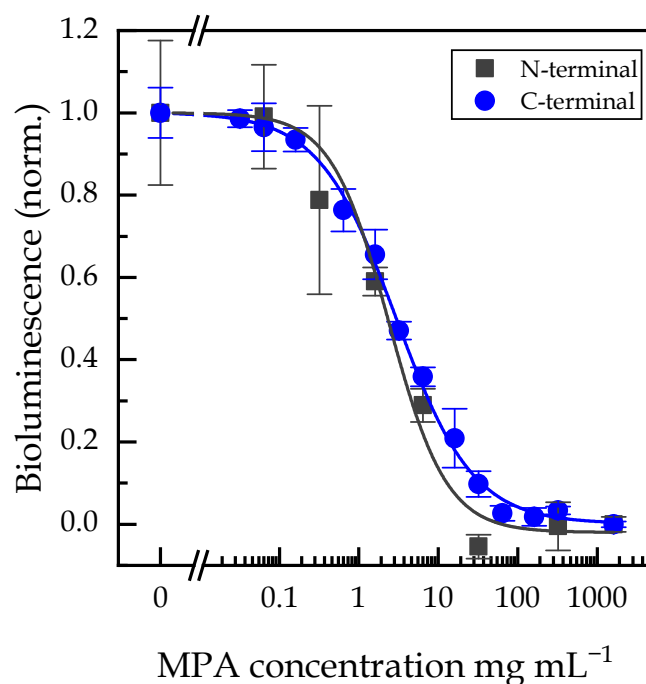


**Figure 56.** Calibrate comparison between the N-terminal (grey) and the C-terminal (blue) fusions. The previously optimized conditions were applied in both calibrates. The results are presented as the normalized bioluminescence mean values  $\pm$  the standard error of the mean ( $n = 3$ ) with a logistic fit (OriginPro 2019)

#### 4.4.6. Analytical characteristics of the bioluminescent assay

The optimized immunoassay with the C-terminal fusion was subject to further characterization as well as a detailed comparison with the previous immunoassays developed with either the phage clone or the cyclic peptide.

##### 4.4.6.1. Calibration

When comparing the sensitivity of the immunoassay using the C-terminal fusion strategy (**Figure 57**) with the previous assays, using the phage clone A2 and the synthesized mimopeptide, the former one improved the dynamic range and the sensitivity of the phage-based and the synthetic mimopeptide-based immunoassays. The limit of detection using the mimopeptide bioluminescent fusion protein was  $0.26 \text{ ng mL}^{-1}$ , compared to the previous values of  $0.61 \text{ ng mL}^{-1}$  and  $1.2 \text{ ng mL}^{-1}$  for the phage-based and mimopeptide-based immunoassays, respectively. The  $\text{IC}_{50}$  value of the NanoLuc-based immunoassay was  $2.9 \pm 0.5 \text{ ng mL}^{-1}$ , whereas the dynamic range was between  $0.64$  and  $14 \text{ ng mL}^{-1}$  MPA. With reference to the interday relative standard deviation (RSD), the value observed was 12% on average ( $n = 3$ ), and the value for the assays carried out on three non-consecutive days was 9%.

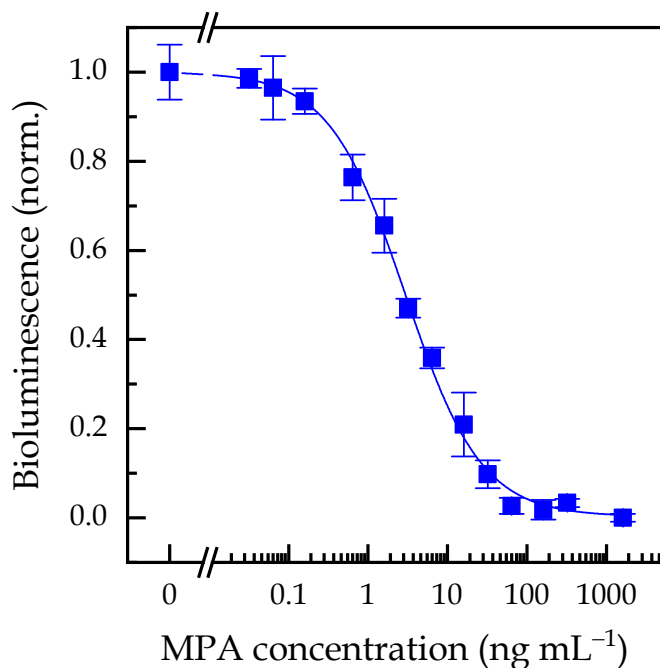


**Figure 57.** Calibration curve of the bioluminescent immunoassay for the determination of MPA in buffer using the C-terminal fusion. Several MPA concentrations were incubated together with the fusion protein and streptavidin magnetic beads coupled to the biotinylated anti-MPA. The bioluminescence signals ( $\lambda_{em} = 470 \pm 80$  nm) were measured after the addition of the NanoLuc substrate, and the values were normalized to the maximum and minimum signals. The results represent as the mean values  $\pm$  the standard error ( $n = 3$ ) adjusted to a logistic fit using OriginPro 2019.

Another improvement of the bioluminescent immunoassay was that it presented a shorter analysis time and more simplicity, compared to the phage-based and mimopeptide-based immunoassays, due to the fact that no secondary antibody is needed. Moreover, the bioluminescent fusion protein immunoassay improves the sensitivity of other immunoassays previously described in the literature as well as commercial kits for the analysis of free MPA. **Table 15** presents a comparison of some relevant immunoassays found in the literature, including some commercial kits from Siemens and Thermo Scientific, as well as several chromatographic methods for the determination of MPA. It can be observed that none of the two commercial kits currently found for the determination of MPA target free MPA, responsible for the pharmacological activity. Furthermore, even if some of the chromatographic methods found in the literature present a considerably wider dynamic range as well as a good limit of detection, they require the use of expensive equipment, longer analysis times, as well as skilled personnel. Additionally, the bioluminescent immunoassay for MPA developed in this thesis is the first one to include a mimopeptide for MPA. This can lead to the production of the mimopeptide fused to a wide variety of bioluminescent or fluorescent proteins in a cost-effective way, avoiding any tedious chemical conjugation of the analyte.

**Table 15.** Comparison of different immunoassays and chromatographic methods for the determination of total and free MPA.

Method	Assay format	Detect	LOD (ng mL <sup>-1</sup> )	Dynamic range (ng mL <sup>-1</sup> )	Ref.
EMIT 2000 MPA	Homog.	Total	<i>n.d.</i>	100-15000	32
CEDIA MPA	Homog.	Total	<i>n.d.</i>	300-10000	33
EMIT	Homog.	Free	1	10-1250	8
PETINIA	Homog.	Total	<i>n.d.</i>	200-30000	9
FPIA	Homog.	Free	3.2	6.8-156	11
UPLC MS/MS	-	Total	2.5	15-15000	34
HPLC-UV	-	Free	4	60-1000	35
HPLC-FLD	-	Total Free	8 <i>n.d.</i>	50-40000 5-1000	36
NanoLuc-mimopeptide	Heterog.	Free	0.26	0.64-14	37
Peptide-Based	Heterog.	Free	0.94	2.4-60	37
Phage-Based	Heterog.	Free	0.69	1.0-4.1	37

*Homog.* Homogeneous immunoassay; *Heterog.* Heterogeneous immunoassay; *nd.* Not determined

#### 4.4.6.2. Cross-reactivity

With the aim of establishing a novel method for the analysis of mycophenolic acid in blood samples of transplanted patients, the selectivity of the bioluminescent immunoassay was tested by reproducing the assay in the presence of several potential interferences. Among these interferences, the main two MPA metabolites typically found in blood, mycophenolic acid glucuronide (MPAG) and acyl-mycophenolic acid glucuronide (Acyl-MPAG) were evaluated. Moreover, other immunosuppressant drugs (tacrolimus and cyclosporin A) generally co-administered with MPA to transplanted patients were also tested (**Figure 58**). The results are shown in **Figure 59**. It can be observed that one of the MPA metabolites, the Acyl-MPAG, presented a similar behavior in the immunoassay, with a cross reactivity of the 58% (calculated as the ratio of the IC<sub>50</sub> for MPA and the IC<sub>50</sub> for Acyl-MPAG). Contrary to the MPAG, the Acyl-MPAG is an active form of MPA.<sup>42</sup> Therefore, the developed immunoassay can be useful for the detection of the active forms of MPA in blood samples. Nonetheless, the Acyl-MPAG is generally found at lower concentrations than MPA, and it might not be detected by the immunoassay.<sup>43</sup> With regard to the inactive form, the MPAG, the cross reactivity was negligible at only 0.03%, and the two other immunosuppressant drugs tested showed a cross reactivity lower than 0.03%.



Immunodetection of mycophenolic acid in blood of transplanted patients using a recombinant peptide mimetic bioluminescent tracer

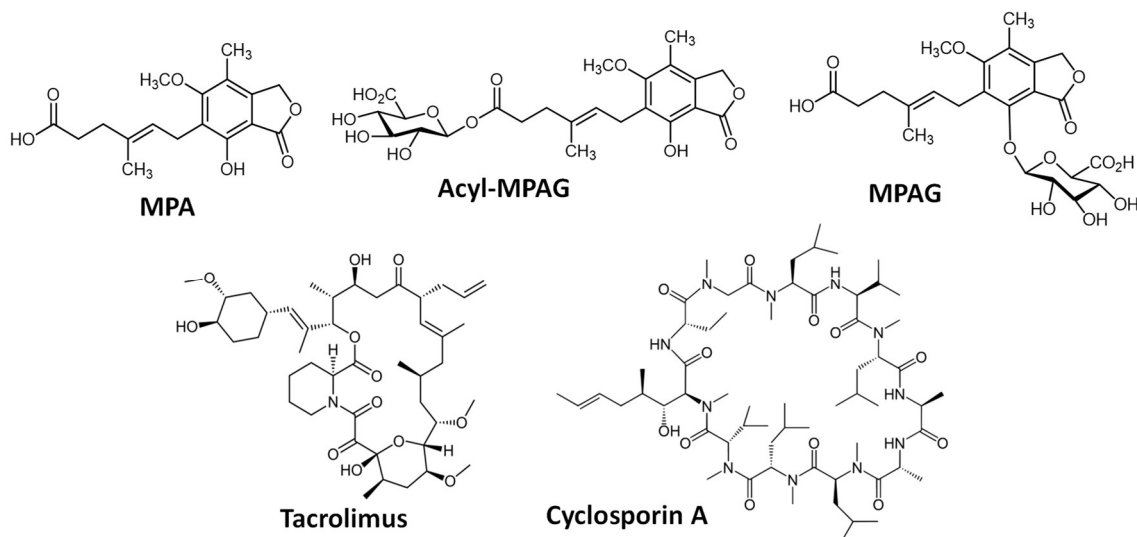


**Figure 58.** Chemical structures of mycophenolic acid (MPA), its two main metabolites, (Acyl-MPAG and MPAG) and two immunosuppressant drugs commonly co-administered to transplanted patients (Tacrolimus and Cyclosporin A).

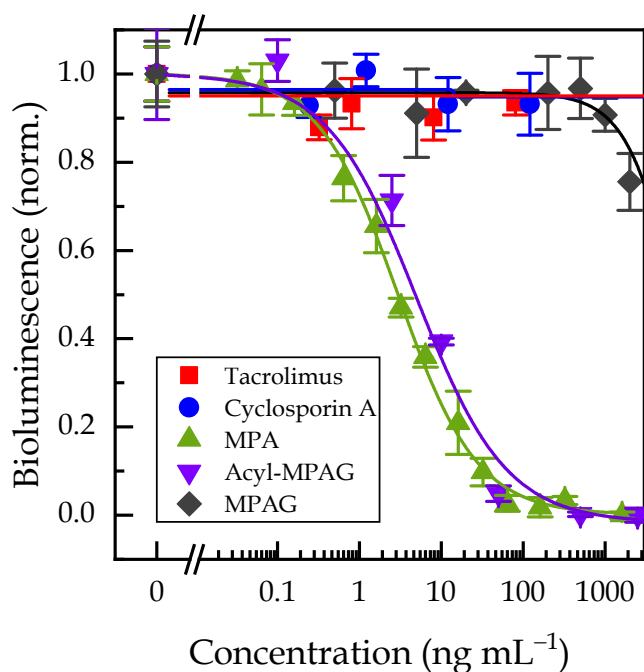


**Figure 59.** Cross-reactivity test of the bioluminescent immunoassay. Acyl-MPAG, an active form of MPA, shows a significant cross-reactivity to MPA, contrary to the inactive form MPAG. The two other immunosuppressant drugs evaluated, tacrolimus and cyclosporin A, showed no significant cross-reactivity at the concentration levels assessed. The bioluminescence values were normalized to the maximum and minimum signals, and the results are shown as the mean values  $\pm$  the standard error of the mean ( $n = 3$ ) adjusted to a logistic fit using OriginPro 2019.

#### 4.4.6.3. Long term stability of the NanoLuc-mimopeptide fusion protein

The NanoLuc-mimopeptide fusion protein proved a good stability upon storage at  $-20\text{ }^{\circ}\text{C}$  in PBS for more than 6 months. The long-term stability was determined by reproducing the immunoassay over a period of time of 6 months and comparing the  $\text{IC}_{50}$  values obtained. The results are displayed in **Figure 60** in a Shewart graph. The center value (straight red line) was calculated as the average of all the values obtained, and the upper and lower limits were calculated as three times the standard deviation. It can be observed that the  $\text{IC}_{50}$  values present no significant differences over the 6-month period tested, although the last calibrate presented a considerably higher error than the previously tested ones. Moreover, after one year, the stability of both products was tested by SDS-PAGE. The results (**Figure 61**) prove that both the N-terminal and the C-terminal fusion proteins presented several products that were very vaguely observed before. The bands observed at  $\sim 40\text{ kDa}$  and  $\sim 70\text{ kDa}$  may correspond to the dimer and the trimer of the fusion protein.

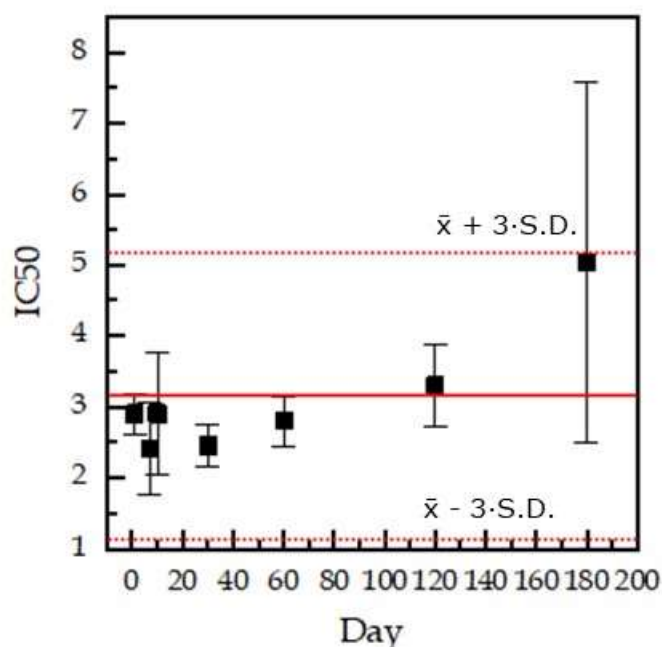


**Figure 60.** Evaluation of the long-term stability for the C-terminal fusion protein stored at  $-20\text{ }^{\circ}\text{C}$  in PBS. The bioluminescent immunoassay was performed under the same conditions and the  $\text{IC}_{50}$  values were consequently compared. The results are shown as the values  $\pm$  the standard error given by OriginPro 2019.

#### 4.4.6.4. Matrix effect

In order to apply the optimized immunoassay to the analysis of blood samples, the matrix effect in the presence of several dilutions of ultrafiltered serum samples (1/2, 1/6, 1/8, (v/v)) in PBS 1 $\times$  supplemented with 0.05% T20 was evaluated. The results (**Figure 62**) prove that no significant differences ( $p > 0.05$ ) were observed when comparing the calibration plots using PBS 1 $\times$  supplemented with 0.05% T20 or a 1/8 dilution of the ultrafiltered serum sample in buffer. Consequently, the 1/8 dilution was applied for further experiments.

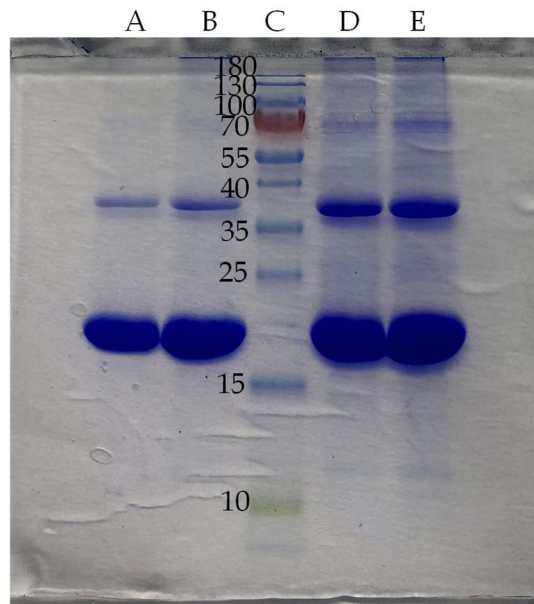


**Figure 61.** SDS-PAGE analysis for the fusion proteins after more than one year of storage with Coomassie brilliant blue protein staining: lane A: C-terminal fusion, B, C-terminal fusion with a 5 min boiling step at 95 °C, C, molecular marker (Thermo Scientific™ PageRuler™ Prestained Protein Ladder, 10 to 180 kDa), D, N-terminal product, E, N-terminal product with a 5 min boiling step at 95 °C.

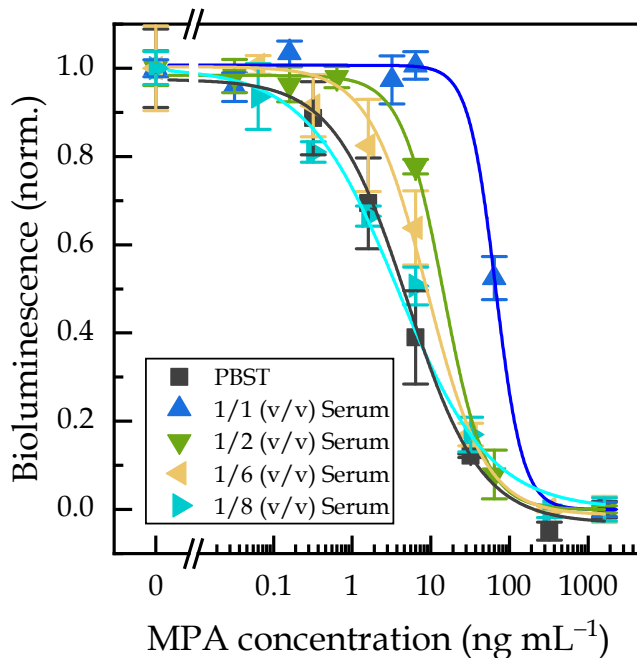


**Figure 62.** Calibration curves obtained for the bead-based immunoassay using various dilutions of ultrafiltered serum samples in PBS 1× supplemented with 0.05% T20. The bioluminescence values were normalized to the maximum and minimum signals and the results are shown as the

mean values  $\pm$  the standard error of the mean ( $n = 3$ ) adjusted to a logistic fit using OriginPro 2019.

#### 4.4.7. Sample analysis

After all the previous evaluations of the immunoassay, blood samples from transplanted patients were examined. Five transplanted patients (T1-T5) and three healthy patients used as control (H1-H3) were analyzed, and the results obtained with the bioluminescent immunoassay were validated by a rapid resolution liquid chromatography coupled to diode array detection (RRLC-DAD) method (**Figure 63**). The samples were provided by Dr. J. Bustamante Munguira from Hospital Clínico Universitario de Valladolid. The concentrations of MPA administered to the transplanted patients and shown in **Table 16**.

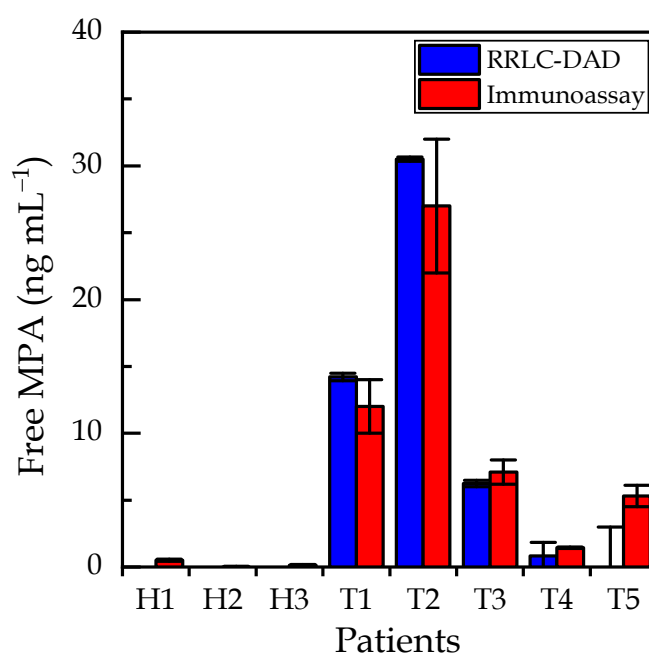


**Figure 63.** Comparison of the results obtained for the analysis of MPA in blood samples from transplanted patients by the immunoassay and the chromatographic method. H patients received no previous treatment with MPA, whereas T patients were previously treated with MPA. The results are presented as the mean values  $\pm$  the standard error of the mean ( $n = 3$ ).

**Table 16.** MPA doses administered to the analyzed transplanted patients.

Patient	Administered drug	Dose
T1	Myfortic	360 mg/12 h
T2	Myfortic	360 mg/12 h
T3	Myfortic	180 mg/8 h
T4	Myfortic	180 mg/8 h
T5	Myfortic	180 mg/8 h

Mycophenolic acid was not detected in any of the control samples analyzed. Furthermore, a statistical comparison using a paired t-test demonstrated no significant differences between the results obtained with the immunoassay and the chromatographic method at a 95% confidence level. A typical chromatogram of the standard mixture of MPA and its two metabolites, MPAG and Acyl-MPAG, is shown in **Figure 64**. The retention times (5.7, 8.8. and 12.0 min for MPAG, Acyl-MPAG and MPA, respectively) proved to be reproducible between different runs on different days, and the elution mode yielded a resolution higher than 2.0 between peaks. The RRLC-DAD results from all the treated patient samples confirmed that the concentration of the active metabolite of MPA was negligible at the dilution level tested. As a result, the signal response obtained in the biosensor was only due to the free MPA. Additionally, all the MPAG levels detected in the blood samples did not exceed the level of quantification of the immunoassay (**Table 17**). Thus, the non-active form of MPA presented no cross-reactivity in the analysis.

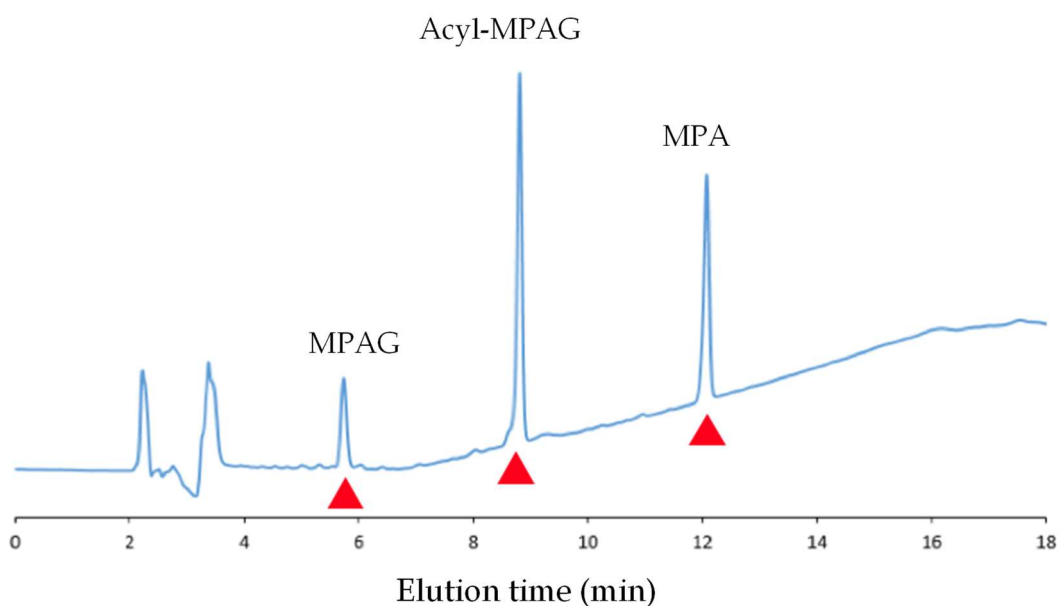


**Figure 64.** RRLC elution profile of MPAG, Acyl-MPAG and MPA. The MPA solution was prepared at 80 ng mL<sup>-1</sup>, whereas the MPAG and the Acyl-MPAG solutions were prepared at 250 ng mL<sup>-1</sup>.

**Table 17.** Concentration levels of MPAG determined in the analyzed samples.

Sample	Average, µg/mL	SD, µg/mL	Remarks
T1	1.7	0	< LOQ (Biosensor)
T2	12.7	1.3	< LOQ (Biosensor)
T3	4.2	0.2	< LOQ (Biosensor)
T4	4.1	0.6	< LOQ (Biosensor)
T5	0.13	0.2	<LOD (RRLC)
H1	0.02	0.1	<LOD (RRLC)
H2	0.02	0.1	<LOD (RRLC)
H3	-0.04	0	<LOD (RRLC)

According to the results, patients T1 and T2 presented the highest levels of MPA out of all the volunteers tested. These results correlate in a favorable manner with the administered doses of MPA to the transplanted patients (**Table 16**). Patients T1 and T2 were given 720 mg Myfortic per day, whereas patients T3, T4 and T5 received only 540 mg Myfortic daily.

## 4.5. Conclusions

The synthetic biotinylated MPA mimopeptide proved its capability to recognize the anti-MPA Fab antibody and compete against free MPA at low concentration levels. Therefore, it was confirmed that the peptide sequence ACEGLYAHWC (with a disulfide bond between the two Cs) is responsible for the interaction with the anti-MPA Fab, and not another moiety of the phage clone. Additionally, the SPR results proved that the mimopeptide presented an affinity constant for the antibody of  $\sim 14 \mu\text{mol L}^{-1}$ , which differs two orders of magnitude from that of the MPA ( $\sim 40 \text{nmol L}^{-1}$ ), turning the mimopeptide into an excellent competitor. Besides that, NMR experiments proved the existence of the disulfide bond in the mimopeptide, and the structural simulation verified the possibility of the existence of that disulfide bond between the two Cs.

The construction of the two bioluminescent fusion proteins (N-terminal and C-terminal) certified that the mimopeptide sequence can be expressed cost-effectively in bacteria, without losing its affinity for the anti-MPA Fab, obtaining a stable conformation of the protein by NMR analysis.

High non-specific binding was observed in a plate-based format or using polystyrene beads. However, the use of a cellulose-based product reduced considerably the non-specific interactions of the NanoLuc-tagged mimopeptide.

Both fusion proteins, the N-terminal and the C-terminal proved competition for the binding sites of the anti-MPA against free MPA. Nonetheless, the C-terminal fusion showed more brightness, a lower dispersity in the measurements at lower concentrations and a wider dynamic range than the N-terminal product.

The bioluminescent immunoassay using the NanoLuc enzyme as a label improved the sensitivities obtained in the phage-based and the peptide-based methods previously described. Furthermore, this immunoassay proved shorter and cost-effective analysis in comparison to other formats utilizing a secondary antibody.

The cross-reactivity tests performed concluded that the immunoassay presented negligible cross-reactivity with other immunosuppressant drugs commonly administered in combination to MPA. Nevertheless, the strong interaction of the Acyl-MPA metabolite, an active form of MPA, with the anti-MPA Fab evidenced that the biosensor can be used to detect the active forms of MPA, rather than just free MPA.

The C-terminal fusion protein proved stability for a period of 6 months, although both proteins were considerably deteriorated after one year of storage at  $-20^\circ\text{C}$  in PBS buffer.

No significant differences were observed when the assay was reproduced in the presence of a 1/8 dilution of ultrafiltered serum in PBS  $1\times$  supplemented with 0.05% T20, allowing the analysis of the active forms of mycophenolic acid in blood samples of transplanted patients.

The analysis of blood samples by RRLC-DAD determined that no Acyl-MPA was observed in any of the analyzed blood samples. Consequently, the response was only due to the presence of free MPA in the treated patients. Moreover, the concentrations of the inactive form of MPA, the MPAG, found by RRLC-DAD, did not exceed the limit of quantification of the biosensor, hence, no cross-reactivity was observed in the determination.

## Conclusions

The MPA concentrations measured with the biosensor were compared to those obtained by RRLC-DAD using a paired t-test at a 95% confidence level, and they were favorably correlated to the administered doses of each patient.



#### 4.6. Bibliography

- (1) Vardanyan, R.; Hruby, V. Chapter 29 - Immunopharmacological Drugs. In *Synthesis of Best-Seller Drugs*; Vardanyan, R., Hruby, V., Eds.; Academic Press: Boston, 2016; pp 549–572. <https://doi.org/10.1016/B978-0-12-411492-0.00029-8>.
- (2) Allison, A. C.; Eugui, E. M. Immunosuppressive and Other Effects of Mycophenolic Acid and an Ester Prodrug, Mycophenolate Mofetil. *Immunol. Rev.* **1993**, *136*, 5–28. <https://doi.org/10.1111/j.1600-065X.1993.tb00652.x>.
- (3) Holt, D. W.; Johnston, A. Chapter 11 - Monitoring Immunosuppressive Drugs. In *Handbook of Analytical Separations*; Hempel, G., Ed.; Drug Monitoring and Clinical Chemistry; Elsevier Science B.V., 2004; Vol. 5, pp 273–296. [https://doi.org/10.1016/S1567-7192\(04\)80012-3](https://doi.org/10.1016/S1567-7192(04)80012-3).
- (4) Gaston, R. S. Chapter 18 - Mycophenolates. In *Kidney Transplantation—Principles and Practice (Seventh Edition)*; Morris, P. J., Knechtle, S. J., Eds.; W.B. Saunders: Philadelphia (PA), 2014; pp 250–266. <https://doi.org/10.1016/B978-1-4557-4096-3.00018-0>.
- (5) Naffouje, R.; Grover, P.; Yu, H.; Sendilnathan, A.; Wolfe, K.; Majd, N.; Smith, E. P.; Takeuchi, K.; Senda, T.; Kofuji, S.; Sasaki, A. T. Anti-Tumor Potential of IMP Dehydrogenase Inhibitors: A Century-Long Story. *Cancers* **2019**, *11*, 1346. <https://doi.org/10.3390/cancers11091346>.
- (6) van Gelder, T.; Hilbrands, L. B.; Vanrenterghem, Y.; Weimar, W.; de Fijter, J. W.; Squifflet, J. P.; Hené, R. J.; Verpooten, G. A.; Navarro, M. T.; Hale, M. D.; Nicholls, A. J. A Randomized Double-Blind, Multicenter Plasma Concentration Controlled Study of the Safety and Efficacy of Oral Mycophenolate Mofetil for the Prevention of Acute Rejection After Kidney Transplantation. *Transplantation* **1999**, *68*, 261–266.
- (7) Kaplan, B. Mycophenolic Acid Trough Level Monitoring in Solid Organ Transplant Recipients Treated with Mycophenolate Mofetil: Association with Clinical Outcome. *Curr. Med. Res. Op.* **2006**, *22*, 2355–2364. <https://doi.org/10.1185/030079906X148481>.
- (8) Nowak, I.; Shaw, L. M. Mycophenolic Acid Binding to Human Serum Albumin: Characterization and Relation to Pharmacodynamics. *Clin. Chem.* **1995**, *41*, 1011–1017. <https://doi.org/10.1093/clinchem/41.7.1011>.
- (9) Bentley, R. Mycophenolic Acid: A One Hundred Year Odyssey from Antibiotic to Immunosuppressant. *Chem. Rev.* **2000**, *100*, 3801–3826. <https://doi.org/10.1021/cr990097b>.
- (10) Renner, U. D.; Thiede, C.; Bornhäuser, M.; Ehninger, G.; Thiede, H.-M. Determination of Mycophenolic Acid and Mycophenolate Mofetil by High-Performance Liquid Chromatography Using Postcolumn Derivatization. *Anal. Chem.* **2001**, *73*, 41–46. <https://doi.org/10.1021/ac0006730>.
- (11) Bolon, M.; Jeanpierre, L.; El Barkil, M.; Chelbi, K.; Sauviat, M.; Bouliou, R. HPLC Determination of Mycophenolic Acid and Mycophenolic Acid Glucuronide in Human Plasma with Hybrid Material. *J. Pharm. Biomed. Anal.* **2004**, *36*, 649–651. <https://doi.org/10.1016/j.jpba.2004.07.034>.
- (12) Łuszczynska, P.; Pawiński, T.; Kunicki, P. K.; Sikorska, K.; Marszałek, R. Free Mycophenolic Acid Determination in Human Plasma Ultrafiltrate by a Validated Liquid Chromatography-Tandem Mass Spectrometry Method. *Biomed. Chromatogr.* **2017**, *31*. <https://doi.org/10.1002/bmc.3976>.
- (13) Gao, X.; Tsai, R. Y. L.; Ma, J.; Bhupal, P. K.; Liu, X.; Liang, D.; Xie, H. Determination and Validation of Mycophenolic Acid by a UPLC-MS/MS Method:

- Applications to Pharmacokinetics and Tongue Tissue Distribution Studies in Rats. *J. Chromatogr. B* **2020**, *1136*, 121930. <https://doi.org/10.1016/j.jchromb.2019.121930>.
- (14) AL, K.; IL, Y.; LN, S. Accurate Method of HPLC-Ms/Ms Determination of Mycophenolic Acid in Human Plasma. *J. Bioequivalence Bioavailab.* **2016**, *09*. <https://doi.org/10.4172/jbb.1000316>.
- (15) Gübitz, G.; Schmid, M. G. Immunoassay Techniques. Luminescence Immunoassays. In *Encyclopedia of Analytical Science (Second Edition)*; Worsfold, P., Townshend, A., Poole, C., Eds.; Elsevier: Oxford, 2005; pp 352–360. <https://doi.org/10.1016/B0-12-369397-7/00265-X>.
- (16) Rebollo, N.; Calvo, M. V.; Martín-Suárez, A.; Domínguez-Gil, A. Modification of the EMIT Immunoassay for the Measurement of Unbound Mycophenolic Acid in Plasma. *Clin. Biochem.* **2011**, *44*, 260–263. <https://doi.org/10.1016/j.clinbiochem.2010.09.025>.
- (17) Dasgupta, A.; Tso, G.; Chow, L. Comparison of Mycophenolic Acid Concentrations Determined by a New PETINIA Assay on the Dimension EXL Analyzer and a HPLC-UV Method. *Clin. Biochem.* **2013**, *46*, 685–687. <https://doi.org/10.1016/j.clinbiochem.2012.11.025>.
- (18) Prémaud, A.; Rousseau, A.; Picard, N.; Marquet, P. Determination of Mycophenolic Acid Plasma Levels in Renal Transplant Recipients Co-Administered Sirolimus: Comparison of an Enzyme Multiplied Immunoassay Technique (EMIT) and Liquid Chromatography-Tandem Mass Spectrometry. *Ther. Drug Monit.* **2006**, *28*, 274–277. <https://doi.org/10.1097/01.ftd.0000197092.84935.ef>.
- (19) Glahn-Martínez, B.; Benito-Peña, E.; Salis, F.; Descalzo, A. B.; Orellana, G.; Moreno-Bondi, M. C. Sensitive Rapid Fluorescence Polarization Immunoassay for Free Mycophenolic Acid Determination in Human Serum and Plasma. *Anal. Chem.* **2018**, *90*, 5459–5465. <https://doi.org/10.1021/acs.analchem.8b00780>.
- (20) Ângela Taipa, M. Affinity separation. Rational Design, Synthesis, and Evaluation: Affinity Ligands. In *Reference Module in Chemistry, Molecular Sciences and Chemical Engineering*; Elsevier, 2014. <https://doi.org/10.1016/B978-0-12-409547-2.10738-3>.
- (21) Peltomaa, R.; Benito-Peña, E.; Barderas, R.; Moreno-Bondi, M. C. Phage Display in the Quest for New Selective Recognition Elements for Biosensors. *ACS Omega* **2019**, *4*, 11569–11580. <https://doi.org/10.1021/acsomega.9b01206>.
- (22) Zhao, F.; Shi, R.; Liu, R.; Tian, Y.; Yang, Z. Application of Phage-Display Developed Antibody and Antigen Substitutes in Immunoassays for Small Molecule Contaminants Analysis: A Mini-Review. *Food Chem.* **2021**, *339*, 128084. <https://doi.org/10.1016/j.foodchem.2020.128084>.
- (23) Hua, X.; Zhou, L.; Feng, L.; Ding, Y.; Shi, H.; Wang, L.; Gee, S. J.; Hammock, B. D.; Wang, M. Competitive and Noncompetitive Phage Immunoassays for the Determination of Benzothiostrubin. *Anal. Chim. Acta* **2015**, *890*, 150–156. <https://doi.org/10.1016/j.aca.2015.07.056>.
- (24) Liu, Z.; Liu, J.; Wang, K.; Li, W.; Shelver, W. L.; Li, Q. X.; Li, J.; Xu, T. Selection of Phage-Displayed Peptides for the Detection of Imidacloprid in Water and Soil. *Anal. Biochem.* **2015**, *485*, 28–33. <https://doi.org/10.1016/j.ab.2015.05.014>.
- (25) Woo, M.-K.; Heo, C.-K.; Hwang, H.-M.; Ko, J.-H.; Yoo, H.-S.; Cho, E.-W. Optimization of Phage-Immobilized ELISA for Autoantibody Profiling in Human Sera. *Biotechnol. Lett.* **2011**, *7*.
- (26) Dong, J.-X.; Xu, C.; Wang, H.; Xiao, Z.-L.; Gee, S. J.; Li, Z.-F.; Wang, F.; Wu, W.-J.; Shen, Y.-D.; Yang, J.-Y.; Sun, Y.-M.; Hammock, B. D. Enhanced Sensitive Immunoassay: Noncompetitive Phage Anti- Immune Complex Assay for the Determination of Malachite Green and Leucomalachite Green. *J. Agric. Food Chem.* **2014**, *7*.

- (27) Kim, H.-J.; Ahn, K. C.; González-Techera, A.; González-Sapienza, G. G.; Gee, S. J.; Hammock, B. D. Magnetic Bead-Based Phage Anti-Immuno-complex Assay (PHAIA) for the Detection of the Urinary Biomarker 3-Phenoxybenzoic Acid to Assess Human Exposure to Pyrethroid Insecticides. *Anal. Biochem.* **2009**, *8*.
- (28) Peltomaa, R.; Agudo-Maestro, I.; Más, V.; Barderas, R.; Benito-Peña, E.; Moreno-Bondi, M. C. Development and Comparison of Mimotope-Based Immunoassays for the Analysis of Fumonisin B1. *Anal. Bioanal. Chem.* **2019**, *411*, 6801–6811. <https://doi.org/10.1007/s00216-019-02068-7>.
- (29) Zou, X.; Chen, C.; Huang, X.; Chen, X.; Wang, L.; Xiong, Y. Phage-Free Peptide ELISA for Ochratoxin A Detection Based on Biotinylated Mimotope as a Competing Antigen. *Talanta* **2016**, *146*, 394–400. <https://doi.org/10.1016/j.talanta.2015.08.049>.
- (30) Wouters, S. F. A.; Vugs, W. J. P.; Arts, R. Bioluminescent Antibodies through Photoconjugation of Protein G–Luciferase Fusion Proteins. *Bioconj. Chem.* **7**.
- (31) NanoLuc® Luciferase: One Enzyme, Endless Capabilities <https://www.promega.es/resources/technologies/nanoluc-luciferase-enzyme/> (accessed 2021 -01 -25).
- (32) Antti Tullila; Tarja Nevanen. Utilization of Multi-Immunization and Multiple Selection Strategies for Isolation of Hapten-Specific Antibodies from Recombinant Antibody Phage Display Libraries. *IJMS* **2017**, *18*, 1169. <https://doi.org/10.3390/ijms18061169>.
- (33) Hall, M. P.; Unch, J.; Binkowski, B. F.; Valley, M. P.; Butler, B. L.; Wood, M. G.; Otto, P.; Zimmerman, K.; Vidugiris, G.; Machleidt, T.; Robers, M. B.; Benink, H. A.; Eggers, C. T.; Slater, M. R.; Meisenheimer, P. L.; Klaubert, D. H.; Fan, F.; Encell, L. P.; Wood, K. V. Engineered Luciferase Reporter from a Deep Sea Shrimp Utilizing a Novel Imidazopyrazinone Substrate. *ACS Chem. Biol.* **2012**, *7*, 1848–1857. <https://doi.org/10.1021/cb3002478>.
- (34) QIAprep Miniprep Handbook - QIAGEN <https://www.qiagen.com/us/resources/resourcedetail?id=22df6325-9579-4aa0-819c-788f73d81a09&lang=en> (accessed 2021 -09 -30).
- (35) PD-10 desalting columns packed with Sephadex G-25 resin <https://www.cytivalifesciences.com/en/us/shop/chromatography/prepacked-columns/desalting-and-buffer-exchange/sephadex-g-25-in-pd-10-desalting-columns-p-05778> (accessed 2021 -10 -01).
- (36) SDS Gel Preparation Kit <https://www.sigmaaldrich.com/Deepweb/Assets/Sigmaaldrich/Product/Documents/594/971/08091dat> (Accessed 2021 - 10 - 01).
- (37) Masseyeff, R. F.; Albert, W. H. W. (Winfried H. W. ); Staines, N. *Methods Immunol. Anal.*; Weinheim, Germany : VCH Verlagsgesellschaft ; New York, NY (USA) : VCH Publishers, 1992.
- (38) Findlay, J. W. A.; Dillard, R. F. Appropriate Calibration Curve Fitting in Ligand Binding Assays. *AAPS J* **2007**, *9*, E260–E267. <https://doi.org/10.1208/aapsj0902029>.
- (39) Fukada, H.; Takahashi, K. Calorimetric Study of the Reduction of the Disulfide Bonds in Insulin. *J. Biochem.* **1980**, *87*, 1111–1117.
- (40) Opstelten, D. J.; de Groote, P.; Horzinek, M. C.; Vennema, H.; Rottier, P. J. Disulfide Bonds in Folding and Transport of Mouse Hepatitis Coronavirus Glycoproteins. *J. Virol.* **1993**, *67*, 7394–7401.
- (41) High Capacity Magne® Streptavidin Beads and Goat Anti-Human Biotinylated IgG <https://www.promega.es/products/protein-purification/antibody-purification/high-capacity-magne-streptavidin-beads-and-goat-anti-human-biotinylated-igg/> (accessed 2021 -10 -10).

## Bibliography

- (42) Bentley, R. Mycophenolic Acid: A One Hundred Year Odyssey from Antibiotic to Immunosuppressant. *Chem. Rev.* **2000**, *100*, 3801–3826. <https://doi.org/10.1021/cr990097b>.
- (43) Ting, L. S. L.; Partovi, N.; Levy, R. D.; Riggs, K. W.; Ensom, M. H. H. Pharmacokinetics of Mycophenolic Acid and Its Phenolic-Glucuronide and Acyl Glucuronide Metabolites in Stable Thoracic Transplant Recipients: *Ther. Drug Monit.* **2008**, *30*, 282–291. <https://doi.org/10.1097/FTD.0b013e318166eba0>.

## **5. PERFORMANCE OF TWO LUCIFERASE PROTEIN FUSIONS WITH A FUMONISIN MIMOPEPTIDE FOR THE ANALYSIS OF THE TOXIN IN WHEAT SAMPLES**

### **5.1. Introduction**

### **5.2. Objectives**

### **5.3. Experimental part**

#### 5.3.1. Reagents and solutions

#### 5.3.2. Analytical instrumentation and materials

#### 5.3.3. Experimental procedures

##### *5.3.3.1. Construction of the GLuc and NLuc fusion proteins*

##### *5.3.3.2. Expression and purification of the fusion proteins*

##### *5.3.3.3. Evaluation of the kinetics of A2-GLuc and A2-NLuc*

##### *5.3.3.4. Optimization of the assay conditions*

##### *5.3.3.5. Bioluminescent bead-based immunoassays for FB<sub>1</sub> analysis*

##### *5.3.3.6. Sample analysis and spiking of fumonisin in wheat samples*

##### *5.3.3.7. HPLC-MS/MS method*

### **5.4. Results and discussion**

#### 5.4.1. Construction of the protein fusions

#### 5.4.2. Bioluminescent characterization of the fusion proteins

#### 5.4.3. Immunoassay optimization

#### 5.4.4. Analytical characteristics of the bioluminescent assays

##### *5.4.4.1. Calibration*

##### *5.4.4.2. Cross-reactivity*

##### *5.4.4.3. Long term stability of the NanoLuc-mimopeptide fusion protein*

##### *5.4.4.4. Matrix effect*

#### 5.4.5. Sample analysis

### **5.5. Conclusions**

### **5.6. Bibliography**



## 5.1. Introduction

In **Chapter 4** of this thesis, we described the development a novel immunoassay for the determination of MPA in blood samples using a novel luciferase, NanoLuc, with remarkably successful results. As an alternative to bioluminescent enzymes, the use of fluorescent proteins is of utmost importance for a wide variety of optical applications, including the development of sensitive immunoassays or fluorescent imaging.<sup>1,2</sup> However, enzymes are a step further in terms of sensing applications, especially for food analysis.<sup>3-5</sup>

A wide range of reactions, such as colorimetric, fluorescent, or luminescent reactions are catalyzed by different enzymes. Their sensitivity depends on a great extent on several factors, such as temperature, pH, or ionic strength. Hence, it has been stated that once these conditions are optimized, a single enzyme molecule can even convert up to  $10^7$  substrate molecules per minute, achieving exceptional sensitivities in immunoassays and other applications.<sup>6</sup>

Luciferases have been previously introduced in this thesis as one of the most relevant type of enzymes applied in the last years for the sensitive detection of different targets. They catalyze reactions that lead to the emission of light, and have been applied to a great diversity of fields, such as drug screening, diagnostics and food analysis.<sup>7</sup> Besides the previously mentioned NanoLuc luciferase (NLuc), *Gaussia* luciferase (GLuc) is also an interesting alternative for these applications. The sizes of both enzymes are similar, 19 kDa for NLuc and 19.9 kDa for GLuc. These luciferases, considered among the brightest luciferases yet discovered, have already contributed to some fascinating applications reported in the literature, such as protein-protein interactions, monitoring of biological processes and bioluminescence resonance energy transfer (BRET) immunoassays.<sup>8-12</sup>

Food quality is a major concern that can affect the health of both humans and animals. As it has been described in the introduction of this thesis, mycotoxins are able to contaminate a vast variety of food and feed and pose a huge risk for human and animal health. This work was focused on the analysis of fumonisin B<sub>1</sub> (FB<sub>1</sub>) and fumonisin B<sub>2</sub> (FB<sub>2</sub>), which are mycotoxins produced by some *Fusarium* species, including *F. verticillioides* and *F. proliferatum*, commonly found in some cereals, such as, maize, wheat, and sorghum.<sup>13,14</sup> As it was mentioned in the introductory chapter of this thesis, fumonisins were first reported in 1988, and despite the fact that there are several metabolites in this group of mycotoxins, FB<sub>1</sub> is the most prominent one.<sup>15,16</sup> Some of the health risks associated to fumonisins are equine leukoencephalomalacia,<sup>17</sup> porcine pulmonary edema,<sup>18</sup> and nephrotoxicity, esophageal cancer and neural tube defects in humans.<sup>14,19,20</sup> Owing to these fatal health risks, several international authorities of utmost relevance in food safety such as the US Food and Drug Administration (FDA) and the European Commission have established maximum levels of fumonisins in a variety of foodstuff.<sup>21,22</sup> The list is most likely to increase in the near future, in order to include several foodstuff that have not been considered yet.

The determination of fumonisins has been traditionally carried out using chromatographic methods, and it has been applied to an extensive range of different matrixes.<sup>23-29</sup> As previously mentioned, chromatographic methods are of considerable robustness, however, they are expensive as well as time consuming. An alternative to traditional chromatographic methods are immunoassays, which have proven over the

last decades excellent reliability and high sensitivity in the analysis of mycotoxins, overcoming some of the limitations of chromatographic methods.<sup>30</sup>

One of the most powerful tools to avoid antigen conjugation as well as potential toxicity to the user are mimopeptides. As it has been described throughout this thesis, mimopeptides can compete for the binding sites of an antibody with the corresponding antigen.<sup>31</sup> As mentioned previously there is a broad variety of mimopeptides already discovered for the most ubiquitous mycotoxins, such as aflatoxins, ochratoxin A, deoxynivalenol, fumonisins and zearalenone, among others.<sup>32-38</sup> In this case, a previously reported mimopeptide for fumonisin B<sub>1</sub>, known as A2,<sup>39</sup> has been chosen for the development of a competition immunoassay using a fusion protein between this mimopeptide and aforementioned luciferases, GLuc and NLuc.

The main goal of this chapter was to conduct a thorough comparison of these two fascinating luciferases for the development of a bioluminescent immunoassay to detect fumonisin B<sub>1</sub> in wheat samples.



## 5.2. Objectives

The main objective of this chapter was to conduct a comparative study of the performance of two of the brightest luciferases currently known, GLuc and NLuc for the analysis of FB<sub>1</sub>. For this aim, both luciferases were expressed in combination with a fumonisin mimopeptide previously isolated by our group. Once the fusion proteins were expressed and purified, two immunoassays were developed for the determination of FB<sub>1</sub>.

The analytical characteristics of both immunoassays were compared, and the best fusion protein was chosen for the analysis of the mycotoxin in wheat samples. First, a spiked wheat extract was analyzed, followed by a reference material and finally a selection of naturally contaminated cereal samples. The results of the real sample analysis were validated with a chromatographic-based method. The objectives of this chapter are summarized below:

- Construction of two different fusion proteins using Gaussia luciferase and NanoLuc luciferase in combination with a fumonisin mimopeptide (A2-GLuc and A2-NLuc).
- Expression and purification of both fusion proteins.
- Development and optimization of two different immunoassays for the analysis of FB<sub>1</sub> in wheat samples.
- Analysis of spiked wheat samples, a wheat reference material and real wheat samples, and method validation by HPLC-MS/MS.

## 5.3. Experimental part

### 5.3.1. Reagents and solutions

#### Cell culture and molecular biology

- LB broth, Lennox (**Thermo Fisher Scientific**)
- Kanamycin (Kan) (**Sigma-Aldrich**)
- Ampicillin (Amp) (**Fluka**)
- LB Agar (**NZYtech**)
- NEB 5-alpha competent *E. coli* cells (**New England Biolabs**)
- BL21 competent *E. coli* cells (**New England Biolabs**)
- Shuffle Express Competent *E. coli* cells (**New England Biolabs**)
- Phusion Hot Start II DNA Polymerase (**Thermo Scientific**)
- PCR Nucleotide Mix (**Roche Diagnostics**)
- KOD Xtreme Hot Start Master Mix (**Sigma-Aldrich**)
- dNTPs (2 mM each) (**Novagen**)
- NEBuilder® HiFi DNA Assembly Master Mix (**New England Biolabs**)
- 5X Phusion HF Buffer (**Thermo Scientific**)
- Betaine (**Sigma Aldrich**)
- Factor Xa (**New England Biolabs**)
- Red Nucleic acid gel stain (**Thermo Fisher Scientific**)
- GelPilot Loading dye (**Qiagen**)
- GeneRuler 1 kb DNA Ladder (**Thermo Scientific**)
- PageRuler™ Prestained Protein Ladder, 10 to 180 kDa (**Thermo Scientific**)
- Bio-Rad Precision Plus Protein Dual Color Standard (**Bio-Rad**)
- ATG-42 plasmid DNA, containing the NanoLuc gene (**Promega**)
- pQE vector (**Qiagen**)
- pMAL-c5X expression vector
- NZY Bacterial Cell Lysis Buffer (**Nzytech**)
- Lysozyme (**Nzytech**)
- DNase I (**Nzytech**)
- Pierce™ Protease Inhibitor Mini Tablets, EDTA-Free (**Thermo Scientific**)
- Bovine serum albumin (**Nzytech**)

#### Antibodies

- Anti-fumonisin monoclonal antibody (**BioTez**)

#### Mycotoxins

- Fumonisin B<sub>1</sub> (FB<sub>1</sub>) (**Fermentek**)
- Fumonisin B<sub>2</sub> (FB<sub>2</sub>) (**Fermentek**)
- Zearalenone (ZEA) (**Sigma-Aldrich**)
- Ochratoxin A (OTA) (**Fermentek**)
- Deoxynivalenol (DON) (**Fermentek**)
- HT-2 toxin (HT-2) (**Fermentek**)
- T-2 toxin (T-2) (**Fermentek**)

### Chemical reagents

- Phosphate buffer saline (PBS) pH 7.4 (**Sigma-Aldrich**)
- Phosphate buffer saline (PBST) (**Sigma-Aldrich**)
- Sodium chloride (**Quimipur**)
- Potassium chloride (Sigma-Aldrich)
- Sodium hydroxide (**Scharlau**)
- Sodium phosphate monobasic monohydrate ( $\geq 98\%$ ) (**Sigma-Aldrich**)
- Sodium phosphate dibasic dehydrate (puriss. p.a.) (**Fluka**)
- Sodium Dodecyl Sulfate (SDS) (**Sigma**)
- Tris base (**Fisher Bioreagents**)
- Dimethyl sulfoxide ( $\geq 99.5\%$ ) (**Sigma-Aldrich**)
- Ethanol Absolute (**Scharlau**)
- Acetonitrile (**Fisher Chemical**)
- Acetic acid glacial (Carlo Erba)
- Formic acid (Scharlau)
- Isopropyl- $\beta$ -d-thiogalactopyranoside (IPTG) (**Sigma-Aldrich**)
- Tween 20 (T20) (**Sigma-Aldrich**)
- Blocker™ Casein (in PBS) (**Thermo Fisher Scientific**)
- Imidazole (**Alfa Aesar**)
- NanoGlo® Reagent for Immunoassay (**Promega**)
- Native coelenterazine (**NanoLight Technology**)
- Furimazine (**Aobious**)

### PCR Primers

- Primers for A2-GLuc:

Forward primer 1: 5'-GAT CCT TTT CGG GGT GGA GGT TCG ATG AAA CCG ACC-3' (**Integrated DNA technologies**)

Forward primer 2: 5'-GTT ACT CCG AAT GAT GAT ACG TTT GAT CCT TTT CGG-3' (**Integrated DNA technologies**)

Forward primer 3: 5'-GGT GGA GGT TCG CAT ATG GTT ACT CCG AAT-3' (**Integrated DNA technologies**)

Reverse primer 1: 5'-CTA ATG ATG ATG ATG ATG ATG ATC ACC ACC TGC-3' (**Integrated DNA technologies**)

Reverse primer 2: 5'-CGA ACC TCC ACC GGA TCC CTA ATG ATG ATG-3' (**Integrated DNA technologies**)

- Primers for A2-NLuc:

pQE-fwd: 5'-TCT GGC GGA AAA CCT GTA TTT TCA GGG C-3' (**Integrated DNA technologies**)

pQE-rv: 5'-GAG TGT GAA GAC CGA ACC TCC ACC CCG AA-3' (**Integrated DNA technologies**)

NLuc-fwd: 5'-AGG TTC GGT CTT CAC ACT CGA AGA TTT CG-3' (**Integrated DNA technologies**)

NLuc-rv: 5'-TAC AGG TTT TCC GCC AGA ATG CGT TCG CA-3' (**Integrated DNA technologies**)

### Other reagents

- Dynabeads Protein G (**Thermo Fisher Scientific**)
- HisTrap™ FF crude columns (**Cytiva**)
- Sephadex™ G-25 M columns (**Cytiva**)
- Illustra NAP-5 columns (**Cytiva**)
- Amylose resin (**New England Biolabs**)
- Blank wheat quality control material (**Romer Labs**)
- Wheat reference matrix material (**Aokin**)
- Contaminated wheat samples were provided by the group of Prof. Belén Patiño at the Department of Microbiology III of Complutense University of Madrid.

### Commercial kit

- QIAquick® PCR & Gel Cleanup Kit (**Qiagen**)
- QIAprep® Spin Miniprep Kit (**Qiagen**)

### Plates

**LB/Amp plates** (for 20 plates approximately): 16 g of LB agar were dissolved in 400 mL of MQ water after cooled at a temperature lower than 70 °C, 400 µL ampicillin were added. The solution was immediately poured into a plate, around 20-25 mL (almost cover all the plate) and left until the mixture solidified. Plates were stored at 4 °C in the dark.

**LB/Kan plates** (for 20 plates approximately): the same protocol was followed substituting ampicillin for kanamycin.

### Solutions and buffers:

**PBS 10×**: one pouch of PBS was dissolved in deionized water. The pH was adjusted to 7.4 for a final volume of 100 mL. The solution was sterilized by autoclaving and stored at room temperature.

**PBS 1×**: the solution was prepared by diluting 10 times in autoclaved water the PBS 10× solution. The final concentration was 0.01 mol L<sup>-1</sup> PBS, pH 7.4.

**Tween-20 solution 10% (v/v)**: 10 mL of Tween® 20 were diluted with 90 mL deionized water. The solution was sterilized by autoclaving and stored at room temperature.

**TAE 50× electrophoresis buffer (2 mol L<sup>-1</sup> Tris base, 1 mol L<sup>-1</sup> acetic acid, 1 mol L<sup>-1</sup> EDTA, pH 8.6)**: 242 g tris base, 18.61 g disodium EDTA and 59.95 g acetic acid were dissolved in 800 mL deionized water. Once dissolved, more deionized water was added for a total volume of 1 L. The pH was not adjusted. The solution was stored at room temperature.

**TAE 1× electrophoresis buffer**: the solution was prepared by diluting 50 times in deionized water the TAE 50× solution.

**SOC media**: 10 g tryptone, 2.5 g yeast extract, 0.25 g NaCl and 5 mL of a solution of 20 mmol L<sup>-1</sup> KCl were dissolved in 400 mL deionized water. The pH was adjusted to 7.4 for a total volume of 500 mL. The solution was autoclaved and then, 2.5 mL of 2 mol L<sup>-1</sup> MgCl<sub>2</sub> (previously autoclaved) and 10 mL of 1 mol L<sup>-1</sup> glucose were added. The solution was stored at 4 °C in the dark.

**Binding buffer (BB) (20 mmol L<sup>-1</sup> sodium phosphate buffer pH 7.4, 500 mmol L<sup>-1</sup> NaCl and 20 mmol L<sup>-1</sup> imidazole):** 0.55 g Na<sub>2</sub>HPO<sub>4</sub>, 0.16 g NaH<sub>2</sub>PO<sub>4</sub>, 7.31 g NaCl and 0.34 g imidazole were dissolved in 200 mL deionized water. The pH was adjusted to 7.4 for a total volume of 250 mL. The solution was stored at room temperature.

**Elution buffer (EB): (20 mmol L<sup>-1</sup> sodium phosphate buffer pH 7.4, 500 mmol L<sup>-1</sup> sodium chloride and 500 mmol L<sup>-1</sup> imidazole):** 0.14 g Na<sub>2</sub>HPO<sub>4</sub>, 0.04 g NaH<sub>2</sub>PO<sub>4</sub>, 1.83 g NaCl and 1.7 g imidazole were dissolved in 50 mL deionized water. The pH was adjusted to 7.4 for a total volume of 250 mL. The solution was stored at room temperature.

**Assay buffer (PBS supplemented with 0.05% T20 and 0.1% BSA, pH 7.4):** 50 µL of a solution of 10% T20 and 1.66 mL of a solution of 3% BSA in PBS were added to a final volume of 10 mL PBS 1×. The solution was stored at 4 °C in the dark.

**Washing buffer (137 mmol L<sup>-1</sup> NaCl, 2.7 mmol L<sup>-1</sup> KCl, 10 mmol L<sup>-1</sup> Na<sub>2</sub>HPO<sub>4</sub>, 1.8 mmol L<sup>-1</sup> KH<sub>2</sub>PO<sub>4</sub>, 0.05% T20, pH 7.4):** 8 g NaCl, 200 mg KCl, 1.44 g Na<sub>2</sub>HPO<sub>4</sub>, 240 mg KH<sub>2</sub>PO<sub>4</sub> and 500 µL T20 were dissolved in 900 mL deionized water. The pH was adjusted to 7.4 for a total volume of 1 L. The solution was stored at room temperature.

### 5.3.2. Analytical instrumentation and materials

- CLARIOstar microplate reader (**BMG Labtech**)
- Nanodrop 1000 spectrophotometer (**Thermo Scientific**)
- Analytical balance with 0.01 mg sensitivity (**Sartorius**)
- pH Meter GLP 21 (**Crison**)
- Eppendorf miniSpin (**Eppendorf**)
- Eppendorf centrifuge 5804 R (**Eppendorf**)
- Shaker incubator KS 4000 i control (**IKA**)
- Autoclave (**Selecta**)
- Thermostatic eppendorf shaker (**Thermo Scientific**)
- Vortex shaker (**Fisher brand**)
- PowerPac™ Basic power supply for gel electrophoresis (**Bio-Rad**)
- Thermocycler SureCycler 8800 (**Agilent Technologies**)
- Automatic plate washer hydro flex (**Tecan**)
- VibraCell Ultrasonic Processor 130 W 20 kHz, Ampl 70% (**Sonics & Materials**).
- High performance liquid chromatography instrument Agilent 1200 (**Agilent technologies**)
- Triple Quadrupole Agilent G6410B (**Agilent technologies**)
- Analytical material of contrasted quality

### 5.3.3. Experimental procedures

#### 5.3.3.1. Construction of the GLuc and NLuc fusion proteins

On one hand, the expression of the A2 mimopeptide with the GLuc luciferase was conducted by amplifying the pColdI-GLuc vector,<sup>40</sup> using the KOD Xtreme Hot Start Master Mix. For this purpose, three sequential PCR reactions were necessary to incorporate both the mimopeptide A2 and a GS-linker on the 5'-end of the luciferase and a polyhistidine tag on the 3'-end. The primers used for these sequential PCR reactions

are shown on **Table 18**. The culminating PCR product was subcloned at the NdeI and BamHI sites of the pMAL-c5X expression vector.

On the other hand, the fusion protein that consisted of the NLuc luciferase and A2 mimopeptide was constructed by amplifying the NLuc gene from the ATG-42 commercial vector,<sup>41</sup> with the help of the Phusion Hot Start II DNA Polymerase. In this case, the sequence encoding for the mimopeptide was also introduced in the 5'-end of the NLuc, from a pQE vector that already contained this sequence, and the polyhistidine tag was included in the 3'-end with the corresponding primers from **Table 18**. To complete the assembly in this case, the vector containing the mimopeptide and the NanoLuc insert were incubated at +50 °C for 15 min with the NEBuilder Master Mix. Also, a transformation of NEB 5-alpha competent *E. coli* cells was performed in a similar way as described on **Section 4.3.3.4.** of **Chapter 4** of this thesis.

**Table 18.** Sequence of the PCR primers used for the construction of the two fusion proteins. The overlapping region with the template plasmid for each case is underlined. The FB<sub>1</sub> mimopeptide sequence appears in bold.

GLuc	
Primer	Sequence
Forward 1	<b>GATCCTTTTCGGGGTGGAGGTT</b> <u>CGATGAAACCGACC</u>
Forward 2	<b>GTTACTCCGAATGATGATACGTTTGATCCTTTTCGG</b>
Forward 3	<b>GGTGGAGGTTGCATATGGT</b> <b>ACTCCGAAT</b>
Reverse 1	CTAATGATGATGATGATGATGAT <u>GATCACCACCTGC</u>
Reverse 2	CGAACCTCCACCGGATCCCTAATGATGATG
NLuc	
pQE-fwd	TCTGGCGGAAAACCTGTATTTTCAGGGC
pQE-rv	GAGTGTAAGACCCGAACCTCCACCCCGAA
NLuc-fwd	AGGTTCCGGTCTTCACACTCGAAGATTTCG
NLuc-rv	TACAGGTTTTCCGCCAGAATGCGTTCGCA

### 5.3.3.2. Expression and purification of the fusion proteins

For the expression of the GLuc-tagged fumonisin mimopeptide (A2-GLuc), Shuffle NEB Express Competent cells were initially used to transform the A2-GLuc plasmid. A single colony harboring the plasmid was picked from an LB agar plate supplemented with 100 µg mL<sup>-1</sup> ampicillin for the inoculation of a 5 mL preculture of LB medium with 100 µg mL<sup>-1</sup>. The aforementioned preculture was previously grown at 37 °C and 250 rpm overnight. This preculture was then expanded the next day to a main culture, consisting of a solution of 180 mL solution of LB with 100 µg mL<sup>-1</sup> ampicillin, and was grown at 37 °C and 200 rpm until reaching an optical density at 600 nm (OD<sub>600</sub>) of 0.7. Then, the addition of a final concentration of 1 mmol L<sup>-1</sup> IPTG served as a way to induce the protein expression on the main culture. After the addition of IPTG, the culture was grown at 15 °C and 175 rpm for 4 h and then, the cells were collected by centrifugation at 5,000 g and 4 °C for 10 min. The cell pellet was subsequently resuspended in 10 mL lysis buffer, consisting of 50 mmol L<sup>-1</sup> Tris-HCl pH 8.7, 150 mmol L<sup>-1</sup> NaCl supplemented with a 5% (v/v) protease inhibitor cocktail. This suspension was frozen overnight at -80 °C, after which a sonication on ice during 10 min with 10 s on/off cycles produced the cell lysis. Once the mixture was centrifuged at 12,000 g and 4 °C for 20 min and the insoluble cell debris were discarded, the supernatant was filtered with a 0.45 µm

filter and purified with amylose resin. To do this, 1 mL of amylose resin was mixed with the clarified lysate and incubated under slow shaking for 30 min at room temperature. A Pierce Centrifuge Column was used to collect the resin, which was thoroughly washed with a total of 10 column volumes of lysis buffer. To proceed to the protein elution, the column was filled with the same lysis buffer, but in this case, it was supplemented with 10 mmol L<sup>-1</sup> maltose. The purified protein was stored at 4 °C for several weeks.

For the expression of the A2-NLuc fusion protein, the plasmid was initially transformed into BL21 *E. coli* competent cells. Similar to the previous case, a single colony was selected from agar plates, but in this case, they were supplemented with 50 µg mL<sup>-1</sup> kanamycin. The single colony was grown overnight at 30 °C on a preculture consisting of 15 mL LB broth with 50 µg mL<sup>-1</sup> kanamycin. Next, an aliquot of the preculture was introduced in a 200 mL LB culture supplemented with 50 µg mL<sup>-1</sup> kanamycin and the mixture was grown at 37 °C and 180 rpm until obtaining an OD<sub>600</sub> of 0.6. At that point, the protein expression was conducted for 4 h at 37 °C and 180 rpm after the addition of IPTG at a final concentration of 0.4 mmol L<sup>-1</sup>. The bacterial culture was subsequently centrifuged at 5000 g for 10 min at 4 °C and the cell pellet was resuspended in NZY Bacterial Cell Lysis containing DNase I, NZY Lysozyme and protease inhibitor cocktail according to the manufacturer's instructions. Then, the cells were sonicated on ice for 10 min with 10 s on/off cycles, following a centrifugation step at 15,000 g for 15 min and 4 °C. The purification of the cell lysate was conducted using HisTrap™ purification columns and Sephadex™ G-25 M columns in a similar way as previously described in **Section 4.3.3.5. of Chapter 4** of this thesis.

For both cases, the purity of both fusion proteins was confirmed by SDS-PAGE analysis, and the concentration of each protein was calculated by measuring the absorbance at 280 nm with a Nanodrop spectrophotometer.

### **5.3.3.3. Evaluation of the kinetics of A2-GLuc and A2-NLuc**

To test the kinetics of both fusion proteins, 50 µL of the same molar concentration of either A2-GLuc or A2-NLuc were added to the wells of a 96-well black plate. The bioluminescence was monitored on a CLARIOstar microplate reader after adding 50 µL of the corresponding substrates, native coelenterazine for GLuc and furimazine or NanoGLO™ for NLuc in PBS buffer.

### **5.3.3.4. Optimization of the assay conditions**

For the A2-GLuc, the evaluation of the optimal antibody and fusion protein concentrations was assessed by a checkerboard-type titration. On the other hand, the A2-NLuc concentration was first optimized, after which a checkerboard-type titration helped to optimize the concentration of both the antibody and magnetic beads on the immunoassay.

### **5.3.3.5. Bioluminescent bead-based immunoassays for FB<sub>1</sub> analysis**

To carry out the immunoassay with the A2-GLuc fusion protein, 200 µL casein were used to block black microtiter plates for 1 h at 37 °C, after which were rinsed twice with washing buffer. Then, a solution of 3 µg mL<sup>-1</sup> A2-GLuc and 1.66 µg mL<sup>-1</sup> of antibody was mixed with varying concentrations of free FB<sub>1</sub>, from 0 to 100 ng mL<sup>-1</sup>, in assay buffer, for a total volume of 60 µL. Once the mixture was incubated for 1 h at room temperature

and slow shaking, 40  $\mu\text{L}$  of a solution of protein G beads in assay buffer were subsequently added to the wells to obtain a final concentration of 0.1  $\text{mg mL}^{-1}$  of magnetic beads. The mixture was incubated for 30 min and then, the wells were rinsed again thrice with an automatic washer under a magnet support. Lastly, 50  $\mu\text{L}$  of a solution containing 2.0  $\mu\text{g mL}^{-1}$  coelenterazine in PBS was added to the wells and the bioluminescence was immediately measured on a CLARIOstar microplate reader.

With reference to the A2-NLuc fusion protein, the initial blocking step consisted of the addition of 200  $\mu\text{L}$  casein on black microtiter plates for 1 h at room temperature. Once the plate was washed thrice with washing buffer, a solution containing a concentration of 8.5  $\mu\text{g mL}^{-1}$  of A2-NLuc and 1.66  $\mu\text{g mL}^{-1}$  of antibody per well was mixed with varying concentrations of free FB<sub>1</sub>, from 0 to 2500  $\text{ng mL}^{-1}$  in assay buffer, for a total volume of 60  $\mu\text{L}$ . After an incubation step for 1 h at room temperature and slow shaking, 40  $\mu\text{L}$  of protein G beads at a concentration of 0.31  $\text{mg mL}^{-1}$  in assay buffer were added and incubated for another 30 min at room temperature and slow shaking. The wells were then washed three times with an automatic washer bearing a magnetic support and finally, the bioluminescence was measured after addition of 60  $\mu\text{L}$  of a solution of NanoGLO™ reagent to each well.

On both cases, for the cross-reactivity tests, the FB<sub>1</sub> concentration was replaced with other mycotoxins at ranging concentrations between 1 and 1000  $\text{ng mL}^{-1}$ .

#### **5.3.3.6. Sample analysis and spiking of fumonisin in wheat samples**

A previously described method reported by Krska et al.<sup>42</sup> was applied for the extraction of FB<sub>1</sub> from wheat samples, with slight modifications. Briefly, 5 mL of a mixture containing acetonitrile/water/acetic acid (79/20/1, v/v/v) were added to 1 g of wheat sample. The samples were incubated for 60 min at room temperature and gentle shaking. Then, the samples were centrifuged for 15 min at 15,000 g and the supernatant was filtered through a 0.22  $\mu\text{m}$  filter and diluted in assay buffer before the analysis.

For the analysis of spiked samples, wheat extracts were supplemented with varying concentrations of FB<sub>1</sub> before they were diluted for the analysis.

#### **5.3.3.7. HPLC-MS/MS method**

The HPLC-MS/MS validation was assessed at the Institute of Food Science, Technology and Nutrition (ICTAN, Madrid, Spain). All the measurements were performed in a high-performance chromatography instrument Agilent 1200, coupled to a Triple Quadrupole Agilent G6410B (Agilent technologies, Santa Clara, CA, USA) using a Poroshell 120 EC C18 (3  $\mu\text{m}$  x 150 mm x 2.7 mm) chromatographic column (Agilent Technologies). The separation was conducted under gradient conditions with the mobile phase consisting of two different solvents: an aqueous solution containing 0.1% formic acid (solvent A) and MeCN supplemented with 0.1% formic acid (solvent B). The separation was carried out at a flow rate of 0.3  $\text{mL min}^{-1}$  (0 min, 30% B; 15 min, 80% B; 17 min, 100% B; 20 min, 100% B; 25 min, 30% B; 30 min, 30% B) and the total injection volume was 5  $\mu\text{L}$ . The precursor ions were 722.4 m/z for FB<sub>1</sub> and 706.4 m/z for FB<sub>2</sub>. To identify and quantify FB<sub>1</sub>, the product ions utilized were 352.3 and 334.3 m/z, respectively, whereas for FB<sub>2</sub> these were 318.3 and 336.3 m/z, respectively.



## 5.4. Results and discussion

### 5.4.1. Construction of the protein fusions

The aforementioned luciferase enzymes GLuc and NLuc were expressed together with a previously characterized fumonisin B<sub>1</sub> mimopeptide, named A2, consisting of the sequence VTPNDDTFDPFR.<sup>39</sup> The enzymes served as a label for the immunoassay and therefore avoided any use of secondary antibodies, as well as tedious conjugations of the mycotoxin to a label or to a protein for immobilization purposes. The expression of both fusion proteins, A2-GLuc and A2-NLuc was carried out in different *E. coli* cells due to their different characteristics.

The A2-GLuc fusion protein was expressed on Shuffle cells since the GLuc luciferase contains disulfide bonds within its structure that ought to be formed in an oxidizing environment. Moreover, the expression of this fusion protein was conducted at 15 °C, because higher temperatures produced a vast protein aggregation and denaturation, obtaining unsatisfactory results. On the other hand, BL21 cells were employed for the expression of the A2-NLuc fusion protein, since this protein did not require the formation of any disulfide bond. On top of that, the expression was easily conducted at 37 °C for 4 h under gentle shaking.

After a purification step using the maltose binding protein (MBP) for the A2-GLuc and the histidine tag for the A2-NLuc, a confirmation of the expression of each fusion protein was performed by SDS-PAGE (Figure 65). The results prove that the theoretical values matched those obtained in the gels. Regarding the A2-GLuc, the theoretical molecular weight was 63,748 g mol<sup>-1</sup> due to the presence of the MBP. With respect to the A2-NLuc, the value was 22,982 g mol<sup>-1</sup> since the MBP was not required in this case.

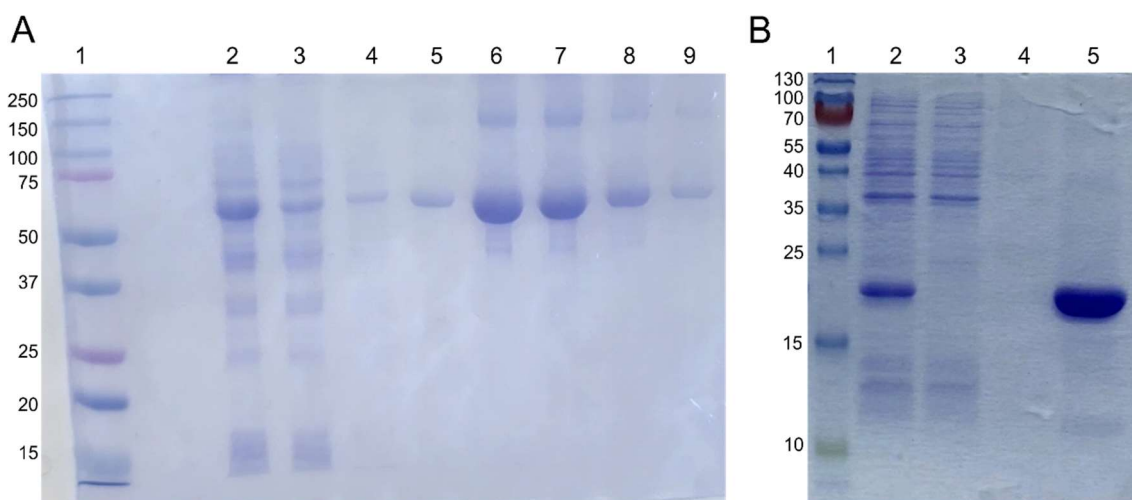


**Figure 65.** SDS-PAGE results obtained for the two fusion proteins. A. A2-GLuc fusion protein; Lane 1: protein ladder (Bio-Rad Precision Plus Protein Dual Color Standard); Lane 2: unpurified protein; Lane 3: flow through of the column; Lanes 4 to 9: elution fractions of the purified protein. B. A2-NLuc fusion protein; Lane 1: protein ladder (Thermo Scientific™ PageRuler™ Prestained Protein Ladder, 10 to 180 kDa); Lane 2: unpurified protein; Lane 3: flow through of the HisTrap™ column; Lane 4: washing solution collected; Lane 5: purified protein eluted from the column.

#### 5.4.2. Bioluminescent characterization of the fusion proteins

Once both fusion proteins were expressed and purified, the addition of the corresponding substrates confirmed their bioluminescent nature. For the A2-GLuc, coelenterazine in PBS was selected as the substrate, whereas furimazine or NanoGLO™ were used for A2-NLuc. The kinetics observed for both luciferases can be observed in **Figure 66**, and it is clearly appreciated there are substantial differences between them. First, the A2-GLuc shows an extremely fast kinetics (flash-type kinetics) after the addition of its substrate, coelenterazine in PBS. In this case, the bioluminescent signal is almost completely attenuated in less than one minute. However, the reaction kinetics experienced by the A2-NLuc are much slower. A similar drop in the signal was observed more than five minutes after the native substrate (furimazine in PBS) was added. On top of that, the NanoGLO™ reagent prolonged much more the bioluminescent signal of the fusion protein (glow-type kinetics) since the same signal decrease was observed, in this case, nearly 25 min after the addition of the substrate. The time increase appreciated in the bioluminescence signal could avoid potential mistakes in the analytical measurement, since a similar value is registered for a longer time than in any reaction following a flash-type kinetics. Therefore, a controlled injection of the substrate inside the microplate reader needed to be implemented for the A2-GLuc fusion protein to avoid any loss of the assay sensitivity and reproducibility. However, the addition of the NanoGLO substrate for the A2-NLuc was conducted outside the microplate reader.

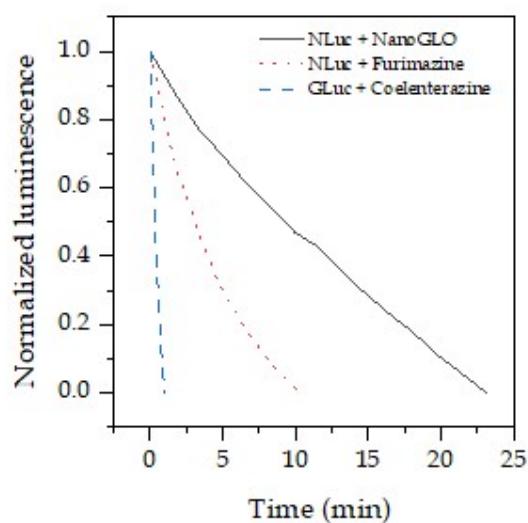


**Figure 66.** Kinetic curves obtained for A2-GLuc (blue dashed line), A2-NLuc with furimazine (red dotted line) and A2-NLuc with NanoGLO reagent (black straight line). In all cases, 50  $\mu$ L of each substrate (coelenterazine for A2-GLuc and furimazine or NanoGLO for A2-NLuc) were added to a solution of 50  $\mu$ L containing the same molar concentration of each of the fusion proteins. Different concentrations of the fusion proteins were assessed in the experiment, obtaining equivalent results in the signal drop for all of them. The graphs represent the normalized bioluminescence of three replicates.

### 5.4.3. Immunoassay optimization

The initial studies for immunoassay optimization were assessed for the A2-GLuc fusion protein. First, the ability of the fusion protein to act as a fumonisin mimopeptide was evaluated by incubating increasing concentrations of the fusion protein, between 0 and 6  $\mu\text{g mL}^{-1}$  with a constant concentration of the anti-fumonisin B<sup>1</sup> antibody ([Ab]= 1.66  $\mu\text{g mL}^{-1}$ ). In this experiment, two different assay formats were tested (**Figure 67**). On the one hand, the fumonisin monoclonal antibody was immobilized on 96-well plates and after a washing step, the mimopeptide was added to the well and incubated during 30 min. On the other hand, a competition between the antibody and the mimopeptide was established in solution and after the incubation, the antibody was collected with protein G-coated magnetic beads. In both cases, low non-specific binding was observed, but better signal-to-background ratios were obtained using the bead-based format. These results are in accordance to previously reported studies, in which the immunoassay sensitivity was improved when the antibody was immobilized on magnetic beads, instead of being coated directly onto the microtiter plate.<sup>43</sup> Therefore, the selected assay format was the one using protein G-functionalized magnetic beads to immobilize the antibody.

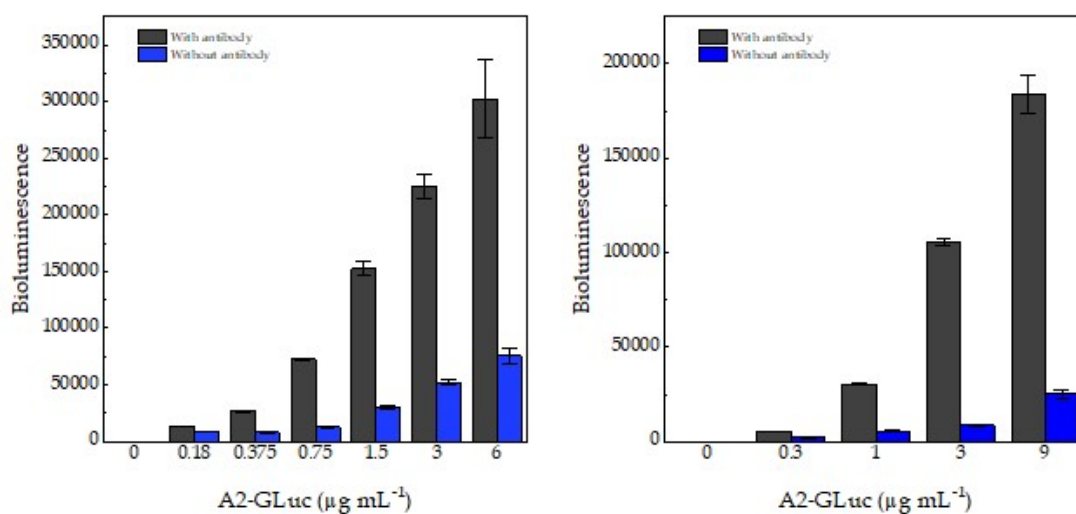


**Figure 67.** Evaluation of the ability of the A2-GLuc fusion protein to act as a mimopeptide on a plate-based (left) or bead-based (right) format. The mimopeptide signal in the presence of antibody (grey) was considerably higher than that in the absence (blue) of the antibody for all the different concentrations tested. The results are displayed as average bioluminescence signals  $\pm$  the standard error of the mean ( $n = 3$ ).

Once the recognition ability was confirmed, and the best assay format was chosen, the competition between the fusion protein and free FB<sub>1</sub> for the binding sites of the antibody was evaluated. In this case, 100 ng of the monoclonal anti-FB<sub>1</sub> antibody were mixed with different A2-GLuc concentrations (0.375–3  $\mu\text{g mL}^{-1}$ ) in the absence and presence of 10 ng mL<sup>-1</sup> free FB<sub>1</sub>. The results (**Figure 68**) prove the competition between the fusion protein and free FB<sub>1</sub> at very low concentration. The best two ratios observed (1.5  $\mu\text{g mL}^{-1}$  and 3  $\mu\text{g mL}^{-1}$ ) were consequently tested at different concentrations of the

mycotoxin (**Figure 68**), confirming that the best signal-to-background ratio was observed for a concentration of A2-GLuc of  $3 \mu\text{g mL}^{-1}$ .

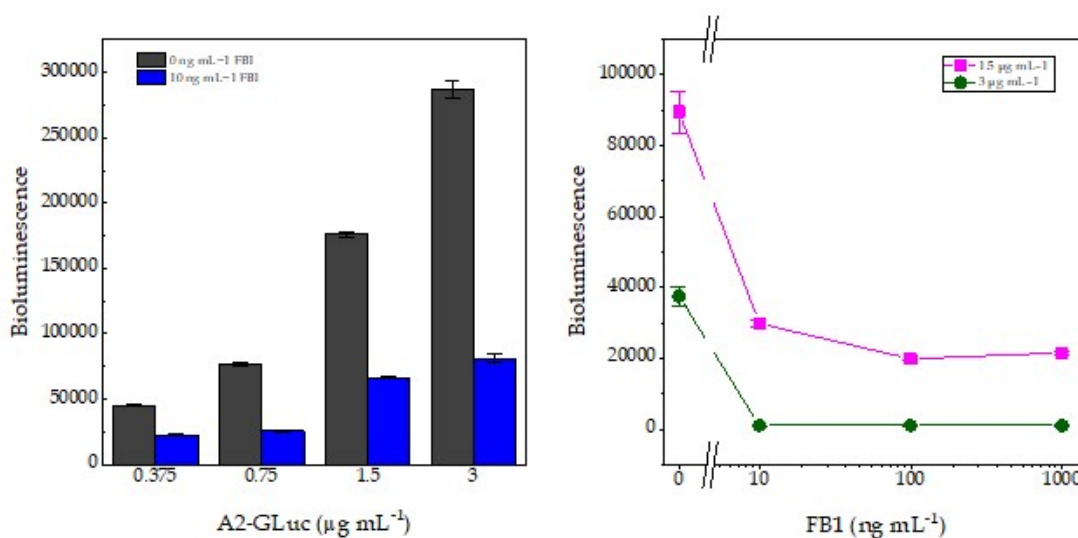


**Figure 68.** Competition evaluation in the bead-based format for A2-GLuc. Left. Preliminary experiments in the absence (grey) and presence (blue) of  $10 \text{ ng mL}^{-1}$  free FB<sub>1</sub> for different fusion protein concentrations. Right. Evaluation of the response of the two A2-GLuc concentrations with the best signal-to-background ratios,  $1.5 \mu\text{g mL}^{-1}$  (green) and  $3 \mu\text{g mL}^{-1}$  (magenta), for different FB<sub>1</sub> concentrations, between 0 and  $1000 \text{ ng mL}^{-1}$ . The results are presented as the average luminescence signals  $\pm$  the standard error of the mean ( $n = 3$ ).

A similar assay was conducted after the MBP was cleaved from the A2-GLuc fusion protein using the factor Xa protease. The lack of reliability of the results (**Figure 69**) was due to the low yield of the cleaved product. Therefore, all the forthcoming experiments were carried out without cleaving the MBP tag.

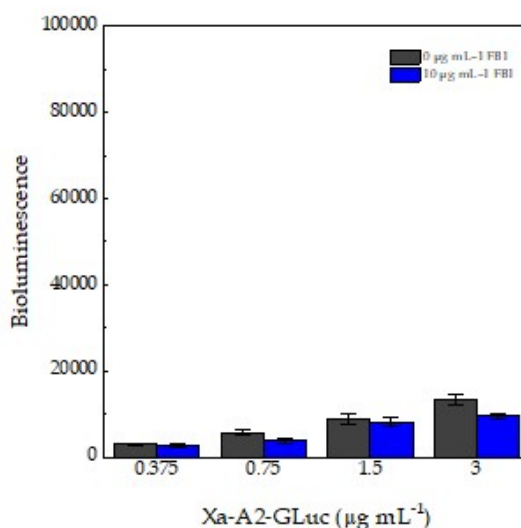


**Figure 69.** Assay response of factor Xa-cleaved A2-GLuc in the absence (grey) or presence (blue) of  $5 \text{ ng mL}^{-1}$  free FB<sub>1</sub> with different concentrations of the fusion protein ( $0.375\text{--}3 \mu\text{g mL}^{-1}$ ). Signal-

to-background ratios are represented in black squares, with the corresponding scale on the right y axis.

To conclude with the optimization of the A2-GLuc, a checkerboard titration was assessed with different monoclonal antibody and fusion protein concentrations, in the absence and presence of free FB<sub>1</sub>. In this experiment, the best ratio between the absence and presence of 10  $\mu\text{g mL}^{-1}$  free FB<sub>1</sub> was chosen for the subsequent immunoassay. As can be observed in **Figure 70** and **Table 19**, the best ratio was observed for 100 ng of antibody per well and 3  $\mu\text{g mL}^{-1}$  of the fusion protein.

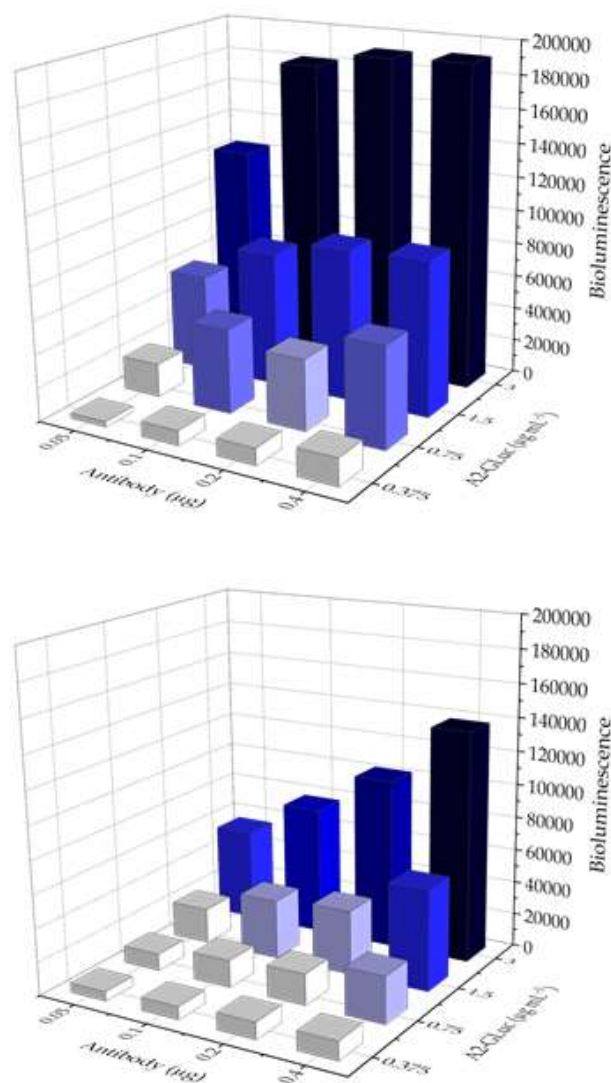


**Figure 70.** Checkerboard titration for the bead-based immunoassay using A2-GLuc. Different concentrations of the antibody (x-axis) and the fusion protein (z-axis) were tested in the absence

(up) and the presence (down) of  $10 \mu\text{g mL}^{-1}$  free FB<sub>1</sub>. The ratio between these two signals (C) was utilized to determine the optimal concentrations for the immunoassay (RSD<16.2%).

**Table 19.** Signal-to-noise ratios obtained in the checkerboard titration in the presence and the absence of free FB<sub>1</sub> for every fusion protein concentration and antibody amount assessed. The optimal combination selected is shown in bold red color (RSD<16.2%).

		Antibody			
		0.05 $\mu\text{g}$	0.1 $\mu\text{g}$	0.2 $\mu\text{g}$	0.4 $\mu\text{g}$
A2-GLuc	3.0 $\mu\text{g mL}^{-1}$	2.1	<b>2.3</b>	1.7	1.5
	1.5 $\mu\text{g mL}^{-1}$	2.0	1.9	1.8	1.2
	0.75 $\mu\text{g mL}^{-1}$	1.9	2.0	1.5	1.3
	0.375 $\mu\text{g mL}^{-1}$	1.7	1.7	1.3	1.2

After the immunoassay with the A2-GLuc fusion protein was optimized, the A2-NLuc was evaluated considering some of the results obtained previously. In this case, a bead-based assay was directly chosen for a better comparison between the two fusion proteins. However, two different assay formats were assessed. On the one hand, the same format as the A2-GLuc was tested, in which the competition was established in solution and then the antibody was captured with magnetic beads. On the other hand, the competition between the fusion protein and free FB<sub>1</sub> was carried out once the antibody was immobilized on magnetic beads. This alternative presented the inconvenience of two washing steps, in comparison with the previous approach that only required a single washing step. The results (**Figure 71**) showed that a better signal-to-background ratio was observed with the same assay format as described before. Therefore, the possibility of previously immobilizing the antibody onto magnetic beads was discarded.

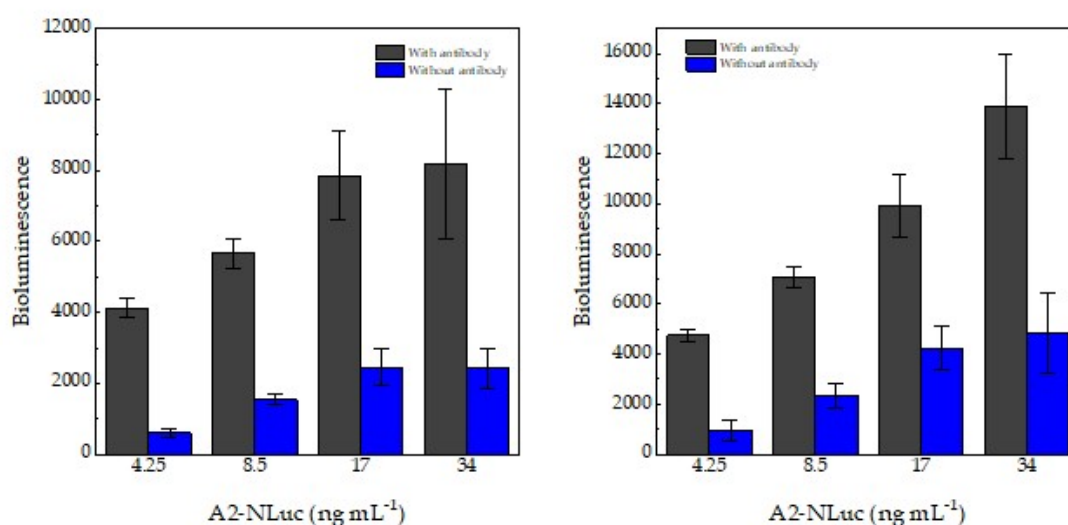


**Figure 71.** Assay comparison for the A2-NLuc fusion protein where the competition was established with the antibody in solution (left) or previously bound onto magnetic beads (right).

Signal-to-background ratios are presented in black squares, with the corresponding scale on the right y axis.

Based on the experimental trials, a concentration of the A2-NLuc almost 10 times higher than for the A2-GLuc fusion protein was required to achieve a similar analytical signal with both luciferases. One of the reasons might be due to the flash kinetics of the A2-GLuc, since all the reagent is consumed extremely fast. Another aspect to bear in mind is that for the A2-GLuc, the total luminescence was measured, whereas for the A2-NLuc it was only measured at  $470 \pm 40$  nm.

For the A2-NLuc, the fusion protein concentration was initially optimized based on the results from **Figure 71**, and a checkerboard titration was conducted for different antibody and magnetic bead concentrations, for a constant A2-NLuc concentration of  $8.5 \mu\text{g mL}^{-1}$ . The results (**Figure 72**, **Table 20**) demonstrate that the best signal-to-noise ratio was obtained for a total antibody amount of 100 ng per well, like the A2-GLuc assay, and a protein G-coated magnetic bead concentration of  $12.5 \mu\text{g mL}^{-1}$ .

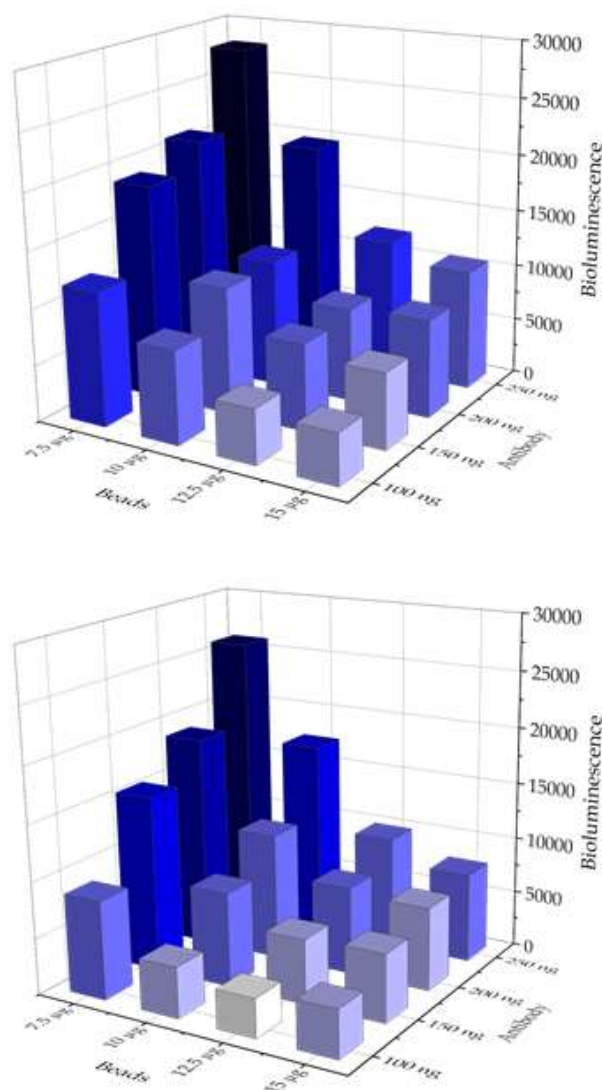


**Figure 72.** Checkerboard titration for the bead-based immunoassay using A2-NLuc. Different concentrations of magnetic beads (x-axis) and antibody (z-axis) were tested in the absence (up)

and the presence (down) of  $10 \mu\text{g mL}^{-1}$  free  $\text{FB}_1$ . The ratio between both signals (C) was utilized to determine the optimal concentrations for the immunoassay (RSD <14.4%).

**Table 20.** Signal-to-noise ratios obtained in the checkerboard titration in the presence and the absence of free  $\text{FB}_1$  for every antibody and bead amount assessed. The optimal combination selected is shown in bold red color. (RSD <14.4%)

		Beads			
		7.5 $\mu\text{g}$	10 $\mu\text{g}$	12.5 $\mu\text{g}$	15 $\mu\text{g}$
Antibody	250 $\mu\text{g}$	<b>1,34</b>	<b>1,23</b>	<b>1,14</b>	<b>1,08</b>
	200 $\mu\text{g}$	<b>1,18</b>	<b>1,07</b>	<b>1,01</b>	<b>1,12</b>
	150 $\mu\text{g}$	<b>1,12</b>	<b>1,34</b>	<b>1,34</b>	<b>1,22</b>
	100 $\mu\text{g}$	<b>1,06</b>	<b>1,41</b>	<b>1,84</b>	<b>1,36</b>

#### 5.4.4. Analytical characteristics of the bioluminescent immunoassays

After the optimization of the conditions were carried out, the two different immunoassays were conducted.

##### 5.4.4.1. Calibration

First, the calibration curves in the presence of varying concentrations of free  $\text{FB}_1$  for each of the developed immunoassays is shown on **Figure 73**. The calibration curves demonstrate the applicability of both fusion proteins for the analysis of  $\text{FB}_1$ , although each fusion protein presents a different behavior.

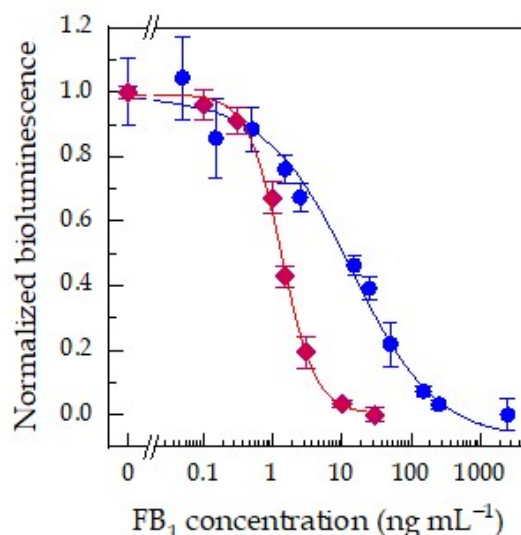


**Figure 73.** Calibration curves for the two bead-based bioluminescent immunoassays developed with either A2-GLuc (red diamonds) and A2-NLuc (blue circles) for the detection of  $\text{FB}_1$  in assay buffer. The competition between the fusion protein and free  $\text{FB}_1$  for the binding sites of the antibody was set in solution. After the corresponding incubation step, the antibody was collected with protein G-coated magnetic beads. The bioluminescence (total luminescence for A2-GLuc,  $\lambda_{\text{em}} = 470 \pm 40 \text{ nm}$  for A2-NLuc) was measured once the substrate was added to the wells. The values presented were normalized to the maximum and minimum values. The results are



displayed as the mean values  $\pm$  the standard error of the mean ( $n = 3$ ) and were adjusted to a logistic fit with OriginPro 2019 software.

A comparison of the analytical performance of both immunoassays reported is provided in **Table 21**. On the one hand, the A2-GLuc immunoassay provided a slightly lower limit of detection, taken as the 10% inhibition,<sup>44</sup> of 0.38 ng mL<sup>-1</sup>, compared to the value obtained for the A2-NLuc of 0.61 ng mL<sup>-1</sup>. The IC<sub>50</sub> for the A2-GLuc was of 1.34 ng mL<sup>-1</sup> and the one for the A2-NLuc resulted to be 13.5 ng mL<sup>-1</sup>. Nevertheless, when it comes to the dynamic range consideration, which was calculated as the 20 – 80% inhibition,<sup>45</sup> the A2-GLuc exhibited a much narrower value, between 0.6 ng mL<sup>-1</sup> and 2.9 ng mL<sup>-1</sup> whereas the A2-NLuc presented a value of almost two orders of magnitude, between 1.9 and 95.2 ng mL<sup>-1</sup>. In terms of reproducibility, relative standard deviations (RSD) of 7.4 % in average ( $n = 3$ ) for intra-day and 15.5 % for the inter-day determinations on 3 different days were observed for the A2-GLuc, and similar ones, 9.0% on intra-day and 15.9% on inter-day ( $n = 3$ ) for the A2-NLuc. One of the benefits that was achieved by introducing protein G-coated magnetic beads was the reduction of the number of washing steps compared to any plate-based method.

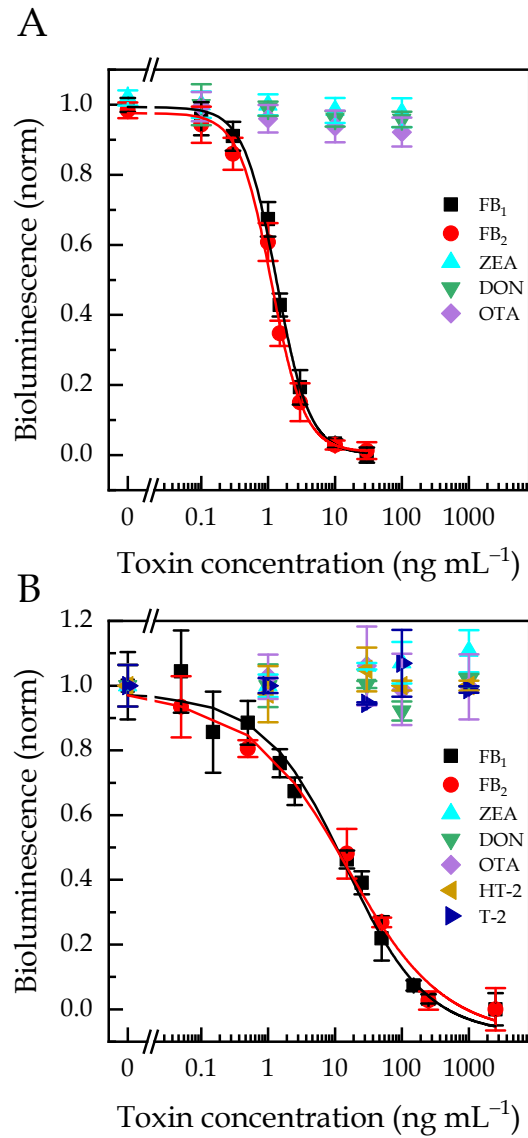
**Table 21.** Analytical characteristics of the two immunoassays described for FB<sub>1</sub>.

Fusion protein	IC <sub>50</sub> (ng mL <sup>-1</sup> )	LOD <sup>[a]</sup> (ng mL <sup>-1</sup> )	DR <sup>[b]</sup> (ng mL <sup>-1</sup> )
A2-GLuc	1.34	0.38	0.61 – 2.9
A2-NLuc	13.5	0.61	1.91 – 95.2

[a] Limit of Detection (taken as 10% inhibition); [b] Dynamic range (taken as 20–80% inhibition).

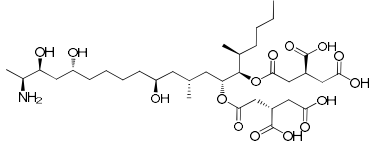
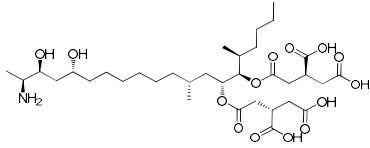
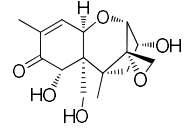
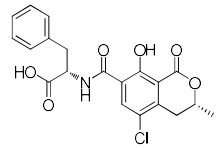
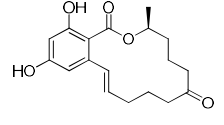
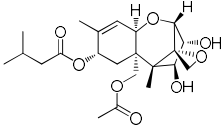
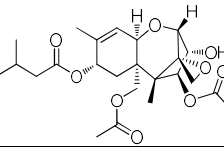
#### 5.4.4.2. Cross-reactivity

Several mycotoxins potentially present together with FB<sub>1</sub> in food samples were used to evaluate the specificity of both immunoassays for the determination of FB<sub>1</sub>. **Figure 74** shows the response curves obtained for each mycotoxin tested, and the results are displayed in **Table 22**. It can be observed that the only mycotoxin that cross reacts with the target analyte is FB<sub>2</sub>, as the remaining mycotoxins show negligible cross reactivity in the immunoassay up to concentration values of 1000 ng mL<sup>-1</sup>. However, the cross reactivity of FB<sub>2</sub> can be easily explained due to its structural similarities with FB<sub>1</sub>. Since it is expected to find both FB<sub>1</sub> and FB<sub>2</sub> together in most samples, it can be concluded that the developed assay would be implemented for the determination of the sum of both FB<sub>1</sub> and FB<sub>2</sub>.



**Figure 74.** Cross reactivity evaluation for the developed immunoassays using (A) A2-GLuc and (B) A2-NLuc. Under identical experimental conditions as the calibration curves, the most abundant mycotoxins that can potentially be found in combination with FB<sub>1</sub> were assessed. The bioluminescent signal values were normalized to the maximum and minimum values. The results are displayed as the average values ( $n = 3$ )  $\pm$  the standard error of the mean. The calibration curves were adjusted to a logistic fit using OriginPro 2019 software.

**Table 22.** Cross reactivity results for the bioluminescent immunoassays with the two fusion proteins, A2-GLuc and A2-NLuc.

Mycotoxin	Structure	A2-GLuc		A2-NLuc	
		IC <sub>50</sub>	CR <sup>[a]</sup>	IC <sub>50</sub>	CR <sup>[a]</sup>
Fumonisin B <sub>1</sub> (FB <sub>1</sub> )		1.34 ± 0.07		13.5 ± 1.7	
Fumonisin B <sub>2</sub> (FB <sub>2</sub> )		1.15 ± 0.05	116%	12.8 ± 2.0	105%
Deoxynivalenol (DON)		> 1000	< 0.1%	> 1000	< 1%
Ochratoxin A (OTA)		> 1000	< 0.1%	> 1000	< 1%
Zearalenone (ZEA)		> 1000	< 0.1%	> 1000	< 1%
HT-2 toxin (HT-2)		<i>n.d.</i>	<i>n.d.</i>	> 1000	< 1%
T-2 toxin (T-2)		<i>n.d.</i>	<i>n.d.</i>	> 1000	< 1%

[a] Cross reactivity

#### 5.4.4.3. Matrix effect

For the implementation of the developed immunoassays to the analysis of wheat samples, different wheat extract concentrations were used in the assay to evaluate the matrix effect. To do this, a certified non-contaminated wheat sample was used. A mixture of acetonitrile/water/acetic acid (79/20/1, v/v) was utilized to perform the extraction protocol. The results are shown in **Figure 75**. When the concentrations of the extract in the assay buffer were higher than 5% a matrix effect was observed in the calibration plots for both assays, probably due to the presence of acetonitrile in the extractand solution. Therefore, this value was selected for further analysis.

As can be observed, the immunoassay with both fusion proteins was similar in terms of cross reactivity and matrix effect. Therefore, owing to the wider dynamic range and similar limit of detection as the A2-GLuc, it was decided to continue with the A2-NLuc fusion protein for the real sample analysis. The LOD in wheat samples calculated for the analysis of FB<sub>1</sub> was 80 µg kg<sup>-1</sup>, whereas the LOQ was 276 µg kg<sup>-1</sup>.

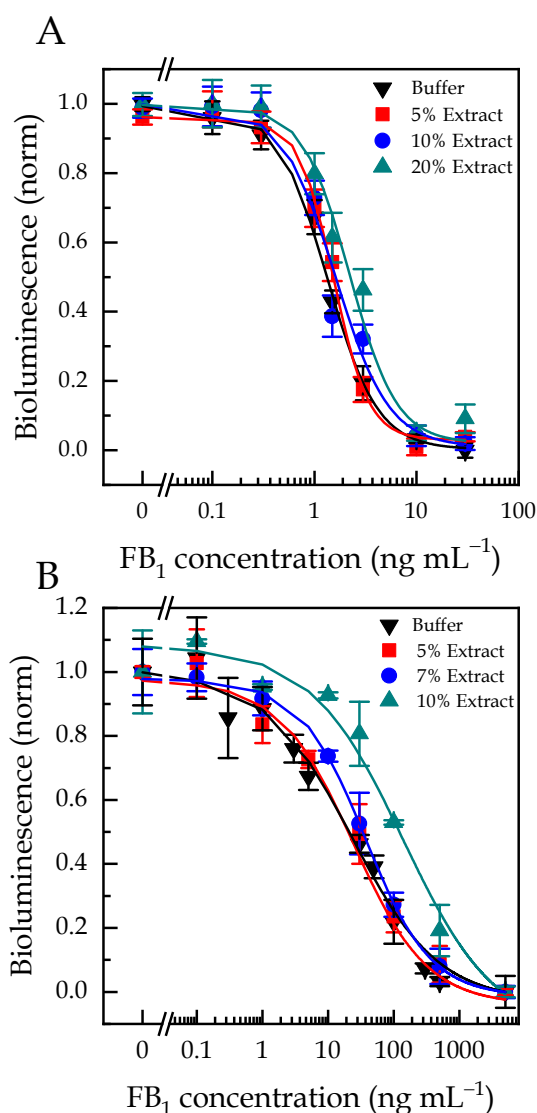


**Figure 75.** Calibration curves obtained for the evaluation of the matrix effect in the bioluminescent immunoassays with (A) A2-GLuc and (B) A2-NLuc. Under identical

experimental conditions as the calibration curves, the wheat extracts were diluted at different concentrations (extract concentration: 5%, 7%, 10%) in the assay buffer and the calibration curves are compared with that in buffer solution. The bioluminescence was normalized to the maximum and minimum signals. The results are presented as the mean bioluminescence  $\pm$  the standard error of the mean ( $n = 3$ ). The calibration curves were adjusted to a sigmoidal fit with OriginPro 2019 software.

#### 5.4.5. Sample analysis

The analysis of spiked wheat samples, a wheat reference material and naturally contaminated wheat samples was conducted with the bioluminescent immunoassay using the A2-NLuc fusion protein. Blank wheat extracts were initially spiked with varying concentrations of free FB<sub>1</sub>, between 200 and 1800 ng mL<sup>-1</sup> (corresponding to 1000 and 8000  $\mu$ g kg<sup>-1</sup>). After the corresponding dilution, all the spiked samples were analyzed, and the results can be observed in **Table 23**. The recoveries obtained were within the values accepted in the legislation, between 81% and 109%, for the different spiked samples, with the corresponding RSD between 3 and 14% ( $n = 3$ ).

**Table 23.** Analysis of spiked wheat samples with FB<sub>1</sub>.

Spiked (ng mL <sup>-1</sup> )	Measured (ng mL <sup>-1</sup> )	Recovery (%)	RSD <sup>[a]</sup> (%)
1600	1482	92.6	8.0
1200	1056	88.0	4.6
1000	815	81.5	9.8
400	430	107	14
200	217	109	3.2

[a] Relative Standard Deviation

The assay was applied to the analysis of a wheat reference material with an FB<sub>1</sub> certified value of  $86,431 \pm 25,900$   $\mu$ g kg<sup>-1</sup>, and the results confirmed that there were not significant differences with the optimized method  $(8 \pm 2) \times 10^4$   $\mu$ g kg<sup>-1</sup> ( $n = 3$ ), obtaining no significant differences at a 95% confidence level.

In parallel, the immunoassay was applied to the analysis of naturally contaminated wheat samples, following the same protocol described above. In this case, an HPLC-MS/MS reference method was used to validate the results of the immunoassay (**Table 24**). As can be observed, some of the analyzed wheat samples contained a very low concentration of FB<sub>1</sub> that could not be quantified by the immunoassay. Nevertheless, three wheat samples presented a higher mycotoxin concentration that could be analyzed with the immunoassay, yet the levels were below the regulatory limits for FB<sub>1</sub> in maize, since maximum levels have not been established in wheat yet.<sup>46</sup> Moreover, there were no significant differences at a 95% confidence level between the results obtained with the optimized method and those measured by HPLC-MS/MS, Therefore, we can

conclude that the developed immunoassay with the A2-NLuc fusion protein can be effectively applied to the analysis of contaminated wheat samples.

**Table 24.** Analysis of real samples and validation with HPLC-MS/MS reference method.

Sample	Fumonisin concentration (sd) <sup>[a]</sup> ( $\mu\text{g kg}^{-1}$ )	
	Immunoassay	HPLC-MS/MS
1	< LOD	< LOQ
2	< LOD	42.6 (1.4)
3	< LOQ	82.7 (1.3)
4	493 (32)	526 (36)
5	< LOD	< LOQ
6	409 (11)	402 (28)
7	< LOQ	291 (5.6)
8	1475 (53)	1512 (2.6)

[a] Standard Deviation

## 5.5. Conclusions

This chapter was focused on the development of novel competitive immunoassays based on protein fusions between a FB<sub>1</sub> mimopeptide and two different bioluminescent proteins: GLuc and NLuc. The correct expression and purification of both fusion proteins proved that they can be expressed in a cost-effective way and a fixed stoichiometry, contributing to the reduction of any possible batch-to-batch variations of chemical conjugation processes.

Both luciferases demonstrated different kinetics. On the one hand, the A2-GLuc fusion protein demonstrated a flash kinetics, consuming most of the reagent in less than one minute after its addition. On the other hand, the A2-NLuc proved a glow-type kinetics, which was especially notorious when the NanoGLO reagent was added instead of the bare substrate, furimazine. A glow-type kinetics supplies an extended luminescence time, reducing potential errors in the measurement of a flash kinetics.

A plate-based immunoassay demonstrated higher non-specific binding than a bead-based assay. Additionally, the competition in solution was a preferable option compared to the previous immobilization of the antibody onto magnetic beads owing to the better signal-to-background ratios observed.

Faster analysis can be fulfilled with a bead-based approach in comparison to the plate-based since the antibody does not require a previous immobilization on the plate and fewer washing steps are needed.

Both immunoassays proved excellent analytical features, with very low limits of detection. Nevertheless, the dynamic range observed for the A2-GLuc was substantially narrower than that of the A2-NLuc. The cross-reactivity results demonstrated a negligible interaction of other mycotoxins in the immunoassay, except for FB<sub>2</sub>. Therefore, the analysis can be used for the detection of these two fumonisins, FB<sub>1</sub> and FB<sub>2</sub>, instead of only FB<sub>1</sub>.

Owing to the fact that both fusion proteins showed a similar matrix effect, which was negligible at a 5% extract concentration, the analysis of wheat samples was conducted with the A2-NLuc for presenting a wider dynamic range and a similar limit of detection compared to the A2-GLuc fusion protein.

The analysis of the spiked wheat extracts, wheat reference material and naturally contaminated wheat samples proved that the developed immunoassay is an effective tool for the fast and sensitive analysis of FB<sub>1</sub> in wheat samples.

## 5.6. Bibliography

- (1) Sharma, A.; Gautam, S.; Bandyopadhyay, N. Enzyme Immunoassays: Overview. In *Encyclopedia of Food Microbiology (Second Edition)*; Batt, C. A., Tortorello, M. L., Eds.; Academic Press: Oxford, 2014; pp 680–687. <https://doi.org/10.1016/B978-0-12-384730-0.00099-9>.
- (2) Chudakov, D. M.; Matz, M. V.; Lukyanov, S.; Lukyanov, K. A. Fluorescent Proteins and Their Applications in Imaging Living Cells and Tissues. *Physiol. Rev.* **2010**, *90*, 1103–1163. <https://doi.org/10.1152/physrev.00038.2009>.
- (3) Sharma, A. ENZYME IMMUNOASSAYS: OVERVIEW. In *Encyclopedia of Food Microbiology*; Robinson, R. K., Ed.; Elsevier: Oxford, 1999; pp 625–633. <https://doi.org/10.1006/rwfm.1999.4500>.
- (4) Stepanenko, O. V.; Stepanenko, O. V.; Shcherbakova, D. M.; Kuznetsova, I. M.; Turoverov, K. K.; Verkhusha, V. V. Modern Fluorescent Proteins: From Chromophore Formation to Novel Intracellular Applications. *Biotechniques* **2011**, *51*, 313–314, 316, 318 passim. <https://doi.org/10.2144/000113765>.
- (5) Sakamoto, S.; Shoyama, Y.; Tanaka, H.; Morimoto, S. Application of Green Fluorescent Protein in Immunoassays. *Adv. Biosci. Biotechnol.* **2014**, *5*, 557–563. <https://doi.org/10.4236/abb.2014.56065>.
- (6) *The Immunoassay Handbook: Theory and Applications of Ligand Binding, ELISA, and Related Techniques*, 4th ed.; Wild, D., Ed.; Elsevier: Oxford ; Waltham, MA, 2013.
- (7) Fleiss, A.; Sarkisyan, K. S. A Brief Review of Bioluminescent Systems (2019). *Curr. Genet.* **2019**, *65*, 877–882. <https://doi.org/10.1007/s00294-019-00951-5>.
- (8) Rathnayaka, T.; Tawa, M.; Sohya, S.; Yohda, M.; Kuroda, Y. Biophysical Characterization of Highly Active Recombinant Gaussia Luciferase Expressed in Escherichia Coli. *BBA Proteins and Proteomics* **2010**, *1804*, 1902–1907. <https://doi.org/10.1016/j.bbapap.2010.04.014>.
- (9) Wu, N.; Rathnayaka, T.; Kuroda, Y. Bacterial Expression and Re-Engineering of Gaussia Princeps Luciferase and Its Use as a Reporter Protein. *BBA Proteins and Proteomics.* **2015**, *1854*, 1392–1399. <https://doi.org/10.1016/j.bbapap.2015.05.008>.
- (10) Song, G.; Wu, Q.-P.; Xu, T.; Liu, Y.-L.; Xu, Z.-G.; Zhang, S.-F.; Guo, Z.-Y. Quick Preparation of Nanoluciferase-Based Tracers for Novel Bioluminescent Receptor-Binding Assays of Protein Hormones: Using Erythropoietin as a Model. *J. Photochem. Photobiol. B* **2015**, *153*, 311–316. <https://doi.org/10.1016/j.jphotobiol.2015.10.014>.
- (11) England, C. G.; Ehlerding, E. B.; Cai, W. NanoLuc: A Small Luciferase Is Brightening Up the Field of Bioluminescence. *Bioconjugate Chem.* **2016**, *27*, 1175–1187. <https://doi.org/10.1021/acs.bioconjchem.6b00112>.
- (12) Tannous, B. A. Gaussia Luciferase Reporter Assay for Monitoring of Biological Processes in Culture and in Vivo. *Nat. Protoc.* **2009**, *4*, 582–591. <https://doi.org/10.1038/nprot.2009.28>.
- (13) Goyal, S.; Ramawat, K. G.; Mérillon, J.-M. Different Shades of Fungal Metabolites: An Overview. In *Fungal Metabolites*; Mérillon, J.-M., Ramawat, K. G., Eds.; Reference Series in Phytochemistry; Springer International Publishing: Cham, 2017; pp 1–29. [https://doi.org/10.1007/978-3-319-25001-4\\_34](https://doi.org/10.1007/978-3-319-25001-4_34).
- (14) Kamle, M.; Mahato, D. K.; Devi, S.; Lee, K. E.; Kang, S. G.; Kumar, P. Fumonisin: Impact on Agriculture, Food, and Human Health and Their Management Strategies. *Toxins (Basel)* **2019**, *11*, 328. <https://doi.org/10.3390/toxins11060328>.
- (15) Gelderblom, W. C.; Jaskiewicz, K.; Marasas, W. F.; Thiel, P. G.; Horak, R. M.; Vlegaar, R.; Kriek, N. P. Fumonisin--Novel Mycotoxins with Cancer-Promoting Activity Produced by Fusarium Moniliforme. *Appl. Environ. Microbiol.* **1988**, *54*, 1806–1811.



- (16) Bezuidenhout, S. C.; Gelderblom, W. C. A.; Gorst-Allman, C. P.; Horak, R. M.; Marasas, W. F. O.; Spiteller, G.; Vlegaar, R. Structure Elucidation of the Fumonisin, Mycotoxins from *Fusarium Moniliforme*. *J. Chem. Soc., Chem. Commun.* **1988**, No. 11, 743–745. <https://doi.org/10.1039/C39880000743>.
- (17) Feijó Corrêa, J. A.; Orso, P. B.; Bordin, K.; Hara, R. V.; Luciano, F. B. Toxicological Effects of Fumonisin B1 in Combination with Other *Fusarium* Toxins. *Food and Chem. Toxicol.* **2018**, *121*, 483–494. <https://doi.org/10.1016/j.fct.2018.09.043>.
- (18) Domijan, A.-M. Fumonisin B: A Neurotoxic Mycotoxin / Fumonizin B: Neurotoksični Mikotoksin. *Arh. Hyg. Rada. Toksikol.* **2012**, *63*, 531–544. <https://doi.org/10.2478/10004-1254-63-2012-2239>.
- (19) Alizadeh, A. M.; Roshandel, G.; Roudbarmohammadi, S.; Roudbary, M.; Sohanaki, H.; Ghiasian, S. A.; Taherkhani, A.; Semnani, S.; Aghasi, M. Fumonisin B1 Contamination of Cereals and Risk of Esophageal Cancer in a High Risk Area in Northeastern Iran. *Asian Pac. J. Cancer Prev.* **2012**, *13*, 2625–2628. <https://doi.org/10.7314/APJCP.2012.13.6.2625>.
- (20) Chu, F. S.; Li, G. Y. Simultaneous Occurrence of Fumonisin B1 and Other Mycotoxins in Moldy Corn Collected from the People's Republic of China in Regions with High Incidences of Esophageal Cancer. *Appl. Environ. Microbiol.* **1994**, *60*, 847–852. <https://doi.org/10.1128/aem.60.3.847-852.1994>.
- (21) EUR-Lex - 02006R1881-20210919 - EN - EUR-Lex <https://eur-lex.europa.eu/legal-content/EN/TXT/?uri=CELEX%3A02006R1881-20210919> (accessed 2021 -11 -30).
- (22) Nutrition, C. for F. S. and A. Guidance for Industry: Fumonisin Levels in Human Foods and Animal Feeds <https://www.fda.gov/regulatory-information/search-fda-guidance-documents/guidance-industry-fumonisin-levels-human-foods-and-animal-feeds> (accessed 2021 -11 -30).
- (23) Kayode, O. F.; Sulyok, M.; Fapohunda, S. O.; Ezekiel, C. N.; Krska, R.; Oguntona, C. R. B. Mycotoxins and Fungal Metabolites in Groundnut- and Maize-Based Snacks from Nigeria. *Food Addit. Contam.* **2013**, *6*, 294–300. <https://doi.org/10.1080/19393210.2013.823626>.
- (24) De Girolamo, A.; Fauw, D. P.; Sizoo, E.; van Egmond, H.; Gambacorta, L.; Bouten, K.; Stroka, J.; Visconti, A.; Solfrizzo, M. Determination of Fumonisin B1 and B2 in Maize-Based Baby Food Products by HPLC with Fluorimetric Detection after Immunoaffinity Column Clean-Up. *World Mycotoxin J.* **2010**, *3*, 135–146. <https://doi.org/10.3920/WMJ2010.1213>.
- (25) Smith, L. L.; Francis, K. A.; Johnson, J. T.; Gaskill, C. L. Quantitation of Fumonisin B1 and B2 in Feed Using Fmoc Pre-Column Derivatization with HPLC and Fluorescence Detection. *Food Chem.* **2017**, *234*, 174–179. <https://doi.org/10.1016/j.foodchem.2017.04.142>.
- (26) Ma, L.; Xu, W.; He, X.; Huang, K.; Wang, Y.; Luo, Y. Determination of Fumonisin B<sub>1</sub> and B<sub>2</sub> in Chinese Rice Wine by HPLC Using AQC Precolumn Derivatization. *J Sci Food Agric* **2013**, *93*, 1128–1133. <https://doi.org/10.1002/jsfa.5862>.
- (27) Dohnal, V.; Jezková, A.; Polisenská, I.; Kuca, K. Determination of Fumonisin in Milled Corn Grains Using HPLC-MS. *J- Chromatogr. Sci.* **2010**, *48*, 680–684. <https://doi.org/10.1093/chromsci/48.8.680>.
- (28) Zhang, B.; Chen, X.; Han, S.-Y.; Li, M.; Ma, T.-Z.; Sheng, W.-J.; Zhu, X. Simultaneous Analysis of 20 Mycotoxins in Grapes and Wines from Hexi Corridor Region (China): Based on a QuEChERS-UHPLC-MS/MS Method. *Molecules* **2018**, *23*, 1926. <https://doi.org/10.3390/molecules23081926>.
- (29) Pradanas-González, F.; Álvarez-Rivera, G.; Benito-Peña, E.; Navarro-Villoslada, F.; Cifuentes, A.; Herrero, M.; Moreno-Bondi, M. C. Mycotoxin Extraction from Edible

- Insects with Natural Deep Eutectic Solvents: A Green Alternative to Conventional Methods. *J. Chromatogr. A.* **2021**, *1648*, 462180. <https://doi.org/10.1016/j.chroma.2021.462180>.
- (30) Zheng, M. Z.; Richard, J. L.; Binder, J. A Review of Rapid Methods for the Analysis of Mycotoxins. *Mycopathologia* **2006**, *161*, 261–273. <https://doi.org/10.1007/s11046-006-0215-6>.
- (31) Zhao, F.; Shi, R.; Liu, R.; Tian, Y.; Yang, Z. Application of Phage-Display Developed Antibody and Antigen Substitutes in Immunoassays for Small Molecule Contaminants Analysis: A Mini-Review. *Food Chem.* **2021**, *339*, 128084. <https://doi.org/10.1016/j.foodchem.2020.128084>.
- (32) Sun, W.; Zhang, Y.; Ju, Z. Mimotopes for Mycotoxins Diagnosis Based on Random Peptides or Recombinant Antibodies from Phage Library. *Molecules* **2021**, *26*, 7652. <https://doi.org/10.3390/molecules26247652>.
- (33) Peltomaa, R.; Benito-Peña, E.; Barderas, R.; Moreno-Bondi, M. C. Phage Display in the Quest for New Selective Recognition Elements for Biosensors. *ACS Omega* **2019**, *4*, 11569–11580. <https://doi.org/10.1021/acsomega.9b01206>.
- (34) Wang, Y.; Wang, H.; Li, P.; Zhang, Q.; Kim, H. J.; Gee, S. J.; Hammock, B. D. Phage-Displayed Peptides That Mimic Aflatoxins and Its Application in Immunoassay. *J. Agric. Food Chem.* **2013**, *61*, 2426–2433. <https://doi.org/10.1021/jf4004048>.
- (35) Zou, X.; Chen, C.; Huang, X.; Chen, X.; Wang, L.; Xiong, Y. Phage-Free Peptide ELISA for Ochratoxin A Detection Based on Biotinylated Mimotope as a Competing Antigen. *Talanta* **2016**, *146*, 394–400. <https://doi.org/10.1016/j.talanta.2015.08.049>.
- (36) Yuan, Q.; Pestka, J. J.; Hespeneheide, B. M.; Kuhn, L. A.; Linz, J. E.; Hart, L. P. Identification of Mimotope Peptides Which Bind to the Mycotoxin Deoxynivalenol-Specific Monoclonal Antibody. *Appl. Environ. Microbiol.* **1999**, *65*, 3279–3286. <https://doi.org/10.1128/AEM.65.8.3279-3286.1999>.
- (37) He, Q.; Xu, Y.; Zhang, C.; Li, Y.; Huang, Z. Phage-Borne Peptidomimetics as Immunochemical Reagent in Dot-Immunoassay for Mycotoxin Zearalenone. *Food Control* **2014**, *Complete*, 56–61. <https://doi.org/10.1016/j.foodcont.2013.10.019>.
- (38) Liu, X.; Xu, Y.; He, Q.; He, Z.; Xiong, Z. Application of Mimotope Peptides of Fumonisin B1 in Peptide ELISA. *J. Agric. Food Chem.* **2013**, *61*, 4765–4770. <https://doi.org/10.1021/jf400056p>.
- (39) Peltomaa, R.; Benito-Peña, E.; Barderas, R.; Sauer, U.; González Andrade, M.; Moreno-Bondi, M. C. Microarray-Based Immunoassay with Synthetic Mimotopes for the Detection of Fumonisin B<sub>1</sub>. *Anal. Chem.* **2017**, *89*, 6216–6223. <https://doi.org/10.1021/acs.analchem.7b01178>.
- (40) Hunt, E. A.; Moutsipoulou, A.; Ioannou, S.; Ahern, K.; Woodward, K.; Dikici, E.; Daunert, S.; Deo, S. K. Truncated Variants of Gaussia Luciferase with Tyrosine Linker for Site-Specific Bioconjugate Applications. *Sci. Rep.* **2016**, *6*, 26814. <https://doi.org/10.1038/srep26814>.
- (41) Hall, M. P.; Unch, J.; Binkowski, B. F.; Valley, M. P.; Butler, B. L.; Wood, M. G.; Otto, P.; Zimmerman, K.; Vidugiris, G.; Machleidt, T.; Robers, M. B.; Benink, H. A.; Eggers, C. T.; Slater, M. R.; Meisenheimer, P. L.; Klaubert, D. H.; Fan, F.; Encell, L. P.; Wood, K. V. Engineered Luciferase Reporter from a Deep Sea Shrimp Utilizing a Novel Imidazopyrazinone Substrate. *ACS Chem. Biol.* **2012**, *7*, 1848–1857. <https://doi.org/10.1021/cb3002478>.
- (42) Krska, R.; Schubert-Ullrich, P.; Molinelli, A.; Sulyok, M.; MacDonald, S.; Crews, C. Mycotoxin Analysis: An Update. *Food Addit. Contam.* **2008**, *25*, 152–163. <https://doi.org/10.1080/02652030701765723>.
- (43) Peltomaa, R.; Agudo-Maestro, I.; Más, V.; Barderas, R.; Benito-Peña, E.; Moreno-Bondi, M. C. Development and Comparison of Mimotope-Based Immunoassays for the

Analysis of Fumonisin B1. *Anal. Bioanal. Chem.* **2019**, *411*, 6801–6811. <https://doi.org/10.1007/s00216-019-02068-7>.

(44) Masseyeff, R. F.; Albert, W. H. W. (Winfried H. W. ); Staines, N. *Methods Immunological Analysis*; Weinheim, Germany : VCH Verlagsgesellschaft ; New York, NY (USA) : VCH Publishers, 1992.

(45) Findlay, J. W. A.; Dillard, R. F. Appropriate Calibration Curve Fitting in Ligand Binding Assays. *AAPS J* **2007**, *9*, E260–E267. <https://doi.org/10.1208/aapsj0902029>.

(46) Official Journal of the European Union. COMMISSION REGULATION (EC) No 1881/2006 of 19 December 2006 Setting Maximum Levels for Certain Contaminants in Foodstuffs.



## 6. FINAL REMARKS

The need of fast and sensitive detection methods for the analysis of mycotoxins in a wide variety of matrixes has led to the design and development of diverse approaches throughout several decades. Scientists have put an enormous effort in finding the best alternatives to provide efficient solutions to this challenge. The results obtained in this doctoral thesis are just a tiny grain that has been added to the huge pyramid of excellent research from all over the world.

In the first part of this thesis, it has been proven that the use of the phage display technology allows to identify novel recognition elements, in our case mycotoxin mimopeptides, from commercially available libraries. In this way, the first, and until now, the only mimopeptide for mycophenolic acid described in the literature was obtained from a library consisting of a series of 7 randomized amino acids flanked by a disulfide constrained loop formed by two cysteines. The selected mimopeptide proved an excellent competition against free MPA for the binding sites of a recombinant Fab anti-MPA antibody, with an  $IC_{50}$  of  $2.1 \text{ ng mL}^{-1}$  and a limit of detection of  $0.61 \text{ ng mL}^{-1}$ . However, it was also evident that the application of this technique was not always successful, as several attempts, in different formats, for the selection of mimopetides for both ochratoxin and alternariol provided dissatisfactory results. Further research needs to be conducted to optimize the selection rounds for the isolation of mimopeptides for these mycotoxins, focusing on bead-based approaches rather than on the direct coating of the antibody to a well plate.

The second part of the thesis consisted of the development of optical immunosensors for the determination of mycotoxins in diverse matrixes. On the one hand, a novel immunoassay for the detection of MPA in blood samples was conducted using the MPA mimopeptide previously selected. Initial experiments proved that the peptide sequence ACEGLYAHWC (with a disulfide bond between the two Cs) was responsible for the interaction with the anti-MPA Fab, and SPR characterization demonstrated the excellent potential of the peptide sequence as a competitor of MPA. Furthermore, the construction of bioluminescent fusion proteins proved that the mimopeptide could be expressed cost-effectively in bacteria without altering its affinity towards the recombinant MPA antibody. A total of three different immunoassays were described in this thesis for MPA: a phage-based immunoassay, utilizing the entire phage clone, a peptide-based immunoassay, using the synthetic mimopeptide, and a bioluminescent immunoassay with the fusion protein. Among them, the bioluminescent immunoassay improved the sensitivities of the former two, with a limit of detection of  $0.26 \text{ ng mL}^{-1}$  and an  $IC_{50}$  of  $2.9 \pm 0.5 \text{ ng mL}^{-1}$ . Moreover, this approach reduced the analysis time since no secondary antibody was required in the assay. The analysis of blood samples proved the potential of the bioluminescent immunoassay for the detection of MPA in complex samples. The results were validated with a reference chromatographic method and favorably correlated with the administered doses of each patient.

On the other hand, two competitive immunoassays were developed for the determination of fumonisin B1 in wheat samples using a previously reported FB<sub>1</sub> mimopeptide fused to two different bioluminescent proteins: *Gaussia* luciferase and

NanoLuc luciferase. A comparison of the performance of both fusion proteins demonstrated the differences between them. The A2-GLuc fusion protein presented a flash kinetics in comparison to the glow-type kinetics of the A2-NLuc fusion protein. Additionally, the A2-GLuc exhibited a comparable limit of detection to that of the A2-NLuc, but a much narrower dynamic range, demonstrating that the A2-NLuc fusion protein is a better alternative for the determination of FB<sub>1</sub> in wheat samples. The applicability of the novel bioluminescent immunoassay using the A2-NLuc fusion protein was demonstrated with the analysis of spiked wheat extracts, a reference material and naturally contaminated wheat samples, and the results were statistically comparable to those obtained with a reference chromatographic method.

Altogether, the results obtained in this thesis confirmed the versatility of mimopeptides and their vast applicability in different assay formats. It is undeniable that phage-based and peptide-based assays can provide efficient results, but the construction of fusion proteins can lead to unlimited production of already-labeled mimopeptides, which can eventually become an excellent alternative for sensing applications.

## **ANNEX: Publications**





## Recombinant Peptide Mimetic NanoLuc Tracer for Sensitive Immunodetection of Mycophenolic Acid

Álvaro Luque-Uría, Riikka Peltomaa, Tarja K. Nevanen,\* Henri O. Arola, Kristiina Iljin, Elena Benito-Peña,\* and María C. Moreno-Bondi\*

Reproduced with permission from: *Anal. Chem.* 2021, 93, 29, 10358–10364

Further permission related to the material excerpted should be directed to the ACS.

Copyright © 2021 American Chemical Society

**ABSTRACT:** Mycophenolic acid (MPA) is an immunosuppressant drug commonly used to prevent organ rejection in transplanted patients. MPA monitoring is of great interest due to its small therapeutic window. In this work, a phage-displayed peptide library was used to select cyclic peptides that bind to the MPA-specific recombinant antibody fragment (Fab) and mimic the behavior of MPA. After biopanning, several phage-displayed peptides were isolated and tested to confirm their epitope-mimicking nature in phage-based competitive immunoassays. After identifying the best MPA-mimetic (ACEGLYAHWC with a disulfide constrained loop), several immunoassay approaches were tested, and a recombinant fusion protein containing the peptide sequence with a bioluminescent enzyme, NanoLuc, was developed. The recombinant fusion enabled its direct use as the tracer in competitive immunoassays without the need for secondary antibodies or further labeling. A bioluminescent sensor, using streptavidin-coupled magnetic beads for the immobilization of the biotinylated Fab antibody, enabled the detection of MPA with a detection limit of 0.26 ng mL<sup>-1</sup> and an IC<sub>50</sub> of 2.9 ± 0.5 ng mL<sup>-1</sup>. The biosensor showed good selectivity towards MPA and was applied to the analysis of the immunosuppressive drug in clinical samples, of both healthy and MPA-treated patients, followed by validation by liquid chromatography coupled to diode array detection (LC-DAD).

### INTRODUCTION

Mycophenolic acid (MPA) is a mycotoxin produced by *Penicillium* fungi, and it is widely used as an immunosuppressant drug to prevent organ rejection in transplanted patients.<sup>1</sup> Recently, it has also been tested as a chemotherapeutic agent as it inhibits the proliferation of cancer cells.<sup>2</sup> Due to the small therapeutic window that MPA has, it is very important to monitor correctly its levels inside the human body.<sup>3</sup> MPA is mainly found in serum, but only 1% of the total MPA exists in the free form, which is the one responsible for its pharmacological activity.<sup>3,4</sup> Therefore, the availability of analytical methods for detecting MPA at low concentrations in serum is of great interest.

Over the past decades, the determination of MPA has been carried out using liquid chromatography (LC) coupled with ultraviolet or mass spectrometry detection.<sup>5–7</sup> However, these methods often require skilled personnel, they are time-consuming and of high cost. Moreover, tedious sample treatment is mandatory in most cases. Fast

screening methods such as immunoassays are highly relevant nowadays, and the use of antibodies has burst over the last years as simple analytical tools. Immunoassays offer outstanding versatility since they can be easily automated or integrated into a routine laboratory or a point-of-care testing device. Also, different immunoassays have been already implemented for the detection of MPA.<sup>8-10</sup> Those assays, however, fail to detect free MPA in blood samples and offer a poor selectivity as several potential interferences may alter the results. We have previously developed a homogeneous fluorescence polarization assay to detect free MPA in blood samples with good sensitivity, low cross-reactivity, and good recovery rates in real samples.<sup>11</sup>

The analysis of low molecular weight molecules can sometimes be challenging. They might present high toxicity, carcinogenicity, high price, or are difficult to functionalize without altering their interaction with the antibody. A feasible solution to this is the use of peptide mimetics, also known as mimotopes, since they can be easily functionalized or fused to other proteins in a cost-effective way. Peptide mimetics have the exceptional ability to bind to the same antibody paratope as the antigen, and they can be applied to the development of competitive immunoassays or biosensors where they can replace the analyte-conjugate used as the competitor.

Phage display is a commonly applied technique for recombinant antibody development as well as to identify peptide mimetics.<sup>12</sup> Phage-based enzyme-linked immunosorbent assays (ELISA) using peptide mimetics have been widely described in the literature. These assays do not require much preparation, and they have good sensitivities as well as selectivities.<sup>13-17</sup> However, the presence of the phage may have a significant effect on the binding kinetics, and previous reports have shown that the assay sensitivity can potentially improve when the peptide is used alone rather than in the phage-displayed form.<sup>18,19</sup> Moreover, the assays would be faster, cheaper and simpler if the peptide is fused to a fluorescent or luminescent protein, since the peptide fusion would be responsible for the analytical signal, and there would be no need to use any secondary antibody for that purpose. The coupling can typically be a genetic fusion or a chemical functionalization, however, the former one is preferred due to the fact that chemical modifications can lead to a series of secondary reactions that may alter the final product. Genetic modifications are more homogeneous and present a well-defined stoichiometry between the peptide and the protein.<sup>20</sup>

In this work, we describe the first peptide mimetic for MPA and a bioluminescent-based immunoassay for the detection of MPA with a NanoLuc-peptide fusion in blood samples. Firstly, the peptide mimetic was selected from a combinatorial peptide library by phage display. The high selectivity of the peptide mimetic for the recombinant MPA antibody fragment was demonstrated by a competitive phage-based ELISA. Moreover, surface plasmon resonance (SPR) was used to confirm the binding properties of the cyclic peptide (named A2) and MPA to the anti-MPA Fab antibody. Thereafter, a bioluminescent protein, NanoLuc, was coupled to the MPA mimicking peptide A2. NanoLuc is reported to be 100 times brighter than firefly or *Renilla* luciferases, and with a size as small as 19 kDa, it is catching the eyes of many researchers for many different applications.<sup>21</sup> The NanoLuc-peptide fusion was genetically crafted and implemented in a magnetic bead-based immunoassay that showed higher sensitivity than the phage-

based ELISA. Finally, the bioluminescent assay was applied to analyze the free active forms of MPA in blood samples from transplanted patients. The results were validated by a reference method using rapid-resolution liquid chromatography with diode array detection (RRLC-DAD).

## EXPERIMENTAL SECTION

**Materials.** Ph.D.-C7C Phage Display Peptide Library Kit was purchased from New England Biolabs (Ipswich, MA, USA). Nunc MaxiSorp 96-well plates, Amplex UltraRed reagent, Phusion Hot Start II DNA Polymerase, high-fidelity DNA Polymerase, SuperBlock blocking buffer (in PBS), LB Broth, Lennox, Human serum type AB, EZ-Link Sulfo-NHS-LC-Biotin, No-Weigh Format, 1-Step™ ultra TMB-ELISA and NeutrAvidin Biotin Binding Protein were from Thermo Fisher Scientific (Waltham, MA, USA). Streptavidin microtiter plates were from Kaivogen (Turku, Finland). PCR Nucleotide Mix and 2,2'-azino-di-(3-ethylbenzthiazoline sulfonic acid) (ABTS) were purchased from Roche Diagnostics (Basel, Switzerland). Black Packard HTRF 96-well plates were from Nunc (Roskilde, Denmark), and the biotinylated peptide A(CEGLYAHWC)GGGSK(Bio)-NH<sub>2</sub> was synthesized at Peptide Synthetics (Fareham, UK). The HRP-conjugated anti-M13 antibody, HisTrap™ FF crude columns, Sephadex™ G-25 M columns and Illustra NAP-5 columns were purchased from Cytiva. (Chicago, IL, USA). Cobalt (II) chloride hexahydrate (for analysis) and hydrogen peroxide 30% were obtained from Merck (Darmstadt, Germany). Phosphate buffer saline (PBS), pH 7.4, Tween 20, Dimethyl sulfoxide (≥99.5%), 5-Bromo-4-chloro-3-indolyl β-D-galactopyranoside (X-Gal) and isopropyl-β-d-thiogalactopyranoside (IPTG) were purchased from Sigma-Aldrich (Saint Louis, MO, USA). LB Agar and Agar Granulated were from NZYtech (Lisbon, Portugal), Imidazole and mycophenolic acid (MPA) were purchased from Alfa Aesar (Maverhill, MA, USA). BcMag IDA-modified magnetic beads (1 μm) were from Bioclone Ltd. (London, UK). PCR primers were purchased from Integrated DNA Technologies, Inc (San Diego, CA, USA). NanoGlo® Reagent for Immunoassay was from Promega Corporation (Madison, WI, USA), and High Capacity Magne™ Streptavidin Beads and ATG-42 plasmid DNA, containing the NanoLuc gene were kindly donated by Promega Corporation (Madison, WI, USA). The recombinant anti-MPA Fab was obtained from a phage display library and produced as described previously.<sup>22</sup>

**Biopanning Rounds.** A commercial phage-displayed peptide library was used to select cyclic peptides that bind to the anti-MPA. The selection rounds were carried out with an automatic magnetic bead processor (KingFisher™ Thermo Fisher Scientific). See Supporting Information for antibody coupling to magnetic beads. Briefly, the phage-displayed peptide library (~ 2.0 × 10<sup>11</sup> phages) was incubated for 2 h with the anti-MPA conjugated beads (50 μg) in a total volume of 505 μL of PBST (PBS, pH 7.4 with 0.05% (v/v) Tween-20). The beads were subsequently washed twice with PBST during 30 s, and then the bound phages were eluted with 100 μL of 0.1 M triethylamine (pH 11.2) for 30 min. The resulting solution containing the eluted phages was immediately neutralized with 70 μL of 1 mol L<sup>-1</sup> Tris-HCl (pH 6.8). Amplification of the eluted phages was carried out by adding 70 μL of the eluate to a 40 mL early-log phase ER2738 culture in LB and incubating at +37 °C for 4.5 h. The cells were harvested by centrifugation

(10 min, 12000 g, +4 °C) and the supernatant was collected. The amplified phages were precipitated overnight at +4 °C after adding to the supernatant 1/6 volume of 20% PEG/2.5 mol L<sup>-1</sup> NaCl. Then, the precipitated phages were collected by centrifugation (15 min, 12000 g, +4 °C) and resuspended in 3 mL of PBS. The precipitation was repeated with 20% PEG/2.5 mol L<sup>-1</sup> NaCl on ice during 1 h, followed by centrifugation (10 min, 12000 g, +4 °C). Finally, the pellet containing the phages was resuspended in 500 µL of PBS. The amplified phage solution was utilized for the consequent selection round.

After the first round, an additional 30-s washing step was introduced to harden the conditions of selection. After three panning rounds, several individual clones were isolated from each round and tested in phage-based ELISAs to select the one showing the highest sensitivity for the anti-MPA. Monoclonal phages were selected from fresh titering plates of each round. Briefly, 80 µL of ER2738 culture containing the monoclonal phages were incubated for 2.5 h at +37 °C and were subsequently streaked out and grown overnight on IPTG/X-Gal plates at 37 °C. Afterwards, individual clones were inoculated on 500 µL of LB and grown for 6 h at +37 °C. Finally, the cells were harvested (5 min, 10000 g, +4 °C), and the supernatant was transferred to a fresh tube. The concentration of the amplified individual clones, determined by titering, ranged from 10<sup>11</sup> to 10<sup>12</sup> pfu mL<sup>-1</sup>.

**Phage-Based ELISA.** The phage-displayed peptides were screened in an ELISA to test their binding to immobilized anti-MPA. The assay was carried out at room temperature (RT). The biotinylated anti-MPA (Supporting Information) (5 µg mL<sup>-1</sup> in assay buffer (SuperBlock supplemented with 0.05% Tween-20); 100 µL per well) was immobilized on streptavidin-coated wells (30 min) followed by three-time washes with PBST. The wells were then blocked with 280 µL of assay buffer for 30 min and washed again three times with PBS. Then, the amplified phage stock (between 10<sup>10</sup> and 10<sup>11</sup> pfu mL<sup>-1</sup>; 100 µL per well) was added to the wells in assay buffer and incubated for 1 h with slow shaking. After washing the wells as described above, the HRP-conjugated anti-M13 monoclonal antibody (1:5000 dilution in assay buffer; 100 µL per well) was added to the wells and incubated for 1 h. Finally, the plate was washed three times as described above and 100 µL of ABTS were added to the wells. After 5 min, absorbance at 405 nm was measured in a Varioksan plate reader (Thermo Scientific)).

The phage clone that showed binding to the anti-MPA Ab was tested in a similar assay in the presence of 100 ng mL<sup>-1</sup> of free MPA. Furthermore, a bead-based assay was developed with the phage that showed significant competition in the plate-based assay. Briefly, black microtiter plates were blocked with 280 µL of assay buffer for 1 h at RT and subsequently washed three times with PBS. Then, the biotinylated anti-MPA (1.2 µg mL<sup>-1</sup>) and neutravidin-coated magnetic beads (125 µg mL<sup>-1</sup>) functionalized as described before,<sup>18</sup> were added to the wells in assay buffer (total volume 260 µL per well) and incubated for 30 min at RT. After washing the beads using a plate washer with a magnetic support, the phage clone (10<sup>11</sup> pfu mL<sup>-1</sup>) and increasing concentrations of free MPA were added to the wells (in assay buffer, 60 µL per well) and incubated for 30 min at RT. The beads were washed again to remove the excess, followed by incubation with HRP-conjugated anti-M13 antibody (1:5000 dilution in assay buffer; 80 µL per well) for 30 min at RT. Finally, after washing, 80 µL of Amplex UltraRed solution was added to

each well and the fluorescence was monitored with a CLARIOstar microplate reader ( $\lambda_{\text{ex}}=530 \text{ nm}$ ,  $\lambda_{\text{em}}=590 \text{ nm}$ ).

**Construction of the NanoLuc Fusion Protein.** The phage clone that showed the best response in the competition assay with free MPA was sequenced to identify the peptide sequence. To express the MPA peptide mimetic A2 in fusion with the NanoLuc protein, the latter one was PCR-amplified from the commercial vector ATG 42<sup>23</sup> using the Phusion Hot Start II DNA Polymerase. The forward primer, RP043, (5'-GAA AAC CTG TAT TTT CAG GGC GTC TTC ACA CTC GAA GAT TTC G-3') hybridized to the 5'-end of the NanoLuc, and the reverse primer, RP044, (5'-ATA CAG ACC CTC ACA ACT GCC ACC TCC AGA GCC GCC ACC CGC CAG AAT GCG TTC GC-3') hybridized to the 3'-end. The hybridizing part of the sequence is underlined. The fusion of the NanoLuc with the cyclic peptide was carried out in the pMAL vector. In order to amplify this vector, the forward primer, RP039, (5'-GT TGT GAG GGT CTG TAT GCG CAT TGG TGC GGA GGC TAG GGA TCC GAA TTC CCT-3') included a 5'-overhang (in bold) for the DNA sequence encoding the peptide mimetic for MPA, whereas the reverse primer, RP040, (5'-G AAA ATA CAG GTT TTC ATG ATG ATG ATG ATG CAT AAT CTA TGG TCC TTG TTG G-3') contained a His-tag. For the assembly, the vector and the insert were incubated at +50 °C for 15 min with the NEBuilder Master Mix. Then, NEB 5-alpha Competent *Escherichia coli* cells were transformed with 2  $\mu\text{L}$  of the assembled product according to the manufacturer's instructions.<sup>24</sup> Successful cloning was proven by DNA sequencing analysis.

**Expression and Purification of the Fusion Protein.** The A2-NanoLuc plasmid (**Figure S1A**, Supporting Information) was first transformed into *E. coli* SHuffle Express cells according to the manufacturer's instructions. A single colony was selected on LB agar plates with 100  $\mu\text{g mL}^{-1}$  ampicillin and grown on 15 mL of LB with 100  $\mu\text{g mL}^{-1}$  ampicillin overnight. The next day, an aliquot of the overnight preculture was added to a 200 mL culture of LB with 100  $\mu\text{g mL}^{-1}$  ampicillin and grown until an OD<sub>600</sub> (optical density at 600 nm) of 0.6 was reached. To induce the protein expression, IPTG was added at a final concentration of 0.4  $\text{mmol L}^{-1}$ , and the expression was continued at +37 °C for 4 h. The culture was then transferred to an ice bath for 10 min to stop the cell growth, and the cells were collected by centrifugation at 5000 g for 10 min at +4 °C and resuspended in NZY Bacterial Cell Lysis Buffer (approximately 5 mL of buffer per gram of cell paste) supplemented with protease inhibitor cocktail, NZY Bacterial Cell Lysis Buffer supplemented with Lysozyme and DNase I according to the manufacturer's instructions. The cell lysis was carried out by sonication (VibraCell Ultrasonic Processor 130 W 20 kHz, Ampl 70%) for 10 s 5 times with 30 s breaks, and the insoluble cell debris was discarded by centrifugation at 15000 g for 15 min at +4 °C. Finally, the cell lysate was purified with HisTrap™ purification columns according to the manufacturer's instructions, and the buffer was exchanged to PBS with Sephadex™ G-25 M columns. The purified proteins were aliquoted and stored at -20 °C. The size and purity of the A2-NanoLuc fusion protein was confirmed by SDS-PAGE (**Figure S1B** Supporting Information). Kinetic constants of the binding of the cyclic peptide (A2) and MPA were determined by Biacore T200 (Supporting Information).

**Bioluminescent Immunoassay for MPA Detection.** To detect MPA with A2-NanoLuc fusion protein, a bead-based assay was carried out on a black microtiter well plate by immobilizing the biotinylated anti-MPA onto streptavidin-coated magnetic beads (**Figure 1**). Briefly, the wells were first blocked with assay buffer (SuperBlock with 0.05% Tween-20) for 1 h. Then, 60  $\mu\text{L}$  of 5  $\mu\text{g mL}^{-1}$  biotinylated anti-MPA in assay buffer and 20  $\mu\text{L}$  of streptavidin beads (1:50 dilution from the stock) were added to the wells and incubated for 30 min at RT. After washing 3 times with PBST, 60  $\mu\text{L}$  of a solution containing different concentrations of MPA and 77  $\mu\text{g mL}^{-1}$  of the A2-NanoLuc in assay buffer was added to the wells and incubated 30 min at RT. Once the beads were washed, 60  $\mu\text{L}$  of NanoGLO substrate in PBS were added and bioluminescence was measured after a 2-min incubation at 470 nm with a bandwidth of 80 nm using a CLARIOstar microplate reader.

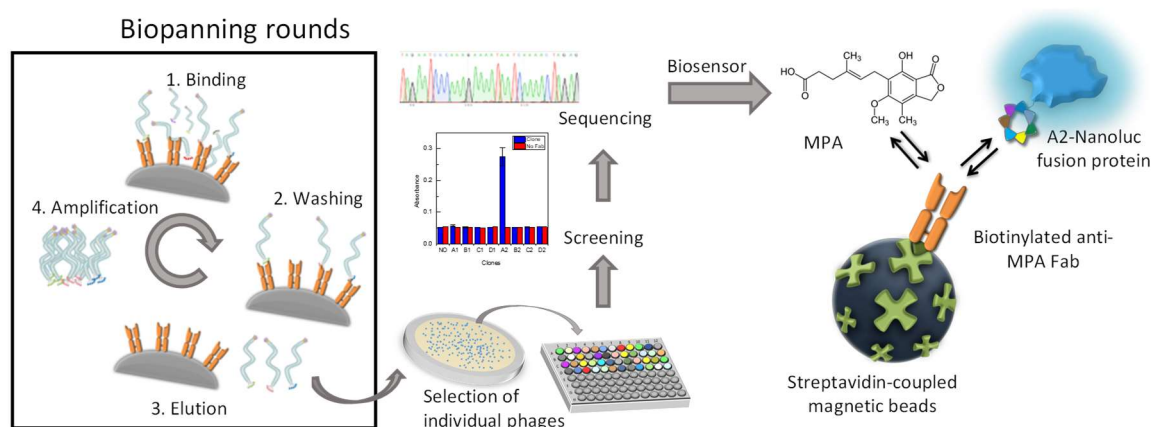


**Figure 1.** Schematic representation of the biopanning rounds followed by the whole process until the biosensor development for the detection of MPA based on the A2-NanoLuc fusion protein. MPA concentration was determined by a competition between the free MPA and the A2-NanoLuc for the binding sites of the biotinylated anti-MPA Fab antibody, previously bound to streptavidin-coupled magnetic beads. Finally, the bioluminescence of NanoLuc was measured after the addition of the NanoGlo substrate.

**Sample analysis.** Volunteers donated whole blood samples with permission from the Ethics Committee from Hospital Clínico Universitario de Valladolid, Spain (no. PI 21-2245). The blood samples were kept at 20 °C during transport and storage. The samples were treated following the procedure described previously (see Supporting Information for details).<sup>11</sup>

## RESULTS AND DISCUSSION

**Selection and Characterization of MPA Peptide Mimetics.** To develop a competitive immunoassay for MPA detection, a peptide mimetic for mycophenolic acid (MPA) was selected from a cyclic 7-mer phage display peptide library (Ph.D.-C7C) in three consecutive panning rounds. Once the three panning rounds were carried out, a total of eight clones were isolated and tested in an ELISA. One of the clones showed a very high signal-to-background ratio, as well as very low nonspecific binding when the assay was performed in the absence of anti-MPA (**Figure 2A**), therefore, this clone (named A2) was selected for further analysis. Next, a competitive ELISA for A2 was carried out under the same assay conditions as before. However, in this case, 100  $\text{ng mL}^{-1}$  of free MPA were added at the same time as the phage clone to test the competition between phage-

displayed A2 and free MPA for the binding sites of the anti-MPA. A significant decrease in the signal was observed in the presence of MPA, demonstrating the success of the selection rounds and excellent performance of clone A2 as a peptide mimetic (data not shown).

A fluorescent bead-based assay was developed to further optimize the assay conditions and confirm the viability of the selected phage clone. Neutravidin-functionalized magnetic beads were incubated with the biotinylated anti-MPA, and the competition was then tested between free MPA in concentrations ranging from 0 to 1600 ng mL<sup>-1</sup> and clone A2. The results were similar to those obtained on the plate-based ELISA, confirming the successful selection of the peptide mimetic (**Figure 2B**).

By DNA sequencing of clone A2, the peptide sequence of ACEGLYAHWC, with a disulfide bond between the two cysteines, was identified. A synthetic biotinylated peptide with this sequence was consequently tested in a competitive neutravidin-bead-based assay, showing competition at the nanomolar level. Contrary to the phage-based assay, this time the biotinylated peptide was bound to neutravidin beads and the non-biotinylated anti-MPA was added thereafter. This antibody was then recognized with an anti-IgG-HRP antibody, measuring the same fluorescent signal as before. Due to the absence of the whole phage in this assay, the results prove that the peptide sequence obtained can be considered an outstanding mimetic for MPA since a similar response was obtained in comparison to the phage-based assay (**Figure S2, Supporting Information**). As can be seen, the phage-based assay showed a slightly lower limit of detection (LOD), calculated as the 10% inhibition,<sup>25</sup> (0.69 ng mL<sup>-1</sup>) compared to the peptide-based assay (0.94 ng mL<sup>-1</sup>). However, the dynamic range, taken as the 20–80% inhibition,<sup>26</sup> is wider in the case of the peptide-based assay (2.4–60 ng mL<sup>-1</sup>) than in the phage-based assay (1.0–4.1 ng mL<sup>-1</sup>). The assay time is the same in both cases, and the detection is done by adding the same fluorescent dye.

**Binding Properties of Cyclic Peptide.** To compare the binding properties of the biotinylated cyclic peptide and mycophenolic acid towards the anti-MPA antibody, label-free surface plasmon resonance (SPR) technology was applied. In the binding experiments, previously identified, produced and purified Fab antibodies recognizing either MPA or ochratoxin A were immobilized onto sensor chip surfaces.<sup>22</sup> The same experimental conditions were used to study the binding properties of cyclic peptide (A2) and mycophenolic acid. The results are presented in **Figures S3 and S4** and summarized on **Table S1 (Supporting Information)**. As expected, both cyclic peptide (A2) and mycophenolic acid showed binding to the anti-MPA Fab antibody surface, and the binding responses increased in a concentration-dependent manner.

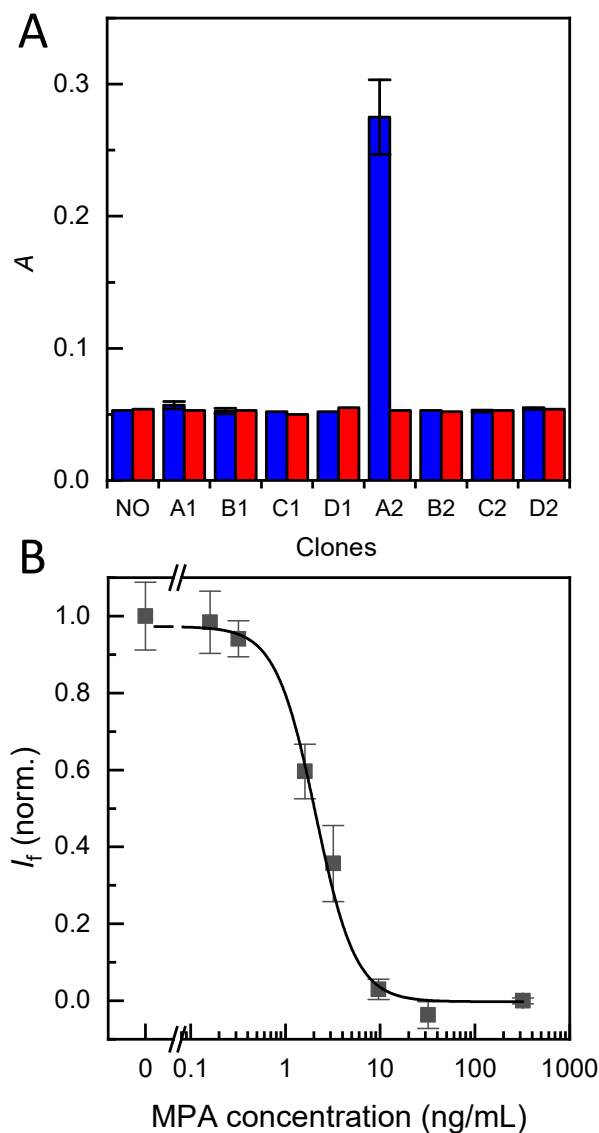


**Figure 2.** (A) Phage-based ELISA with 8 different monoclonal phages. Clone A2 showed high specificity towards anti-MPA (blue) and very low nonspecific binding in the absence of anti-MPA (red), similar to the background wells (NO clone). (B) Competitive phage-based ELISA with clone A2. Free MPA was added simultaneously with the phage clone A2 to the wells containing the anti-MPA immobilized onto magnetic beads in assay buffer. The results are shown as the average fluorescence intensity  $\pm$  the standard error of the mean ( $n = 3$ ). The response was fitted to a logistic fit using OriginPro 2019.

In agreement with our previous results from the SPR assay using affinity in solution approach, the affinity constant for MPA and anti-MPA Fab antibody interaction was  $\sim 40 \text{ nmol L}^{-1}$ .<sup>22</sup> The affinity of the interaction between cyclic peptide (A2) and anti-MPA Fab antibody is two orders of magnitude lower compared to the affinity of MPA–anti-MPA Fab antibody interaction. This is due to the slower association and faster dissociation of cyclic peptide (A2)–anti-MPA Fab antibody complex compared to the corresponding values for MPA–anti-MPA Fab antibody complex.

**Bioluminescent Bead-Based Immunoassay for MPA Detection.** To improve the assay sensitivity and to provide a faster and cheaper assay, the peptide mimetic was fused to a bioluminescent enzyme, both in the N-terminus and the C-terminus (A2-Nanoluc and



NanoLuc-A2, respectively), and a simple immunoassay for MPA detection was established using the A2-NanoLuc fusion protein. The fusion protein was produced cost-effectively by bacteria, in which the bioluminescent protein can be already incorporated. After purification, both NanoLuc-A2 and A2-NanoLuc fusion proteins showed bright luminescence in the presence of the substrate, proving that the assay did not require a secondary antibody or any other chemical modification to obtain the analytical signal. Both fusion proteins also proved to recognize the anti-MPA and compete with free MPA at the nanomolar level for the binding sites of the antibody (**Figure S5**, Supporting information), however, the A2-Nanoluc product showed a wider dynamic range and lower dispersity at low concentrations, and it was selected for further characterization (**Figure 3**). This confirmation was carried out with a bead-based assay, in which streptavidin-coated beads were incubated first with the biotinylated anti-MPA, and then, the A2-NanoLuc and the free MPA were added simultaneously to the solution. This bead-based immunoassay improved both the dynamic range and the sensitivity compared to similar bead-based assays carried out with the phage-displayed A2 and with the synthetic peptide A2-bio (**Figure S2**, Supporting Information). The limit of detection (LOD) was  $0.26 \text{ ng mL}^{-1}$  and the  $\text{IC}_{50}$  value was  $2.9 \pm 0.5 \text{ ng mL}^{-1}$ . The dynamic range ranged between  $0.64$  and  $14 \text{ ng mL}^{-1}$ . The interday relative standard deviation (RSD) was 12% on average ( $n = 3$ ), whereas the value for assays on three different, non-consecutive days was 9%. The A2-NanoLuc fusion protein proved to be stable for more than 6 months upon storage at  $-20 \text{ }^{\circ}\text{C}$  in PBS. For comparison purposes, this bioluminescent assay provided a better sensitivity, a shorter analysis time and simplicity, since there is no need to add a secondary antibody, than those described previously using horseradish peroxidase (HRP) as the label and fluorometric detection. In addition, the sensitivity of this assay is better than for other immunoassays described in the literature, as well as for several commercially available kits for the analysis of MPA (**Table S2**, Supporting Information).

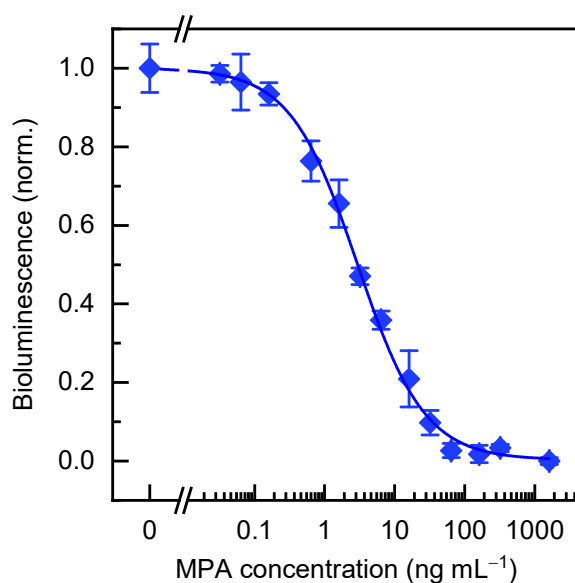


**Figure 3.** Bead-based bioluminescent MPA calibration in assay buffer using A2-NanoLuc fusion protein. Different MPA concentrations were incubated with A2-NanoLuc, and magnetic beads coupled to the biotinylated anti-MPA. The bioluminescence signals ( $\lambda_{\text{em}} = 470 \pm 80 \text{ nm}$ ) were

measured after adding the NanoGLO substrate, and the values were normalized to the maximum and minimum signals. The results are presented as the mean values  $\pm$  the standard error ( $n = 3$ ) adjusted to a logistic fit using OriginPro 2019.

**Cross-Reactivity.** To prove the selectivity of the method, the assay was performed in the presence of different MPA metabolites found in blood, such as the mycophenolic acid glucuronide (MPAG) and the acyl-mycophenolic acid glucuronide (acyl-MPAG), as well as other immunosuppressant drugs commonly co-administered to transplanted patients, tacrolimus and cyclosporin (Figure S6 Supporting Information). As can be observed in Figure 4, the acyl-MPAG showed a very similar behavior as the MPA in the assay (58% cross-reactivity, calculated as the  $IC_{50}$  for MPA divided by the  $IC_{50}$  of acyl-MPAG). This metabolite is an active form of the MPA, contrary to the MPAG,<sup>27</sup> therefore the assay can be designed to detect the active forms of MPA in blood. Nevertheless, the acyl-MPAG is found at lower concentrations than MPA<sup>28</sup> and it was not detected by HPLC in any of the analyzed samples. Concerning MPAG, the cross-reactivity was negligible at 0.03%, and for the two other immunosuppressant drugs, it was lower than 0.03%.

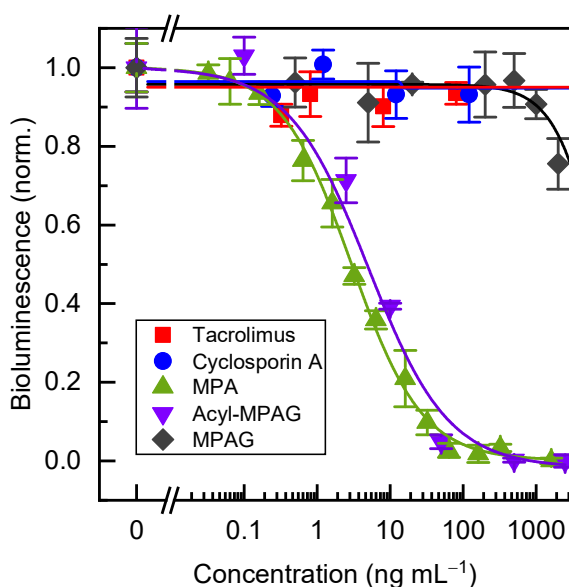


**Figure 4.** Cross-reactivity of the bead-based bioluminescent immunoassay. MPAG and acyl-MPAG are metabolites that can be found in blood together with MPA. Tacrolimus and cyclosporine are two immunosuppressant drugs that can be administered in combination with MPA to transplanted patients to prevent organ rejection. The bioluminescence values were normalized to the maximum and minimum signals, and the results are presented as the mean values  $\pm$  the standard error of the mean ( $n = 3$ ) adjusted to a logistic fit using OriginPro 2019.

**Matrix Effect.** The matrix effect was tested in the presence of different dilutions of the ultrafiltered serum samples (1/2, 1/6, 1/8, (v/v)), treated following a previously described procedure,<sup>11</sup> in PBST. **Figure 5** shows that no significant differences ( $p > 0.05$ ) were observed between the dose response curves obtained in PBST or in ultrafiltered serum diluted 1/8 (v/v) with the buffer. Therefore, such dilution was used for further experiments.

**Sample Analysis.** The optimized assay was applied to the analysis of blood samples from transplanted patients (T1-T5) and healthy control patients (H1-H3), and the results

were validated by rapid resolution liquid chromatography coupled to diode array detection (RRLC-DAD) (Supporting Information) (**Figure 6**). **Figure S7** (Supporting information) shows a chromatogram of a standard mixture of the metabolites. As expected, no MPA was detected in the control samples. A statistical comparison of the results obtained by both methods using a paired t-test demonstrated that there are not significant differences between them at a 95% confidence level. The RRLC-DAD results confirmed that the active metabolite, acyl-MPAG, was not present in any of the samples, and therefore, the biosensor response was only due to the free MPA. Furthermore, the MPAG levels found in the analyzed samples were below the limit of quantification of the biosensor, hence, the non-active metabolite of the MPA did not cross-react in the analysis. (**Table S3**, Supporting Information). The results show that patients T1 and T2 had the highest MPA concentration levels and the results in all cases correlate favorably with the administered doses (**Table S4** Supporting Information).

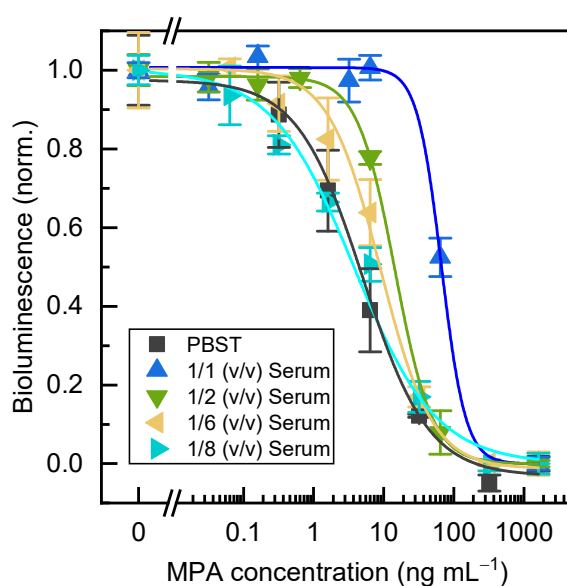


**Figure 5.** Comparison of the calibration curves for the bead-based bioluminescent immunoassay in PBST and with different dilutions of ultrafiltered serum. No significant differences were found with the 1:8 (v/v) dilution. The bioluminescence values were normalized to the maximum and minimum signals and the results are presented as the mean values  $\pm$  the standard error of the mean ( $n = 3$ ). The graph was adjusted to a logistic fit using OriginPro 2019.

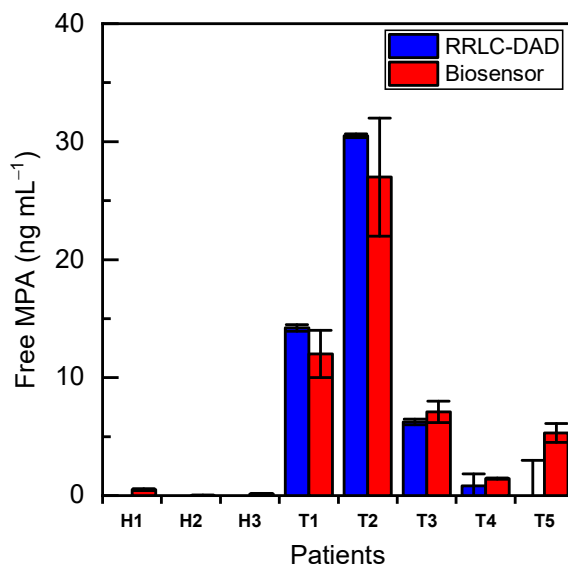


**Figure 6.** Results comparison of the analysis of blood samples from transplanted patients by the biosensor and RRLC-DAD. H refers to healthy patients, not treated with MPA, and T to MPA treated patients. The results are presented as the mean values  $\pm$  the standard error of the mean ( $n = 3$ ).

## CONCLUSIONS

In this work, we proved that phage display is a useful technique for the selection of mycophenolic acid peptide mimetics for the development of immunoassays and biosensors. A bioluminescent bead-based assay using a luciferase enzyme as reporter provided higher sensitivities, shorter analysis times and cost-effective assays than other formats using HRP as the label and fluorometric detection. The assay allows the analysis of the active forms of mycophenolic acid in plasma, *i.e.*, free mycophenolic acid and acyl-MPAG. No relevant cross-reactivity was observed with other non-active forms of MPA in plasma as well as with other drugs jointly administered to transplanted patients. The results were compared favorably with a reference RRLC-DAD based method.

## ASSOCIATED CONTENT

### Supporting Information

The Supporting Information is available free of charge on the ACS Publications website.

Protocols for antibody coupling to magnetic beads and antibody biotinylation. Details about the synthetic peptide-based ELISA. Description about the SPR measurements. Details about the RRLC-DAD method. Blood sample treatment. Construction of the NanoLuc-peptide mimetic fusion. Calibrate comparison of both NanoLuc-peptide mimetic fusions. Chemical structures of MPA, its main metabolites and two other co-administered immunosuppressant drugs. Comparison of different analytical methods reported for MPA detection. MPAG levels found in transplanted patients. Administered doses of MPA to the analyzed transplanted patients.

## AUTHOR INFORMATION

### Corresponding Authors

**Elena Benito-Peña** – Department of Analytical Chemistry, Faculty of Chemistry, Complutense University, Ciudad Universitaria s/n, 28040 Madrid, Spain;

orcid.org/0000-0001-5685-5559

Email: [elenabp@quim.ucm.es](mailto:elenabp@quim.ucm.es)

**María C. Moreno-Bondi** – Department of Analytical Chemistry, Faculty of Chemistry, Complutense University, Ciudad Universitaria s/n, 28040 Madrid, Spain; orcid.org/0000-0002-3612-0675

Email: [mcmbondi@ucm.es](mailto:mcmbondi@ucm.es)

**Tarja K. Nevanen** – VTT Technical Research Centre of Finland Ltd, Tietotie 2, FI-02150 Espoo, Finland

Email: [Tarja.Nevanen@vtt.fi](mailto:Tarja.Nevanen@vtt.fi)

### Authors

**Álvaro Luque-Uria** – Department of Analytical Chemistry, Faculty of Chemistry, Complutense University, Ciudad Universitaria s/n, 28040 Madrid, Spain

**Riikka Peltomaa** – Department of Analytical Chemistry, Faculty of Chemistry, Complutense University, Ciudad Universitaria s/n, 28040 Madrid, Spain; orcid.org/0000-0001-7041-3722

**Henri O. Arola** – VTT Technical Research Centre of Finland Ltd, Tietotie 2, FI-02150 Espoo, Finland

**Kristiina Iljin** – VTT Technical Research Centre of Finland Ltd, Tietotie 2, FI-02150 Espoo, Finland

### Present Addresses

**Riikka Peltomaa** – Department of Life Technologies/Biotechnology, University of Turku, Kiinamyyllykatu 10, 20520, Turku, Finland

### Author Contributions

A.L.U.: Conceptualization, methodology, investigation, writing – original draft, visualization. R.P.: Conceptualization, methodology, investigation, writing – review & editing, visualization. T.N.: Conceptualization, methodology, writing – review & editing, funding acquisition. H.A.: Conceptualization, methodology, investigation, writing – review & editing, visualization. K.I.: investigation, visualization, writing – review & editing; E.B.P.: Conceptualization, methodology, investigation, writing – review & editing. M.C.M.B.: Conceptualization, methodology, writing – review & editing, funding acquisition.

### Notes

The authors declare no competing financial interest.

### ACKNOWLEDGMENT

This study was supported by the Spanish Ministry of Science, and Innovation (MICINN, RTI2018-096410-B-C21). A. L.-U. acknowledges MICINN for a predoctoral grant (BES-2016-078137)

We thank Dr. J. Bustamante Munguira from Hospital Clinico Universitario de Valladolid (Spain) for his invaluable help and the access to the blood samples and B. Glahn-Martínez for helpful discussions.

### REFERENCES

- (1) Allison, A. C.; Eugui, E. M. Immunosuppressive and Other Effects of Mycophenolic Acid and an Ester Prodrug, Mycophenolate Mofetil. *Immunol Rev* **1993**, *136* (1), 5–28.

- (2) Naffouje, R.; Grover, P.; Yu, H.; Sendilnathan, A.; Wolfe, K.; Majd, N.; Smith, E. P.; Takeuchi, K.; Senda, T.; Kofuji, S.; Sasaki, A. T. Anti-Tumor Potential of IMP Dehydrogenase Inhibitors: A Century-Long Story. *Cancers* **2019**, *11* (9), 1346.
- (3) Kaplan, B. Mycophenolic Acid Trough Level Monitoring in Solid Organ Transplant Recipients Treated with Mycophenolate Mofetil: Association with Clinical Outcome. *Current Medical Research and Opinion* **2006**, *22* (12), 2355–2364.
- (4) Bentley, R. Mycophenolic Acid: A One Hundred Year Odyssey from Antibiotic to Immunosuppressant. *Chem. Rev.* **2000**, *100* (10), 3801–3826.
- (5) Renner, U. D.; Thiede, C.; Bornhäuser, M.; Ehninger, G.; Thiede, H.-M. Determination of Mycophenolic Acid and Mycophenolate Mofetil by High-Performance Liquid Chromatography Using Postcolumn Derivatization. *Anal. Chem.* **2001**, *73* (1), 41–46.
- (6) Łuszczynska, P.; Pawiński, T.; Kunicki, P. K.; Sikorska, K.; Marszałek, R. Free Mycophenolic Acid Determination in Human Plasma Ultrafiltrate by a Validated Liquid Chromatography-Tandem Mass Spectrometry Method. *Biomed Chromatogr* **2017**, *31* (10).
- (7) Gao, X.; Tsai, R. Y. L.; Ma, J.; Bhupal, P. K.; Liu, X.; Liang, D.; Xie, H. Determination and Validation of Mycophenolic Acid by a UPLC-MS/MS Method: Applications to Pharmacokinetics and Tongue Tissue Distribution Studies in Rats. *J. Chromatogr. B* **2020**, *1136*, 121930.
- (8) Rebollo, N.; Calvo, M. V.; Martín-Suárez, A.; Domínguez-Gil, A. Modification of the EMIT Immunoassay for the Measurement of Unbound Mycophenolic Acid in Plasma. *Clin. Biochem.* **2011**, *44* (2–3), 260–263.
- (9) Dasgupta, A.; Tso, G.; Chow, L. Comparison of Mycophenolic Acid Concentrations Determined by a New PETINIA Assay on the Dimension EXL Analyzer and a HPLC-UV Method. *Clin. Biochem.* **2013**, *46* (7–8), 685–687.
- (10) Prémaud, A.; Rousseau, A.; Picard, N.; Marquet, P. Determination of Mycophenolic Acid Plasma Levels in Renal Transplant Recipients Co-Administered Sirolimus: Comparison of an Enzyme Multiplied Immunoassay Technique (EMIT) and Liquid Chromatography-Tandem Mass Spectrometry. *Ther. Drug Monit.* **2006**, *28* (2), 274–277.
- (11) Glahn-Martínez, B.; Benito-Peña, E.; Salis, F.; Descalzo, A. B.; Orellana, G.; Moreno-Bondi, M. C. Sensitive Rapid Fluorescence Polarization Immunoassay for Free Mycophenolic Acid Determination in Human Serum and Plasma. *Anal. Chem.* **2018**, *90* (8), 5459–5465.
- (12) Peltomaa, R.; Benito-Peña, E.; Barderas, R.; Moreno-Bondi, M. C. Phage Display in the Quest for New Selective Recognition Elements for Biosensors. *ACS Omega* **2019**, *4* (7), 11569–11580.

- (13) Hua, X.; Zhou, L.; Feng, L.; Ding, Y.; Shi, H.; Wang, L.; Gee, S. J.; Hammock, B. D.; Wang, M. Competitive and Noncompetitive Phage Immunoassays for the Determination of Benzothiostrubin. *Anal. Chim. Acta* **2015**, *890*, 150–156.
- (14) Liu, Z.; Liu, J.; Wang, K.; Li, W.; Shelver, W. L.; Li, Q. X.; Li, J.; Xu, T. Selection of Phage-Displayed Peptides for the Detection of Imidacloprid in Water and Soil. *Anal. Biochem.* **2015**, *485*, 28–33.
- (15) Woo, M.-K.; Heo, C.-K.; Hwang, H.-M.; Ko, J.-H.; Yoo, H.-S.; Cho, E.-W. Optimization of Phage-Immobilized ELISA for Autoantibody Profiling in Human Sera. *Biotechnol Lett* **2011**, *7*.
- (16) Dong, J.-X.; Xu, C.; Wang, H.; Xiao, Z.-L.; Gee, S. J.; Li, Z.-F.; Wang, F.; Wu, W.-J.; Shen, Y.-D.; Yang, J.-Y.; Sun, Y.-M.; Hammock, B. D. Enhanced Sensitive Immunoassay: Noncompetitive Phage Anti- Immune Complex Assay for the Determination of Malachite Green and Leucomalachite Green. *J. Agric. Food Chem.* **2014**, *7*.
- (17) Kim, H.-J.; Ahn, K. C.; González-Techera, A.; González-Sapienza, G. G.; Gee, S. J.; Hammock, B. D. Magnetic Bead-Based Phage Anti-Immuno-complex Assay (PHAIA) for the Detection of the Urinary Biomarker 3-Phenoxybenzoic Acid to Assess Human Exposure to Pyrethroid Insecticides. *Anal. Biochem.* **2009**, *8*.
- (18) Peltomaa, R.; Agudo-Maestro, I.; Más, V.; Barderas, R.; Benito-Peña, E.; Moreno-Bondi, M. C. Development and Comparison of Mimotope-Based Immunoassays for the Analysis of Fumonisin B1. *Anal. Bioanal. Chem.* **2019**, *411* (26), 6801–6811.
- (19) Zou, X.; Chen, C.; Huang, X.; Chen, X.; Wang, L.; Xiong, Y. Phage-Free Peptide ELISA for Ochratoxin A Detection Based on Biotinylated Mimotope as a Competing Antigen. *Talanta* **2016**, *146*, 394–400.
- (20) Wouters, S. F. A.; Vugs, W. J. P.; Arts, R. Bioluminescent Antibodies through Photoconjugation of Protein G–Luciferase Fusion Proteins. *Bioconjugate Chem.* **2020**, *31* (3) 656–662.
- (21) NanoLuc® Luciferase: One Enzyme, Endless Capabilities <https://www.promega.es/resources/technologies/nanoluc-luciferase-enzyme/> (accessed 2021 -01 -25).
- (22) Tullila, A.; Nevanen, T.K.. Utilization of Multi-Immunization and Multiple Selection Strategies for Isolation of Hapten-Specific Antibodies from Recombinant Antibody Phage Display Libraries. *IJMS* **2017**, *18* (6), 1169.
- (23) Hall, M. P.; Unch, J.; Binkowski, B. F.; Valley, M. P.; Butler, B. L.; Wood, M. G.; Otto, P.; Zimmerman, K.; Vidugiris, G.; Machleidt, T.; Robers, M. B.; Benink, H. A.; Eggers, C. T.; Slater, M. R.; Meisenheimer, P. L.; Klaubert, D. H.; Fan, F.; Encell, L. P.; Wood, K. V. Engineered Luciferase Reporter from a Deep Sea Shrimp Utilizing a Novel Imidazopyrazinone Substrate. *ACS Chem. Biol.* **2012**, *7* (11), 1848–1857.

(24) High Efficiency Transformation Protocol  
<https://international.neb.com/protocols/0001/01/01/high-efficiency-transformation-protocol-c2987> (accessed 2021 -01 -25).

(25) Masseyeff, R. F.; Albert, W. H. W. (Winfried H. W. ); Staines, N. *Methods of Immunological Analysis*; Weinheim, Germany : VCH Verlagsgesellschaft ; New York, NY (USA) : VCH Publishers, 1992.

(26) Findlay, J. W. A.; Dillard, R. F. Appropriate Calibration Curve Fitting in Ligand Binding Assays. *AAPS J* **2007**, *9* (2), E260–E267.

(27) Bentley, R. Mycophenolic Acid: A One Hundred Year Odyssey from Antibiotic to Immunosuppressant. *Chem. Rev.* **2000**, *100* (10), 3801–3826.

(28) Ting, L. S. L.; Partovi, N.; Levy, R. D.; Riggs, K. W.; Ensom, M. H. H. Pharmacokinetics of Mycophenolic Acid and Its Phenolic-Glucuronide and Acyl Glucuronide Metabolites in Stable Thoracic Transplant Recipients: *Ther. Drug Monit.* **2008**, *30* (3), 282–291.



## Supporting Information

### Experimental

#### Antibody Coupling to Magnetic Beads

Recombinant anti-MPA Fab, previously described by Tullila and Nevanen,<sup>1</sup> was conjugated to carboxylated paramagnetic beads. Briefly, 4.5 mg of beads were suspended in 150  $\mu\text{L}$  of buffer A (100  $\text{mmol L}^{-1}$  sodium phosphate, pH 6.8, 1  $\text{mol L}^{-1}$  NaCl, 20% EtOH) and vortexed. The beads were washed three times with water and resuspended in 750  $\mu\text{L}$  of 100  $\text{mmol L}^{-1}$   $\text{CoCl}_2$ . The reaction was incubated for 30 min at room temperature in shaking and subsequently the beads were washed five times with buffer B (20  $\text{mmol L}^{-1}$  sodium phosphate, pH 7.0, 0.5  $\text{mol L}^{-1}$  NaCl). Then, the beads were mixed with anti-MPA (1 mg of anti-MPA per 2 mg of beads in a total volume of 1 mL) in PBS buffer, and the solution was incubated overnight at +4 °C under rotation. After collecting the beads and aspirating the buffer, 1 mL of 0.03%  $\text{H}_2\text{O}_2$  in milli-Q water was added to the suspension and incubated for 4 h at room temperature under rotation. Finally, the beads were washed twice with buffer B and stored at +4 °C in the same buffer. Success of the immobilization of the anti-MPA Fab fragments onto the magnetic beads was confirmed by bead ELISA using MPA-alkaline phosphatase enzyme conjugate and para-Nitrophenylphosphate as a substrate for the detection.<sup>21</sup> A total of 260  $\mu\text{g}$  of anti-MPA Fab fragment was bound to the magnetic beads.

#### Antibody Biotinylation

Anti-MPA Fab antibody (anti-MPA)<sup>1</sup> was biotinylated using EZ-Link Sulfo-NHS-LC-Biotin, according to the manufacturer's instructions,<sup>2</sup> using a 3 $\times$  molar excess of Sulfo-NHS-LC-Biotin in comparison to the antibody. Purification was carried out with Illustra NAP-5 columns according to the manufacturer's instructions.

#### Synthetic Peptide-Based ELISA

The amino acid sequence of clone A2 was identified by DNA sequencing and the biotinylated peptide with the sequence A(CEGLYAHWC)GGGSK(Bio)- $\text{NH}_2$  was synthesized at Peptide Synthetics (Fareham, UK). The two C's were bound by a disulfide bridge. GGGs was included in the sequence as a linker, the same as in the phage of origin, and biotin was included in the side chain of C-terminal lysine residue.

In order to optimize the conditions of the assay, a checkerboard-type titration was performed using different concentrations of the biotinylated peptide A2 (A2-bio) and anti-MPA. Briefly, 100  $\mu\text{L}$  of different concentrations of A2-bio (ranging from 0.05 to 5  $\mu\text{g mL}^{-1}$ ) dissolved in assay buffer were added to neutravidin-coated clear plates blocked with SuperBlock and incubated during 30 min at room temperature. After washing the wells 3 times with PBS, 100  $\mu\text{L}$  of a solution containing different concentrations of non-biotinylated anti-MPA (ranging from 0.05 to 5  $\mu\text{g mL}^{-1}$ ) in the presence and absence of 16  $\text{ng mL}^{-1}$  of free MPA (anti-MPA and MPA previously incubated for 15 min at room temperature) in assay buffer were added to the wells and incubated for 30 min at room temperature. Once the plates were washed, HRP-conjugated anti-IgG monoclonal antibody (0.27  $\mu\text{g mL}^{-1}$  in assay buffer; 80  $\mu\text{L}$  per well) was added and incubated for

30 min at room temperature followed by a washing step. Then, 80  $\mu\text{L}$  of TMB was added to the solution, and after 1 min the reaction was stopped with 2 mol  $\text{L}^{-1}$   $\text{H}_2\text{SO}_4$ . The absorbance at 450 nm was measured with a CLARIOstar microplate reader

For comparison purposes, a bead-based assay was also developed using a similar strategy as the bead-based assay for the phage-displayed peptide with slight modifications. In this case, 100  $\mu\text{L}$  of a 0.1  $\mu\text{g mL}^{-1}$  bio-A2 solution were added to the neutravidin-functionalized beads solution as described before. After a 30-min incubation and a similar washing step, 100  $\mu\text{L}$  of a solution containing 0.5  $\mu\text{g mL}^{-1}$  of anti-MPA and different concentrations of free MPA, previously incubated during 10 min, were added to the beads and incubated for another 30 min. After washing, an anti-IgG-HRP antibody was added, incubated 30 min and washed thereafter. Finally, 80  $\mu\text{L}$  of Amplex UltraRed was added and the fluorescence was monitored as described above.

### SPR Measurements

The binding experiments using Biacore T200 instrument (Cytiva, formerly GE Healthcare Life Sciences) and Sensor Chip CM5 with carboxymethylated dextran matrix (Cytiva) were performed at +25 °C. EDC/NHS chemistry was used according to manufacturer's instructions to immobilize anti-mycophenolic acid Fab fragment on active surface (flow channel 2) and anti-ochratoxin A (OTA) Fab fragment on reference surface (flow channel 1). As running buffer, 1 $\times$  PBS-P (20 mmol  $\text{L}^{-1}$  phosphate buffer, 2.7 mmol  $\text{L}^{-1}$  KCl, 0.137 mol  $\text{L}^{-1}$  NaCl, 0.05% P20, Cytiva) was used. Seven serially diluted concentrations (0, 0.12, 4.9, 19.5, 78.1, 312.5 and 1250 nmol  $\text{L}^{-1}$ ) of cyclic peptide or mycophenolic acid (Sigma-Aldrich, St. Louis, MO, USA) in 1 $\times$  PBS-P were injected at a flow rate of 20  $\mu\text{L min}^{-1}$  for 2 min. After dissociation phase of 5 min, regeneration was done with 10 mmol  $\text{L}^{-1}$  NaOH 0.05% P20 (contact time 60 s, flow rate: 30  $\mu\text{L min}^{-1}$ ) followed by stabilization period of 60 s. All samples were analyzed in replicates. The results were analyzed with the Evaluation T200 -software with a 1:1 Langmuir binding model.

### RRLC-DAD Method

The optimized separation of the three metabolites was performed in gradient elution mode, yielding a resolution ( $R_s$ ) higher than 2.0 and with retention times (rt) of 5.7, 8.8 and 12.0 min for MPAG, Acyl-MPAG and MPA respectively. The rt were reproducible between runs. **Figure S7** shows a chromatogram of a standard mixture of the metabolites. The three metabolites were quantified using an internal standard (MPA-LuciferYellow) calibration model using a nine-point calibration curve, with a concentration range (0.5–80 ng  $\text{mL}^{-1}$  for MPA; 50–15000 ng  $\text{mL}^{-1}$  for MPAG and 12–250 ng  $\text{mL}^{-1}$  for Acyl-MPAG) for the three metabolites. The  $r^2$  value for standard curves was >0.99 for all compounds tested.

### Blood Sample Treatment

To isolate the plasma, blood samples from five different transplanted patients under different treatments (T1–T5) and three healthy patients (H1–H3) were centrifuged at 2000 g for 15 min at room temperature. The supernatant was then transferred to a 1.5 mL tube and 500  $\mu\text{L}$  of that supernatant were added to ultrafiltration 3K Amicon Ultra tubes, previously rinsed with PBST, and centrifuged at 12,045 g for 30 min. The ultrafiltered

plasma samples were kept at  $-20\text{ }^{\circ}\text{C}$  until analyzed. Free MPA was analyzed in plasma samples after a 1:8 dilution in SuperBlock + 0.05% T20.

For the RRLC-DAD analysis, 1000  $\mu\text{L}$  of acetonitrile were added to the ultrafiltered plasma samples and vortexed for 5 minutes at 1000 rpm. The samples were then centrifuged at 12045 g for 10 minutes and the supernatant was transferred to a new tube. The supernatant was evaporated up to circa 30  $\mu\text{L}$  and it was reconstituted in a final volume of 150  $\mu\text{L}$  PBST acidified with 0.4% TFA (final concentration).

## Results

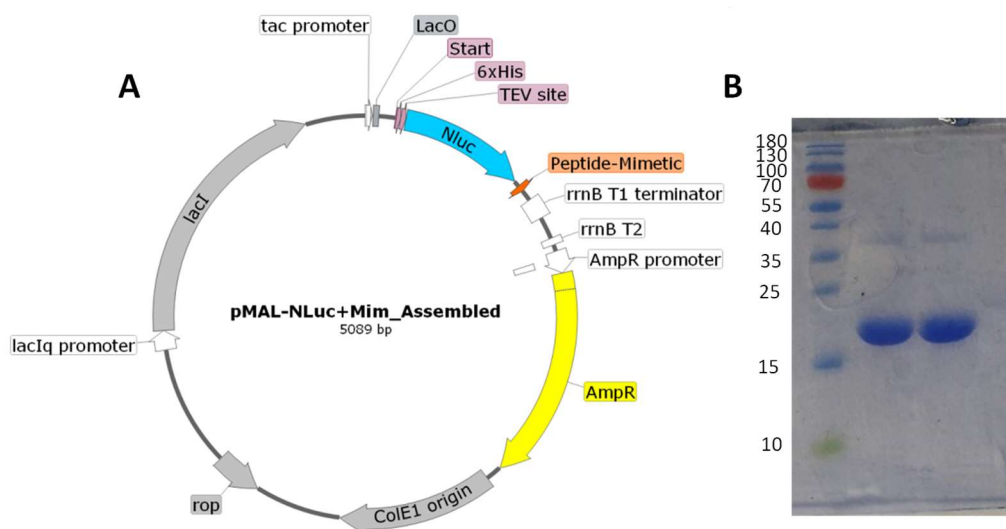


**Figure S1.** Construction of the NanoLuc-peptide mimetic fusion. (A) Scheme of the fusion protein construct with its main features. (B) SDS-PAGE analysis of the purified fusion protein with Coomassie brilliant blue protein staining: lane 1, molecular marker (Thermo Scientific™ PageRuler™ Prestained Protein Ladder, 10 to 180 kDa); 2, purified product with a 5-minute boiling step at  $+95\text{ }^{\circ}\text{C}$ ; 3, purified fusion protein without a boiling step. The thickest band corresponds to the molecular weight of the fusion protein (22 kDa).

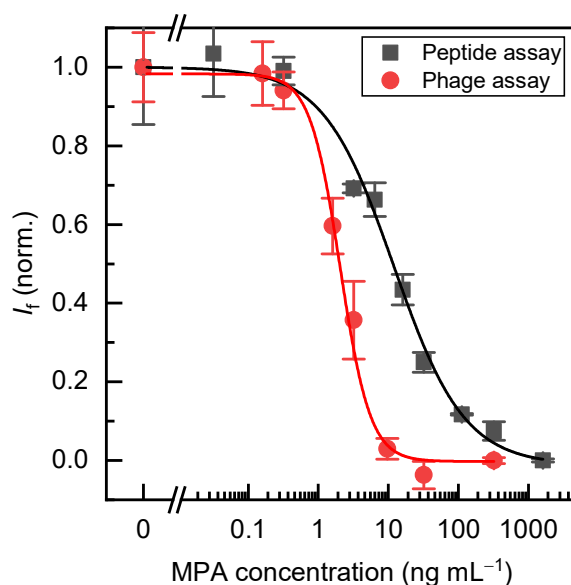


**Figure S2.** Bead-based immunoassays with the phage clone A2 (red) and the synthetic biotinylated peptide mimetic (black). In both cases, neutravidin-functionalized magnetic beads were used. The fluorescent substrate was also the same in both cases. Fluorescence signals ( $\lambda_{\text{ex}} = 530 \text{ nm}$ ,  $\lambda_{\text{em}} = 590 \text{ nm}$ ) were measured after adding the Amplex UltraRed substrate. The results are shown as the normalized mean values  $\pm$  the standard error of the mean ( $n = 3$ ) with a logistic fit (OriginPro 2019).

**Table S1.** Kinetic constants determined for anti-MPA (14) Fab interaction with MPA, and cyclic peptide (A2) measured by BIAcore. The values present the averages ( $\pm$  SE) obtained with seven analyte (MPA or cyclic peptide (A2)) concentrations.

	<b>Association rate constant <math>k_a</math> (1/Ms)</b>	<b>Dissociation rate constant <math>k_d</math> (1/s)</b>	<b>Affinity constant <math>K_D</math> (M)</b>
MPA	$(1.846 \pm 0.009) \times 10^6$	$0.0741 \pm 0.0004$	$4.016 \times 10^{-8}$
Cyclic peptide (A2)	$(4.06 \pm 0.02) \times 10^5$	$0.583 \pm 0.001$	$1.434 \times 10^{-6}$

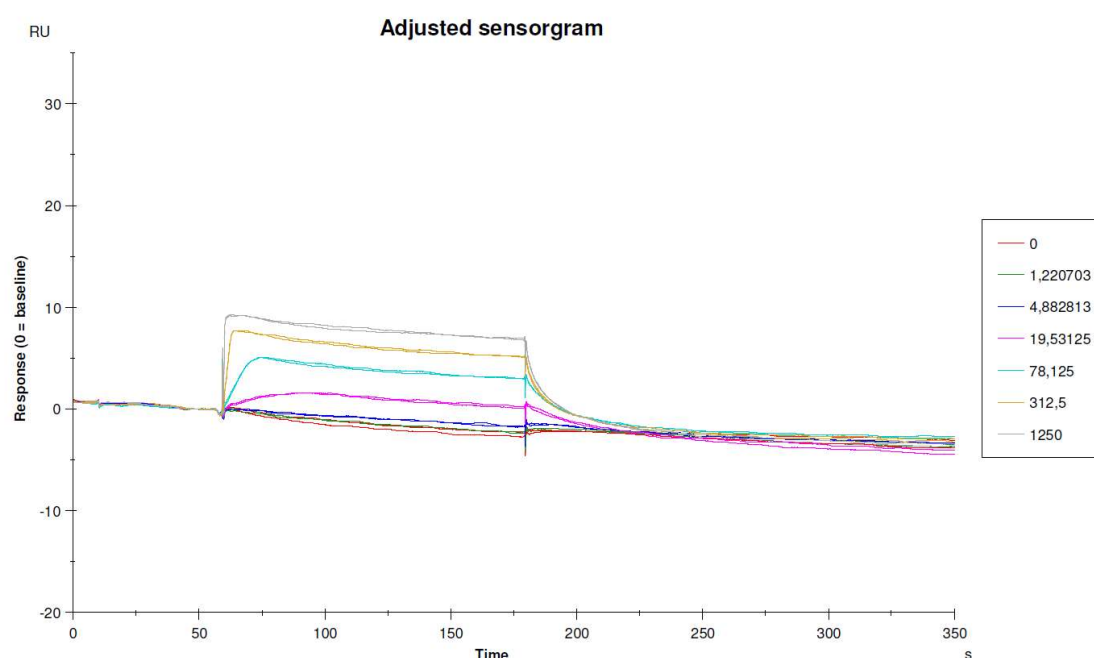


**Figure S3.** Sensorgrams presenting mycophenolic acid (MPA) interaction with anti-MPA Fab fragment using Biacore T200. The colors indicate different nanomolar concentrations of MPA.

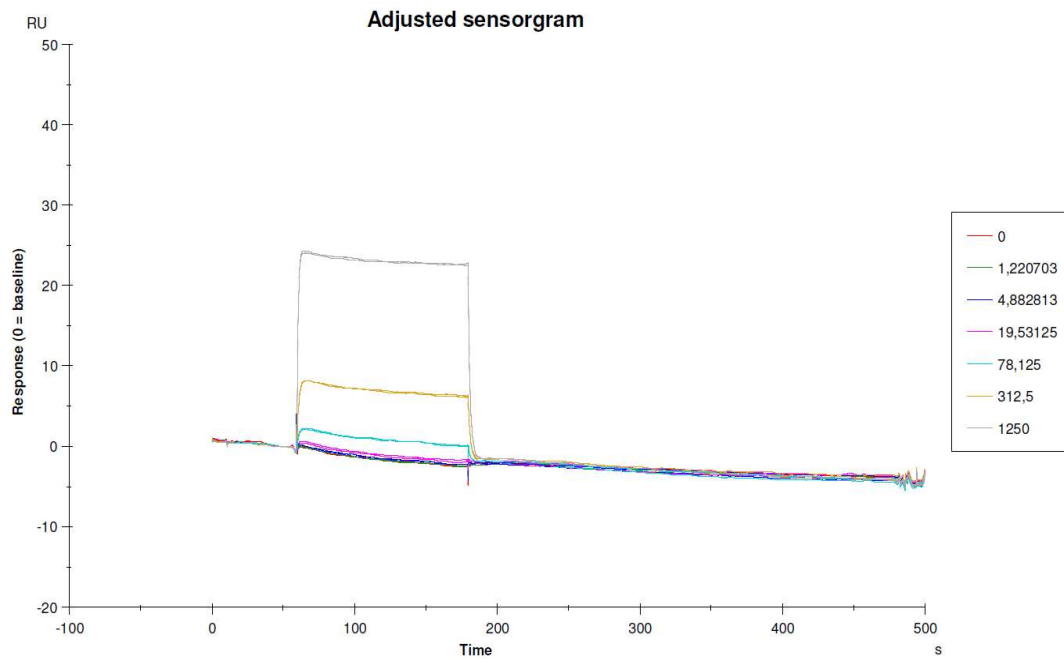


**Figure S4.** Sensorgrams presenting cyclic peptide interaction with anti-MPA Fab fragment using Biacore T200. The colors indicate different nanomolar concentrations of cyclic peptide.

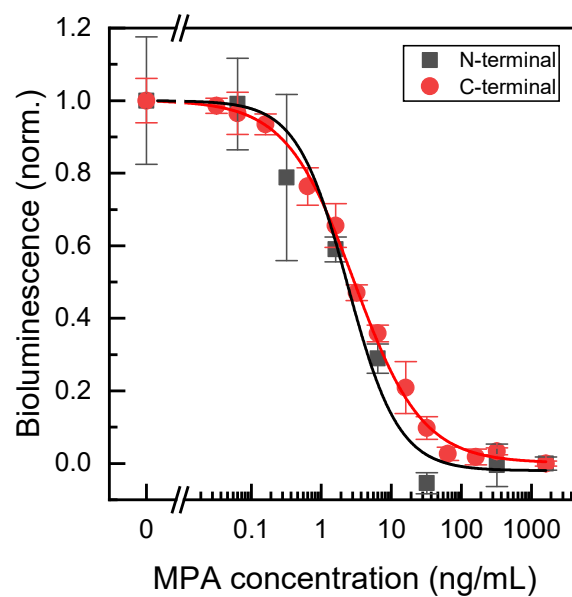


**Figure S5.** Calibrate comparison between the N-terminal (NanoLuc-A2) and the C-terminal (A2-Nanoluc) fusions, under the same assay conditions described in the main text. The results are shown as the normalized mean values  $\pm$  the standard error of the mean ( $n = 3$ ) with a logistic fit (OriginPro 2019).

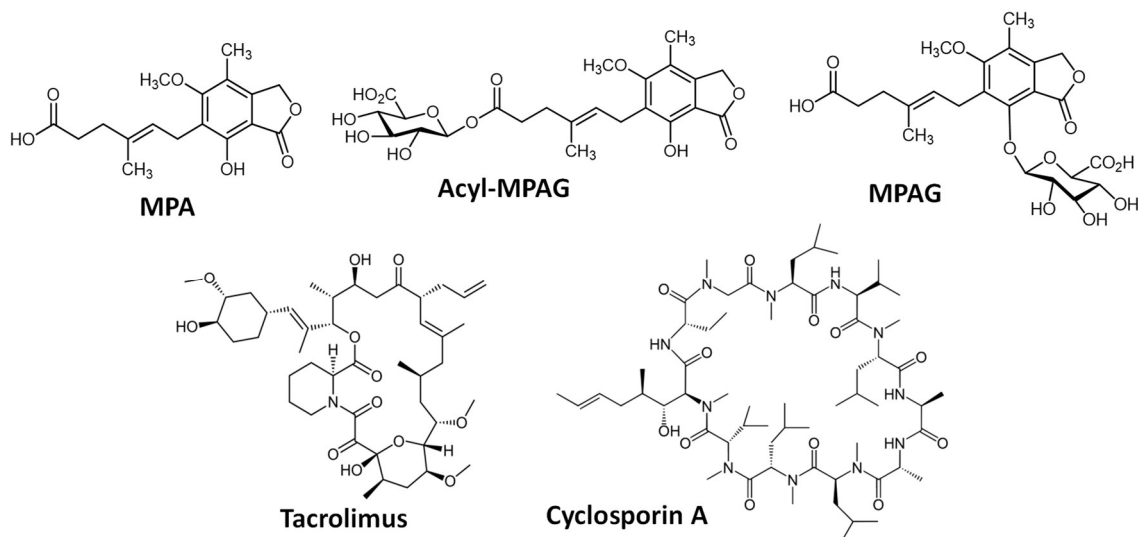


**Figure S6.** Chemical structures of mycophenolic acid (MPA), its two main metabolites, (Acyl-MPAG and MPAG) and two immunosuppressant drugs commonly co-administered to transplanted patients (Tacrolimus and Cyclosporin A).

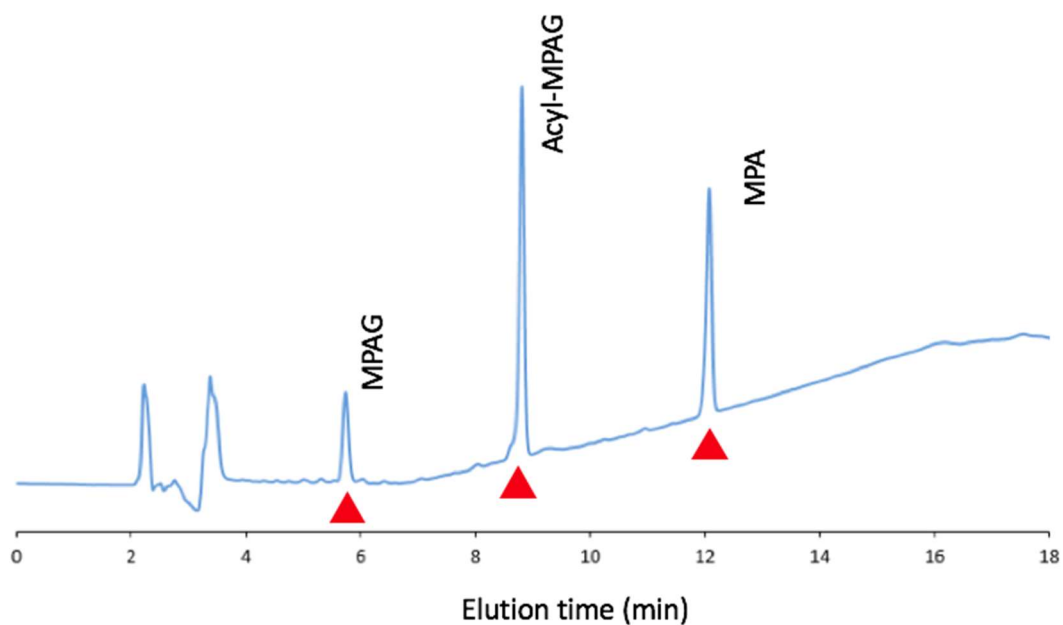


**Figure S7.** HPLC elution profile of MPA and its metabolites MPAG and acyl-MPAG. Standard solution of MPA prepared at  $80 \text{ ng mL}^{-1}$ ; and MPAG, acyl-MPAG prepared at  $250 \text{ ng mL}^{-1}$ .

**Table S2.** Assays comparison for the detection of MPA.

Method	Assay format	Detect	LOD (ng mL <sup>-1</sup> )	Dynamic range (ng mL <sup>-1</sup> )	Ref.
EMIT 2000 MPA	Homogeneous	Total	<i>n.d.</i>	100–15000	Siemens
CEDIA MPA	Homogeneous	Total	<i>n.d.</i>	300–10000	Thermo Scientific
Roche total MPA (EMIT)	Homogeneous	Total	300	400–15000	Roche
EMIT	Homogeneous	Free	1	10–1250	(3)
PETINIA	Homogeneous	Total	<i>n.d.</i>	200–30000	(4)
FPIA	Homogeneous	Free	3.2	6.8–156	(5)
ELISA	Heterogeneous	-	<i>n.d.</i>	<i>n.d.</i>	(1)
UPLC MS/MS	-	Total	70	200–30000	(6)
HPLC-UV	-	Free	4	60–1000	(7)
HPLC-FLD	-	Total Free	8 <i>n.d.</i>	50–40000 5–1000	(8)
Peptide-Nanoluc	Heterogeneous	Free	0.26	0.64–14	This work
Peptide-Based	Heterogeneous	Free	0.94	2.4–60	This work
Phage-Based	Heterogeneous	Free	0.69	1.0–4.1	This work

*n.d.* not determined

**Table S3.** MPAG concentration levels found in the analyzed samples.

Samples	Average, µg/mL	SD, µg/mL	Remarks
T1	1.7	0.0	< LOQ (Biosensor)
T2	12.7	1.3	< LOQ (Biosensor)
T3	4.2	0.2	< LOQ (Biosensor)
T4	4.1	0.6	< LOQ (Biosensor)
T5	0.13	0.2	<LOD (RRLC)
H1	0.02	0.1	<LOD (RRLC)
H2	0.02	0.1	<LOD (RRLC)
H3	-0.04	0.0	<LOD (RRLC)

**Table S4.** Administered doses of MPA to the analyzed transplanted patients

Patient	Administered drug	Dose
T1	Myfortic	360 mg/12 h
T2	Myfortic	360 mg/12 h
T3	Myfortic	180 mg/8 h
T4	Myfortic	180 mg/8 h
T5	Myfortic	180 mg/8 h

## References

- (1) Tullila, A.; Nevanen, T. Utilization of Multi-Immunization and Multiple Selection Strategies for Isolation of Hapten-Specific Antibodies from Recombinant Antibody Phage Display Libraries. *IJMS* **2017**, *18*, 1169.
- (2) EZ-Link™ Sulfo-NHS-LC-Biotin, formato No-Weigh™ <https://www.thermofisher.com/order/catalog/product/A39257> (accessed Jan 25, 2021).
- (3) Rebollo, N.; Calvo, M. V.; Martín-Suárez, A.; Domínguez-Gil, A. Modification of the EMIT Immunoassay for the Measurement of Unbound Mycophenolic Acid in Plasma. *Clin Biochem* **2011**, *44*, 260–263.
- (4) Dasgupta, A.; Tso, G.; Chow, L. Comparison of Mycophenolic Acid Concentrations Determined by a New PETINIA Assay on the Dimension EXL Analyzer and a HPLC-UV Method. *Clin Biochem* **2013**, *46*, 685–687.
- (5) Glahn-Martínez, B.; Benito-Peña, E.; Salis, F.; Descalzo, A. B.; Orellana, G.; Moreno-Bondi, M. C. Sensitive Rapid Fluorescence Polarization Immunoassay for Free Mycophenolic Acid Determination in Human Serum and Plasma. *Anal Chem* **2018**, *90*, 5459–5465.
- (6) Reséndiz-Galván, J. E.; Romano-Aguilar, M.; Medellín-Garibay, S. E.; Milán-Segovia, R. del C.; Chevaile-Ramos, A.; Romano-Moreno, S. Determination of Mycophenolic Acid in Human Plasma by Ultra-performance Liquid Chromatography-Tandem Mass Spectrometry and Its Pharmacokinetic Application in Kidney Transplant Patients. *Biome Chromatogr* **2019**, *33*.
- (7) Aresta, A.; Palmisano, F.; Zambonin, C. G.; Schena, P.; Grandaliano, G. Simultaneous Determination of Free Mycophenolic Acid and Its Glucuronide in Serum of Patients under Mycophenolate Mophetil Therapy by Ion-Pair Reversed-Phase Liquid Chromatography with Diode Array UV Detection. *J Chromatogr B* **2004**, *810*, 197–202.
- (8) Shen, J.; Jiao, Z.; Yu, Y.-Q.; Zhang, M.; Zhong, M.-K. Quantification of Total and Free Mycophenolic Acid in Human Plasma by Liquid Chromatography with Fluorescence Detection. *J Chromatogr B* **2005**, *817*, 207–213.



## Comparative Study of the Performance of Two Different Luciferases for the Analysis of Fumonisin B<sub>1</sub> in Wheat Samples

Álvaro Luque-Uría<sup>[a]</sup>, Riikka Peltomaa<sup>[a][b]</sup>, Marina Navarro-Duro<sup>[a]</sup>, Sabrina Fikacek<sup>[a]</sup>, Trajen Head<sup>[c]</sup>, Sapna Deo<sup>[c]</sup>, Sylvia Daunert<sup>[c]</sup>, Elena Benito-Peña<sup>\*[a]</sup>, María C. Moreno-Bondi<sup>\*[a]</sup>

[a] A. Luque-Uría, Dr. R. Peltomaa, M. Navarro-Duro, S. Fikacek, Prof. E. Benito-Peña, Prof. M.C. Moreno-Bondi

Department of Analytical Chemistry  
Faculty of Chemistry, Complutense University of Madrid  
Ciudad Universitaria s/n, 28040 Madrid, Spain  
E-mail: elenabp@quim.ucm.es, mcmbondi@ucm.es

[b] Dr. R. Peltomaa  
Department of Life Technologies, Turku Collegium for Science, Medicine and Technology, TCSMT  
University of Turku  
Kilnamyllynkatu 10, 20520, Turku, Finland

[c] Dr. Trajen Head, Prof. Sapna Deo, Prof. S. Daunert  
Department of Biochemistry and Molecular Biology, Miller School of Medicine; University of Miami Clinical and Translational Science Institute  
University of Miami  
Miami, FL 33136, USA

ACCEPTED ARTICLE.

Analysis and Sensing (Wiley)

**Abstract:** The development of two different immunoassays for the determination of fumonisin B<sub>1</sub> in wheat samples is reported. A previously described mimopeptide for fumonisin B<sub>1</sub> (FB<sub>1</sub>) was used to produce fusion proteins in combination with two different luciferases: Gaussia luciferase (GLuc) and NanoLuc luciferase (NLuc). The production, expression and the development of two immunoassays based on these fusion proteins (A2-GLuc and A2-NLuc) is detailed. The assay showing the best performance, A2-NLuc, with a limit of detection of 0.61 ng mL<sup>-1</sup> and a dynamic range from 1.9 to 95 ng mL<sup>-1</sup>, was employed for the analysis of spiked wheat samples, a reference matrix material, as well as naturally contaminated wheat samples. The recoveries obtained in the spiked samples were acceptable, between 81.5 and 109%, with relative standard deviations lower than 14%. The analysis of naturally contaminated wheat was validated by a liquid chromatography coupled to tandem mass detection method.

### Introduction

Enzymes and fluorescent proteins are considered of great importance for many optical applications, including fluorescent imaging and immunoassay development. Despite the great applicability of fluorescent proteins in current research, enzymes are considered the most prevalent in sensing applications.<sup>[1,2]</sup> High sensitivities can be obtained with their use as it has been estimated that, under optimal pH, ionic strength and temperature conditions, a single enzyme molecule is able to convert up to 10<sup>7</sup> molecules of its corresponding substrate per minute.<sup>[3]</sup>

Luciferases are a specific type of enzymes that have been considered of utmost relevance over the last years. They are able to catalyze reactions that emit light, and are currently applied in highly relevant fields, such as food testing, diagnostics or drug screening.<sup>[4,5]</sup> Two of the smallest luciferases currently known are Gaussia luciferase (GLuc) and NanoLuc luciferase (NLuc), with a size of only 19.9 kDa and 19 kDa, respectively. These two luciferases offer an exceptional performance in protein–protein interactions or bioluminescence resonance energy transfer (BRET) immunoassays, as they are considered two of the brightest luciferases yet discovered.<sup>[6–8]</sup>

Fumonisin is a mycotoxin produced as secondary metabolites by several *Fusarium* species, such as *F. verticillioides* and *F. proliferatum*, two common pathogens found in some cereals, maize, wheat, and sorghum.<sup>[9,10]</sup> Fumonisin was reported and characterized back in 1988, and among the different metabolites found in this group, fumonisin B<sub>1</sub> (FB<sub>1</sub>) is the most prevalent one.<sup>[11,12]</sup> Fumonisin poses a dangerous health risk for both humans and animals, as they have been reported to cause equine leukoencephalomalacia,<sup>[13]</sup> porcine pulmonary edema,<sup>[14]</sup> and in humans, fumonisin has been associated with esophageal cancer, neural tube defects and nephrotoxicity.<sup>[10,15,16]</sup> Due to their high risk, the detection of fumonisin in foodstuff is of great importance. In fact, some of the most eminent international authorities regarding food safety, such as the European Commission and the US Food and Drug Administration (FDA), have set maximum limits of these mycotoxins in a variety of foodstuff.<sup>[17,18]</sup>

Traditional chromatographic methods, especially those based on mass spectrometry detection (LC-MS/MS), have been extensively applied to the determination of fumonisin in a wide variety of matrices.<sup>[19–25]</sup> Despite the fact that these methods offer sensitive determinations ( $\mu\text{g Kg}^{-1}$  level using triple quadrupole analyzers)<sup>[26]</sup> in a wide variety of matrices, in many cases they suffer from matrix effects, requiring extensive sample preparation and chromatographic optimization to reduce them to a minimum.<sup>[26]</sup>

As an alternative, fast screening methods, such as immunoassays, have proven to give reliable results providing high sensitivity (limits of detection in the microgram per kilogram detection levels) in cereal samples (Table S1),<sup>[26,27]</sup> at a substantially reduced cost and in a lesser time. Epitope-mimicking peptides, also known as mimopeptides or mimotopes, have become a successful tool to avoid the main limitations of tedious antigen conjugations and its potential toxicity to the user. Mimopeptides have the intriguing ability to bind to the same antibody paratope as the corresponding antigen and establish a competition for its binding sites.<sup>[28]</sup> A broad variety of mimopeptides have been obtained by phage display technology.<sup>[29]</sup> Among them, mimopeptides have been obtained for some of the most ubiquitous mycotoxins, such as aflatoxin, fumonisin B<sub>1</sub>, ochratoxin A, or deoxynivalenol.<sup>[30–33]</sup> The potential of bioconjugating mimopeptides to optical labels such as the aforementioned luciferases, GLuc and NLuc, has opened a great scope of sensing possibilities.

This work aims for a closer comparison of these two fascinating luciferases in the development of a bioluminescent immunoassay for the detection of FB<sub>1</sub> in wheat samples. For this aim, the construction of two different fusion proteins, A2-GLuc and A2-NLuc, in combination with a previously reported mimopeptide for FB<sub>1</sub> is detailed. Then, the analytical characteristics of both fusion proteins is tested and compared. Finally, the best bioluminescent system was chosen for the analysis of fumonisin in wheat samples, validating the results with a chromatographic-based method.

## Results and Discussion

### A2-GLuc and A2-NLuc expression and purification

The construction of the recombinant fusion proteins was based on the bioluminescent GLuc and NLuc proteins in combination with a fumonisin B<sub>1</sub> mimopeptide, A2, previously obtained by phage display.<sup>[31]</sup> To carry out the expression of the fusion proteins (A2-GLuc and A2-NLuc), the plasmids were transformed into different *E. coli* cells. In the case of the A2-GLuc fusion protein, Shuffle cells were utilized because the GLuc contains disulfide bonds that ought to be formed in an oxidizing environment. An especially important indication to point out in the expression of the A2-GLuc fusion

protein is that this expression was carried out at 15 °C. Low temperature was critical due to the fact that higher temperatures led to the protein aggregation and consequent denaturation, obtaining dissatisfactory results. On the other hand, the A2-NLuc needed no formation of disulfide bonds, and therefore BL21 cells were used. In this case, the expression was successfully conducted at 37 °C for 4 h. Once both fusion proteins were purified, the correct expression was confirmed by SDS-PAGE (Figure S1). As can be seen, the molecular mass obtained on both cases was in accordance with the theoretical values of 63748 g mol<sup>-1</sup> for A2-GLuc, due to the presence of the maltose binding protein (MBP) and 22982 g mol<sup>-1</sup> for A2-NLuc since the fusion protein was not expressed in combination with the MBP.

### Bioluminescent characterization and kinetics of the fusion proteins

The bioluminescent nature of the fusion proteins was confirmed after the addition of the respective substrates, coelenterazine for A2-GLuc and furimazine or NanoGLO for A2-NLuc. As can be observed in **Figure 1**, the kinetics observed for each of the luciferases vary significantly. On the one hand, the A2-GLuc fusion protein experiences a remarkably fast kinetics, decreasing the bioluminescence signal by a third of the original value in just one minute. On the opposite site, the A2-NLuc presents a much slower reaction kinetics, with a similar decrease of the signal in more than five minutes after the bare substrate (furimazine in PBS) was added. Moreover, the Nano-GLO™ Luciferase Assay Reagent provided a glow-like kinetics, avoiding any flash consumption of the reagent and increasing the time of the bioluminescent signal more than two times with respect to the bare substrate. Taking these results into account, the assay using the A2-GLuc fusion protein was carried out with the help of a controlled injection of the substrate inside the microplate reader for a higher reproducibility and sensitivity of the assay. However, this was not necessary in the case of the A2-NLuc when the Nano-GLO substrate was used.

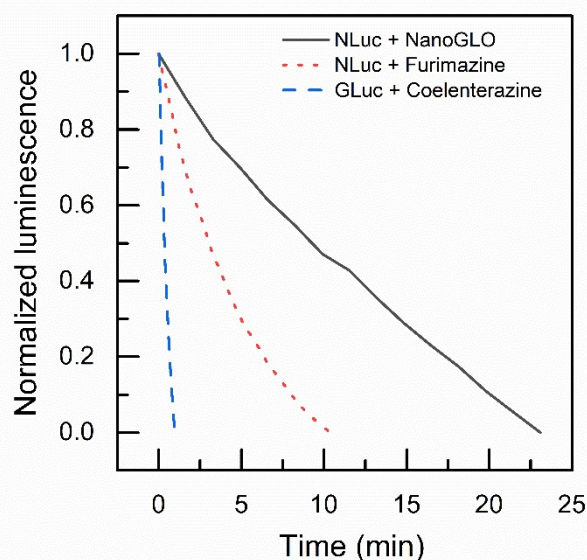


**Figure 1.** Kinetic curves for A2-GLuc (blue dashed line), A2-NLuc with furimazine (red dotted line) and A2-NLuc with NanoGLO reagent (black straight line). To obtain these curves, 50 µL of each substrate (coelenterazine for A2-GLuc and furimazine or NanoGLO for A2-NLuc) were added to a solution of 50 µL of each fusion protein. Different concentrations of the fusion proteins were tested in the experiment, obtaining similar results for all of them. The graphs represent the normalized bioluminescence of three replicates.

## Assay optimizations

It has been previously reported that the immunoassay sensitivity can be improved if the antibody is immobilized on the surface of magnetic beads, instead of coating it directly to a well plate.<sup>[34]</sup> This was the main reason why the assay was developed using protein G-coupled magnetic beads to immobilize the antibody. Prior to that, the competition step was established in solution between the free FB<sub>1</sub> and the corresponding fusion protein for the binding sites of the antibody (**Figure 2**).

A checkerboard titration was conducted for the A2-GLuc fusion protein varying the antibody and fusion protein concentration, for a fixed magnetic bead concentration of 0.1 mg mL<sup>-1</sup>, in the absence and presence of free FB<sub>1</sub>. In order to obtain the optimal concentrations for the immunoassay, the maximum signals obtained in the absence of free FB<sub>1</sub> were compared to those signals obtained in the presence of 10 µg mL<sup>-1</sup> free FB<sub>1</sub>. The best maximum/minimum signal ratio was chosen for the development of the immunoassay. The best ratio was obtained for a total antibody amount of 100 ng per well and a concentration of 3 µg mL<sup>-1</sup> fusion protein (**Figure S2**).

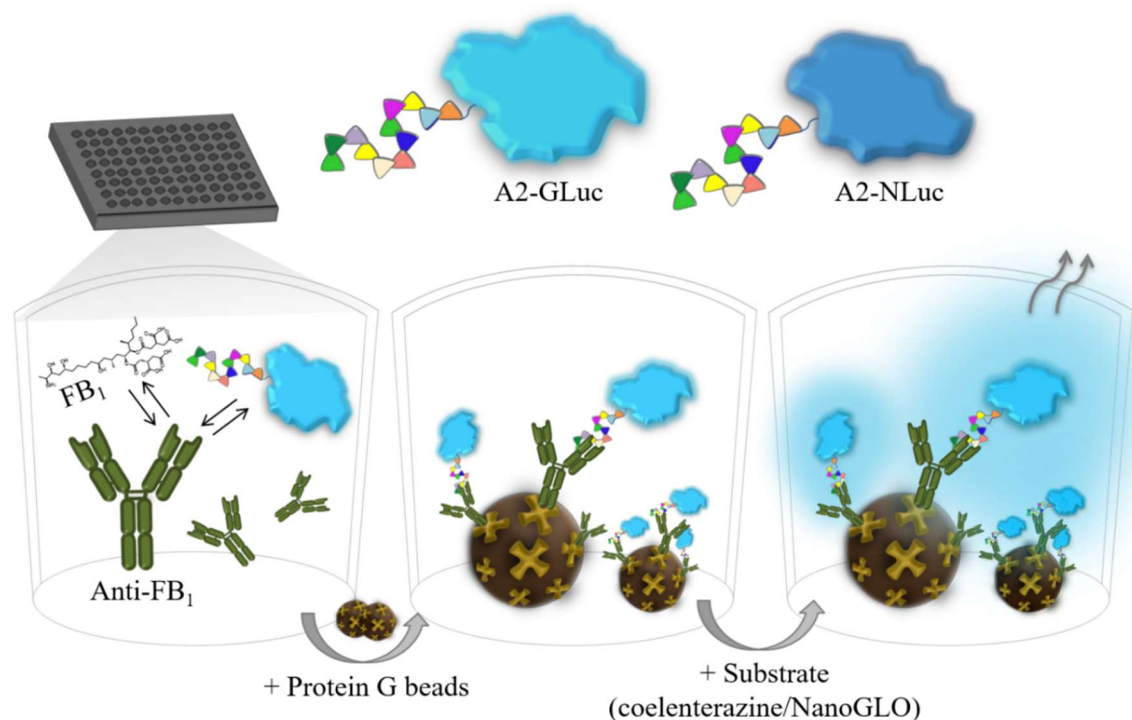


**Figure 2.** Scheme of the bioluminescent immunoassay. On black microtiter wells, competition between free FB<sub>1</sub> and the fusion protein (either A2-GLuc or A2-NLuc) for the binding sites of the anti-FB<sub>1</sub> antibody is established in solution. Then, protein G-coated magnetic beads are added to capture the formed immunocomplex. After a washing step using a magnetic support to retain the beads, the corresponding substrate is added (coelenterazine for GLuc and furimazine for NLuc) and the bioluminescence is measured on a microplate reader.

With reference to the A2-NLuc fusion protein, a much higher concentration of the fusion protein was needed to obtain measurable bioluminescence signals. Taking into account the lower molecular weight of the A2-NLuc fusion protein in comparison to the A2-GLuc, it would be expected that a lower concentration of the protein would provide similar results. However, based on the experimental trials, it was determined that the molar concentration of the A2-NLuc fusion protein needed to be almost 10 times higher than that of the A2-GLuc. In this case, once the fusion protein concentration was optimized, a checkerboard titration was carried out varying the antibody and magnetic

bead concentration, for a concentration of  $8.5 \mu\text{g mL}^{-1}$  A2-NLuc. In this case, the best ratio was observed for a total antibody amount of 100 ng per well, similar to the A2-GLuc assay, and a bead concentration of  $12.5 \mu\text{g mL}^{-1}$  (Figure S3).

### Bioluminescent-based immunoassays

Once the conditions for each of the fusion proteins were optimized, the bioluminescent-based immunoassays were conducted for both of them. Figure 3 shows the calibration curves for both fusion proteins in the presence of increasing concentrations of FB<sub>1</sub>. As can be observed, both the A2-GLuc and A2-NLuc provide a great analytical performance, but their behavior was not exactly the same.

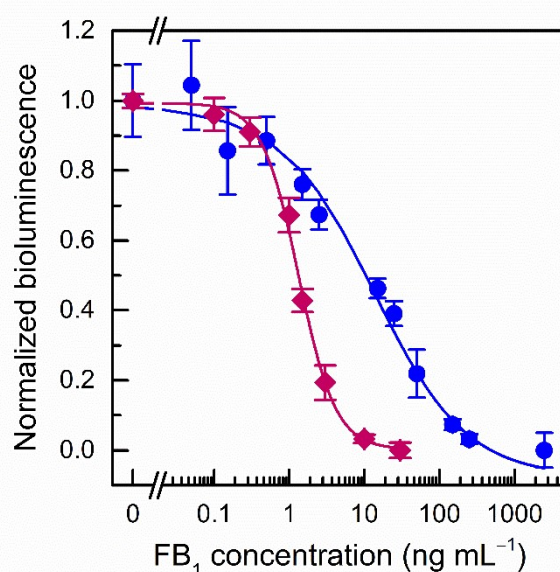


**Figure 3.** Bead-based bioluminescent immunoassays for the determination of FB<sub>1</sub> in assay buffer using A2-GLuc (purple diamonds) and A2-NLuc (blue circles) fusion protein. In both cases, a competition was established between FB<sub>1</sub> and the fusion protein containing the FB<sub>1</sub> mimopeptide for the binding sites of the antibody. Then, magnetic beads were added to collect the antibody in solution. The bioluminescence (total luminescence for A2-GLuc,  $\lambda_{em} = 470 \pm 40$  nm for A2-NLuc) was measured after the addition of each substrate. The bioluminescence values were normalized to the maximum and minimum values. The results show the mean values  $\pm$  the standard error of the mean ( $n = 3$ ) adjusted to a logistic fit using OriginPro 2019 software.

**Table 21** **Table 1** provides a comparison of the main analytical characteristics of the two different assays described for the determination of FB<sub>1</sub>. The A2-GLuc assay provided an IC<sub>50</sub> of  $1.34 \text{ ng mL}^{-1}$  and a limit of detection (LOD), taken as the 10% inhibition,<sup>[35]</sup> of  $0.38 \text{ ng mL}^{-1}$ . The dynamic range, calculated as the 20–80% inhibition,<sup>[36]</sup> for the bead-based approach for A2-GLuc was between  $0.6$  and  $2.9 \text{ ng mL}^{-1}$ . However, the results of the bead-based approach utilizing the A2-NLuc fusion protein proved a much wider dynamic range, of almost two orders of magnitude, with a relatively similar LOD as the A2-GLuc approach. The A2-GLuc presents a good reproducibility, with relative standard deviations (RSD) of 7.4 % in average ( $n = 3$ ) for intra-day determinations and 15.5 % for the inter-day assays on 3 different days. The A2-NLuc provides an average intra-day RSD of 9.0 % ( $n = 3$ ) and 15.9 % for the inter-day assays on 3 different days. The implementation of magnetic beads allowed a competition between the free FB<sub>1</sub> and the fusion protein for the binding sites of the antibody, for a later capture of the antibody with the magnetic beads. This approximation reduces the number of washing steps in

comparison to any other plate-based method. When comparing these results to other methods described in the bibliography, the bioluminescent-based immunoassays described here present higher sensitivities than most of the immunoassays previously described, and are within the most sensitive methods applied to the analysis of real samples (**Table S1**).

**Table 1.** Analytical characteristics of the immunoassays for FB<sub>1</sub>.

Fusion protein	IC <sub>50</sub> [ng mL <sup>-1</sup> ]	LOD <sup>[a]</sup> [ng mL <sup>-1</sup> ]	DR <sup>[b]</sup> [ng mL <sup>-1</sup> ]
A2-GLuc	1.3 ± 0.1	0.38 ± 0.09	0.61–2.9
A2-NLuc	13.5 ± 1.7	0.61 ± 0.18	1.91–95.2

<sup>[a]</sup> Limit of Detection (taken as 10% inhibition) <sup>[b]</sup> Dynamic range (taken as 20–80% inhibition)

### Cross reactivity evaluation

The specificity of each of the bead-based immunoassays for the determination of FB<sub>1</sub> was assessed with several mycotoxins that could be potentially present in the same food samples. The response curves are represented in **Figure 4**, and the results can be observed in **Table S2**. It is noted that for both cases, the FB<sub>2</sub> presents a cross reactivity of circa 100%, with the remaining toxins evaluated proving a negligible cross reactivity in the immunoassay. The high cross reactivity of FB<sub>2</sub> is associated to the extremely similar structure between both fumonisins. The antibody used in this case could not differentiate between them. Therefore, the assays could be implemented for the determination of the total amount of fumonisin in the analyzed samples.

### Sample analysis

#### Matrix effect

In order to implement the immunoassays to the analysis of wheat samples, the matrix effect was tested with different percentages of wheat extract in the assay. To carry out these experiments, a non-contaminated wheat sample was utilized. The extraction procedure was conducted according to a previously reported method, in which a mixture of acetonitrile/water/acetic acid (79/20/1, v/v) was used.<sup>[37]</sup> As can be observed, only low percentages of the extract, 5% in both cases, could give a similar response in the immunoassay with negligible interferences (**Figure 5**). Higher concentrations of the extract severely interfered with the immunoassay, mainly because of the high percentage of acetonitrile. Due to the similarities in the cross reactivity and matrix effect, the immunoassay with the A2-NLuc fusion protein was chosen for the analysis of real samples due to the wider dynamic range and similar LOD in comparison with the A2-GLuc fusion protein. The LOD calculated for the analysis of FB<sub>1</sub> in wheat samples was 80 µg kg<sup>-1</sup>, whereas the LOQ was 276 µg kg<sup>-1</sup>.

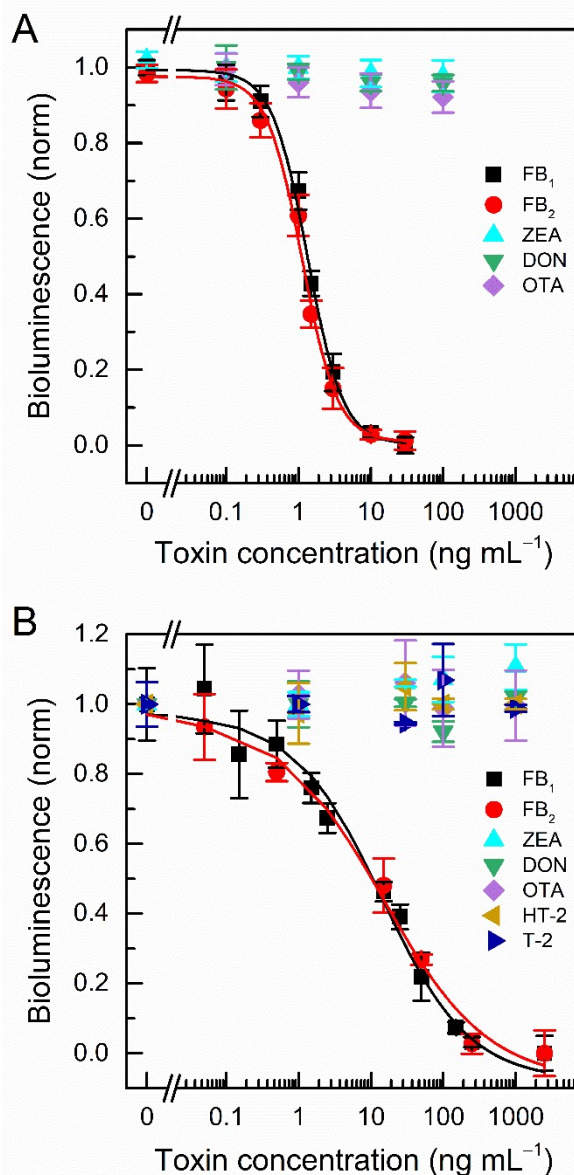


**Figure 4.** Cross reactivity evaluation for the bead-based immunoassay with (A) A2-GLuc and (B) A2-NLuc. Some of the most abundant mycotoxins which can be found in combination with fumonisin were tested in the immunoassay under identical experimental conditions. The results were normalized to the maximum and minimum values. The results show the average values ( $n = 3$ )  $\pm$  the standard error of the mean and they were adjusted to a logistic fit using OriginPro 2019.

### Analysis of wheat samples

The bioluminescent assay using the A2-NLuc fusion protein was applied to the analysis of spiked wheat samples, a wheat reference material and naturally contaminated wheat samples. First, the blank wheat quality control material extracts were spiked with ranging concentrations of FB<sub>1</sub> from 200 to 1800 ng mL<sup>-1</sup> (corresponding to 1000 to 8000  $\mu$ g kg<sup>-1</sup>). These spiked samples were analyzed according to the developed immunoassay and the results are shown in **Table 2**. As can be seen, mean recoveries of 81–109% were obtained for the different spiked samples analyzed, with the corresponding RSD ranging from 3% to 14%. The assay was applied to the analysis of a

wheat reference material with a total fumonisin certified value of  $86431 \pm 25900 \mu\text{g kg}^{-1}$ , and the results confirmed that there were not significant differences at a 95% confidence level with the optimised method, obtaining a total fumonisin value of  $80000 \pm 20000 \mu\text{g kg}^{-1}$  ( $n = 3$ ).

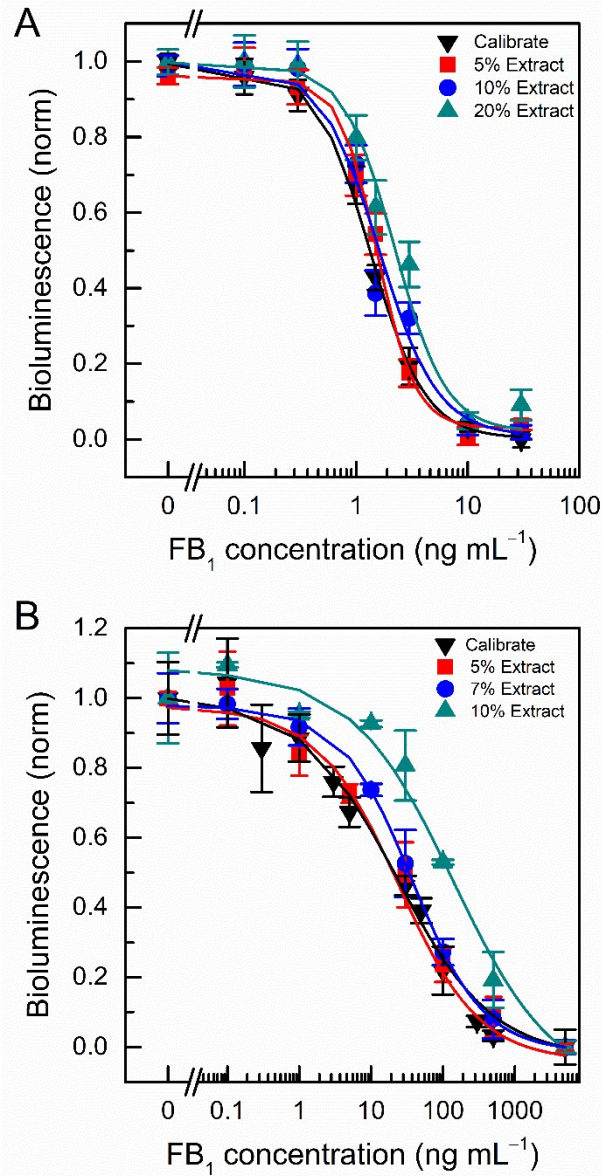


**Figure 5.** Matrix effect evaluation for the bead-based immunoassay with (A) A2-GLuc and (B) A2-NLuc. Different calibrate curves in the presence of a certain percentage of wheat extract were compared to a calibrate in assay buffer. The bioluminescence results were normalized to the maximum and minimum signals. The results are shown as the mean bioluminescence  $\pm$  the standard error of the mean ( $n = 3$ ). The calibrate curves were adjusted to a sigmoidal fit with OriginPro 2019.



**Table 2.** Analysis of spiked wheat samples with FB<sub>1</sub>

Spiked [ng mL <sup>-1</sup> ]	Measured [ng mL <sup>-1</sup> ]	Recovery [%]	RSD <sup>[a]</sup> [%]
1600	1482	92.6	8.0
1200	1056	88.0	4.6
1000	815	81.5	9.8
400	430	107	14
200	217	109	3.2

<sup>[a]</sup> Relative Standard Deviation

Finally, eight wheat samples were analyzed, following the same extraction protocol, and the results were validated by an HPLC-MS/MS reference method. The results appear on **Table 3**. It can be seen that the majority of the wheat samples analyzed contained a very low total fumonisin concentration which could not be quantified by the immunoassay. However, some of the samples contained enough analyte to be detected by the immunoassay, proving that it presented enough sensitivity to detect fumonisin in wheat samples at levels well below the regulatory limits for fumonisin in maize (1000 µg kg<sup>-1</sup> for direct human consumption), since it has not been established yet maximum levels for wheat samples.<sup>[38]</sup> All these results demonstrate that the bioluminescent method can be efficiently applied to the analysis of contaminated wheat samples.

**Table 3.** Analysis of real samples and validation by HPLC-MS/MS reference method

Sample	Fumonisin concentration (sd) <sup>[a]</sup>	
	[µg kg <sup>-1</sup> ]	
	Immunoassay	HPLC-MS/MS
1	< LOD	< LOQ
2	< LOD	42.6 (1.4)
3	< LOQ	82.7 (1.3)
4	493 (32)	526 (36)
5	< LOD	< LOQ
6	409 (11)	402 (28)
7	< LOQ	291 (5.6)
8	1475 (53)	1512 (2.6)

<sup>[a]</sup> Standard Deviation

## Conclusions

This work reports the development of competitive bioluminescent immunoassays for the determination of fumonisin in wheat samples. Two different bioluminescent proteins, GLuc and NLuc, were expressed in combination with the FB<sub>1</sub> mimopeptide previously obtained. The recombinant nature of both fusion proteins can guarantee an unlimited source as well as a fixed stoichiometry of the components of the fusion protein, greatly reducing batch-to-batch variations. It was proven that both luciferases presented different kinetics when the corresponding substrate was added. On the one hand, the GLuc fusion protein presented a flash kinetics, whereas the NLuc showed a more glow-type kinetics, especially if the NanoGLO substrate was added instead of the bare substrate diluted in PBS. The glow-type luminescence allows an extended luminescence and permits a longer measuring time than a flash-type luminescence.

A bead-based immunoassay was conducted for both fusion proteins, A2-GLuc and A2-NLuc. The implementation of a bead-based immunoassay offers faster analysis in comparison to plate-based methods in which the antibody needs to be immobilized onto the well plates. Both fusion proteins proved a reproducible, selective and sensitive detection of fumonisin at very low concentrations. However, the dynamic range obtained using the A2-GLuc was much narrower than that of the A2-NLuc possibly due to the lower amount of fusion protein added to the immunoassay. Once it was proven that the matrix effect was negligible at 5% extract concentration, the A2-NLuc fusion protein was used for the analysis of wheat samples, obtaining satisfactory results. Therefore, it can be concluded that the favorable analytical performance obtained makes the developed immunoassay a very useful tool for a fast and sensitive analysis of fumonisin in wheat samples. Further work will be aimed to the implementation of bioluminescent immunoassays in different food matrixes and for a wider scope of analytes for a development of multiplexing analysis.

## Experimental Section

### Materials

Phusion Hot Start II DNA Polymerase, high-fidelity DNA Polymerase, Blocker™ Casein (in PBS), LB Broth Lennox, Dynabeads Protein G, 96 flat well chimney base black plates and Pierce Centrifuge Columns were from Thermo Fisher Scientific (Waltham, MA, USA). PCR Nucleotide Mix was obtained from Roche Diagnostics (Basel, Switzerland). HisTrap™ FF crude columns, Sephadex™ G-25 M columns and Illustra NAP-5 columns were purchased from Cytiva. (Chicago, IL, USA). Phosphate buffer saline (PBS), pH 7.4, Tween 20, dimethyl sulfoxide (≥99.5%), ampicillin, kanamycin, protease inhibitor cocktail, SDS gel preparation kit, Amicon Ultra 3K centrifugal filters, isopropyl-β-d-thiogalactopyranoside (IPTG), D-(+)-maltose monohydrate, KOD Xtreme Hot Start Master Mix and the mycotoxin zearalenone were from Sigma-Aldrich (Saint Louis, MO, USA). Fumonisin B<sub>1</sub>, fumonisin B<sub>2</sub>, HT-2 toxin, T-2 toxin, deoxynivalenol, and ochratoxin A were acquired from Fermentek Ltd. (Jerusalem, Israel). LB Agar and bovine serum albumin were from NZYtech (Lisbon, Portugal). Imidazole was purchased from Alfa Aesar (Maverhill, MA, USA). PCR primers were procured from Integrated DNA Technologies, Inc (San Diego, CA, USA). Shuffle Express Competent and BL21 Competent *E. coli* cells and amylose resin were obtained from New England Biolabs (Ipswich, MA, USA). The anti-fumonisin monoclonal antibody was purchased from BioTez (Berlin, Germany). NanoGLO® Reagent for Immunoassay was from Promega Corporation (Madison, WI, USA), furimazine was purchased from Aobious (Gloucester,

MA, USA) and the native coelenterazine was acquired from NanoLight Technology (Pinetop, AZ, USA). The blank wheat quality control material was from Romer Labs (Getzersdorf, Austria) and the wheat reference matrix material was acquired from Aokin (Berlin, Germany).

### Construction of the GLuc and NanoLuc fusion proteins

The expression of a previously characterized fumonisin mimopeptide, A2 (VTPNDDTFDPFR) with GLuc bioluminescent protein was carried out through an amplification of the pColdI-GLuc vector,<sup>[39]</sup> using KOD Xtreme Hot Start Master Mix. Both the DNA encoding for the mimopeptide A2 and a GS-linker were added to the 5'-end of GLuc, and a polyhistidine tag was incorporated to the 3'-end in three sequential PCR reactions with the primers that are shown in **Table S3**. The final PCR product was subcloned at the NdeI and BamHI sites of the pMAL-c5X expression vector.

With reference to the expression of the A2 mimopeptide together with NanoLuc, an amplification of the later one was conducted from the ATG-42 commercial vector,<sup>[40]</sup> using Phusion Hot Start II DNA Polymerase. Similar to the previous case, the DNA sequence encoding for the fumonisin mimopeptide (VTPNDDTFDPFR) was included in pQE vector in the 5'-end of NanoLuc, whereas a polyhistidine tag was added to the 3'-end using the corresponding primers from **Table S3**.

### Expression and purification of the fusion protein

To express the GLuc-tagged fumonisin mimopeptide (A2-GLuc), the plasmid was initially transformed into Shuffle NEB Express Competent cells. A single colony containing was selected from an LB agar plate supplemented with 100  $\mu\text{g mL}^{-1}$  ampicillin to inoculate a 5 mL preculture of LB medium with 100  $\mu\text{g mL}^{-1}$  ampicillin which was previously grown overnight at 37 °C and 250 rpm. The overnight preculture was expanded the following day to a main culture of 180 mL solution of LB with 100  $\mu\text{g mL}^{-1}$  ampicillin. The main culture was grown at 37 °C and 200 rpm until an optical density at 600 nm (OD<sub>600</sub>) of 0.7 was achieved. At that point, the protein expression was induced with the addition of IPTG to the main culture at a final concentration of 1 mmol L<sup>-1</sup>. The culture was allowed to grow for 4 h at 15 °C and 175 rpm and then, the cells were collected by centrifugation at 5,000 g and 4 °C for 10 min. The pellet was then resuspended in 10 mL lysis buffer (50 mmol L<sup>-1</sup> Tris-HCl pH 8.7, 150 mmol L<sup>-1</sup> NaCl) containing 5 % (v/v) protease inhibitor cocktail. The mixture was frozen at -80 °C overnight, and the following day the cells were lysed by sonication on ice during 10 min doing 10 s on/off cycles. The insoluble cell debris was discarded by centrifugation at 12,000 g and 4 °C for 20 min, and the supernatant was filtered through a 0.45  $\mu\text{m}$  filter. Then, the lysate was purified with amylose resin. For this, the clarified lysate was mixed with 1 mL of the amylose resin and incubated 30 min at room temperature and slow shaking. The resin was then collected on a Pierce Centrifuge Column and washed with 10 column volumes of lysis buffer. The purified protein was eluted from the column with lysis buffer supplemented with 10 mmol L<sup>-1</sup> maltose. The protein was stored at 4 °C for several weeks.

A similar protocol with some modifications was conducted for the expression of the NLuc-tagged fumonisin mimopeptide (A2-NLuc). Briefly, a plasmid containing the fusion of the NanoLuc and the fumonisin mimopeptide was transformed into E. coli BL21 Competent cells. A single colony was picked from LB agar plates containing

50  $\mu\text{g mL}^{-1}$  kanamycin and was grown overnight on a 15 mL LB preculture supplemented with 50  $\mu\text{g mL}^{-1}$  kanamycin. The following day, an aliquot of the aforementioned preculture was transferred to a 200 mL LB culture with 50  $\mu\text{g mL}^{-1}$  kanamycin and grown at 37 °C and 180 rpm until an OD<sub>600</sub> of 0.6 was reached. To induce the expression, a final concentration of 0.4  $\text{mmol L}^{-1}$  IPTG was added to the culture, and it was grown for 4 h at 37 °C and 180 rpm. Next, the culture was centrifuged at 5000 g for 10 min at 4 °C to collect the cells, and the pellet was resuspended in NZY Bacterial Cell Lysis supplemented with protease inhibitor cocktail, NZY Lysozyme and DNase I according to the manufacturer's instructions. The cells were subsequently sonicated on ice for 10 min doing 10 s on/off cycles, and the insoluble cell debris was separated by centrifugation at 15000 g for 15 min at 4 °C. The purification of the cell lysate was carried out with HisTrap™ purification columns and Sephadex™ G-25 M columns were utilized afterwards to change the buffer to PBS. The purified A2-NLuc fusion protein was stored at -20 °C for several weeks. The purity of all the fusion proteins was verified by SDS-PAGE analysis, and the concentration was determined by measuring the absorbance at 280 nm with a Nanodrop spectrophotometer.

## **Optimization of the assay conditions for each luciferase**

### **Consideration of kinetics**

A total of 50  $\mu\text{L}$  of the fusion protein, either A2-GLuc or A2-NLuc, were added to a 96-well black plate. The bioluminescence was measured immediately after the addition of 50  $\mu\text{L}$  of the substrates in PBS buffer, coelenterazine for GLuc and furimazine or NanoGLO for NLuc, on a CLARIOstar microplate reader.

### **Optimized immunoassays for FB<sub>1</sub>**

#### **Bead-based assay with immobilized antibody**

A checkerboard-type titration was carried out to evaluate the optimal concentrations of the antibody and fusion protein on the immunoassay for A2-GLuc. However, for A2-NLuc, the fusion protein concentration was initially optimized and then a checkerboard-type titration evaluated the optimal concentrations of antibody and magnetic beads.

#### **A2-GLuc**

Black microtiter plates were blocked with 200  $\mu\text{L}$  Casein for 1 h at 37 °C and then, rinsed thrice with washing buffer (137  $\text{mmol L}^{-1}$  NaCl, 2.7  $\text{mmol L}^{-1}$  KCl, 10  $\text{mmol L}^{-1}$  Na<sub>2</sub>HPO<sub>4</sub>, 1.8  $\text{mmol L}^{-1}$  KH<sub>2</sub>PO<sub>4</sub>, 0.05% T20, pH 7.4). Varying concentrations of free FB<sub>1</sub>, from 0 to 100  $\text{ng mL}^{-1}$  in assay buffer (PBS supplemented with 0.05% T20 and 0.1% BSA, pH 7.4), were mixed with a solution of 3  $\mu\text{g mL}^{-1}$  A2-GLuc and 1.66  $\mu\text{g mL}^{-1}$  of antibody per well. The mixture was incubated for 1 h at room temperature and slow shaking and subsequently 40  $\mu\text{L}$  of a solution of protein G beads were added to the wells for a final concentration of 0.1  $\text{mg mL}^{-1}$ . After incubation for 30 min, the wells were washed thrice with an automatic washer under a magnet. Finally, the bioluminescence was measured immediately after the addition of 50  $\mu\text{L}$  of a solution of 2.0  $\mu\text{g mL}^{-1}$  coelenterazine in PBS.

## A2-NLuc

Black microtiter plates were blocked with 200  $\mu\text{L}$  Casein for 1 h at room temperature. After rinsing the plate three times with washing buffer, varying concentrations of free  $\text{FB}_1$ , from 0 to 2500  $\text{ng mL}^{-1}$  in assay buffer were added to the wells containing 8.5  $\mu\text{g mL}^{-1}$  of A2-NLuc and 1.66  $\mu\text{g mL}^{-1}$  of antibody per well in a total volume of 60  $\mu\text{L}$ . The mixture was incubated for 1 h at room temperature and slow shaking and then, 40  $\mu\text{L}$  of a solution of 0.31  $\text{mg mL}^{-1}$  of protein G beads in assay buffer were added to each well and incubated for 30 min at room temperature and slow shaking. The wells were then washed thrice with an automatic washer under a magnet and finally, the bioluminescence was measured after the addition of 60  $\mu\text{L}$  of a solution of NanoGLO reagent. For the cross reactivity tests, the  $\text{FB}_1$  concentration was replaced with other mycotoxins at ranging concentrations between 1 and 1000  $\text{ng mL}^{-1}$ .

## Sample analysis and spiking

Wheat samples were collected in an Experimental Field and a Flour Company. Fumonisin extraction was carried out following a method previously described by Krska et al.<sup>[37]</sup> with some modifications. Briefly, 5 mL of a mixture containing acetonitrile/water/acetic acid (79/20/1 v/v/v) were added to 1 g of wheat sample. The samples were gently shaken for 60 min at room temperature and then centrifuged for 15 min at 15000 g. The supernatant was filtered with a 0.22  $\mu\text{m}$  filter and conveniently diluted in assay buffer prior to the analysis.

For the analysis of spiked samples, different concentrations of  $\text{FB}_1$  were added to the wheat extract and conveniently diluted to carry out the analysis.

## Acknowledgements

This study was supported by the Spanish Ministry of Science, and Innovation (MICINN, RTI2018-096410-B-C21). A.L.U. acknowledges MICINN for a predoctoral grant (BES-2016-078137). Prof. Belen Patiño from the Department of Biology (Universidad Complutense of Madrid) is gratefully acknowledged for providing the wheat samples analyzed in this work.

**Keywords:** Bioluminescence • Fumonisin B1 • Fusion Proteins • Immunoassays • Luciferases

- [1] O. V. Stepanenko, O. V. Stepanenko, D. M. Shcherbakova, I. M. Kuznetsova, K. K. Turoverov, V. V. Verkhusha, *Biotechniques* 2011, 51, 313–314, 316, 318 passim.
- [2] S. Sakamoto, Y. Shoyama, H. Tanaka, S. Morimoto, *Adv. Biosci. Biotechnol.* 2014, 5, 557–563.
- [3] D. Wild, Ed., *The Immunoassay Handbook: Theory and Applications of Ligand Binding, ELISA, and Related Techniques*, Elsevier, Oxford ; Waltham, MA, 2013.
- [4] A. Fleiss, K. S. Sarkisyan, *Curr. Genet.* 2019, 65, 877–882.
- [5] Á. Luque-Uría, R. Peltomaa, T. K. Nevanen, H. O. Arola, K. Iljin, E. Benito-Peña, M. C. Moreno-Bondi, *Anal. Chem.* 2021, 93, 10358–10364.

- [6] T. Rathnayaka, M. Tawa, S. Sohya, M. Yohda, Y. Kuroda, *Biochim. Biophys. Acta Prot. Proteom.* 2010, 1804, 1902–1907.
- [7] N. Wu, T. Rathnayaka, Y. Kuroda, *Biochim. Biophys. Acta Prot. Proteom.* 2015, 1854, 1392–1399.
- [8] C. G. England, E. B. Ehlerding, W. Cai, *Bioconjug. Chem.* 2016, 27, 1175–1187.
- [9] S. Goyal, K. G. Ramawat, J.-M. Mérillon, in *Fungal Metabolites* (Eds.: J.-M. Mérillon, K.G. Ramawat), Springer International Publishing, Cham, 2017, pp. 1–29.
- [10] M. Kamle, D. K. Mahato, S. Devi, K. E. Lee, S. G. Kang, P. Kumar, *Toxins (Basel)* 2019, 11, 328.
- [11] W. C. Gelderblom, K. Jaskiewicz, W. F. Marasas, P. G. Thiel, R. M. Horak, R. Vlegaar, N. P. Kriek, *Appl. Environ. Microbiol.* 1988, 54, 1806–1811.
- [12] S. C. Bezuidenhout, W. C. A. Gelderblom, C. P. Gorst-Allman, R. M. Horak, W. F. O. Marasas, G. Spiteller, R. Vlegaar, *J. Chem. Soc., Chem. Commun.* 1988, 743–745.
- [13] J. A. Feijó Corrêa, P. B. Orso, K. Bordin, R. V. Hara, F. B. Luciano, *Food Chem. Toxicol.* 2018, 121, 483–494.
- [14] A.-M. Domijan, *Archives of Industrial Hygiene and Toxicology* 2012, 63, 531–544.
- [15] A. M. Alizadeh, G. Roshandel, S. Roudbarmohammadi, M. Roudbary, H. Sohanaki, S. A. Ghiasian, A. Taherkhani, S. Semnani, M. Aghasi, *Asian Pac. J. Cancer Prev.* 2012, 13, 2625–2628.
- [16] F. S. Chu, G. Y. Li, *Appl. Environ. Microbiol.* 1994, 60, 847–852.
- [17] “EUR-Lex - 02006R1881-20210919 - EN - EUR-Lex,” can be found under <https://eur-lex.europa.eu/legal-content/EN/TXT/?uri=CELEX%3A02006R1881-20210919>, n.d.
- [18] C. for F. S. and A. Nutrition, “Guidance for Industry: Fumonisin Levels in Human Foods and Animal Feeds,” can be found under <https://www.fda.gov/regulatory-information/search-fda-guidance-documents/guidance-industry-fumonisin-levels-human-foods-and-animal-feeds>, 2021.
- [19] O. F. Kayode, M. Sulyok, S. O. Fapohunda, C. N. Ezekiel, R. Krska, C. R. B. Oguntona, *Food Addit. Contam. Part B* 2013, 6, 294–300.
- [20] A. De Girolamo, D. P. Fauw, E. Sizoo, H. van Egmond, L. Gambacorta, K. Bouten, J. Stroka, A. Visconti, M. Solfrizzo, *World Mycotoxin J.* 2010, 3, 135–146.
- [21] L. L. Smith, K. A. Francis, J. T. Johnson, C. L. Gaskill, *Food Chem.* 2017, 234, 174–179.
- [22] L. Ma, W. Xu, X. He, K. Huang, Y. Wang, Y. Luo, *J. Sci. Food Agric.* 2013, 93, 1128–1133.
- [23] V. Dohnal, A. Jezková, I. Polisenská, K. Kuca, *J. Chromatogr. Sci.* 2010, 48, 680–684.
- [24] B. Zhang, X. Chen, S.-Y. Han, M. Li, T.-Z. Ma, W.-J. Sheng, X. Zhu, *Molecules* 2018, 23, 1926.
- [25] F. Pradanas-González, G. Álvarez-Rivera, E. Benito-Peña, F. Navarro-Villoslada, A. Cifuentes, M. Herrero, M. C. Moreno-Bondi, *J. Chromatogr. A* 2021, 1648, 462180.

- [26] A. Malachová, M. Stránská, M. Václavíková, C. T. Elliott, C. Black, J. Meneely, J. Hajšlová, C. N. Ezekiel, R. Schuhmacher, R. Krska, *Anal. Bioanal. Chem.* 2018, 410, 801–825.
- [27] D. A. Vargas Medina, J. V. Bassolli Borsatto, E. V. S. Maciel, F. M. Lanças, *Trends Analyt. Chem.* 2021, 135, 116156.
- [28] F. Zhao, R. Shi, R. Liu, Y. Tian, Z. Yang, *Food Chem.* 2021, 339, 128084.
- [29] R. Peltomaa, E. Benito-Peña, R. Barderas, M. C. Moreno-Bondi, *ACS Omega* 2019, 4, 11569–11580.
- [30] Y. Wang, H. Wang, P. Li, Q. Zhang, H. J. Kim, S. J. Gee, B. D. Hammock, *J. Agric. Food Chem.* 2013, 61, 2426–2433.
- [31] R. Peltomaa, E. Benito-Peña, R. Barderas, U. Sauer, M. González Andrade, M. C. Moreno-Bondi, *Anal. Chem.* 2017, 89, 6216–6223.
- [32] X. Zou, C. Chen, X. Huang, X. Chen, L. Wang, Y. Xiong, *Talanta* 2016, 146, 394–400.
- [33] Q. Yuan, J. J. Pestka, B. M. Hespeneide, L. A. Kuhn, J. E. Linz, L. P. Hart, *Appl. Environ. Microbiol.* 1999, 65, 3279–3286.
- [34] R. Peltomaa, I. Agudo-Maestro, V. Más, R. Barderas, E. Benito-Peña, M. C. Moreno-Bondi, *Anal. Bioanal. Chem.* 2019, 411, 6801–6811.
- [35] R. F. Masseyeff, W. H. W. (Winfried H. W. ) Albert, N. Staines, *Methods of Immunological Analysis*, Weinheim, Germany : VCH Verlagsgesellschaft ; New York, NY (USA) : VCH Publishers, 1992.
- [36] J. W. A. Findlay, R. F. Dillard, *AAPS J* 2007, 9, E260–E267.
- [37] R. Krska, P. Schubert-Ullrich, A. Molinelli, M. Sulyok, S. MacDonald, C. Crews, *Food Addit. Contam.: Part A* 2008, 25, 152–163.
- [38] Commission Regulation (EC) No 1881/2006 of 19 December 2006 Setting Maximum Levels for Certain Contaminants in Foodstuffs (Text with EEA Relevance)Text with EEA Relevance, 2022
- [39] E. A. Hunt, A. Moutsiopoulou, S. Ioannou, K. Ahern, K. Woodward, E. Dikici, S. Daunert, S. K. Deo, *Sci. Rep.* 2016, 6, 26814.
- [40] M. P. Hall, J. Unch, B. F. Binkowski, M. P. Valley, B. L. Butler, M. G. Wood, P. Otto, K. Zimmerman, G. Vidugiris, T. Machleidt, M. B. Robers, H. A. Benink, C. T. Eggers, M. R. Slater, P. L. Meisenheimer, D. H. Klaubert, F. Fan, L. P. Encell, K. V. Wood, *ACS Chem. Biol.* 2012, 7, 1848–1857. [10] M. Kamle, D. K. Mahato, S. Devi, K. E. Lee, S. G. Kang, P. Kumar, *Toxins (Basel)* 2019, 11, 328.

## Supporting information

### HPLC-MS/MS method

The validation by HPLC-MS/MS was conducted at the Institute of Food Science, Technology and Nutrition (ICTAN, Madrid, Spain). Briefly, all the measurements were performed in a high-performance chromatography instrument Agilent 1200, coupled to a Triple Quadrupole Agilent G6410B (Agilent technologies, Santa Clara, CA, USA). The column utilized was a Poroshell 120 EC C18 (3  $\mu\text{m}$  x 150 mm x 2.7 mm) chromatographic column (Agilent Technologies). The separation was performed under gradient conditions with the mobile phase consisting of an aqueous solution containing 0.1% formic acid (solvent A) and MeCN supplemented with 0.1% formic acid (solvent B) at a flow rate of 0.3 mL min<sup>-1</sup> (0 min, 30% B; 15 min, 80% B; 17 min, 100% B; 20 min, 100% B; 25 min, 30% B; 30 min, 30% B). The injection volume was 5  $\mu\text{L}$ . The precursor ions were 722.4 m/z for FB<sub>1</sub> and 706.4 m/z for FB<sub>2</sub>. The product ions utilized to identify and quantify FB<sub>1</sub> were 352.3 and 334.3 m/z, respectively, and for FB<sub>2</sub>, 318.3 and 336.3 m/z, respectively.

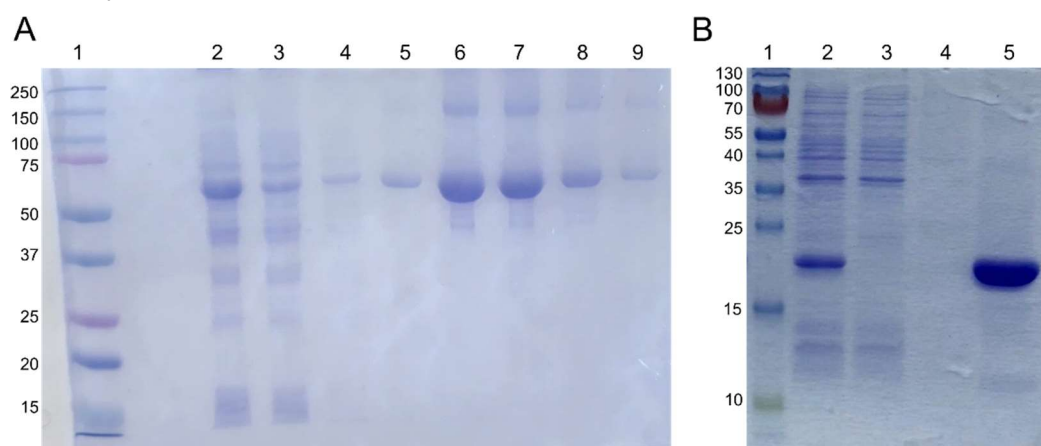


**Figure S1.** SDS-PAGE results for both fusion proteins. A. A2-GLuc fusion protein; Lane 1: protein ladder (Bio-Rad Precision Plus Protein Dual Color Standard); Lane 2: unpurified protein; Lane 3: flow through of the column; Lanes 4 to 9: elution fractions of the purified protein collected from the column. B. A2-NLuc fusion protein; Lane 1: protein ladder (Thermo Scientific™ PageRuler™ Prestained Protein Ladder, 10 to 180 kDa); Lane 2: unpurified protein; Lane 3: flow through of the column; Lane 4: washing solution; Lane 5: purified protein.



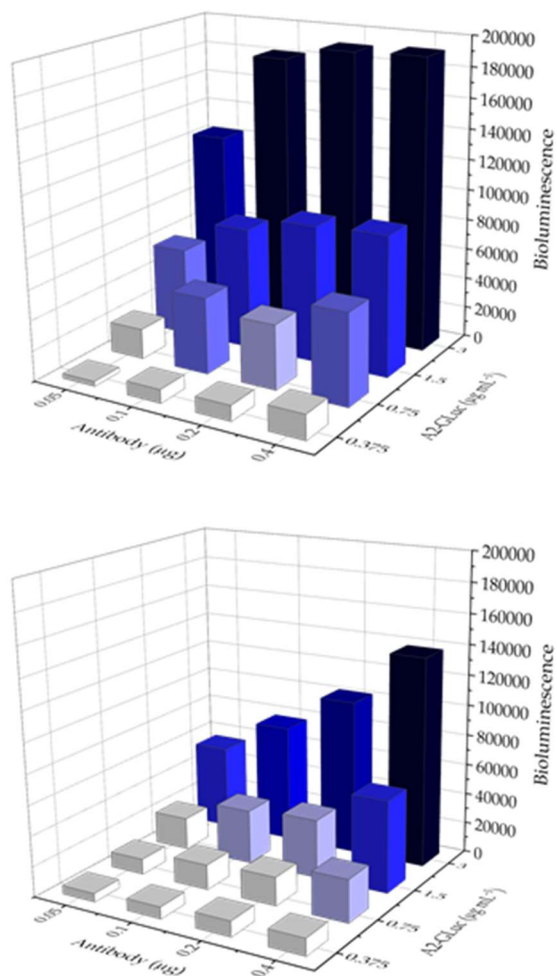


**Figure S2.** Checkerboard titration for the bead-based immunoassay using A2-GLuc. Different concentrations of the antibody (x-axis) and the fusion protein (z-axis) were tested in the absence (up) and the presence (down) of 10 µg mL<sup>-1</sup> free FB<sub>1</sub>. The ratio between these two signals (C) was utilized to determine the optimal concentrations for the immunoassay (RSD < 16.2%).

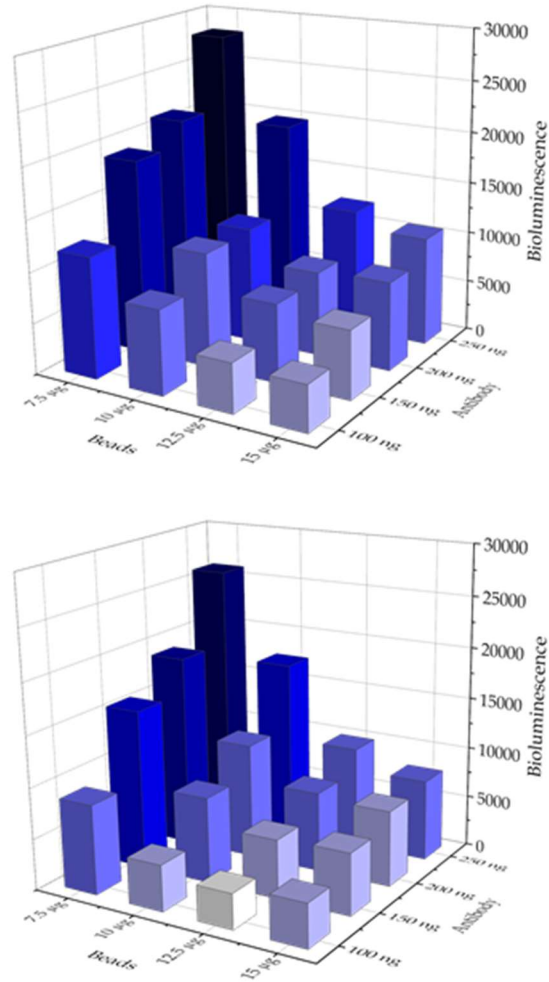


**Figure S3.** Checkerboard titration for the bead-based immunoassay using A2-NLuc. Different concentrations of magnetic beads (x-axis) and antibody (z-axis) were tested in the absence (up) and the presence (down) of 10 µg mL<sup>-1</sup> free FB<sub>1</sub>. The ratio between both signals (C) was utilized to determine the optimal concentrations for the immunoassay (RSD < 14.4%).

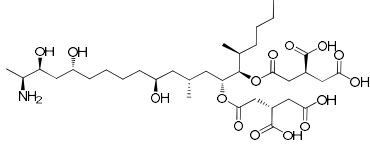
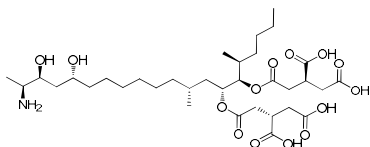
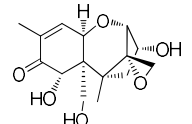
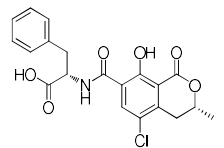
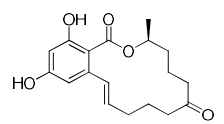
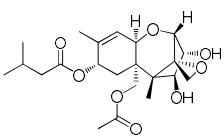
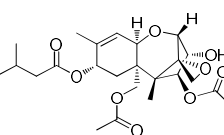
**Table S1.** Comparison of the analytical characteristics of reported immunoassays for the detection of FB<sub>1</sub>.

Assay type	Label	Measurement	IC50 and DR	LOD	Sample	Reference
Microarray-based ELISA with immobilized FB <sub>1</sub> -BSA and PcAb	AP	Absorbance	- -	43 ng mL <sup>-1</sup>	-	1
ELISA with immobilized FB <sub>1</sub> mimotope-BSA and McAb	HRP	Absorbance	6.06 ng mL <sup>-1</sup> 1.77 – 20.73 ng mL <sup>-1</sup>	1.18 ng mL <sup>-1</sup>	Maize, feedstuff, and wheat	2
Multiplex ELISA on reusable biochips with imobilized FB <sub>1</sub> -BSA and McAb	HRP	Chemiluminescence	644.8 µg kg <sup>-1</sup> 10.5–138.5 ng mL <sup>-1</sup>	9.9 ng mL <sup>-1</sup> (159.0 µg kg <sup>-1</sup> )	Oat, wheat, rye, corn	3
ELISA with recombinant scFv and immobilized FB <sub>1</sub> -OVA	HRP	Absorbance	12.67 ng mL <sup>-1</sup> 2.10 – 76.45 ng mL <sup>-1</sup>	8.32 µg kg <sup>-1</sup>	Spiked corn	4
ELISA on ICG-strip with immobilized FB <sub>1</sub> -OVA and PcAb-CGC	Golloidal gold	Visual	-	5 ng mL <sup>-1</sup>	Maize, wheat, sorghum, and paddy	5
Magnetoimmunosensor on CSPE with McAb immobilized on magnetic beads and FB <sub>1</sub> -HRP	HRP	Amperometry	2.86 ng mL <sup>-1</sup> 0.73–11.2 ng mL <sup>-1</sup>	0.33 ng mL <sup>-1</sup>	Maize, beer	6
ELISA with anti-FB <sub>1</sub> mAb coated plates	Ab2β-Nb-AP	Absorbance	2.69/0.93- 7.73 ng mL <sup>-1</sup>	0.35 ng mL <sup>-1</sup>	Corn	7
		Chemiluminescence	0.89/ 0.29- 2.68 ng mL <sup>-1</sup>	0.12 ng mL <sup>-1</sup>		
Multiplex homogeneous immunoassay for FB <sub>1</sub> , DON and T-2 using selective McAbs	AlexaFluor 647	Fluorescence polarization	1918 µg kg <sup>-1</sup> 587.0–6265 µg kg <sup>-1</sup>	331.5 µg kg <sup>-1</sup>	Maize	8

Microarray-based immunoassay with covalently immobilized FB1 mimopeptide and McAb	AlexaFluor 647	Fluorescence	37.1 ng mL <sup>-1</sup> 17.3–79.6 ng mL <sup>-1</sup>	11.1 ng mL <sup>-1</sup>	Spiked maize and wheat	9
Homogeneous assay with Au NPs coated with protein G and McAb	FB <sub>1</sub> mimotope fused to YFP	Fluorescence	12.9 ng mL <sup>-1</sup> 7.3 - 22.6 ng mL <sup>-1</sup>	1.1 ng mL <sup>-1</sup>	Wheat	10
FB1-KLH coated on the Au chip surface	None	Mass-sensitive	Singleplex	2.0/0.5 - 8.0 ng mL <sup>-1</sup>	---	-----
			Multiplex	3.6/0.9–14.3 ng mL <sup>-1</sup>		
Magnetic beads coated with protein G and McAb	FB <sub>1</sub> mimotope fused to GLuc	Bioluminescence	1.3/0.61–2.9 ng mL <sup>-1</sup>	0.38 ng mL <sup>-1</sup>	Wheat	This work
	FB <sub>1</sub> mimotope fused to NLuc		13.5/1.91–95.2 ng mL <sup>-1</sup>	0.61 ng mL <sup>-1</sup>		

Abbreviations: NP: nanoparticle; McAb: monoclonal antibody; scFv: single-chain fragment variable antibody; PcAb: polyclonal antibody conjugated to colloidal gold; OVA: ovalbumin; HRP: horse-radish peroxidase; BSA: bovine serum albumin; SAM: self-assembled monolayer; CSPE: carbon screen-printed electrode; DR: dynamic range; AP: alkaline phosphatase; ICG: immunochromatographic; Ab2 $\beta$ -Nb-AP: anti-idiotypic nanobody-alkaline phosphatase; DON: Deoxynivalenol; YFP: yellow fluorescent protein; GLuc: Gaussia luciferase; NLuc: NanoLuc luciferase.

**Table S2.** Cross reactivity results for the bead-based immunoassays with A2-GLuc and A2-NLuc

Mycotoxin	Structure	A2-GLuc		A2-NLuc	
		IC <sub>50</sub>	CR <sup>[a]</sup>	IC <sub>50</sub>	CR <sup>[a]</sup>
Fumonisin B <sub>1</sub> (FB <sub>1</sub> )		1.34 ± 0.07	100%	13.5 ± 1.7	100%
Fumonisin B <sub>2</sub> (FB <sub>2</sub> )		1.15 ± 0.05	116%	12.8 ± 2.0	105%
Deoxynivalenol (DON)		> 1000	< 0.1%	> 1000	< 1%
Ochratoxin A (OTA)		> 1000	< 0.1%	> 1000	< 1%
Zearalenone (ZEA)		> 1000	< 0.1%	> 1000	< 1%
HT-2 toxin (HT-2)		n.d.	n.d.	> 1000	< 1%
T-2 toxin (T-2)		n.d.	n.d.	> 1000	< 1%

<sup>[a]</sup> Cross reactivity

**Table S3.** PCR primers utilized in the construction of the A2-GLuc and A2-NLuc fusion proteins. The overlapping region with the template plasmid for each case is underlined. The FB<sub>1</sub> mimopeptide sequence appears in bold.

GLuc	
Primer	Sequence
Forward 1	GATCCTTTTCGGGGTGGAGGTTTCGATGAAACCGACC
Forward 2	GTTACTCCGAATGATGATACGTTTGATCCTTTTCGG
Forward 3	GGTGGAGGTTTCGCATATGGTTACTCCGAAT
Reverse 1	CTAATGATGATGATGATGATGATCACCACCTGC
Reverse 2	CGAACCTCCACCGGATCCCTAATGATGATG
NLuc	
pQE-fwd	TCTGGCGGAAAACCTGTATTTTCAGGGC
pQE-rv	GAGTGTGAAGACCGAACCTCCACCCCGAA
NLuc-fwd	AGGTTTCGGTCTTCACACTCGAAGATTTTCG
NLuc-rv	TACAGGTTTTCCGCCAGAATGCGTTCGCA

## Bibliography

- [1] I. Lamberti, C. Tanzarella, I. Solinas, C. Padula, L. Mosiello, *Mycotoxin Res.* 2009, 25, 193–200.
- [2] X. Liu, Y. Xu, Q.H. He, Z.Y. He, Z.P. Xiong, *J. Agric. Food Chem.* 2013, 61, 4765–4770.
- [3] S. Oswald, X.Y. Karsunke, R. Dietrich, E. Martlbauer, R. Niessner, D. Knopp, *Anal. Bioanal. Chem.* 2013, 405, 6405–6415.
- [4] L. Zou, Y. Xu, Y. Li, Q. He, B. Chen, D. Wang, *J. Sci. Food Agric.* 2014, 94, 1865–1871.
- [5] M. Venkataramana, K. Navya, S. Chandranayaka, S.R. Priyanka, H.S. Murali, H.V. Batra, *J. Food Sci. Technol.* 2014, 51, 1920–1928.
- [6] A. Jodra, M.A. López, A. Escarpa, *Biosens. Bioelectron.* 2015, 64, 633–638.
- [7] M. Shu, Y. Xu, X. Liu, Y. Li, Q. He, Z. Tu, J. Fu, S.L. Gee, B.D. Hammock, *Anal. Chim. Acta* 2016, 924, 53–59.
- [8] C. Li, K. Wen, T. Mi, X. Zhang, H. Zhang, S. Zhang, J. Shen, Z. Wang, *Biosens. Bioelectron.* 2016, 79, 258–265.
- [9] R. Peltomaa, E. Benito-Peña, R. Barderas, U. Sauer, M. González Andrade, M.C. Moreno-Bondi, *Anal. Chem* 2017, 89, 6216 – 6223.
- [10] R. Peltomaa, F. Amaro-Torres, S. Carrasco, G. Orellana, E. Benito-Peña, M.C. Moreno-Bondi, *ACS Nano* 2018, 12, 11333–11342.
- [11] P. Nolana, S. Auerb, A. Speharb, M. Oplatowska-Stachowiaka, K. Campbella, *Talanta*, 2021, 222, 121521.

